Thesis for the Master's Degree in Chemistry

Jochen Grudzinski

Determination of Major Particulate Matter (PM_{10}) Components in Urban Aerosol From Taiyuan City, China

60 Study Points

Supervisor: Prof. H.M. Seip

DEPARTMENT OF CHEMISTRY
Faculty of Mathematics and Natural Sciences

UNIVERSITY OF OSLO 06/2007

Acknowledgements

First of all, I want to thank my God, Saviour and Brother **Jesus** for how wonderfully He led my wife and me to Oslo, opened up all necessary doors and gave me the great opportunity to undergo a master education, just like He had promised three years ago. His unconditional love and favour, also during this time of studying, have made it all so smooth, easy and blessed. He provided for all my needs and blessed me with the following people, who I want to dearly thank:
My wonderful wife Sigga, for her unconditional love and constant encouragement, and the time she gave me to study when I needed it, even though these were our first two years of marriage; **My family**, who gave me the greatest food of another kind; My supervisor, **Prof. Hans Martin Seip**, for the great chance of studying environmental chemistry, for his kindness and constructive advice; **Anne-Marie Skramstad**, for her awesome teachings, advice and help with ICP-MS and AES. **Hege** and **Hanne**, for their ever so kind help with all IC related issues, laboratory equipment, etc.; **Steve Kohl** from the Nevada Desert Research Institute, who helped me a lot with finding out about carbon analysis; **Ruikai Xie**, for all his wisdom, especially during the actual sampling time in Taiyuan. **Karl Espen Yttri**, from NILU, for his supervision during TOA analysis and helpful input at all other times; **Inge Mikalsen**, who in no time at all built a great cutting mould for the quartz filters; and last but not least, the entire **environmental chemistry group**, for the warm atmosphere and their individual kindness. It was an honour for me being here and meeting you all.

Table of Contents

ABSTRACT **5**

1.0 INTRODUCTION **6**

2.0 SITE DESCRIPTION **8**

2.1 China **8**
2.2 The Shanxi Province **9**
2.3 Taiyuan **10**
2.3.1 Occupational, Meteorological, and Geographical Information 10
2.3.2 Emission Sources 11

3.0 ATMOSPHERIC PARTICULATE MATTER **12**

3.1 Physical Characteristics and Processes **13**
3.1.1 Particle Diameters 13
3.1.2 Size Distribution Function 15
3.1.3 Definition of Particle Size Fractions 19
3.1.3.1 Occupational Health or Dosimetry Size Cuts 19
3.1.3.2 Size Selective Sampling – Cut Points 20
3.1.4 Relative Humidity's Impact on Particle Size 21
3.2 Chemistry of Atmospheric Particulate Matter **22**
3.2.1 Chemical Composition 22
3.2.2 Primary and Secondary Particulate Matter 22
3.2.3 Particle-Bound Water (PBW) 23
3.3 Dispersion, Lifetime, and Removal of Atmospheric Particulate Matter **23**
3.4 Carbonaceous Particulate Matter **28**
3.5 Effects of Atmospheric Particulate Matter **29**
3.5.1 Environmental Effects 29
3.5.1.1 Effects on Vegetation 29
3.5.1.2 Effects on Visibility 32
3.5.1.3 Effects on Materials 33
3.5.1.4 Effects on Global Warming 34
3.5.2 Effects on Human Health 36
3.5.2.1 The Human Lung 37
3.5.2.2 Toxicological Effects and Epidemiology 38
3.5.2.2.1 Cardiovascular Effects 38
3.5.2.2.2 Respiratory Effects 40
3.5.2.2.3 Mutagenic/Genotoxic Effects 40
3.5.2.2.4 Compositional Effects 41

4.0 MATERIALS AND METHODS **42**

4.1 Sampling **42**
4.1.1 The Sampling Site 42
4.1.2 Air Samplers and Filters 43
4.2 Microwave Decomposition **46**
4.2.1 The Closed Vessel Microwave Decomposition System 46
4.2.1.1 Absorption of Microwave Energy 46
4.2.1.2 Advantages of the Closed Vessel System 47

4.2.1.3 Chemical Reaction Profile Inside the Closed Vessel 48
4.2.2 The Instrumental Setup 49
4.2.3 The Microwave Decomposition Method 50
4.3 Inductively Coupled Plasma Mass Spectrometry (ICP-MS) 54
4.3.1 Theory, Components and Function 54
4.3.2 ICP-MS Method of Analysis 59
4.3.2.1 The Daily Test 60
4.3.2.2 SRM and Sample Preparation 60
4.3.2.3 ICP-MS Analysis 64
4.4 Inductively Coupled Plasma Atomic Emission Spectrometry (ICP-AES) 65
4.4.1 Theory, Components and Function 65
4.4.2 ICP-AES Method of Analysis 68
4.4.2.1 Sample (SRM) Preparation 68
4.4.2.2 ICP-AES Analysis 70
4.5 Ion Chromatography (IC) 71
4.5.1 Theory, Components and Function 71
4.5.2 Sample Preparation 74
4.5.3 IC Analysis 77
4.6 Thermal/Optical Carbon Analysis 78
4.6.1 Theory, Components and Function 78
4.6.2 Protocols for Thermal/Optical Carbon Analysis 80
4.6.3 TOA Analytical Practise 81
5.0 RESULTS AND DISCUSSION 84
5.1 Method Validation – Recoveries and Uncertainties 84
5.1.1 ICP-MS and ICP-AES Analysis 84
5.1.2 IC Analysis 87
5.1.3 Thermal/Optical Carbon Analysis 88
5.2 Atmospheric Mass Concentrations and PM Composition of Taiyuan Samples 89
5.3 Discussion of Results from Taiyuan Sampling 92
5.3.1 Aerosol-Crust Enrichment Factors (EF) 94
5.3.2 Correlations and Source Apportionment 96
5.3.3 Comparison with Other Results and Air Quality Standards 99
5.4 Discussion of Results of Other TOA analyses 103
5.4.1 Comparison of the Thermal Protocols NIOSH-Derived and JRC-IMPROVE 103
5.4.2 Backup Filter Results 105
6.0 CONCLUSION AND SUGGESTIONS FOR FURTHER WORK 106
REFERENCES 107
APPENDIX 115

Abstract

Atmospheric particulate matter samples (PM_{10}) have been collected on quartz and Teflon filters, for 12 days from 16th to 28th of March 2006 on the 4th floor of the University of Science and Technology in Taiyuan, China. The samples were analysed for the metal elements aluminium (Al), iron (Fe), calcium (Ca), magnesium (Mg), sodium (Na), silicon (Si), titanium (Ti) and zinc (Zn), with inductively coupled plasma atomic emission spectrometry (ICP-AES); copper (Cu), lead (Pb), manganese (Mn), arsenic (As), cadmium (Cd), cobalt (Co), nickel (Ni), antimony (Sb), selenium (Se) and vanadium (V), with inductively coupled plasma mass spectrometry (ICP-MS); ammonium (NH_4^+), sulphate (SO_4^{2-}) and nitrate (NO_3^-), with ion chromatography (IC) and organic and elemental carbon (OC, EC) with a thermal/optical carbon analyser. The average aerosol composition was determined and the mass closure yielded (60.8±12.5)% crustal material, (11.4±3.9)% OC, (5.5±2.0)% EC, (4.4±1.4)% SO_4^{2-}, (1.2±0.6)% NO_3^-, (1.6±0.8)% NH_4^+ and (15.1±21.2)% unknown. The dominating ammonium specie, averaged over the 12 days of sampling, was ammonium sulphate $(NH_4)_2SO_4$. Aerosol-crust enrichment factors and correlation coefficients were applied to identify potential sources of anthropogenic pollutants, and the results pointed towards coal-burning activities as the dominating source. The mean bulk PM_{10} atmospheric mass concentration was (385±105)μg/m³, significantly exceeding all Chinese air quality guidelines. Nevertheless, a trend towards improved air quality was noticed by comparing the results with a previous study from the same location and almost same time of year.

Additionally, two more studies were carried out with samples provided by the Norwegian Institute of Air Research (NILU). A new temperature protocol for the thermal/optical carbon analysis was tested and the results were compared to an existing protocol, with surprisingly good agreement. Further, backup filters from sampling of different size fractions (PM_{10}, $PM_{2.5}$, $PM_{1.0}$) were analysed with the thermal/optical carbon analyser and the found amounts of vapour phase OC were compared among the various size fractions with satisfactory results.

1.0 Introduction

The Environmental Protection Agency (EPA), in their exposure factors handbook (1997), has determined the average amount of air a male or female inhales in the duration of one day to be 15.2 and 11.3m³ respectively. These figures are mean values taking into account that the inhalation rate (also called breathing or ventilation rate) is a function of several parameters, such as age, gender, weight, health status, activity, and metabolism. This large amount of air travelling through the lungs poses certain demands on the cleanness of this transparent, viscous and life-sustaining fluid in order not to impart any adverse health effects. It is exactly this cleanness of the air that has been compromised by increasing industrialisation particularly in rapidly developing countries, such as China and India (EIA, 2003, and 2004 respectively), with considerable toll to human health.

Having one of the world's fastest growing economies (Mestl and Fang, 2003) China has been paying for this upswing with a stark deterioration of its environment. The 1.3 billion people nation (CPIRC, 2007) has strongly built its economic ascent on coal as a major source of energy (Aunan et al., 2006), with the result that according to a World Bank survey, carried out in 2006, 16 of the world's 20 most polluted cities are now situated in China (Walker, 2006). Most of them lie in the north-east, particularly the Shanxi province, which is the Chinese centre for coal extraction (Aunan et al., 2005). Taiyuan is the capitol of Shanxi and was ranked "most polluted city in China" according to a State Environmental Protection Administration (SEPA) report of 2000. Even though more recent reports (SEPA, 2005) indicate a slight improvement in the number of cities increasing their air quality, the situations remains rather serious and inhalable particles are still the major air pollutants. Taiyuan is particularly prone to intense air pollution due to its geographic location.

Amongst all constituents of urban air pollution, **p**articulate **m**atter with an aerodynamic diameter (see section 3.1.1 for more details) less than 10μm (PM_{10}), which can be inhaled into the human respiratory system (Harrison, 1999), is related to the most serious health effects including lung cancer and other cardiopulmonary mortality (WHO, 2002). The same world health report (2002) states, that outdoor urban particulate matter air pollution is responsible for 1.4% of the total annual global

mortality, an estimated number of 0.8 million people. Besides its effects on health particulate matter also impairs visibility, plays an important role in the formation of acid rain, affects the amount of sunlight reaching the ground, and in turn interferes with a variety of environmental processes.

Particulate matter is either directly emitted into the atmosphere from various natural and anthropogenic sources, or can be formed from gases through chemical reactions. The most noteworthy anthropogenic sources with regard to quantity stem from incomplete combustion processes, such as fossil fuel and biomass burning (Seinfeld and Pankow, 2003).

The particles contain a myriad of chemical species, such as inorganic salts, siliceous crustal minerals, carbonaceous materials, and water (Seinfeld and Pankow, 2003). In order to identify any potential effect of atmospheric particles it is of utter importance to determine their composition to an as large as possible degree.
The goal of this thesis is to determine and classify the basic constituents of the particles collected in Taiyuan City, China, to investigate potential correlations of selected constituents to sources and to compare the obtained data with figures from previous studies at the same location.

2.0 Site Description

2.1 China

The nation of China is expanding in every respect. Its urban population has grown by 15% from 1990 to 2004, while on the energy side, China's total consumption increased by 200% from 1980 to 2004 making it the world's largest energy consumer second only to the US. China now accounts for 10% of the total global consumption, a figure that underlines the nation's remarkable economic growth and increasing population density, particularly in urban areas. China has abundant coal resources but at the same time lacks petroleum and natural gas, which gives the country a different energy structure than for instance the Organisation for Economic Co-operation and Development (OECD) countries, the European Union or the world, as can be seen in figure 1 (Yi et al., 2007).

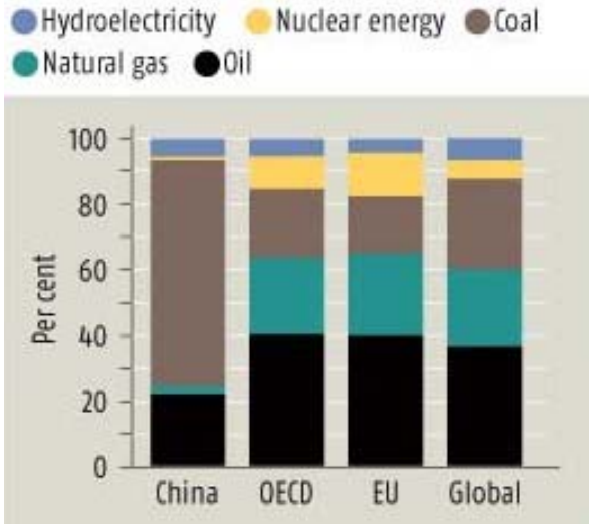

Figure 1 – Energy structure comparison between China, OECD, EU, and world (2004)
[source: Yi et al., 2007]

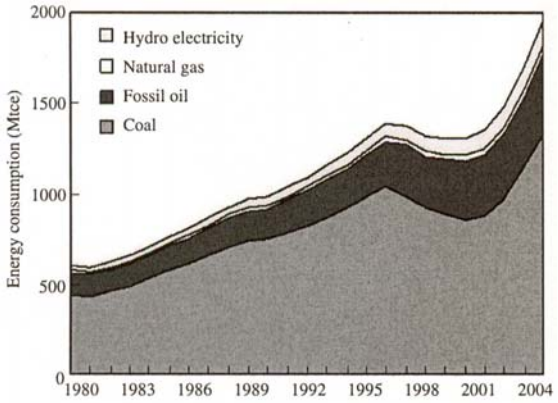

Figure 2 – Energy consumption growth and structure in China from 1980 – 2004
[source: Yi et al., 2007]

Figure 2 illustrates quite clearly the rapid change in the rate of coal consumption within the last six years. Furthermore, there are no signs that coal will soon be replaced by other energy sources (see figure 3). Even though the proportion of coal to the total amount of energy consumed will be reduced from 67% (in 2000) to 54% (in 2020), according to Yi et al. (2007), the demand for coal will increase because of the increase of total energy consumption, which is estimated to have reached 1677 million tons of coal equivalent (Mtce) in 2010 and about 2057 Mtce by the year 2020 (figure 3).

Since coal is the “dirtiest” kind of fossil fuel, and probably dirtier than any energy source, it does not surprise that its burden on the environment is equally enhanced with the amount burned. Figure 4 illustrates this by projecting the potential emissions of the major pollutants up to the year 2020. Coal burning power plants and industry are the main sources for particulate pollution of the Chinese atmosphere.

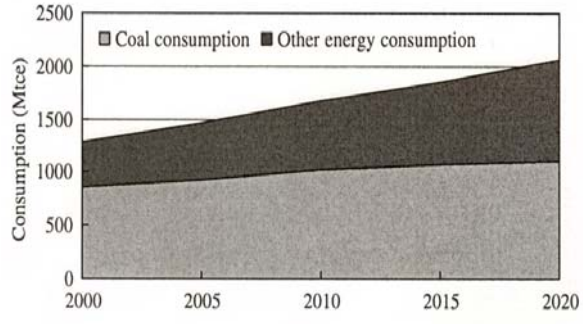

Figure 3 – Forecast of energy consumption in China [source: Yi et al., 2007]

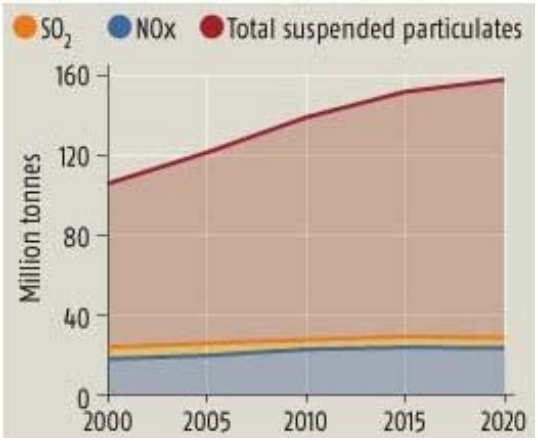

Figure 4 – Projected Pollutant Emissions [source: Yi et al., 2007]

It needs to be said that China is taking measures to improve its air quality. Nevertheless, the quantity of suspended particles in the air will not plateau before at least the year 2020. The total suspended particulates (TSP) (figure 4) are the sum of all airborne particulate matter.

2.2 The Shanxi Province

As already mentioned in the introduction the Shanxi province is the Chinese heart of coal production and features some of the world’s most polluted cities as a consequence. Coal is practically lying in the streets; it is omnipresent and thus rather difficult to be replaced by an alternative, possibly more expensive but less polluting source of energy. An estimated 261.2 billion tons of coal are verified reserves in this province and account for one-third of the country’s total. The energy output of all coal and coal-related industries accounts to also one-third of the nation’s total, while Shanxi’s coal production amounts to one-fourth overall (Aunan et al., 2004). Being

Figure 5 – Shanxi province and capital Beijing [source: Province View-China, 2004]

located in the central north-west of China (figure 5) Shanxi covers an area of about 156,000km² and is home to more than 33.4 million people (2004). Its geographical location, i.e. west of the Taihang mountains, has given Shanxi its name, which means “west of the mountains” (Province View-China, 2004). Climatically Shanxi is predominantly influenced by continental monsoon and hence receives most of its annual precipitation (60%) in summer time (Aunan et al., 2004, and Food and Agriculture Organisation (FAO), 2006).

2.3 Taiyuan

2.3.1 Occupational, Meteorological, and Geographical Information

Taiyuan city is the capital of Shanxi province and the site where air has been collected for analysis. It is home to about 2.93 million people who live in the wider metropolitan area including approximately 1.83 million urban dwellers (Answers.com, 2006). Geographically it is situated between 37°27’N-38°25’N and 111°30’E-113°09’E, lies 800m above sea level and has a continental, temperate and monsoonal climate. The prevailing wind directions are Northerly and North-westerly with an average wind speed of 1.98m/s. The temperatures vary on average between -5.6°C in January and 24.4°C in July resulting in an annual average of 10.8°C. Rainfall is rather irregular due to the monsoonal climate and occurs mostly during summer with an annual average (determined between 1996 and 2000) of 393mm. The average relative humidity is 54%. The occurrence of a so-called inversion layer is rather frequent with on average 60% of all days during summer – having an average thickness of 490m – and 80% with average thickness of 247m in winter time (Xie, 2002).

Location – Taiyuan [source: www.warriortours.com/images/map/chinamap.gif]

As mentioned earlier, Shanxi's topography is coined by mountain ranges with a valley stretching to the north-south. Taiyuan is situated in this valley, surrounded by mountains on the west and east side which narrow in towards the north. The south side of the city is open terrain (Mestl & Fang, 2003).

2.3.2 Emission Sources

Emission sources are either stationary or mobile. In Taiyuan the mobile sources, such as those of the transport sector, contribute merely 0.4% to the energy consumption of the stationary ones. Emissions from transportation significantly affect the air quality of their immediate surroundings, while the distribution of emissions from stationary sources strongly depends on the height at which they are released into the environment. The latter can be subdivided into three categories:

- The domestic sector, including all emissions from private homes, cooking, hot water and heating activities
- The commercial sector, summarising all service companies, such as hotels and restaurants, as well as schools, public organisations and government
- The industrial sector, containing all types and sizes of power plants and metal smelters.

TSP emissions are either related to combustion or to production processes and according to Mestl and Fang (2003) are both of the same order of magnitude. However, emissions from production processes are generally low-level emissions and are more difficult to pinpoint.

Taiyuan's industrial status already indicates that the majority of its TSP emissions (76% of combustive TSP) are generated by industry. The Taiyuan Cogeneration Power Plant No. 1 and 2 with installed capacities of 1000MW and 600MW, and the Taiyuan Iron and Steel Company, which is one of the major iron and steel complexes in China, are the three largest industrial emitters accounting for 50% of all industrial TSP emissions. All three companies are located in central areas of the city (Mestl and Fang, (2003), and Aunan et al., (2004)).

3.0 Atmospheric Particulate Matter

Ever since that bleak day on 5 December 1952, when Londoners suddenly found themselves overshadowed by clouds of a corrosive cocktail of fog mixed with smoke and gas from domestic fires and power stations, the awareness of anthropogenic emissions into the atmosphere received a sudden boost (Brimblecombe, 2002). Reason for what later became to be known as “smog” was the unusual weather phenomenon called *inversion*, which takes place when warm air masses are pushed over colder ones, leading to an increase in temperature with altitude and thus interrupting the vertical exchange of air (see section 3.3). The smog stayed put for four days and an estimated number of 4000 people died of bronchitis. Research into the effects of airborne particles on human health and the environment has become more intensive and a necessary priority of many countries.

Generally, atmospheric particles, also called aerosols or particulate matter (PM), exist in two different aggregate states: liquid and solid. Their contents cover a wide range of substances, from inorganic ions, elemental carbon, metallic-, organic-, and crustal compounds. Hygroscopic particles, furthermore, contain particle-bound water (EPA, 2004). Particles can be emitted directly into the atmosphere – *primary particles* – or they can be formed in the atmosphere thus being termed *secondary particles* (see section 3.2.2). The latter ones are produced through condensation processes of a semi-volatile component either on its own or on pre-existing particle surfaces or volumes (Steven et al., 2004), and via reactions of more than one gas forming a new particle (Wayne, 2000).

The compounds which are involved in the formation process of secondary particles are atmospheric oxygen (O_2), water vapour (H_2O), reactive species such as ozone (O_3), radicals such as hydroxyl ($\bullet OH$) and nitrate ($\bullet NO_3$) radicals, and pollutants such as sulphur dioxide (SO_2), nitrogen oxides (NO_x), ammonia (NH_3) and organic gases from natural and anthropogenic sources. Due to the variety of formation processes and components involved, any given atmospheric particle may contain particulate matter from a number of sources, giving the collective of particles the name “mixture of mixtures”. In this thesis, the terms particulate matter or particles are used to clearly denote the suspended particles only (EPA, 2004).

3.1 Physical Characteristics and Processes

Generally, individual particles are invisible to the naked eye, however, when appearing collectively, they are noticeable due to their light scattering ability (see section 3.5.1.2). Figure 6 gives a good indication of the differences of two important particle sizes when compared to an average human hair.

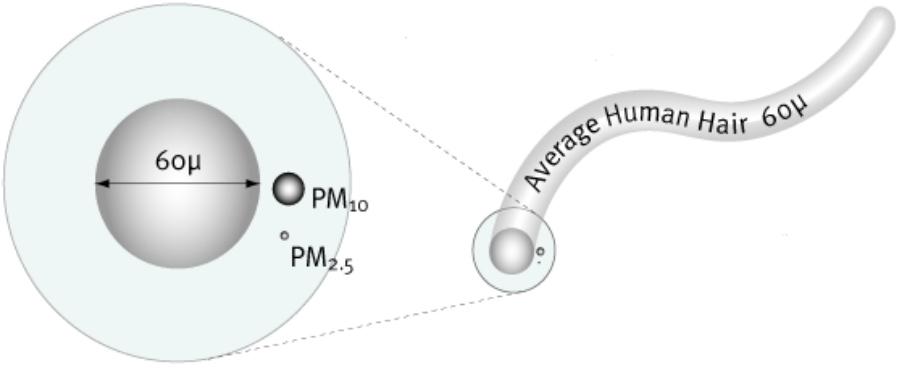

Figure 6 – Size Comparison – Human hair vs. particles [source: EPA, 2006]

3.1.1 Particle Diameters

Particles come in many different shapes, sizes and are seldom spherical (figure 7). Hence their diameters have to be described by an *equivalent diameter*, i.e. the diameter a sphere would have with the same physical behaviour as the particle in question. The type of equivalent diameter used depends on the importance of the physical process involved. For instance, while diffusion is the dominant process for smaller particles (smaller than 0.5µm), the larger particles are more strongly controlled by their gravitational settling behaviour. The former particles are best described by the **Stokes** diameter, while the **aerodynamic diameter** is a more useful quantity to characterise the latter. The two mentioned physical processes have a strong impact on particle transport, collection, and removal processes, including deposition in the respiratory tract.

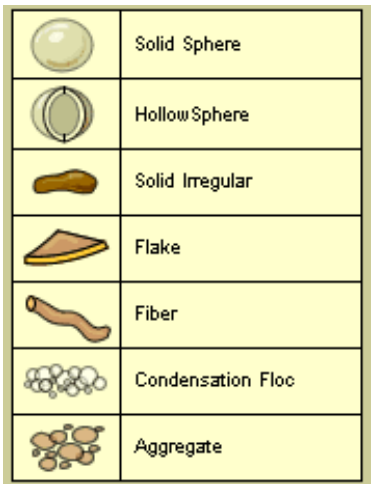

Figure 7 – Particle Shapes [source: http://www.epa.gov/eogapti1/module3/diameter/diameter.htm]

The Stokes diameter ($\mathbf{D_s}$) of a particle is based on its aerodynamic drag force, which it experiences when its velocity differs from that of the surrounding fluid. A

smooth, spherically shaped particle would have a Stokes diameter exactly equal to its physical diameter, while irregularly shaped ones have a D_s of an equivalent sphere having the same aerodynamic resistance. Moreover, the Stokes diameter is independent of density (EPA, 2004).

The aerodynamic diameter (**D_a**) depends on the density of the particle and is defined as being the diameter of a spherical particle with an equal gravitational settling velocity but a material density of 1g/cm³. D_a is the quantity of interest for particles that are **larger than 0.5μm**. The relationship between the aerodynamic diameter and the Stokes diameter is given in equation 1.

$$D_a = D_s \sqrt{\frac{\rho \cdot C_s}{C_a}} \qquad \text{Equation 1}$$

with ρ: particle density

$C_{s,a}$: Cunningham slip factor evaluated for D_s and D_a

The Cunningham slip factor is a function of the ratio between particle diameter and the mean free path length of air molecules. It accounts for the reduction in drag force on the particles because of the “slip” of gas molecules on the surface of the particles, and is empirically determined. For larger particles (>0.5μm), with diameters greater than the mean free path length of the air molecules (λ), i.e. all particles collide with the air molecules, the Cunningham slip factors are approximated to be equal to one. Smaller particles have C-values larger than one. The following equations result from the two considerations.

$$D_a = D_s \sqrt{\rho} \quad \text{for } D_s >> \lambda \qquad \text{Equation 2}$$

$$D_a = D_s \cdot \rho \quad \text{for } D_s << \lambda \qquad \text{Equation 3}$$

The equivalent diameters are a very important quantity in order to:

- Determine the properties, effects, and fate of atmospheric particles,
- Investigate their atmospheric deposition rates and residence times,
- Establish the deposition patterns of the particles in the lung, and to
- Characterise their light scattering ability (EPA, 2004).

The size of the smallest suspended particles is about 1nm – size of typical gaseous molecules is between 0.1 and 1nm – while the upper limit lies in the vicinity of 100μm (Baird and Cann, 2005).

3.1.2 Size Distribution Function

The size distribution is a very important physical quantity governing the behaviour of the particles. Since the particle sizes cover several orders of magnitude, distributions are usually expressed on a logarithmic scale on the x-axis and expressed according to the formula

$\frac{\Delta N}{\Delta(\log D_p)}$ = Number of particles per cm³ of air which have diameters in the size range from $\log(D_p)$ to $\log(D_p+\Delta D_p)$, on the y-axis.

The particle diameter D_p stands for a variety of different equivalent diameters which are measured by various instruments to cover the whole range from 1nm till 100μm. Moreover, it is necessary to include a unit term in the log function to give it the dimension one. Hence, the term $\log(D_p)$ has to be considered as being in fact $\log(D_p/D_{p0})$, with D_{p0} having a value of 1μm. When plotting the "number distribution function" $dN/d(\log D_p)$ on a linear scale, the area under the curve between D_p and $D_p+\Delta D_p$ is proportional to the number of particles in this range. Surface, volume, and mass distributions are treated equivalently and an example of a grand average continental size distribution by Whitby (1978) is shown in figure 8 below. Whitby analysed more than 1000 particle size distributions by collecting particles at various locations all across the United States. One pattern typically emerged from all size distributions: There are three distinctive peaks, also called "modes", which can be distinguished and the overall distribution can be approximated by three additive log-normal distributions. Whitby stated his results as follows:

> "*The distinction between 'fine particles' and 'coarse particles' is a fundamental one. There is now an overwhelming amount of evidence that not only are two modes in the mass or volume distribution usually observed, but that these fine and coarse modes are usually chemically quite different. The physical separation of the fine and coarse modes originates because condensation produces fine particles while mechanical processes produce mostly coarse particles…the dynamics of fine particle growth ordinarily operate to prevent the fine particles from growing larger than about 1μm. Thus, the fine and coarse*

> *modes originate separately, are transformed separately, are removed separately, and are usually chemically different…practically all of the sulphur found in atmospheric aerosol is found in the fine particle fraction. Thus, the distinction between fine and coarse fractions is of fundamental importance to any discussion of aerosol physics, chemistry, measurement, or aerosol air quality standards*" (Whitby, 1978).

Whitby's results for two modes (accumulation and coarse) have been validated with numerous new measurements over the last decades. However, new results had to be included in the diameter range below 0.1μm yielding a more complete picture.
The nomenclature of the determined modes is as follows:

- **Nucleation Mode**: Particle diameter below 10nm;
  Freshly formed particles observed during active nucleation events;
  Particles did not have a chance to grow by condensation or coagulation;
- **Aitken Mode**: Particle diameter between 10nm and 100nm;
  Also recently formed particles that still actively undergo coagulation;
  Due to either higher concentrations of precursors or more time for condensation and coagulation, they have reached larger diameters;
- **Accumulation Mode**: Particle diameter between 0.1μm and 1-3μm;
  With increasing particle size the rate of growth via coagulation and condensation goes down and the particles accumulate in this mode;
- **Coarse Mode**: Particle diameter mostly greater than the minimum in the mass or volume distribution (1-3μm) (Figure 8c); Particles have been generated by mechanical breakdown of minerals, crustal material, and organic debris; in addition sea salts, nitrate formed from reactions between HNO_3 and NaCl, and sulphate from reactions of SO_2 and basic particles may also be included.

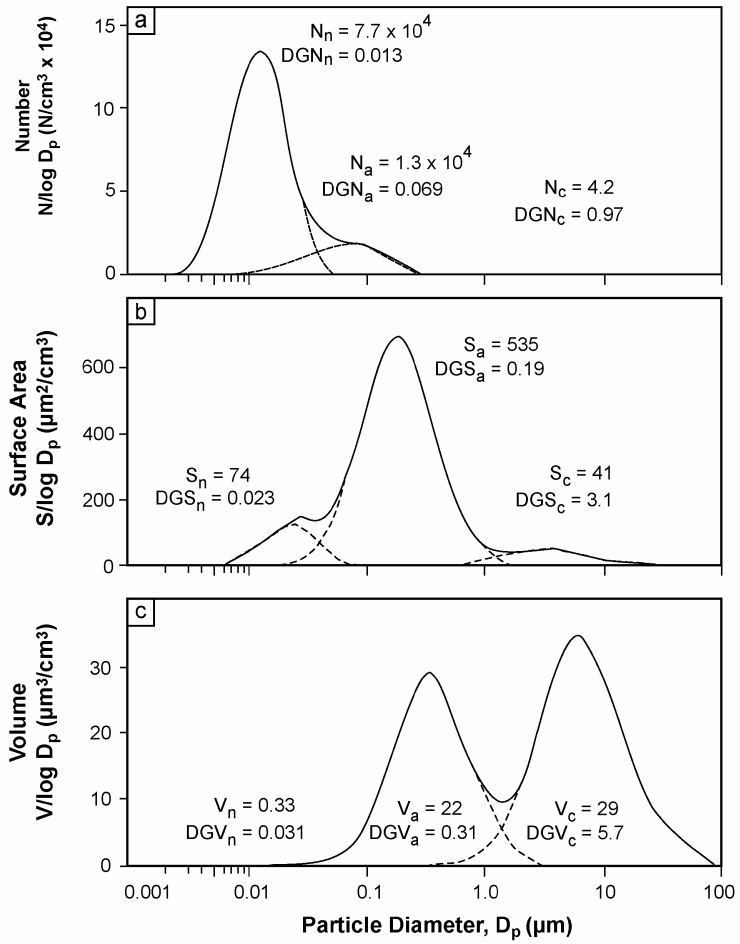

Figure 8 – Particle number (N), surface area (S), and volume (V) distributions of the nucleation, accumulation, and coarse mode. Particle number, surface area, and volume figures correspond to the areas under the curves. Geometric mean diameter by volume, surface, and number (DGV, DGS, and DGN respectively) are also stated. Abbreviations n, a, and c stand for the three modes. [Source: Whitby, 1978].

As can be seen in figure 8, the nucleation and/or Aitken mode are best observed in the number distribution. Nevertheless, the Aitken mode can be identified in the volume distribution in emissions from traffic or other sources of ultra-fine particles. The three distributions from figure 8 clearly show that most particles are smaller than 0.1μm, and that most of the volume (mass) can be found in particles larger than 0.1μm. Of course, peak heights will vary with the location (rural, urban, etc.), source, temperature, saturated vapour pressure of the components, and age of the aerosol, which may remove or include a mode in the ultra-fine particle region, yet the overall pattern remains. The three most important size categories for particles are called coarse, fine, and ultra-fine. The **coarse** particles range between 1 and 100μm, **fine** particles have a diameter below 1μm with **ultra-fine** particles at diameters smaller than 0.1μm.

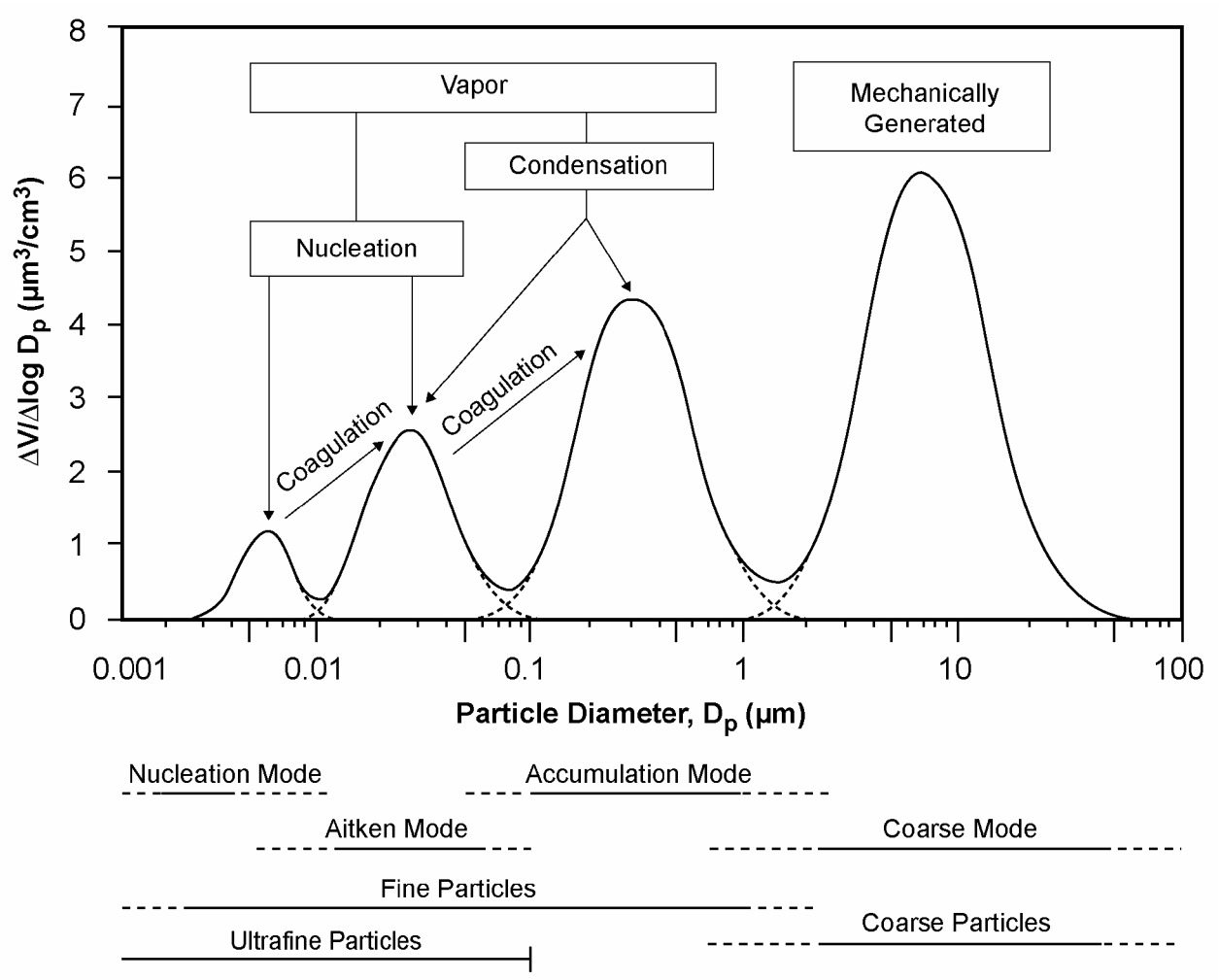

Figure 9 – Idealised size distribution observable in traffic, including fine and coarse particles in the nucleation, Aitken, accumulation, and coarse mode. [Source: EPA, 2004].

All four basic modes, illustrated in figure 9, are generally defined according to the underlying mechanisms of formation. Combustion and chemical reactions of gases leading to products with low saturation vapour pressure are the major pathways to the generation of fine particles, which are composed of metals (also metal oxides), elemental carbon, primary and secondary organic compounds, and sulphate, nitrate, ammonium, and hydrogen ions. Particles from the accumulation mode usually do not grow into the coarse mode. Nevertheless, during periods of high relative humidity, hygroscopic accumulation mode particles grow and increase the overlap between fine and coarse particles (EPA, 2004).

3.1.3 Definition of Particle Size Fractions

In order to classify atmospheric particles by their sizes, aerosol scientists apply several definitions. The most common ones are: (1) the already stated modes, which are based on the observed size distributions and formation mechanisms, (2) occupational health sizes or dosimetry, based on the entrance into various compartments of the respiratory system, and (3) cut points, which are usually based on the 50% cut point of the specific sampling device.

3.1.3.1 Occupational Health or Dosimetry Size Cuts

This particular convention classifies particles as inhalable, thoracic, and respirable, according to their *upper size cuts*. While inhalable particles only enter the respiratory tract, beginning with the head airways, and thoracic ones travel past the larynx reaching the lung airways and gas-exchange regions of the lung, respirable particles, a subset of thoracic particles, are more likely to reach the gas-exchange region of the lung. Exact, unified definitions of the three terms were only established in 1993 and are shown through the respective curves in figure 10. These specific particle penetration curves were collected through an ideal (no-particle-loss) inlet for the individual size-selective sampling criteria. With the use of the curves it is possible to establish that, for instance from all particles with an aerodynamic diameter of 10μm, about 70% penetrate through an inlet representing the condition (diameter) of the respiratory tract (i.e. inhalable fraction), circa 35% of all those particles are thoracic, and none or very few are respirable (EPA, 2004).

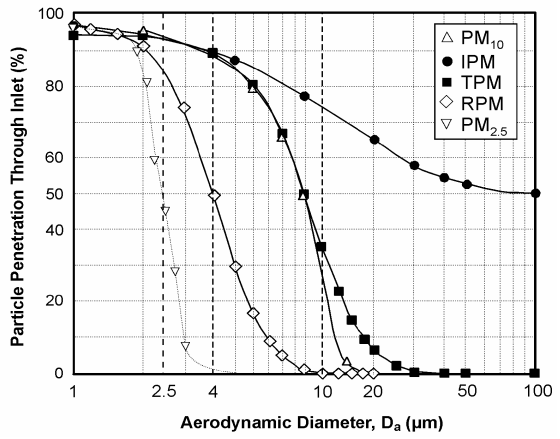

Figure 10 – Specific particle penetration (size-cut curves) with focus on inhalable (IPM), thoracic (TPM), and respirable particulate matter (RPM). [Source: EPA, 2004].

3.1.3.2 Size Selective Sampling – Cut Points

This particular set of definitions of particle size fractions refers to the collection of particles above or below a specific aerodynamic size range. This is the description method used within this thesis and the commonly used abbreviation PM_x (particulate matter with aerodynamic diameter below xμm) arises from these considerations. The size fractions (x) are most often specified by the 50% cut point size, i.e. a sampling device collects 50% of the particles with xμm aerodynamic diameter and rejects 50%. Furthermore, the size fractions are not only defined by the 50% cut points but also by the entire penetration curve (figure 10). It depends to a large extent on the sampler and thus two samplers with the same 50% cut point, but different penetration curves, would collect different fractions of the particulate matter. The reason why size selective sampling has gained a lot of attention is due to the need of measuring particle size fractions that have a special importance, such as for health studies, visibility, source apportionment, to measure mass size distributions, or to collect segregated particles for chemical analysis. An example of the size fractions collected by various samplers is given in figure 11. It also becomes clear from those curves that PM_x samplers do not collect all particles with diameter smaller than xμm, but rather reject a given amount before their characteristic curves (dotted lines in figure 11) merge with the overall size distribution curves.

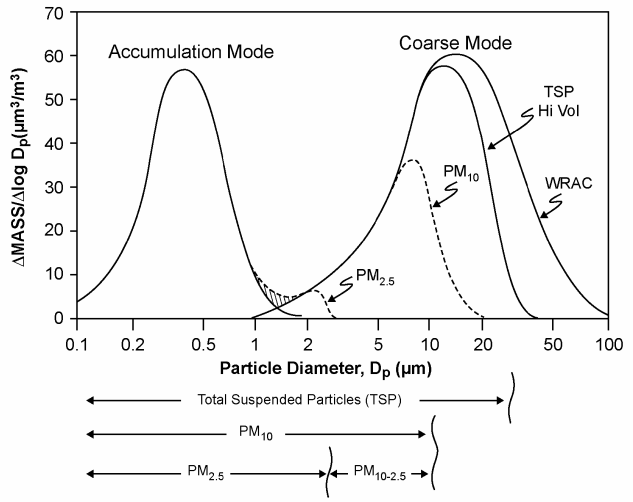

Figure 11 – Idealised distribution of ambient particulate matter including the fractions collected by size-selective samplers. WRAC: Wide Range Aerosol classifier, collecting the entire coarse mode. [Source: EPA, 2004].

The exact definitions of which particles have been size-selectively sampled vary but need to be explicitly stated in order not to arrive at misleading conclusions. For example, samplers that sample with total rejection of all particles greater than 10μm in diameter lack the amount of coarse thoracic PM collected by samplers with a 50% cut at 10μm. When considering figure 10, it seems reasonable to assign the thoracic particle fraction to the particles collected with a PM_{10} sampler, although, in this case, some thoracic particles are not included. Health considerations were thus the reason for the selection of PM_{10} as an indicator.

3.1.4 Relative Humidity's Impact on Particle Size

Relative humidity influences the particle size distribution in both the accumulation and coarse modes (EPA, 2004). Of particular interest is the region between 1.0 and 3.0μm, also called intermodal region, where the accumulation and coarse mode overlap. High RH causes hygroscopic accumulation-mode particles to grow in size due to the accumulation of particle-bound water, thus enabling some initially sub-micrometer sized accumulation-mode particles to reach aerodynamic diameters above 1μm. At RH of 100%, as in fog and clouds, these accumulation-mode particles may even extend above 2.5μm in aerodynamic diameter. Conversely, at very low RH, coarse particles may be fragmented into smaller sizes, and small amounts of coarse-mode particles can be found having aerodynamic diameters below 2.5μm (Lundgren et al., 1984; Lundgren and Burton, 1995). Misclassifications of accumulation and coarse-mode particles can occur when neglecting the influence of RH. However, within the framework of this thesis, only PM_{10} particles were collected which will include the intermodal region (see figure 11), rendering a necessary distinction between the two modes obsolete.

3.2 Chemistry of Atmospheric Particulate Matter

Atmospheric particulate matter can be divided into several **major categories**, such as **nitrates**, **sulphates**, **ammonium**, **hydrogen ions**, **particle-bound water**, **elemental carbon** and **organic compounds**, **crustal material**, **sea salts** (at coastal locations), and a large amount of **elements** in numerous compounds and concentrations (EPA, 2004).

3.2.1 Chemical Composition

The chemical compositions stated are based on results collected in studies in most parts of the United States. The results indicate that sulphate, ammonium, hydrogen ions, elemental carbon, primary and secondary organic compounds from cooking and combustion, as well as certain transition metals are predominantly found in the fine particle mode, while crustal materials such as calcium, aluminium, silicon, magnesium, and iron are mostly discovered in coarse particles. Also found in the coarse mode are primary organic materials such as pollen, spores, and plant and animal debris. Furthermore, nitrate and potassium are found in both the fine and the coarse modes as their sources and mechanisms of formation may vary.
While potassium in coarse particles originates from soil, the potassium in the fine particle mode comes from burning wood or cooking meat. The nitrate in fine particles is caused by the reaction of gas-phase nitric acid with gas-phase ammonia forming particulate ammonium nitrate. Reactions of gas-phase nitric acid with pre-existing coarse particles lead to nitrate ending up in the coarse mode (EPA, 2004).

3.2.2 Primary and Secondary Particulate Matter

The two major types of particulate matter, defined in section 3.0, not only differ in their pathway of formation but also in their chemical composition. *Primary coarse particles* are usually formed by mechanical processes including wind blown dust, sea salt, road dust, and combustion-generated particles such as fly ash and soot. *Primary fine particles* can either be emitted directly as particles or as vapours that quickly condense forming nucleation-mode particles. Included in this category is soot from diesel engines, a large range of organic compounds from incomplete combustion or cooking, and compounds of As, Se, Zn, etc which condense from vapour formed during combustion or smelting.

Condensable vapours generated by chemical reactions of gas-phase precursors are the source of fine secondary particulate matter. Most sulphates and nitrates along with some of the organic compounds in atmospheric particles are formed in these chemical reactions. It is, however, much more difficult to trace ambient secondary species back to their origins, as the entire formation process depends on numerous factors, such as the concentration of precursors and other gaseous reactive species, e.g. ozone, hydroxyl and peroxy radicals, or hydrogen peroxide, and atmospheric conditions such as solar radiation and relative humidity (EPA, 2004).

3.2.3 Particle-Bound Water (PBW)

Some atmospheric aerosols are in equilibrium between the gas phase and the condensed phase and are therefore called semi-volatile. Examples of this kind are water, ammonium nitrate and certain organic compounds. The equilibrium between water vapour and liquid water in **hygroscopic particles** is the reason why many ambient particles contain particle-bound water. In order not to measure PBW as a part of the particle mass, it has to be removed by drying. PBW has a large impact on the chemistry and physics of the atmospheric particles, such as:

- Particle size and light scattering;
- Aerodynamic properties, which play an important role in dry deposition to surfaces, deposition to airway surfaces during breathing, and deposition in sampling instruments;
- Provides medium for reactions of dissolved gases;
- Acts as carrier for potentially toxic species to the respiratory system.

3.3 Dispersion, Lifetime, and Removal of Atmospheric Particulate Matter

The local meteorological conditions play an important role in the fate of emitted particles and consequently in the extent of human exposure towards them. Therefore, the degree of dispersion, or in other words, the concentration of the atmospheric particles, will strongly depend on **wind speed** and **atmospheric stability**. Wind speed and pollutant concentration (includes PM) are correlated reciprocally, i.e. low wind speeds will result in high pollutant concentrations and vice versa. This becomes very clear when considering a chimney that emits smoke at a constant rate. The volume of air into which the smoke is blown will increase with

increasing wind speed. Thus, the pollutant concentration will be directly proportional to the rate of emission but inversely proportional to the wind speed. It is important to consider the prevailing wind directions as the pollution situation is worse down-wind of the sources. In reality, however, the concentration of pollutants in urban areas usually does not drop as quickly as predicted by wind speed.

In addition to the direction and velocity of the wind, the vertical mixing of air in the boundary layer of the troposphere [lowest 1 – 2km of the atmosphere, IPCC (2001)] also affects the concentration of the pollutants. The larger the **surface roughness** the stronger the resulting turbulence when wind blows across it, and as a result, the larger the vertical mixing of air. The roughness coefficient signifies the degree of surface roughness and increases with an increase in obstacles in the pathway of the wind. Large scale vertical mixing is dominated by the stability of the atmosphere, which in turn is largely controlled by the **thermal buoyancy**. An air package that is warmed at the ground will rise due to buoyancy, i.e. the surrounding air is colder and heavier. It will then ascend at a rate and to a degree given by the stability of the atmosphere. The rate at which it will cool and expand is called the **adiabatic lapse rate**, which is about 1°C over 100m for dry air and approximately 0.6°C/100m for moist air. This effect occurs because the pressure in the atmosphere decreases exponentially with height, and as the air cools, it expands. In the real atmosphere the lapse rate can be smaller, almost equal to, or larger than the adiabatic lapse rate. This has consequences on the extent of vertical mixing. There are various stability categories of the atmosphere. It shall suffice to mention only the ground level and aloft inversion condition, as these will inhibit the dispersion of the pollutants (figure 12a and 12b respectively).

Ground level inversion (figure 12a) most often occurs when the lowest layer of air is cooled by the underneath ground, which frequently takes place during overnight radiative cooling of the same in cloudless nights. This condition usually does not last longer than midmorning when the warming effect of the sun removes that low-lying layer. Furthermore, the ground

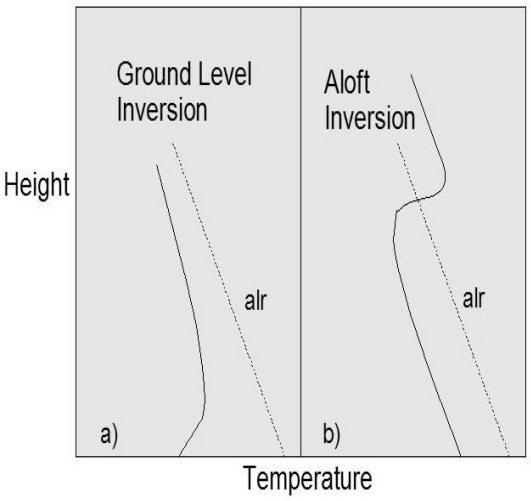

Figure 12 – Illustration of ground level inversion (a) and aloft inversion (b) [source: adapted from Harrison, 1999]

level inversion layer is not very thick (often 100 – 200m) and factories with very high chimneys will emit into the well mixed higher altitude layer above. Increasing the concentration of pollutants during inversion is the decrease in wind speed, since fast moving air above the inversion layer does not mix with the low level air. Consequently there will be no exchange in downward momentum and the air in the inversion layer becomes stagnant. The situation is different in the case of the **aloft inversion** (a.k.a. subsidence inversion) shown in figure 12b, which occurs during a certain meteorological condition termed anticyclonic. Within an anticyclone, air diverges from a high pressure system and at the centre it subsides from high levels of the atmosphere to lower levels. As the air subsides it warms resulting in the emergence of a high level inversion layer. It is possible for the air underneath the inversion layer to be well mixed up to the inversion height. The local pollution situation is generally worse during episodes of ground level inversion (Harrison, 1999). The local geography also has a considerable impact on the potential of pollutants to accumulate. Cities located in valleys, such as Taiyuan, are especially susceptible to increased pollution levels, as cool air tends to flow down the valley triggering low level inversion. A quite similar situation occurs in cities located by the sea. A sea breeze during the day from the cooler sea towards the warmer land will result in cooler air from the sea being forced underneath warmer air on land.

Chimney emission from factories is a major contributor to air pollution in Taiyuan (Mestl and Fang, 2003). However, the dispersion of pollutants from chimneys strongly depends on the stability of the atmosphere, the wind speed, chimney (stack) height, and the temperature and exit velocity of the flue gasses. While the ground-level concentration of pollutants is zero close to the chimney, as some time is necessary for vertical mixing to transport pollutants to the ground, it will reach a maximum at some distance down-wind that will be larger with increasing stack height and atmospheric stability. As a rule of thumb, the maximum ground level concentration is inversely proportional to the square of the chimney height. Thus very high chimneys tend to shift a local problem to a regional and/or transboundary one (Harrison, 1999).

Atmospheric lifetimes of particles, in the same way as most other particle characteristics, depend on their size. The nucleation-mode particles will rather quickly

coagulate and hence grow into the accumulation mode, where no further growth into the coarse mode takes place. The fine particles from the accumulation mode remain in the atmosphere for a number of days and can travel over thousands of kilometres before they are deposited to surfaces. On the other hand, coarse-mode particles do not remain suspended in the atmosphere for more than minutes to a few hours. As a consequence the possible range they can travel is considerably shorter. The only exception arises during extreme weather events, such as strong dust storms, when coarse particles of smaller sizes can reach higher altitudes and be transported over longer distances (EPA, 2004).

The deposition of suspended particles to surfaces occurs in several possible ways (figure 13). **Dry deposition** describes the process in which the particles eventually settle down as a result of gravity. Turbulence may also cause particles to hit surfaces and be deposited. In contrast, **wet deposition**, describes the atmospheric removal of particles via rain or snow (Harrison, 1999). During **occult deposition**, named because it was previously hidden in measurements that determined the first two types, particles are being removed from the air via fog, cloud-water, and mist interception (EPA, 2004). The dry deposition velocity reaches a minimum for particle sizes between 0.1 and 1.0μm in aerodynamic diameter. Cloud processes are the predominant removal pathway for accumulation-mode particles. Fine particles, in particular those containing a hygroscopic component, grow with increasing relative humidity into cloud condensation nuclei, and eventually into cloud droplets. When they have reached sizes larger than 100μm they form rain and fall out of the air (Baird and Cann, 2005). Falling rain drops also remove coarse-mode particles by mechanical impact and ultra-fine particles via diffusion. The cloud processes are, however, much more efficient in removing accumulation-mode particles than falling rain drops (EPA, 2004). Table 1 below summarizes the characteristics of the different particle modes.

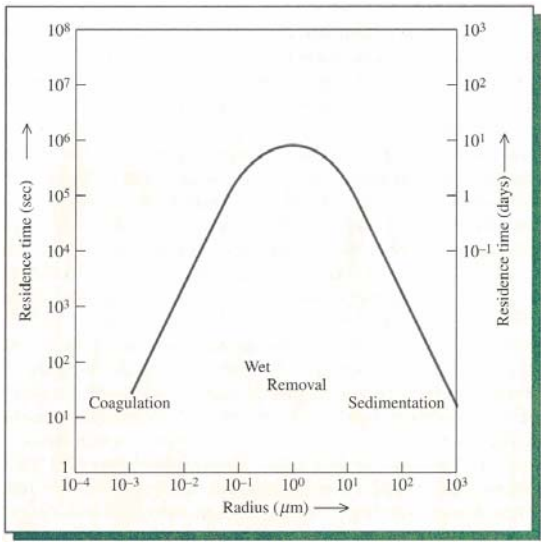

Figure 13 – Residence times and removal pathways as a function of particle size [source: Baird and Cann, 2005]

Table 1 – Characteristics and properties of the individual particle modes [source: EPA, 2004]

Particle Mode	Fine		Coarse
	Ultra-Fine	**Accumulation**	
Formation Processes	Combustion, high-temperature processes, atmospheric reactions		Break-up of large solids/droplets
Formed by:	Nucleation Condensation Coagulation	Condensation Coagulation Reactions of gases in or on particles Evaporation of fog and cloud droplets in which gases have dissolved and reacted	Mechanical disruption (crushing, grinding, abrasion of surfaces) Evaporation of sprays Suspension of dusts Reactions of gases in or on particles
Composed of:	Sulphate Elemental carbon Metal compounds Organic compounds with very low saturation vapour pressure at ambient temperature	Sulphate, nitrate, ammonium, and hydrogen ions Elemental carbon Large variety of organic compounds Metals: compounds of Pb, Cd, V, Ni, Cu, Zn, Mn, Fe, etc. Particle-bound water	Suspended soil or street dust Fly ash from uncontrolled combustion of coal, oil, and wood Nitrates/chlorides/sulphates from HNO_3/HCl/SO_2 reactions with coarse particles Oxides of crustal elements (Si, Al, Ti, Fe) $CaCO_3$, $CaSO_4$, NaCl, sea salt Pollen, mould, fungal spores Plant and animal fragments Tire, brake pad, and road wear debris
Solubility	Probably less soluble than accumulation mode	Largely soluble, hygroscopic, and deliquescent	Largely insoluble and non-hygroscopic
Sources	Combustion Atmospheric transformation of SO_2 and some organic compounds High-temperature processes	Combustion of coal, oil, gasoline, diesel fuel, wood Atmospheric transformation products of NO_x, SO_2, and organic compounds, including biogenic organic species (e.g. terpenes) High-temperature processes, smelters, steel mills, etc.	Resuspension of industrial dust and soil tracked onto roads and streets Suspension from disturbed soil (e.g. farming, mining, unpaved roads) Construction and demolition Uncontrolled coal and oil combustion Ocean spray Biological sources
Atmospheric Half-Life	Minutes to hours	Days to weeks	Minutes to hours
Removal Processes	Grows into accumulation mode Diffuses into raindrops	Forms cloud droplets and rains out Dry deposition	Dry deposition by fallout Scavenging by falling raindrops
Travel Distance	<1 to 10s of km	100s to 1000s of km	<1 to 10s of km (small size tail, 100s to 1000s km in dust storms)

3.4 Carbonaceous Particulate Matter

The contribution of carbonaceous matter to the total particle composition deserves to be mentioned individually, due to its effects on health, visibility, and climate, and furthermore, according to Steven et al. (2004), because it composes about 37% of the global sub-micrometer particle emissions. The percentage composition of an atmospheric particle varies from location to location (e.g. urban, rural, continental, coastal, etc.) and so does the content of carbonaceous material, which traditionally has been divided into an organic carbon (OC), elemental carbon (EC), and a **carbonate carbon** fraction. The latter is almost exclusively derived from soil dust and of the least importance with regard to climatic effects (Seinfeld and Pankow, 2003). It is in the form of K_2CO_3, Na_2CO_3, $MgCO_3$, and $CaCO_3$.

Elemental (graphitic) **carbon** is defined as soot, black carbon or light-absorbing carbon (EPA, 2004). It strongly absorbs both visible and near-infrared light and is viewed as entirely non-volatile but only existing in the particle phase. Generally, EC is considered to exclusively derive from primary emissions, which makes it a useful tracer for the primary component of atmospheric particles (Seinfeld and Pankow, 2003). The incomplete combustion of coal, oil, gasoline, and diesel fuel produces fine crystalline particles of carbon which are called **soot** (see figure 14). About one half of the carbon emissions from heavy-duty diesel vehicles are elemental carbon, clearly visible as black smoke (Baird and Cann, 2005). However, a clear definition does not exist and EC may not be the best suited name, as it does not consist entirely of graphite (see Chow et al., 2001 for more definitions).

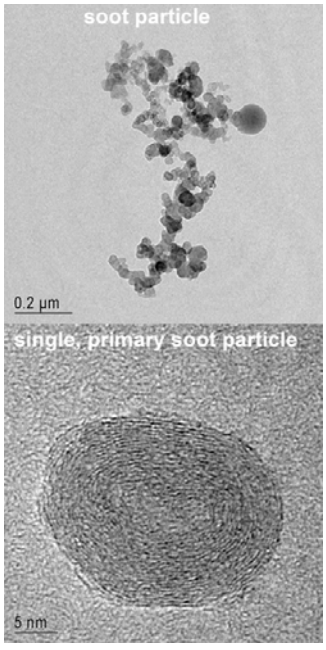

Figure 14 – Transmission Electron Microscopy (TEM) image of soot [source: EMPA]

The **organic carbon** fraction is defined as the semi-volatile or non-visible light absorbing carbon (EPA, 2004) and is an aggregate mix of countless individual compounds with a large range of chemical and thermodynamic properties (Seinfeld and Pankow, 2003). All three types of carbonaceous material are summarised as **total carbon** (TC) content of the atmospheric PM.

3.5 Effects of Atmospheric Particulate Matter

The role of atmospheric particulates in the London smog (also called **classic smog**) of winter 1952 jumpstarted the public's awareness of their impact on environment and human health, and began to draw worldwide attention to the effects of smoke and fog (smog). The particles catalyse the oxidation of SO_2 to SO_3 and provide nuclei for water to condense on forming fog (both ways ultimately leading to acid rain – see section 3.5.1.1) (Whittaker et al., 2004). Atmospheric particles are ubiquitous and according to their characteristics consequently interact and/or interfere with several natural processes affecting humans and the environment to a larger or lesser degree.

3.5.1 Environmental Effects

3.5.1.1 Effects on Vegetation

It is beyond the scope of this work to exhaustively discuss the diverse effects of airborne particles on vegetation. Thus, a very basic introduction mentioning only the most important direct effects and one indirect effect shall suffice.
Any particles deposited on plant parts that are above the ground may exert physical or chemical effects (EPA, 2004). The plants, which are key members of ecosystems, then often respond to the induced stress by the elimination of the more sensitive population and an increase in abundance of the species that tolerate the stress (Woodwell, 1970; Guderian, 1985). Particles become available to the vegetation via the three deposition pathways mentioned in section 3.3. Measurable direct responses of the vegetation to particulate matter, both coarse and fine, include **reduction in photosynthesis**, **changes in soil salinity**, and **foliar effects** that result from sulphate, nitrate, acidic, and heavy metal deposition.
"Inert" particles mainly cause physical effects, while the effects of toxic particles are both chemical and physical. It is usually the chemical composition of the particles that acts as the key phytotoxic (poisonous to plants) factor leading to plant injury.

The settling of **coarse particles** on above-ground plant organs may coat them with a layer of dust that can cause changes in the amount of received radiation, rise leaf temperature and block the stomata (EPA, 2004).

The major effect of fine particles on vegetation is dominated by occult and wet deposition of dissolved ions containing hydrogen, sulphates and nitrates. This process is called **acid rain** which severity is dominated by the formation of sulphuric acid (H_2SO_4) in the atmosphere according to several processes:

1. Gas phase reaction starting with SO_2 and hydroxyl radicals (HO•)

   $HO\bullet + SO_2 + M \rightarrow HOSO_2\bullet + M^*$

   (M: is just any molecule for energy and momentum conservation)

   $HOSO_2\bullet + O_2 \rightarrow HOO\bullet + SO_3$

   $SO_3 + H_2O \rightarrow H_2SO_4(g)$

   $H_2SO_4 + \text{many } H_2O \rightarrow H_2SO_4(aq)$ (Baird and Cann, 2005)

2. Oxidation within droplets

   If there is significant cloud, fog or mist content in the air, the somewhat water soluble SO_2 will be oxidised to sulphuric acid in the water phase:

   $SO_2(g) + H_2O(aq) \rightarrow H_2SO_3(aq)$ (sulphurous acid)

   plus SO_2 is oxidised to SO_4^{2-} by trace amounts of O_3 and H_2O_2 present in the droplet (see figure 15).

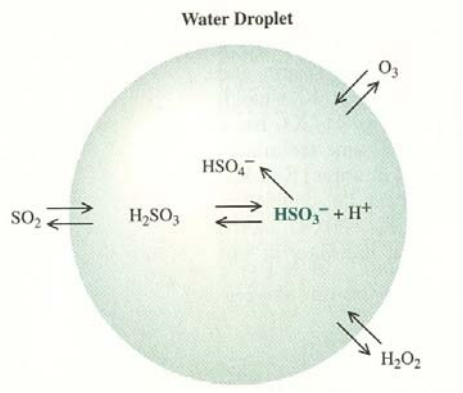

Figure 15 – Sulphuric acid formation within droplets
[source: Baird and Cann, 2005]

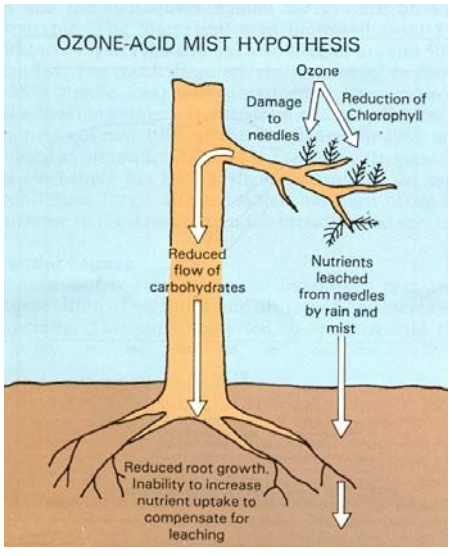

Figure 16 – Ozone-acid mist hypothesis
[source: Roberts, 1987]

The acidity of particles is due almost entirely to the presence of H_2SO_4 or NH_4HSO_4. Therefore, the acidity of the atmospheric particles depends on both the amount of SO_2 that is oxidised to SO_3 forming H_2SO_4 as well as the amount of ammonia available to react with the sulphuric acid (EPA, 2004).

Fine particles containing sulphates have a strong acidification potential and can exert harmful effect on forests when included in mists (see figure 16). The ozone-acid mist hypothesis proposes the damaging effect of ozone on cell membranes and thus increased leaching of nutrients from needles by acid rain and mist. The leached nutrients can not be recycled by the tree roots as ozone reduced the flow of carbohydrates from the shoot resulting in impaired root growth (Roberts, 1987).

Vegetational surfaces, especially the foliage, act as major reaction and filtration surfaces to the atmosphere and accumulate particles that have been deposited via wet and dry processes (Tong, 1991; Youngs et al., 1993). The leaf-surfaces may then take up the constituents of the particles. The foliar uptake of **heavy metals**, for example, could result in metabolic effects in plant tissues above ground.

One example of indirect effects of particles on vegetation is the **brown haze** over India (figure 17). Between October and May, a 3-kilometer-thick brown haze resides over much of South Asia and the northern Indian Ocean. The haze is caused by urban pollution such as vehicle emissions, industrial soot, the burning of wood and crops and forest fires.

This dirty cloud affects the region by reflecting sunlight back into space, thus having a cooling effect, but at the same time it also lessens the monsoon rainfalls by reducing evaporation. Auffhammer et al. (2006) combined historical rice data and a climate model and showed that rice harvests would have been up to 11% higher without the brown haze.

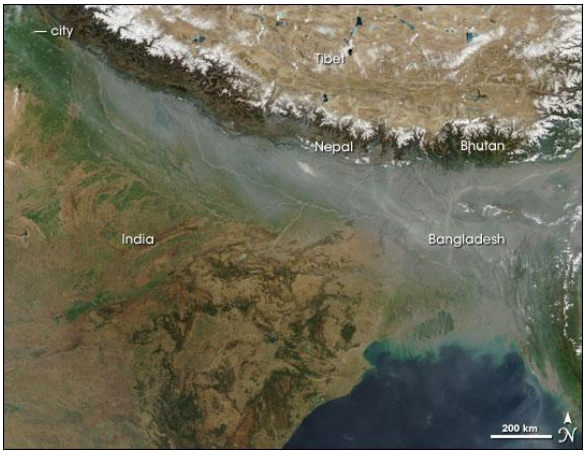

Figure 17 – Brown haze over India
[source: Ravilious, 2006]

Rice is particularly sensitive to brown haze because it needs a lot of water to grow successfully. Nevertheless, a variety of other crops may be affected as well.

3.5.1.2 Effects on Visibility

As one can imagine, the brown haze over India does not only affect crop yields but also visibility. Reason for this reduction in visibility is primarily the scattering and absorption of light by the fine suspended particles in the atmosphere. Traditionally, visibility has been defined by meteorologists as the visual range defined as the furthest distance at which a black object can be distinguished against the horizon sky (EPA, 1979). As a consequence, visibility can only be quantified for a sight path and depends on the illumination of the atmosphere and the direction of view. When determining it as a quantity, the concentration of particles in the atmosphere plays a key role. Particles and gases in the atmosphere attenuate light on its way from an object to the observer. The fractional attenuation of light per unit distance is termed light extinction coefficient (b_{ext}) and expressed in unit 1/distance.

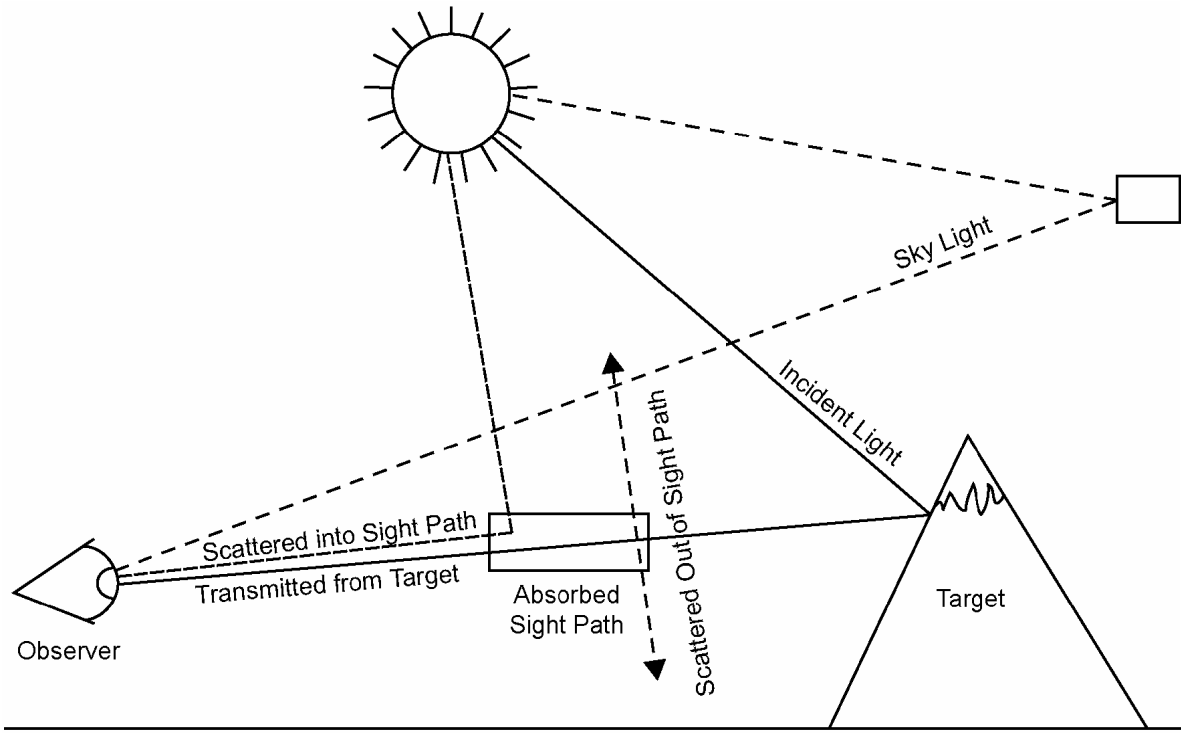

Figure 18 – Reflected light from a target to the observer. A portion of the light is scattered out of the sight path and light from the sun is scattered into the sight path by the intervening atmosphere. Some particles and gases also absorb some of the light from the target. Light scattered into the sight path increases and light transmitted from the target decreases with distance from the target. The visual range is defined as being the closest distance between the target and the observer at which the transmitted light can no longer be distinguished from the light scattered into the sight path. [Source: Watson and Chow, 1994].

It is composed of the sum of light scattering and light absorbing coefficients of particles and gases (EPA, 2004):

$$b_{ext} = b_{ap} + b_{ag} + b_{sg} + b_{sp}$$ with p, g (particles, gases)
s, a (scattering, absorption)

The light scattering (**Rayleigh scattering** – caused by molecular components of the air, which diameter is much smaller than the wavelength of the incident light) and absorption (mostly NO_2 – absorbs blue → looks yellow, brownish) of gases only dominate the light extinction under pristine atmospheric conditions. Otherwise, it is the particles that have the greatest effect on visibility. The corresponding extinction coefficient can be determined when the particle size, refractive index, and shape of the particles are known (EPA, 2004). The whole situation is illustrated in a simple way in figure 18. Light absorption by particles is predominantly caused by soot (black carbon) and to a lesser extent by minerals in crustal particles. **Mie scattering** is caused by particles with diameters larger than the wavelength of the light (Quaschning, 1999). The single most important factor determining the amount of light scattered by a particle is its size and the maximum single-particle scattering efficiency (i.e. scattering per cross-sectional area of a particle) is achieved by particles with diameters of about the wavelength of visible light, centred at around 0.53μm (EPA, 2004). Therefore, the effects of relative humidity on particle size will significantly affect the amount of particle light scattering.

3.5.1.3 Effects on Materials

The presence of particulate matter (especially particulate sulphate) may have an impact on the corrosion of metals. However, results have been found for and against their contribution and a final conclusion has not been drawn yet (EPA, 2004). Nevertheless, the effects of acid rain on materials, such as stone and concrete are well known. The stones most susceptible to deterioration are calcareous stones, such as limestone, marble and carbonated cement. The damage occurs when salts are formed in the stone which are subsequently washed away and will leave the surface of the stone more susceptible to the effects of pollution. The sulphates in acid rain will trigger the formation of gypsum ($CaSO_4$), a grey-black crusty material (EPA, 2004). The chemical reaction follows: $CaCO_3 + H_2SO_4 \rightarrow CaSO_4 + CO_2 + H_2O$

3.5.1.4 Effects on Global Warming

The issue of global warming has materialised into what can *safely* be considered 'the biggest threat to human kind and nature since the last ice-age or the Great Flood', depending on the individual's world view.

Its effects infiltrate and influence all ecosystems due to their either direct or indirect dependence on temperature. Contrary to the public believe, that noticeable effects will only occur many decades into the future, Sir John Houghton [former co-chair of the UN Intergovernmental Panel on Climate Change (IPCC)] in his interview to The Guardian (2003), calls global warming a "weapon of mass destruction", that already kills more people than terrorism.

Global warming can be best described as the trapping (absorption) of outgoing terrestrial infrared radiation by greenhouse gasses (GHG), such as water vapour, CO_2 and other trace gases such as CH_4, N_2O, O_3, CFCs, HCFCs, and HFCs. Human activities have added especially CO_2 to this global GHG-budget and introduced the so-called anthropogenic 'greenhouse effect' (Brasseur at al., 1999).

As extensive research has shown, it is not only the GHGs that affect the global radiation budget, but also atmospheric particulate matter (IPCC, 2007). **Particles** in the atmosphere **directly affect climate**, as they, on the one hand, absorb and scatter a significant amount of the incoming solar radiation back into space and thus have a cooling effect, and, on the other hand, also absorb terrestrial infrared radiation and cause a significant heating in dense aerosol layers (Brasseur et al., 1999).

Figure 19 is the summary of the effects of several agents on the global climate expressed in radiative forcing. **Radiative forcing** is defined as the response in the net radiative energy flux at the tropopause to changes in the concentration of a given global warming agent (Brasseur et al., 1999). With the release of the latest IPCC report (2007), the picture of the climatic impact of aerosols has changed. Increased scientific understanding allows for a better quantification of the total direct radiative forcing of all aerosol types combined together [$(-0.5\pm0.4)W/m^2$]. Less certain is the direct radiative forcing of the individual species. Those have been estimated from models to be $(-0.4\pm0.2)W/m^2$ for sulphate, $(-0.05\pm0.05)W/m^2$ for fossil fuel OC, $(+0.2\pm0.15)W/m^2$ for fossil fuel EC, $(+0.03\pm0.12)W/m^2$ for biomass burning, $(-0.1\pm0.1)W/m^2$ for nitrate and $(-0.1\pm0.2)W/m^2$ for mineral dust. It has to be noted, however, that the impact of particles (for the larger part) is spatially different from that of GHGs. The anthropogenic aerosol forcing occurs mostly in the mid-latitudes of the

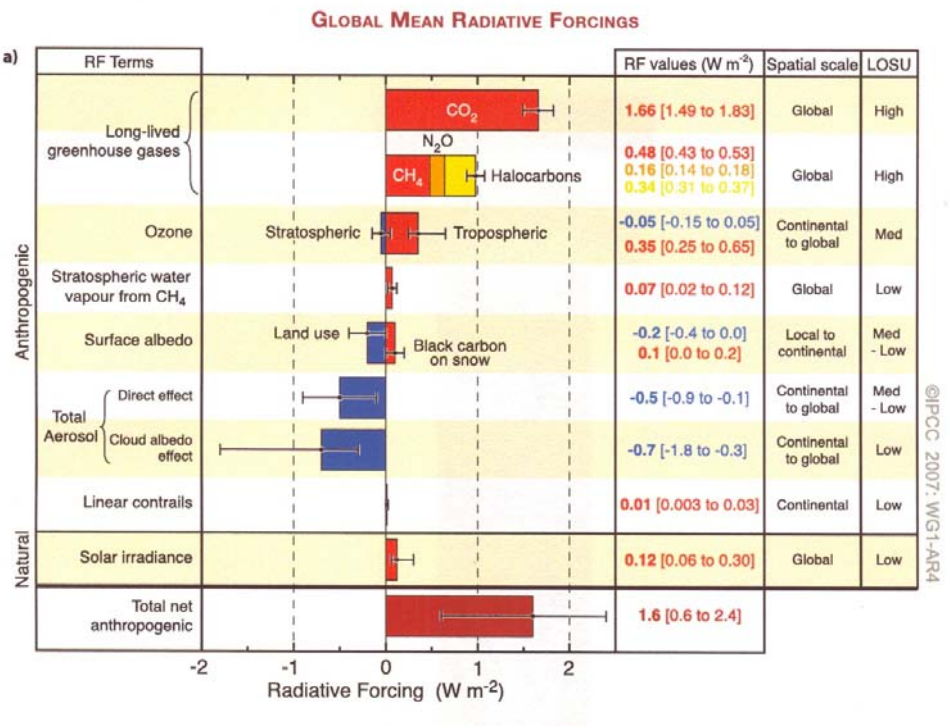

Figure 19 – Global annual mean radiative forcings (W/m²) due to several agents for a period from pre-industrial (1750) to 2005
(LOSU: Level of Scientific Understanding) [source: IPCC, 2007]

Northern Hemisphere, where most of the sources are located, while GHGs (except O_3) are generally well mixed in the troposphere and thus their radiative effects are strongest between -30° and +30° latitude.

As a result, the combined effects may not cancel each other out but rather change global temperature gradients (Brasseur et al., 1999). The radiative forcing of aerosols does not only depend on their spatial distributions, but also on their size, shape, and chemical composition (IPCC, 2001). Particles are always mixtures of a multitude of components, some of which such as sulphates and organic carbon compounds have a cooling effect (negative radiative forcing), others like soot a warming effect (positive radiative forcing). As a consequence of the latest findings (figure 19), the cooling effect of PM dominates and thus a large scale reduction of the emission of PM may contribute to global warming as a negative side effect. Another direct effect of particles arises from the decrease of the **albedo** (fraction of light from the sun, that is reflected off the surface of the earth or clouds; range from 0 to 1 – Harrison, 1999) of snow and ice surfaces when soot is deposited upon them (Brasseur et al., 1999).

Atmospheric particles also affect the climate in **indirect ways**. Sulphate particles, due to their hygroscopic nature, act as **cloud condensation nuclei** (**CCN**) and thus influence formation and radiative properties of clouds. They act as ‘seeds’ for water

molecules to condense on, coagulate and grow into a water droplet, that when it has reached a size of 100μm and larger, will fall out as rain. In doing so, they alter the albedo of clouds by changing the nucleated droplet number concentration. An increase in droplet number concentration, for a fixed amount of liquid water content, follows a decrease in mean droplet size and thus an increase in the reflectivity of the clouds. Moreover, the altitude and type of the clouds play a significant role in their climatic impact. It is believed that high-altitude cirrus clouds contribute to warming, while low-level stratus clouds have a cooling effect (Brasseur et al., 1999). Research from Zhao et al. (2006) has found that smoke particles prevent raindrops from forming. The team detected a decrease in rainfall of 0.4% per year between 1961 and 2000 over eastern central China which strongly correlated to an increase in aerosol particles. The reason why particles affect rainfall in this way is that after they have acted as CCNs the formed small cloud droplets tend to repel each other, discouraging the formation of the heavy droplets needed for rain. Menon et al. (2002) have earlier published their results on the effects of black carbon on large scale atmospheric circulation and the hydrological cycle over China and India. With the aid of numerical simulations they isolated a clear tendency that increased amounts of soot do in fact correlate with the flooding scenarios occurring in southern China and the increasing drought over northern China which has persisted for several years at the time the results were published. The increase of rising air, heated by the light absorption of soot in the atmosphere, is balanced by an increase of sinking air (subsidence) and drying in northern China. Sinking air does not form clouds or rain and is thus creating dry conditions.

3.5.2 Effects on Human Health

While all the effects of particles mentioned so far surely indirectly affect humans, there are also of course effects that impact us directly leading to a variety of pathologic patterns. In toxicological assessments it is of utter importance to determine the route of exposure for any given toxicant. In the case of atmospheric particles the exposure route is rather unambiguous and straight forward: INHALATION. This makes the lung the priority organ of exposure and the centre of focus on PM effects on human health.

3.5.2.1 The Human Lung

Naturally our lungs are well endowed with several protective mechanisms preventing them from being invaded by natural irritants. It is particularly the fine and ultra-fine PM that harbour the capacity to outsmart the natural defence functions within our respiratory system. The deadliest particles are the finest ones and it is predominantly us who are responsible for their emissions (Merefield, 2002).
Figure 20 shows the entire human respiratory system and indicates some of its defence mechanisms. Any particles larger than 10μm in diameter are deposited in the nose and throat, filtered out by the mucus. Particles between 4 and 10μm are trapped by the mucus coating the airways, which is constantly driven towards the mouth by billions of hairs. Once it arrives at the mouth it is swallowed. Particles smaller than 4μm, however, can bypass the natural removal system and reach the naked gas-exchange surfaces of the tiny air sacs called **alveoli** (Merefield, 2002).
Due to our high metabolic requirements we need a tremendous amount of air. At rest, around 7.5 litres per minute of air are moved in and out of the lungs. At the extreme end, lungs can take as much as 80 litres of air every minute during strenuous exercise (Lee and Manning, 1995).
Giving these numbers there is a huge opportunity for airborne substances to accumulate and gradually damage the lung tissue.

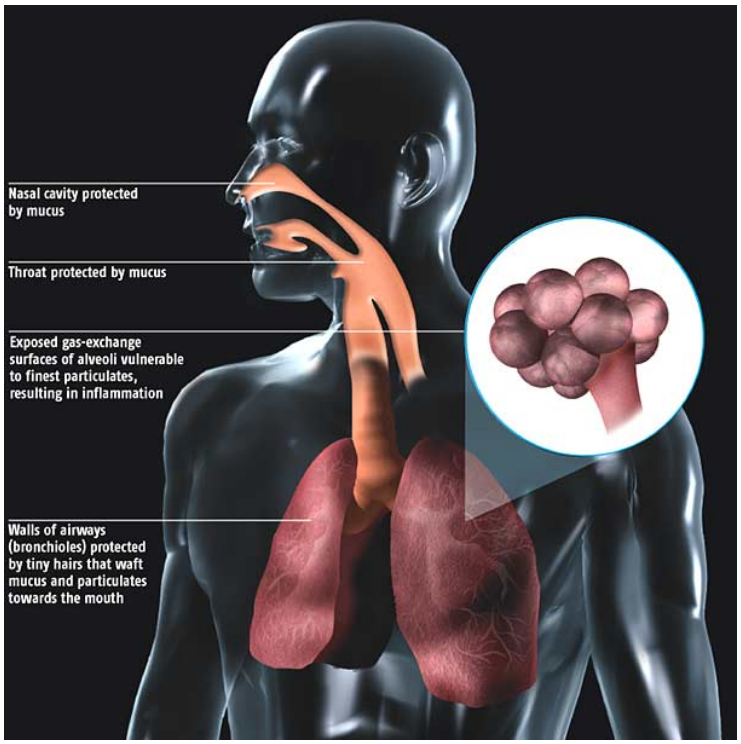

Figure 20 – Overview of the total respiratory system [source: Merefield, 2002]

These airborne substances do not only directly affect the lung but also leave it more vulnerable to infection. This susceptibility can already be caused by particles that only mildly irritate the lungs (Lee and Manning, 1995).

3.5.2.2 Toxicological Effects and Epidemiology

The recent toxicological research on particulate matter has mainly focused on several interrelated issues, such as (1) the types of pathophysiological effects exerted by ambient PM or constituent substances and their underlying mechanisms, (2) which characteristics of the particulate matter (i.e. size, chemical composition, etc.) cause or contribute to health effects, (3) which susceptible subgroups are at increased risk and what factors contribute to increasing susceptibility, (4) what types of interactive effects of particles and gaseous co-pollutants have been demonstrated, and (5) are the toxicological findings on PM-related mutagenic/genotoxic effects supporting the plausibility of the airborne PM – lung cancer relationship observed epidemiologically in the population (EPA, 2004).

It is very difficult to determine and assign possible mechanisms of damage, as PM is a mixture with diverse physicochemical properties, ranging from physical characteristics of the particles to chemical components in or on the surface of the particles. Any of those properties could change at any given time in the atmosphere, which makes it rather challenging to duplicate real properties in controlled laboratory experiments (EPA, 2004). Much work has been done in recent years to address these issues and the results confirm that fine particulate matter and associated combustion-related air pollutants are largely responsible for the observed health effects (Pope, 2004).

3.5.2.2.1 Cardiovascular Effects

An ever increasing amount of epidemiological studies find relationships between ambient PM and increases in cardiac-related deaths and/or morbidity indicators. Furthermore, those PM-related cardiac effects may be as great as or even greater than those attributed to respiratory causes (see chapter 8 of EPA, 2004 for an extensive list). The cardiovascular mortality and morbidity effects were observed for both acute and chronic PM exposure and appear to be induced via direct particle uptake into the blood and/or mediation via the nervous system. An illustration of the hypothetic mechanisms involved in the cardiovascular responses to PM exposure is shown in figure 21. The effects seem to be most detrimental for individuals already predisposed to disease states such as ischemic heart disease (characterised by reduced blood flow to the heart), cardiac arrhythmias and COPD (chronic obstructive

pulmonary disease). Figure 21 shows that the heart receives both parasympathetic and sympathetic inputs via the central nervous system (CNS), which serve to decrease or increase heart rate respectively. Vasoconstriction, possibly caused by the release of endothelin (induced by PM), could cause increased blood pressure. Consequently the parasympathetic neural input may then be decreased to the heart in order to slow down the heart rate and to decrease the cardiac output. This in turn may cause sympathetic input resulting in increased heart rate and cardiac output. This arrythmogenesis and altered cardiac output in either direction can be life-threatening to susceptible individuals.

Another way in which PM could induce cardiovascular effects is by affecting endothelial (*endothelium: the cells lining the inside of all blood vessels*) function as proposed by Seaton et al. (1995). Exposure to particulate matter could cause blood coagulation via injury of the endothelium resulting in platelet activation. A series of possible effects can be triggered by that process, e.g., increased fibrinogen and fibrin formation leading to increased formation of clots (EPA, 2004). Moreover, PM exposure could cause vascular (from vessel) inflammation promoting the release of C-reactive proteins and cytokines, which cause further inflammatory responses which can lead to arteriosclerosis on a chronic basis.

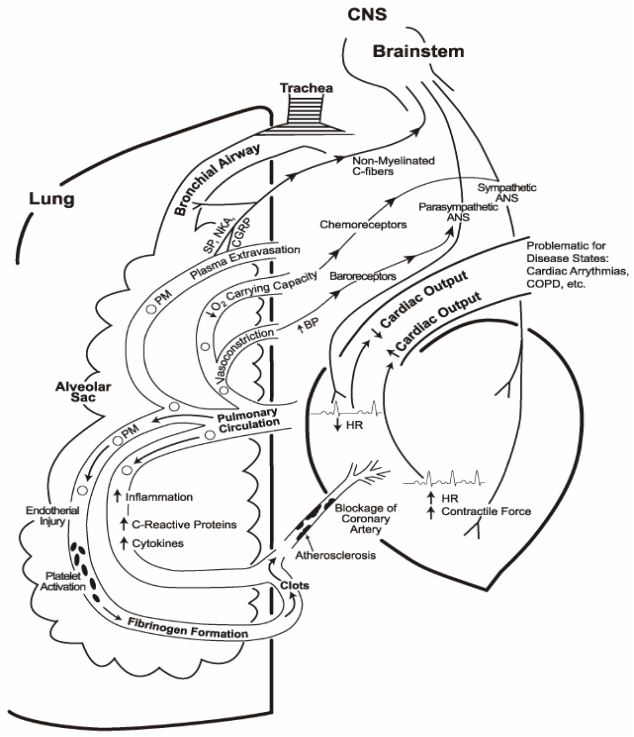

Figure 21 – Illustration of hypothetic pathways/mechanisms potentially underlying the cardiovascular effects of PM
[source: EPA, 2004]

Nevertheless, these are all hypotheses lacking extensive toxicological backup. Healthy human (voluntary) tests have been scarce and yielded only limited evidence for the PM – cardiovascular effects relationships. However, the blood clotting hypothesis has been supported by both epidemiological studies and animal experiments (Maynard, 2004). Pope et al. (2004) linked fine PM air pollution to the

increased risk of cardiovascular disease mortality (CDM) via pulmonary and systemic inflammation, accelerated atherosclerosis and altered cardiac autonomic function. Smoking is still a larger risk for CDM but could be synergistic with fine PM exposure.

3.5.2.2.2 Respiratory Effects

How particles affect the lung is strongly correlated with where inside the lung they are deposited and how chemically reactive they are. The subsequent damage can occur within minutes, slowly over a period of months and years, or very slowly over decades, depending on how the damage takes place. So-called **obstructive lung diseases** are characterised by a blockage that prevents air reaching the gas-exchange regions of the lung. Asthma and chronic bronchitis are two examples of this condition. In **restrictive lung disease** the location of harmful activity lies mainly within the gas-exchange tissue of the lung, as in many diseases that result from heavy exposure to dust and particles. Toxicological studies investigating the respiratory effects of inhaled PM are again in short supply.
However, a large number of epidemiological studies, carried out in recent years, substantiate the positive correlations between ambient PM and (a) increased respiratory-related hospital admissions, emergency department and other medical visits, (b) increased incidence of asthma and other respiratory symptoms, and (c) decrements in pulmonary functions. New findings indicate that not only the fine particle fraction causes exacerbations of various respiratory conditions (e.g. asthma), but also the coarse thoracic particles ($PM_{10-2.5}$). Further findings seem to indicate that the increased occurrences of chronic bronchitis are associated with (particularly chronic) PM exposure (EPA, 2004 – for an exhaustive list).

3.5.2.2.3 Mutagenic/Genotoxic Effects

The mutagenicity of particulate matter is a function of its chemical composition and size (EPA, 2004). Pope et al. (2002) carried out an analysis of the longer-term database of the American Cancer Society and found that long-term exposure to combustion-related fine PM is an important environmental risk factor for lung cancer mortality. A large amount of work examining the emissions from coal combustion has demonstrated the mutagenicity of both the polar and the aromatic fraction of the ambient particulate matter. Populations with a high occurrence of lung cancer have been linked to exposure with the PAH component of coal smoke (EPA, 2004).

Dockery et al. (1993) established robust associations between air pollution and mortality and further verified in their six-city study a positive correlation of air pollution with death from lung cancer (and cardiopulmonary disease), particularly related to fine particles, including sulphates. These results are quite compelling as the team also accounted for potentially confounding explanatory variables such as smoking and other risk factors. A meta-analysis, carried out by Zhao et al. (2006), confirmed the association between lung cancer and indoor air pollution and found significant odds ratios for indoor exposure to coal dust.

3.5.2.2.4 Compositional Effects

All the above with regard to health effects of PM comprises merely a tiny fraction of a rather complicated issue originating from the complex nature of airborne particles. There still remains to be done a lot of research aiming towards gaining better insights into potential synergetic effects of particle size and composition alongside underlying mechanisms. The particle size appears to have a carrier capacity for associated chemicals. The fine and ultra-fine particles, for instance, with their potential of entering the blood-stream, carry along with them their constituents enabling them to cause all sorts of systemic effects. Of those constituents some of the polycyclic aromatic hydrocarbons (**PAH**) have been shown to have carcinogenic capacity (especially benzo[a]pyrene) (Baird and Cann, 2005). **Iron** and **nickel** have been identified as being potentially important in mediating the toxicological properties of particles (Gilmour et al., 1996). **Cadmium** and **arsenic** are both carcinogens and have been found to induce lung cancer in humans via inhalation (WHO, 2000). Furthermore, particle-bound water contains soluble compounds which are partitioned between the gas phase and the aerosol liquid-water phase. Since highly soluble compounds usually deposit in the upper airways, there is a chance of particles providing a vector for deposition of these compounds in the lower airways (EPA, 2004). Closing this section on PM health effects it shall suffice to mention that an in-depth treatment lies beyond the scope of this work and the interested reader may be referred to the exhaustive EPA review (2004) quoted so many times above.

4.0 Materials and Methods

4.1 Sampling

4.1.1 The Sampling Site

The sampling site was located at the roof of a four-story building at the Taiyuan University of Science and Technology. The height above ground where the air samplers were positioned may be approximately 8 – 9m (see figure 22a).
The university is situated rather central in the city of Taiyuan (figure 22c) with a heavy traffic road nearby.
The sampling site was characterised by a multitude of local particulate matter sources, making it perhaps not the most suitable location for obtaining representative data.
The roof itself was covered with dust that was re-suspended in the air during the frequent episodes of stronger winds. Merely about 300 to 400m away was a huge construction site (figure 22b) of a new university building.
Moreover, the sampling location was in the middle of several domestic dwellings and frequent emissions were noted, ranging from black-smoke chimney emissions to white-smoke backyard incinerations. The actual building on which roof the samples were collected is the smallest one of all the surrounding buildings and thus lying in a “hole” which most likely causes turbulent wind conditions and may thus alter the condition and composition of the air that reaches the samplers. The air samples have been collected over a period of 12 consecutive days from Thursday, the 16th of March to Tuesday, the 28th of March 2006 (see also table 2).

Figure 22 – Pictures of the sampling location (a), a construction site nearby (b), and location (green point) of the site in Taiyuan [sources: a) and b) mine; c) Google Earth, 2007]

4.1.2 Air Samplers and Filters

The air samplers used were medium flow samplers [Wuhan Tianhong Intelligent Instrument Plant – TH 150A] provided by the Environmental Monitoring Department of Taiyuan City. An air sampling unit consists of a pump that was programmed to suck in air for a certain amount of time each hour at a flow rate of 100l/min, and an atmospheric particle collector. The flow rate was quite constant and only occasionally changed by ±2l/min. A PM_{10} particle collector was used and mounted onto the pumping unit according to figure 23. Figure 23 also shows the makeup of the PM_{10} collector. Each part had to be washed with water and afterwards cleaned with alcohol (<75Vol.%). Alcohol on all the parts that were in direct contact with the filter was left to evaporate and not cleaned off with a tissue due to the risk of contamination.

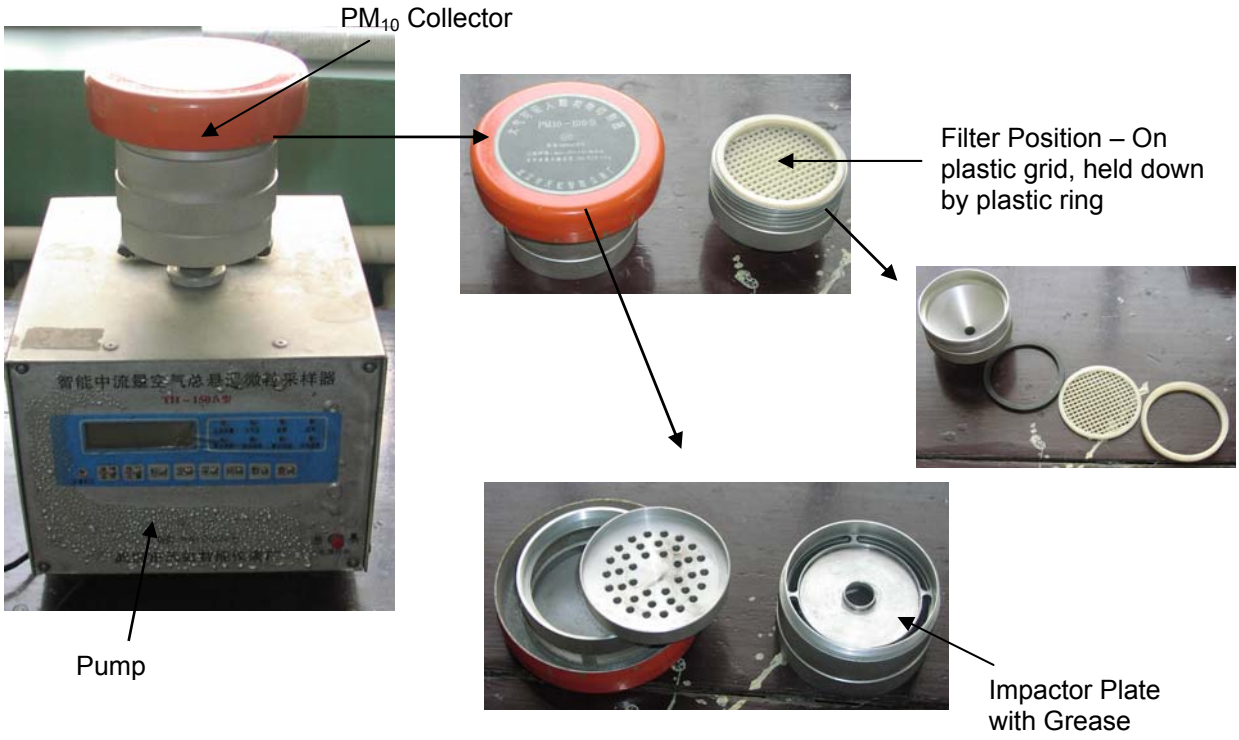

Figure 23 – Basic makeup of PM_{10} air sampling unit [pictures mine]

The air and included particles are sucked into the collector right underneath the orange top lid. It then passes through a metal plate with an arrangement of small holes preceding the impactor plate. The impactor plate is covered with a small layer of grease that has to be changed every other day when there is a visible accumulation of particles. If the grease is not changed, there is a chance of a particle bounce-off resulting in larger particles being collected on the filter. The flow rate of 100l/min is the crucial parameter that controls the particle size fraction collected. At

this flow, all particles which are larger and thus heavier, will not be able to avoid the grease on the impactor plate and collide with it due to inertia. All smaller particles will follow the air stream around the impactor plate and are collected on the filter that is situated underneath on a plastic grid, firmly held in place by a plastic ring. The plastic ring had to be applied and removed with care due to its quite sharp edges, in order not to break off pieces from the edge of the filter. Four PM_{10} samplers were used and set up in the arrangement shown in figure 24. Two were actively operating holding two different types of filters, while the other two served as field blanks. The maximum time span covered was 22 hours and not 24, as the pumps needed 2-hour breaks ensuring them to be still operational the next day.

Figure 24 – Arrangement of samplers at the sampling location [picture mine]

Table 2 – Sampling information (each new sampling started between 5 and 6pm for 22 hours)

Name of Sample and Blank				Date When New Sampling Started	Sampling: Minutes Each Hour		Total Sampling Time Over 22 Hours [min]	
Quartz		**Teflon**						
Sample	Blank	Sample	Blank		**Quartz**	**Teflon**	**Quartz**	**Teflon**
Q1	Q2	T51	T52	16.03.06	30	30	660	660
Q3	Q4	T53	T54	17.03.06	20;30*	20;30*	460	460
Q5	Q6	T55	T56	18.03.06	20	20	440	440
Q7	Q8	T57	T58	19.03.06	15	15	330	330
Q9	Q10	T59	T60	20.03.06	10	10	220	220
Q11	Q12	T61	T62	21.03.06	10	10	220	220
Q13	Q14	T63	T64	22.03.06	10	10	220	220
Q15	Q16	T65	T66	23.03.06	10	15	220	330
Q17	Q18	T67	T68	24.03.06	10	20	220	440
Q19	Q20	T69	T70	25.03.06	10	15	220	330
Q21	Q22	T71	T72	26.03.06	10	15	220	330
Q23	Q24	T73	T74	27.03.06	10	15	220	330

*) Power cut – 1 hour with 30min, 14 hours with 20min each, and 5 hours with 30min

The PM_{10} collector units were not cleaned again with water and alcohol but rather via pumping air through them for four minutes without filters prior to the beginning of each new sampling period. The pumps were working well at all times when checked upon. At the start-up phase the pumps quickly reached a flow rate of 80l/min and then over the duration of approximately 30s reach the set value of 100l/min.
Two different types of **filters** were used for PM sampling, **Tissuequartz** and **Teflon** filters. The reason for utilising two types of filters lies with their individual advantages

with regard to the particle components to be analysed and the analytical methods to be applied. The Teflon filters are Fluoropore® (PTFE) hydrophobic membrane filters with a diameter of 90mm, a pore size of 3μm and a collection efficiency of 98% for particles larger than 0.035μm, while the quartz filters are Pallflex® Tissuequartz (Pall Life Sciences – type: 2500QAT-UP) filters, also having a diameter of 90mm, made of pure quartz with no added binder, have a collection efficiency of 99.9% for typical aerosols and a maximum operating temperature (air) of 1093°C. The high operating temperature of the quartz filters is very important for their applicability in the thermal-optical carbon analysis (described later), where temperatures up to 850°C are reached. Both filter types were pre-treated prior to being packed and transported to the sampling site in Taiyuan. The Teflon filters were dried in a desiccator (silica gel) for 24 hours and afterwards weighed on a Sartorius® analytical balance (readability 0.1mg). They were then put into plastic zipper bags (see figure 25) and transported in a cardboard box. A much larger amount of preparation is necessary for the quartz filters. They must be protected from carbonaceous contamination and thus cleaned and sealed as good as possible. For this purpose aluminium foil was pre-heated in a Nabertherm® [T_{max}=1100°C; P=3kW] oven for 3 hours at 450°C. The quartz filters were stacked up and put in the same type of oven for 3 hours at 900°C [according to Chow et al., 2005]. This should remove all the residual carbonaceous contamination. According to Karl Espen Yttri (pers. comm.), many companies treat their quartz filters with a fungicide which would introduce unwanted carbons. This pre-firing process, however, increases the brittleness of the filters.

Figure 25 – Packaging of Teflon filters (left) and quartz filters (right – aluminium foil) [pictures mine]

The quartz filters were weighed and packed into the aluminium foil (see figure 25) and plastic zipper bags. At all times the filters were handled with metal tweezers,

which were retrofitted with plastic tips, and rubber gloves (no powder gloves). After a filter was used for air sampling in Taiyuan, it was transferred into a Tupperware® box and stored in a freezer provided by some nice local people. They had to share their space in the freezer, however, with some huge bones from a lamb or cow. The loading on the first day of sampling was too high (30min per hour), as can be seen in figure 26, and had to be reduced on the following days.

Figure 26 – Quartz filters before (left) and after sampling (right – Q1) [pictures mine]

After transport from China to Norway the filters were again stored in a freezer room and weighed only prior to analysis.

4.2 Microwave Decomposition

Sample preparation is an important step in the analytical sequence and since a homogeneous solution is required to conduct inductively coupled plasma mass spectrometry (ICP-MS) and atomic emission spectrometry (ICP-AES), a method of dissolving the solid matrix (i.e. filter and particles) has to be applied. The most efficient answer to what was historically done using acid solutions and a hot plate or convection oven, is the closed vessel microwave acid decomposition system (Kingston and Walter, 1998).

4.2.1 The Closed Vessel Microwave Decomposition System

4.2.1.1 Absorption of Microwave Energy

Microwave energy is absorbed and transformed into heat in two primary mechanisms: dielectric polarisation and ionic conduction. Both mechanisms originate from the alignment of charged or partially charged atoms or molecules with an applied electric field. The ability of molecules to convert microwave energy into heat

is directly proportional to the loss tangent, $\tan\delta = \varepsilon''/\varepsilon'$, which defines the ability of a solvent to absorb microwave energy. The symbol ε'' is called the dielectric loss and defines the efficiency of the molecule in converting microwave energy into thermal heat, while ε' is the dielectric constant and a measure of the molecules' ability to be polarised in an electric field. The loss tangent is a function of microwave frequency and temperature. Since solvents such as water, mineral acids and some organic solvents possess dipole moments, they can interact with the applied electric field. Dielectric polarisation depends on the rapid alignment of polar molecules in solution and their random relaxation and reorientation. This motion results in friction converting the electromagnetic microwave energy into heat.
The free ions in solution (e.g. ionised acids) are attracted by the oppositely charged directions of the electromagnetic field, which oscillates and reverses approximately 5 billion times per second (f=2450Hz). The ionic conduction is less affected by microwave frequency (Kingston and Walter, 1998).

4.2.1.2 Advantages of the Closed Vessel System

The microwave assisted closed vessel acid digestion has several unique attributes that considerably improve the sample preparation process. The high temperature achieved inside the closed vessel result in a kinetic advantage that is not given at low temperatures. Elevated temperatures improve the oxidation potential of several acids (e.g. nitric acid) and in doing so make them more capable reagents. Moreover, the analytical blank is reduced in the closed system due to the fact that (1) the reaction atmosphere is closed and controlled, (2) acid amount is reduced to stoichiometric quantities of the necessary reactions, (3) the vessel is usually made of Teflon or quartz (best materials for trace element analysis), and the analyst is assisted by a viable instrumental interface (Kingston and Walter, 1998). Furthermore, no volatilisation of elements occurs and the reaction times are shortened. As a significant drawback the limited sample amount of less than 2g needs to be mentioned. This may exclude some matrices (e.g. polymers) from being digested in the closed system if not ICP-MS is used as the analytical instrument, as its low detection limit may be able to compensate for the restricted sample amount (Kingston and Walter, 1998).

4.2.1.3 Chemical Reaction Profile Inside the Closed Vessel

The conditions inside the closed vessel are monitored with aid of a pressure and temperature sensor. The resulting graph typically looks something like given in figure 27 and is important to be understood correctly in order to develop a digestion procedure. With the beginning of the experiment the acid and the vessel walls it is in contact with are being heated up by the microwave energy. At this stage, the acid is below its atmospheric boiling point, its vapour pressure is minimal, and no noticeable amount of vapour heats the vessel walls. Is the atmospheric boiling point exceeded by the temperature inside the vessel, then a large amount of gas phase acid is produced. The efficiency of microwave absorption of the gaseous acid is quite small and when it comes in contact with the cool vessel walls it condenses, releasing energy to them. Consequently, and depending on the heat capacity of the vessel wall, heat is released to the air inside the microwave cavity. At this stage of the digestion process, the liquid acid is heated and its vapours heat the walls of the vessel. What follows is the final stage of heating, which is called "**sustained dynamic non-equilibrium**". This equilibrium, which is balanced through the microwave energy absorbed by the acid and the energy released by the vessel, maintains reaction temperatures during digestion. Due to the heat loss from the vessel, its top can never reach the temperature attained by the reagents and sample. Test with PFA Teflon have shown temperature differences between the top of the vessel and the liquid phase of up to 100°C (Kingston and Walter, 1998). Due to the heat loss a normal thermodynamic equilibrium between gas and liquid cannot be attained. This bears a significant advantage for microwave digestion over, for instance, convection oven bombs, that is that the pressure inside the vessel will be about 5 times lower.

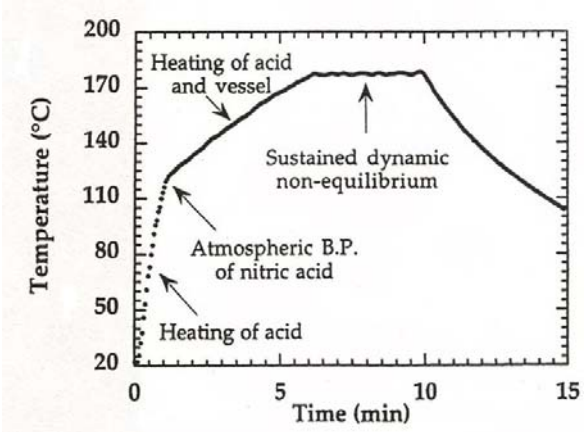

Figure 27 – Interpretation of microwave heating [source: Kingston and Walter, 1998]

4.2.2 The Instrumental Setup

The microwave oven (Milestone ETHOS 1600) is depicted in figure 28, including the computer system. The oven has been designed with a fume hood and a safety door, which will elastically (controlled by feathers) release pressure in case of any explosions inside.

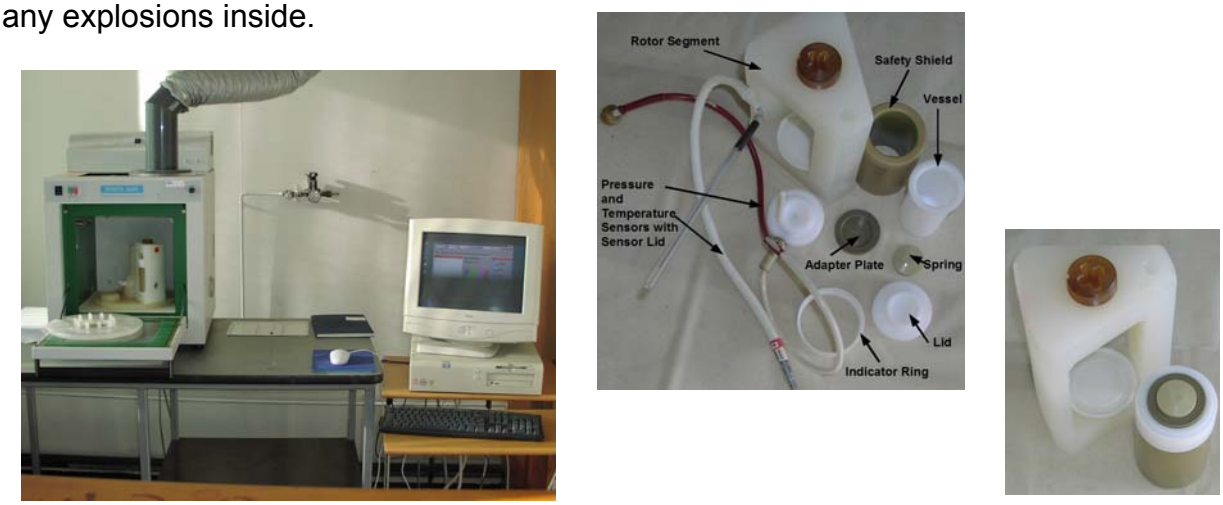

Figure 28 – Microwave oven and computer system (left), individual components of microwave bomb: rotor segment, safety shield, vessel, indicator ring, lid, adapter plate and spring (middle), fully assembled bomb (right) [pictures mine]

The rotor inside the oven has a maximum capacity of holding ten rotor segments, which fixate the microwave bombs (figure 28). However, due to space requirements of the temperature and pressure sensors, only 8 rotor segments with bombs can be used at any time. The individual parts are shown in figure 28 (middle). The correct assembly is crucial to ensure maximum safety and operating conditions. The safety shield acts as a radial protection of the vessel and the surroundings. The indicator ring has a small hole allowing gasses to ventilate when the bomb is opened. It also functions as an indicator of ventilation during microwave decomposition. When the pressure inside the bomb reaches a critical value, the spring on top of the adaptor plate will bend, pressure be released, and the indicator ring will be lifted up somewhat giving an observable indication of ventilation. Should this occur then some elements may have been lost in the process. The springs are always checked for cracks and shape. If they can be pushed through a “control gap”, they are not to be used. When the bomb is fully assembled and positioned in the rotor segment, it is held in place by tightening of a screw on top of the rotor segment. This is done first with a plastic screwdriver and afterwards with a torque wrench to ensure equal torque for all segments. The one bomb that is endowed with the temperature and pressure

sensors has a different lid and rotor segment allowing the connection of the sensors. It is important that the minimum amount of liquid inside the vessels (**8ml**) is not violated. This is necessary, as the temperature sensor would otherwise not be immersed in the liquid anymore, leading to irreproducible temperature profiles.

4.2.3 The Microwave Decomposition Method

The method applied to decompose the filter samples did not have to be developed from scratch and is a slightly modified version of an already existing method. However, Kingston and Walter (1998) offer a great deal of noteworthy help when attempting to develop a new method from step one.

In order to validate the method and for the purpose of parameter testing, a suitable **standard reference material (SRM)** was decomposed first. SRM 1648 was the best choice, which is an urban aerosol (see appendix A). The **Teflon** filter samples were used in the decomposition process due to their suitability for element analysis. Equivalent amounts of total mass of the SRM 1648 to the amount of particulate matter collected on the Teflon filters were weighed into seven microwave vessels on a Sartorius® analytical balance (0.1mg). Furthermore, one new Teflon filter was cut into small pieces with a clean scalpel (ethanol cleaned) and added to each vessel as well, in order to simulate the conditions of the decomposition of the PM filter samples as closely as possible. As during all filter handling, the specially prepared tweezers were used and cleaned beforehand. A new Teflon filter that was cut and put into another decomposition vessel served as a blank. It needs to be mentioned that the transferring of the cut Teflon pieces into the plastic decomposition vessels is a very tricky business due to electrostatic charging of the Teflon. Nevertheless, with a bit of force and careful handling of the vessels, especially when the plastic lid is put on top, the process is doable. The Teflon filters were cut on a clean plastic disk. Figure 29 shows the filter cutting arrangement.

Figure 29 – Cutting of the Teflon filters for microwave decomposition [pictures mine]

To each vessel were added (automatic pipette) 10ml of an acid mixture consisting of concentrated nitric acid (65% **HNO_3** – from MERCK, Germany) and concentrated hydrofluoric acid (40% **HF** – from MERCK, Germany) in a 5+1 v/v ratio. This was achieved by preparing a stock mixture of 80ml (65%) HNO_3 and 16ml of (40%) HF. The proper choice, handling and use of acids are of uttermost importance in the microwave decomposition method. Generally, the **acids** are classified according to their primary role in the decomposition reaction, and fall into either of the two categories: **oxidising** or **non-oxidising**. HF is a non-oxidising acid and thus dissolves metals with a negative reduction potential greater than hydrogen. HNO_3, on the other hand, is an oxidising acid dissolving most metals by forming soluble metal nitrates. Its oxidising strength is most powerful in the concentrated form and merely poorly developed at concentrations below 2mol/l. It is possible to enhance its oxidising strength by adding chlorate, permanganate, hydrogen peroxide, or bromide or by increasing the reaction temperature and pressure. Gold and platinum are not oxidised by HNO_3 and some metals, such as Al, B, Cr, Ga, In, Nb, Ta, Th, Ti, Zr, and Hf form insoluble oxides when attacked by HNO_3 and therefore a combination of acids is necessary to dissolve those. Organic matrices are most commonly oxidised using nitric acid.

The reactivity of HF is based on its strong complexing nature and it is one of only a few acids that can dissolve silicates according to:

$$SiO_2 + 6HF \rightarrow H_2SiF_6 + 2H_2O$$

Its strong complexation capability prevents the formation of sparingly soluble products of the IV's to the VI's group in the periodic table and thus increases the solubility and stability of certain elements, e.g. Si, Sn, Ti, Zr, Hf, Nb, Ta, Pa. HF dissolution produces predominantly soluble fluorides with the exception of insoluble or merely sparingly soluble fluorides of the alkaline earths elements, lanthanides, and actinides. It was not necessary for the succeeding analysis to remove the HF after decomposition, as both the ICP-MS and ICP-AES can handle HF. It is extremely important to be conscious about the harmfulness of HF when handling it. HF attacks any glassware due to its affinity to silicon. More important for the user is to be always protected with adequate gloves (at least 3mm thickness and HF resistant), goggles, and laboratory coat (preferably with an HF resistant apron). It is very advisable to always have the HF antidote gel nearby and knowledge of the *special* emergency phone number. HF can remain on clothing for longer time and still cause damage

when finding its way onto the skin, etc. HF does not 'only' very aggressively eat through skin and bones, but upon entering the human body and blood stream, it causes systemic effects, mostly by binding to the calcium in bones causing fractures. In case of any spillage onto skin, the area should be washed with water immediately and the HF antidote gel be applied in large quantities. The gel contains calcium which shall serve as a binding site for the fluorides. All handling of chemicals was carried out in a fume hood.

After the 10ml of the acid mixture were added to the vessels, the bombs were fully assembled and fastened in the rotor segments. Before putting them into the microwave oven the fully assembled segments were gently shaken to ensure that all SRM is immersed in and homogenised with the acids. The temperature/pressure control vessel requires a special adapter plate and spring. The vessel with the largest amount of SRM was used for the temperature/pressure bomb. This will ensure that the measured conditions will not be exceeded in another bomb. It was inserted last into the oven and both the pressure and the temperature cables were connected to their respective ports. It is important to test if the cables are placed correctly inside the entire arrangement in order for them not interfere with each other during the process of rotation while the microwave oven is activated. This can be done by activating the rotor table over the computer software.
The EasyWave® software is very user-friendly, easy to operate and works by dividing the decomposition process into individual steps, which are in turn defined by the user. Table 3 contains information on the program that was applied for the dissolution of the standard reference material 1648. The third step serves as a cool-down or ventilation step, while pressure and temperature are still measured. An extra 30 minutes of waiting time was added to reduce the acidic gas pressure resulting in lower gas emissions when loosening the connection of the pressure sensor. Afterwards, the rotor segments and bombs were transferred into an ice-bath and left for about two hours to cool down.

Table 3 – Microwave decomposition program for dissolution of SRM1648

Decomposition			
Step	Time [min]	Temperature [°C]	Power [W]
1 – Ramping	15	180	1000
2 – Dwelling	15	180	1000
3 – Ventilation	10	0	0

The cooled bombs were carefully opened under the fume hood and 50ml of Milli-Q® type-1 water were added to each individual bomb. This was done according to Xie et al. (2006) in order to completely dissolve any fluorides present. All bombs were closed again, vigorously shaken for all bits and pieces stuck to the vessel walls (potentially containing elements) to be dissolved, and left overnight for the decomposition to be completed. The bombs were opened again the following day and their contents were observed and carefully transferred into 100ml PP (polypropylene) bottles, which were then stored in the fume hood at room temperature. All vessels were cleaned by adding the same amount of the same acid mixture to them that was also used for the SRM decomposition. The cleaning program is shown in table 4.

Table 4 – Cleaning program

Cleaning			
Step	Time [min]	Temperature [°C]	Power [W]
1 – Ramping	5	180	1000
2 – Dwelling	10	180	1000
3 - Ventilation	15	0	0

After the decomposition method was tested by determining the recovery of the certified NIST values (appendix A) of the present elements in the SRM1648 with ICP-MS, the Teflon filter samples from Taiyuan were prepared in the same way as outlined above and decomposed according to the same method. The samples were decomposed in two batches, each containing six samples, one field blank and one solution blank. The decomposed samples, as well as the decomposed SRM, still contained a large amount of black particles and Teflon.

Table 5 – Amounts of SRM and Teflon filter samples for microwave decomposition

Standard Reference Material 1648							
Name	2SRM1	2SRM2	2SRM3	2SRM4	2SRM5	2SRM6	2SRM7
Mass [mg]	11.0	8.7	5.7	3.0	12.1	15.3	33.3
Teflon Filter Samples - Taiyuan							
Name	T51	T53	T55	T57	T59	T61	T63
Mass [mg]	32.3	11.4	14.1	18.7	8.7	5.9	2.7
Name	T65	T67	T69	T71	T73		
Mass [mg]	8.8	12.3	11.7	13.4	7.5		

When transferring the decomposed solution into the PP bottles it can be helpful to avoid as much of the Teflon and particles as possible, as no larger particles should enter the analytical instruments. Filters may introduce contamination and have hence

not been applied. The final decomposed solutions were stored in the fume hood until analysis. Table 5 lists the different amounts of bulk particulate matter used either from the SRM or what was adsorbed onto the Teflon filters in Taiyuan. Moreover, one SRM blank (only empty, pre-dried filter, no SRM) and two field blanks from Taiyuan (T54, T74) were prepared and selected respectively for later analysis. The standard reference material 1648 had to be **dried** in an oven at 105°C for 8 hours according to NIST (1998). The certified NIST concentrations are reported on a dry-weight basis and thus any absorbed water has to be removed and accounted for in the considerations. For this purpose one pre-cleaned (5% HNO_3) glass vial with cap was weighed (Sartorius balance – readability 0.1mg) and 44.7mg of SRM1648 were added into it. The oven (Nabertherm® 30-3000°C) was programmed to reach the set temperature of 105°C after 20min and to hold it for 8 hours. SRM and vial were re-weighed and the water content was determined from the weight difference.

4.3 Inductively Coupled Plasma Mass Spectrometry (ICP-MS)

The first of the applied instrumental analysis techniques (ICP-MS) was developed commercially in the early 1980's and has since been utilised for the determination of trace, minor and major elements in almost every analytical field. It is a particularly powerful technique because of its a) wide elemental coverage, b) high performance (low detection limits [ng/l], high sensitivity and low background signals), c) fast analysis time, d) wide analytical working range (up to nine orders of magnitude), e) isotopic information and f) excellent chromatographic detector (Agilent Technologies, 2005).

4.3.1 Theory, Components and Function

Principally, the ICP-MS consists of several individual components. These are **sample introduction**, **ion generation**, **plasma/vacuum interface**, **ion focusing** and **ion separation and measurement**, all of which will be discussed briefly in this section. The overall process from sample introduction to mass analysis is illustrated in figure 30 and a schematic diagram of the ICP-MS instrument is shown in figure 31. The principal components are similar to the ones in the instrument used for analysis. The **introduction** of the liquid sample, which is the most important process of the entire ICP-MS system, is achieved by passing it through a pneumatic nebuliser that

transforms the liquid into an aerosol. Larger aerosol droplets need to be removed from the gas stream, as they would not be fully decomposed in the plasma. This is done by a spray chamber, while the smaller droplets are transported by a carrier gas (Ar) into the central channel of the argon plasma.

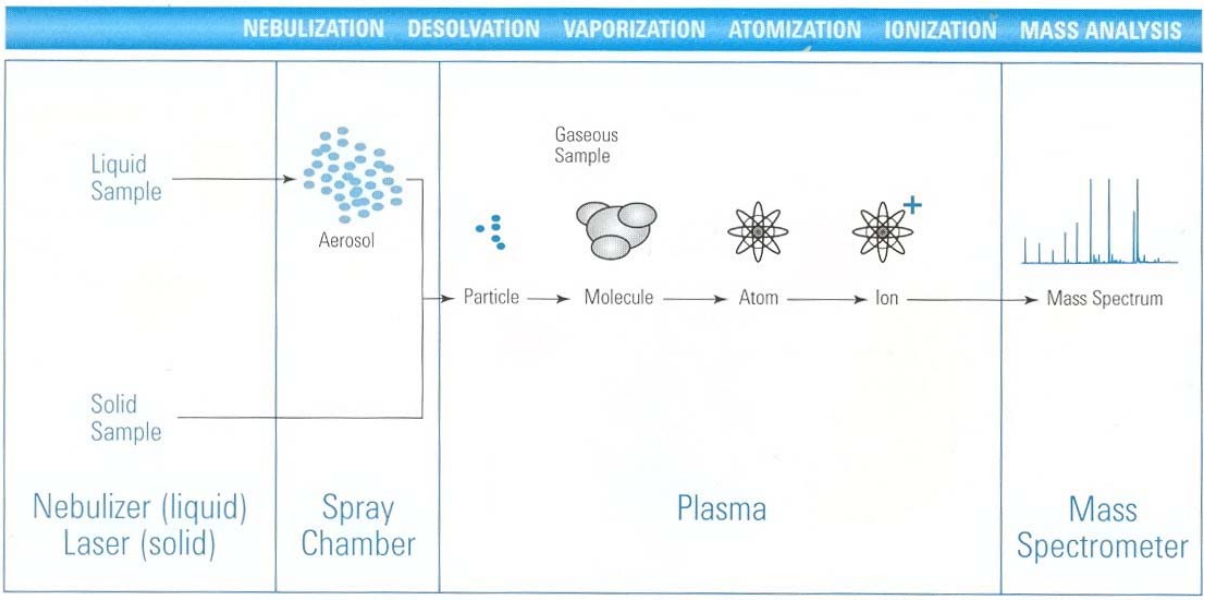

Figure 30 – Processes involved in ICP-MS [source: Agilent Technologies, 2005]

A well-designed sample introduction system will reduce maintenance and boost analytical performance.

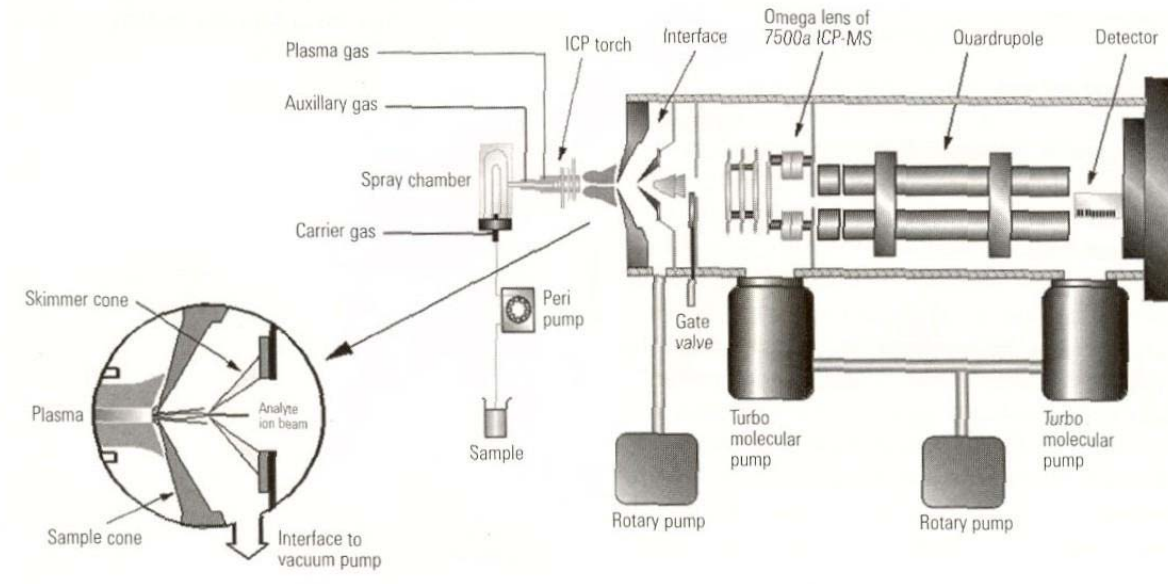

Figure 31 – Illustration of ICP-MS system [source: Agilent Technologies, 2005]

The major objective of the sample introduction system is to ensure a stable, high temperature plasma (necessary for high matrix samples, e.g. environmental), which is achieved by reducing the sample load on the plasma.

The performance of the sample introduction system is strongly affected by the:

a) Nebuliser Sample Uptake Rate (1-1.5ml/min, with increasing sensitivity from lower to higher values but at the same time increasing water loading on the plasma, which will reduce its temperature); **b) Nebuliser Type** – The nebuliser has to be capable of creating an aerosol with uniformly small droplet size. Figure 32 shows a sketch of the cross-flow nebuliser. Its operation can be compared to that of a perfume atomiser. The high speed argon gas stream is directed at 90° towards the capillary tube of the sample. The caused impact breaks up the sample into an aerosol (Boss and Fredeen, 2004); **c) Spray Chamber Temperature** – The plasma loading and efficiency can be significantly influenced by the temperature of the spray chamber, as it affects the amount of solvent vapour that enters the plasma; and **d) Spray Chamber Design** – The major role of the spray chamber is to guarantee that the larger sample aerosol droplets are being filtered out (see figure 33).

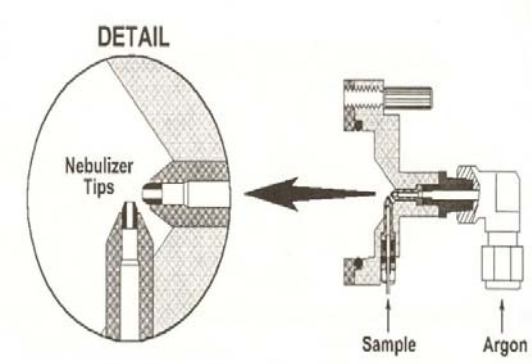

Figure 32 – Cross-flow nebuliser
[source: Boss and Fredeen, 2004]

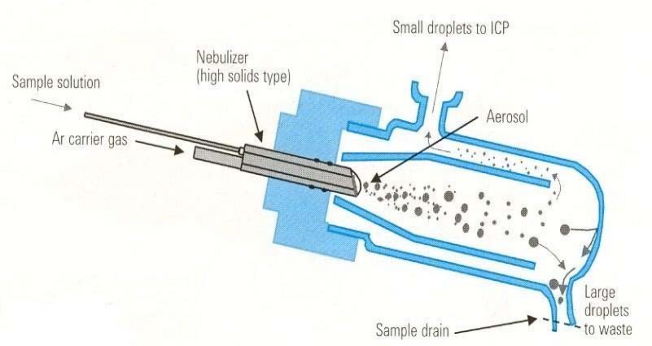

Figure 33 – Spray chamber design with Babington nebuliser
[source: Agilent Technologies, 2005]

The **ion generation** takes place in the plasma which main purpose is to form positively charged ions from the sample aerosol. In order to achieve good results from samples with high or varying matrices, the plasma loading should be optimised to maintain high ionisation temperatures while retaining good sensitivity. The objective is to attain the highest possible degree of matrix decomposition and analyte ionisation. Such high matrix decomposition will reduce the deposition on the interface and contamination of the expansion stage pump oil. A well optimised and high

temperature plasma has the capability of ionising even elements with rather high ionisation potential, such as Hg, Be and As. As already pointed out in figure 30, in order for the sample droplets to be ionised they have to undergo several stages beginning with a) approaching the plasma and being dried, b) then, as particles, being decomposed and atomised, c) all the way to the ionisation process, which requires the plasma to have more energy than for example in ICP-AES. Ionisation is carried out by the removal of a single electron, the ease of which depends on the first ionisation potential (i.e. the amount of energy required to remove one electron from a neutral atom) of the element. An illustration of the most commonly used **plasma torch** (Fassel design) is depicted in figure 34. Individual torches only vary in the diameter of the carrier or injector gas tube. A larger diameter will result in a more diffuse and slower moving aerosol, leading to improved matrix decomposition. The RF (radio frequency) generator produces an oscillating field of around 40MHz, which in turn causes rapid oscillations in the Ar gas atoms producing heat of up to 10000K (hot spot).

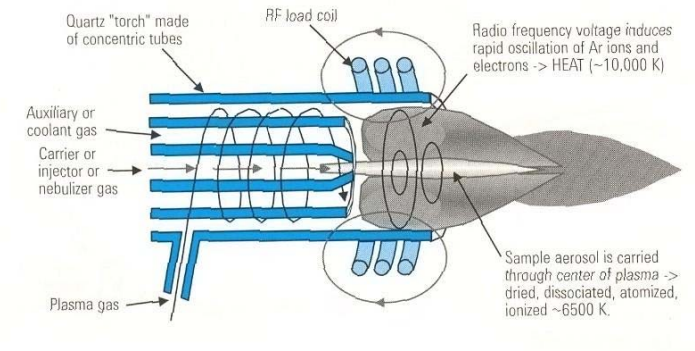

Figure 34 – Plasma torch [source: Agilent Technologies, 2005]

Once ionised, the sample has to enter into the detection system, the mass spectrometer (MS). The MS operatres at high vacuum conditions and in order for the sample ions, at atmospheric pressure, to enter into the MS, a **plasma/vacuum interface** is crucial (see figure 35).
The high vacuum significantly reduces the background and scattering effects of of residual gas molecules. The purpose of the interface is to extract a representative sample of the ions generated in the plasma and efficiently transfer it into the MS. It is impossible to do this in one single step. Hence, a series

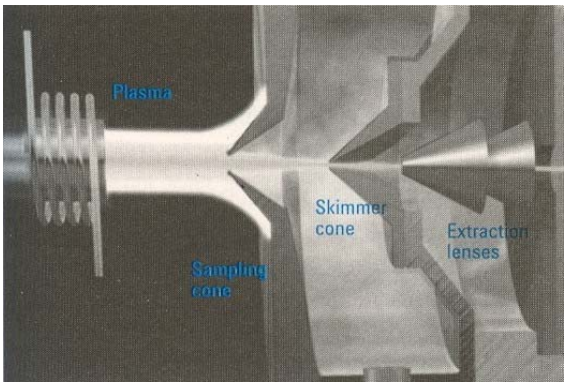

Figure 35 – Plasma/vacuum interface [source: Agilent Technologies, 2005]

of vacuum chambers are used (3 steps). The first step (step down vacuum), in the interface vacuum chamber between the first two conical metal plates (sampling and skimmer cone respectively = Interface), is from atmospheric pressure to approximately 1mbar. The extracted ion beam supersonically expands due to the sudden decrease in pressure and its composition is retained, arriving unchanged at the skimmer cone. The size and shape of the orifices (usually about 1mm) of the interface cones has a large impact on sensitivity, mass response, oxide and double charged formation, as well as robustness to high matrix samples.
The other two stages are called intermediate and analyser vacuum stages with progressively lower pressure. Both of these regions are isolated from the interface region by a gate valve. Turbo pumps enable vacuum pressure below $1.3 \cdot 10^{-3}$Pa (10^{-5} torr) in the ICP-MS utilised for analysis.

The **ion focusing** is achieved by electrostatic plates, also known as ion “lenses”. They are located in the intermediate stage. The ion beam is focused as it enters through the skimmer cone and the analyte ions are separated from the neutral species and photons, to avoid a random background signal upon detection. This separation is done by the electrostatic fields, which deflect the ions away from the photons and neutrals. The focusing lenses prevent any loss of ions from the beam and transfer them efficiently to the detector (Agilent Technologies, 2005).

In the final stage (analyser vacuum stage), the ions are **separated** according to their mass to charge ratio (m/q) by a quadrupole (see figure 36). The quadrupole mass analyser is most widely used in ICP-MS applications because of its ease of use, robustness, mass range, high scanning speed and relatively low cost.
It consists of four parallel cylindrical rods, arranged in a square around the trajectory of the ions. AC (alternating current) and DC (direct current) voltages are applied to the two pairs of rods creating a dynamic hyperbolic electric field. The field can be set selectively to only allow ions with the given mass-to-charge ratio to pass,

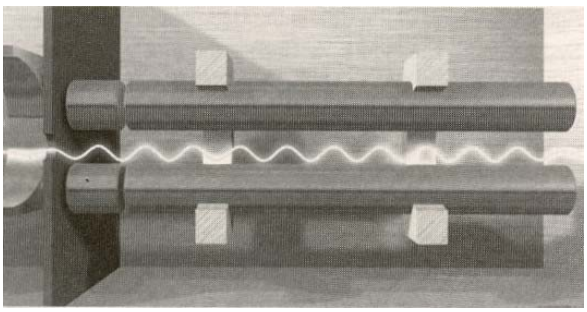

Figure 36 – Quadrupole mass analyser
[source: Agilent Technologies, 2005]

while all others will have unstable trajectories and thus are lost from the ion beam. The voltages can be adjusted very rapidly, thus allowing for the determination of a mass spectrum for all elements and their isotopes virtually simultaneously.

The characteristics of ICP-MS having a high sensitivity and a low random background are largely attributed to the **detector**, an electron multiplier. It is capable of generating a measurable signal pulse from only a single ion. The performance of the detector is characterised by high sensitivity (counts per second per unit concentration), wide linear dynamic range (concentration range over which the detector gives a linear count rate response) and a low random background.

Spectral interference in ICP-MS is caused by polyatomic ions or, to a lesser extent, by multiply charged ions. Both will result in mass-to-charge ratios of single-charged element ions, rendering a clear determination ambigious. There are only a few elements that possess sufficiently low ionisation potentials to allow the generation of noticible amounts of doubly charged ions. The relative percentage of doubly charged ions is usually smaller then 2%. The condition of the plasma has a large impact on the occurrence of polyatomic ions. High plasma temperatures significantly reduce their level. The level of polyatomic ions is monitored by using the production of oxide ions in specific elements. Cerium oxide (CeO^+) is measured due to its strong oxide bond and associated high oxide formation rate. Ce-O decomposition efficiencies are expressed in $\%CeO^+$, relative to the parent ion Ce^+. The CeO^+/Ce^+ ratio is adjusted to be below 3% (Agilent Technologies, 2005).

4.3.2 ICP-MS Method of Analysis

The ICP-MS utilised for analysis was a 13-year old Perkin Elmer Sciex Elan 5000 (figure 37) endowed with all the above mentioned hardware and characteristics, with only some small exceptions, such as a cross-flow nebuliser instead of the Babington depicted in figure 33 and probably a

Figure 37 – Image of the Perkin Elmer Sciex Elan 5000 [picture mine]

different ion lens system than the Omega shown in figure 31. A **routine start-up procedure** was followed each time the ICP-MS was used, that, in sequence, comprised of the turning on of the ventilation system, a check of the correct distance between the tip of the plasma torch and coil, observation of the small orifice in the sampling cone (no dirt), proper fastening of the sample tubing system and subsequent check of sample flow rate (≈1ml/min), a cleaning of the tubing system with type 1 water followed by 5% HNO_3, the ignition of the plasma and continuous cleaning with 5% HNO_3. The plasma was left to stabilise for about 15min.

4.3.2.1 The Daily Test

Prior to each analysis it was necessary to perform an optimisation procedure, which is called a "**daily-test**", in order to check and adjust the sensitivity range across the mass spectrum, the amount of oxides and doubly charged ions. For this purpose, a special daily test solution was prepared according to the details given in appendix C. The sensitivity distribution across the mass spectrum is adjusted according to figure 38 in two steps: (1) by first optimising the nebuliser gas flow to achieve a high Rhodium (Rh[103]) sensitivity (minimum of $4.5 \cdot 10^4$) while at the same time maintaining a low oxide sensitivity (max 3%), and (2) by adjusting the optics (lenses) to achieve equal sensitivity of the other two elements used in the process – Magnesium (Mg[24]) and Lead (Pb[208]) (both min of $7.5 \cdot 10^3$). This optimises the sensitivity according to figure 38 (arbitrary sensitivity scale), giving highest sensitivity to the elements in the middle of the mass range.

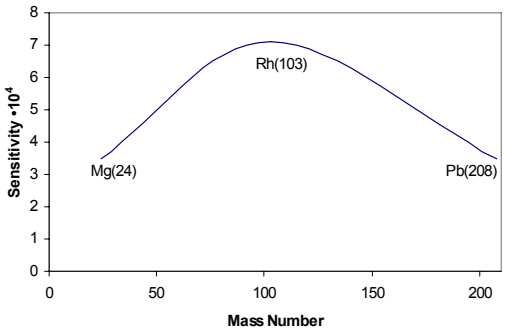

Figure 38 – Sensitivity optimisation [graph mine]

4.3.2.2 SRM and Sample Preparation

The ICP-MS was used to determine the elements arsenic (**As[75]**), manganese (**Mn[55]**), nickel (**Ni[60]**), antimony (**Sb[121]**), selenium (**Se[77]**), vanadium (**V[51]**), cadmium (**Cd[111]**), cobalt (**Co[59]**), lead (**Pb[208]**) and copper (**Cu[63]**). The numbers in brackets correspond to the mass numbers of the individual elements. These metals were selected as their concentration ranges and relative

aerosol abundance (according to NIST values in the SRM1648) in the reference material and samples were either below the suggested maxiumum concentration for the IPC-MS of 100μg/l (ppb), or could easily be diluted to match this requirement.

Cleaning Procedures and Analytical Practise

All used labware, such as flasks, scintillation bottles, Erlenmayer flasks, various PP (polypropylen) bottles, etc., not only for ICP-MS but for all applied analytical methods, were always pre-cleaned by filling them with 5% HNO_3 and leaving them overnight. The items were then rinsed two times with **type 1 water** [Resistivity: 18.2MΩcm @ 25°C; TOC (μg/l): <10; Na (μg/l): <1; Cl (μg/l): <1; silica (μg/l): <3] and air-dried until the following day. In case of imminent need for clean volumetric flasks, they were rinsed with concentrated nitric acid and afterwards washed twice with type 1 water. Pipette tips were rinsed twice with type 1 water prior to use. By shaking the pipettes rigurously it is rather easy to remove all residual water. The first volume to be transferred was discarded to further clean the pipettes. It is not recommendable to pre-clean pipette tips with acid, as the acid tends to attack the inner surface of the tips and causes some droplets to be retained in them when transferring solutions (Skramstad, pers. comm.).

The SRM and sample preparation was carried out in the following steps:

1. **SRM**: The volumetric concentration of each element in the 60ml of decomposition solution was determined according to the certified NIST values (see appendix A and appendix D).

2. The HF load on the instrument was determined (see appendix D) and found to be considerably lower than the maximum acceptable limit of 10%.

3. Based on these results, the concentration range of the standards was determined and multiplied by a factor of 5, since **standard addition** (see point 5) was chosen as an appropriate method due to strong matrix effects. The following standard concentrations were selected, in μg/l:

   0 (only sample); 5; 10; 30; 50; 80, for all elements except:

   Pb[208]: 0 (only sample); 10; 30; 50; 80; 100.

Again, these are not the concentrations that were prepared but the resulting concentrations after standard addition. Prepared concentrations were: 0; 25; 50; 150; 250; 400, and 0; 50; 150; 400 and 500 μg/l respectively.

4. Single element stock standards [*SESS*], all produced by TEKNOLAB A/S, having the characteristics given in table 6, were diluted to yield a 10mg/l (ppm) and 1mg/l (ppm) stock solution, accoring to the following procedure:

   1ml of SESS into 100ml volumetric glass flask → 10mg/l

   5ml of 10mg/l stock into 50ml volumetric PP flask → 1mg/l

Table 6 – Characteristics of single element stock standards [data from manufacturer]

Element	**V**	**Mn**	**Co**	**Ni**	**Cu**	**As**	**Se**	**Cd**	**Sb**	**Pb**
Conc. in mg/l	1000 ±1	1000 ±0.5	1000 ±0.5	1002 ±2	1000 ±3	1000 ±0.5	1000 ±0.5	1000 ±0.5	1003 ±3	1002 ±3
Matrix	2.5% HNO_3	2.5% HNO_3	2.5% HNO_3	1.4% HNO_3	2.5% HNO_3	2.5% HNO_3	2.5% HNO_3	2.5% HNO_3	0.7% HNO_3, 3% Tartaric Acid	0.35% HNO_3

Unfortunately, some of the SEES were very old and way past their recommended time of use. Pre-calibrated automatic pipettes were used for all volumetric preparations.

5. The standards were obtained by transferring different amounts from the two stock solutions with automatic pipettes into 100ml volumetric glass flasks (see table 7).

Table 7 – Standard preparation for ICP-MS

Standard Concentration in μg/l	**25.0**	**50.0**	**150**	**250**	**400**	**500**
Amount Added From 10μg/l Stock in ml	---	---	1.50	2.50	4.00	5.00
Amount Added From 1μg/l Stock in ml	2.50	5.00	---	---	---	---

6. The standard addition procedure was carried out by either directly working with the original sample or SRM, or by first diluting it, as had to be done in the cases of Mn[55], Cu[63] and Pb[208]. Dilution caused the acid concentration to fall below the minum of 1% and had to be accounted for by adding HNO_3 according to table D-2 (appendix D). The nitric acid will ensure that the elements remain in solution and will not precipitate and deposit on the walls of the tubing. Because of the presence of particles in the decomposed sample

bottles, they were not shaken before pipetting and the required volume was collected in the middle region of the solution to avoid particle uptake.

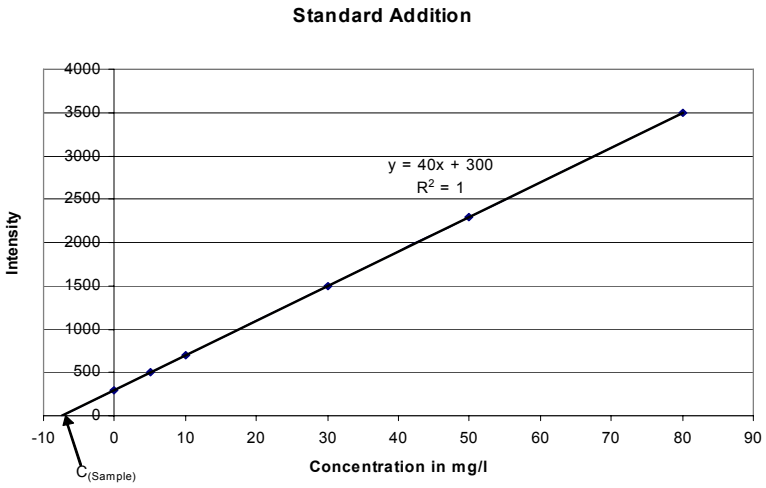

Figure 39 – Example of standard addition calibration [graph mine]

For the purpose of standard addition, "**spiked**" standard solutions had to be prepared. In other words, the standards were added to a known and constant amount of one, so-called **representative sample** or **SRM**. The representative sample should not be an outlier but rather lie within the most frequently occurring PM or SRM mass range. Several different representative samples (SRMs) were used in all the analyses due to the limited amount of sample solution available. The spikes can either be very small amounts of sample (SRM), causing a negligible change in total volume, or, as applied in this work, a larger quantitiy, under consideration of the increase in volume. *Hence, 1ml of each standard was added with automatic pipettes to 4ml of each sample or SRM in a small (20ml) scintillation bottle*. This leads to the total volume of 5ml and thus a dilution factor of 5 for all the original standards, as mentioned above. Figure 39 illustrates the standard addition procedure and how the unknown concentration of the added sample (SRM) is determined. It is simply the point of intersection between the absciss and the calibration graph. For further calculation of the concentrations of all other samples (SRMs), only the slope of the calibration graph for the corresponding element is needed, while the intercept equals the intensity of the to be determined sample (SRM). Solving this equation by setting y equal to zero (figure 39), the unknown sample (SRM) concentration is found, after correcting for the applied dilutions and blank values. For the sake of simple data acquisition, it is important to also dilute all other samples (SRMs) and blanks, etc., in the same way as the representative sample (SRM) for the standard addition. Then all samples (SRMs) were prepared and ready for ICP-MS analysis.

4.3.2.3 ICP-MS Analysis

After the ICP flame was ignited and stabilised, while cleaning the tubing, nebuliser, spray-chamber and plasma with 5% HNO_3 and type 1 water, the daily test was performed and the acquired instrument characteristics were noted down in a data book. It is very important to never let the plasma run “dry”, i.e. not having any solution circulating through the sample introduction system, in which case the plasma would simple switch off. The Elan 5000 computer software, which is rather easy to use, despite its outdated design, was the data acquisition and processing tool. It allows the user to define a data set, parameter set and a calibration file, which contain all the necessary procedures for analysis.

Table 8 – Software settings on the Elan 5000 program for ICP-MS

Time Factor	1	Points/Spectral Peak	1	Spectral Peak Processing	Average
Replicate Time (ms)	1000	Resolution	Normal		
Dwell Time (ms)	1000	Transfer Frequency	Replicate	Dead Time Correction	51
Sweeps/Reading	1	Baseline Time (ms)	0		
Readings/Replicate	1	Polarity	+	Dilution Factor	1
Number of Replicates	3(SRM); 5(Sample)	Signal Profile Processing	Average	Sample Read Delay (s)	45

In order to properly clean the system before analysis and after each standard, sample, SRM, etc., and to not disturb the plasma too much by a rather different matrix, a “washing acid mix” was prepared. This washing solution had almost the same acid matrix as all the analytes, except that it was slightly stronger to increase its dissolving power for a better removal of potentially deposited solids (see also appendix D-5). The washing was done for 2min each time and no memory effects were detected. A summary of all the settings applied on the Elan 5000 software is given in table 8 and the manual should be consulted for detailed definitions of each parameter.

In order to monitor any possible **instrumental drift**, a standard from the middle of the concentration range was re-analysed in the **middle** and **end** of the overall analysis. A maximum drift of ±10% was defined as being acceptable. Otherwise, the analysis was repeated. At the end of each individual analysis, the instrumental limit of detection (**LOD**) was determined by measuring the acid matrix (washing solution) ten times and multiplying the resulting standard deviation by a factor of three.

4.4 Inductively Coupled Plasma Atomic Emission Spectrometry (ICP-AES)

The ICP-AES technique is in many ways similar to the ICP-MS instrumentation and hence does not necessitate an as exhaustive description as given for the ICP-MS procedure. In the following, only the major differences between the two techniques will be stressed and illustrated, incorporating the characteristics of the actually utilised instrument.

4.4.1 Theory, Components and Function

As already implied in the name – atomic emission spectrometry – the technique involves the emission of electromagnetic radiation from atoms (and ions) in the sample. It is the detection of radiation that leads to quantitative (amount of radiation) and qualitative (wavelength) information about the sample, whereas this information was retrieved by the detection of the mass-to-charge ratio in ICP-MS.

The electromagnetic radiation (mostly ultra-violet [UV] and visible [VIS], from 160nm – 800nm) is emitted by the sample atoms (ions) which were formed after they have undergone the same transformations as illustrated in figure 30. The use of the UV-

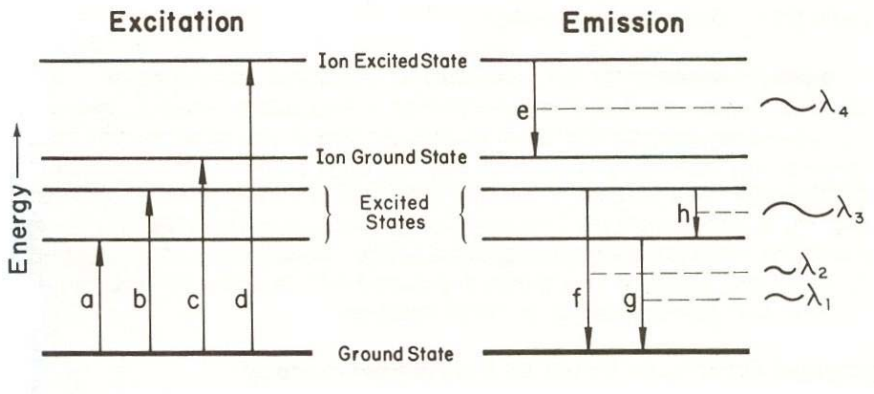

Figure 40 – Energy level diagram, showing different energy transitions, such as excitation [a, b], ionisation [c], ionisation/excitation [d], ion emission [e] and atom emissions [f, g, h] [source: Boss and Fredeen, 2004]

VIS region has some unique advantages over techniques that operate at different wavelengths, in that the UV-VIS techniques are accurate, precise, flexible and relatively inexpensive. The electrons in the atoms and ions are excited by the energy provided by the plasma and radiation, characteristic for the particular element, is emitted as the excited electron decays back to a lower and more stable energy state. Energy that exceeds the ionisation potential of the individual element will cause its atoms to be ionised. Figure 40 gives a simplified overview of the transitions involved in the mentioned processes.

Generally, the majority of the sample elements will be transformed into ions in the plasma, while only a small fraction of the argon gas, sustaining the plasma, is ionised. The reason for this is the high ionisation potential of Ar (Octet rule). The electromagnetic field (between 700 – 1500W power – 40MHz) around the top of the plasma torch, and an ignition spark, will ionise some of the argon atoms. The liberated electrons are accelerated by the electromagnetic field with the use of a coil. This mechanism is called **inductive coupling**. The electrons collide with other argon atoms continuing the chain reaction that breaks down the gas into a plasma consisting of argon atoms, electrons and argon ions [Boss and Fredeen, 2004].

The principle setup of the ICP-AES instrument is depicted in figure 41. Different to the ICP-MS is the V-groove nebuliser, shown in figure 42 and, of course, the optical arrangement for the collection and separation of the generated electromagnetic radiation, as well as the detection component.

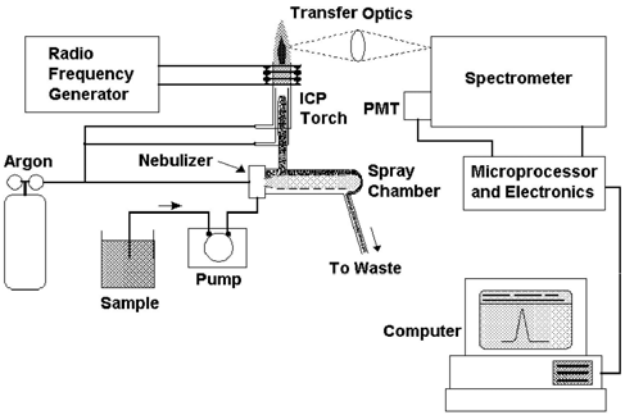

Figure 41 – ICP-AES basic component layout
[source: Boss and Fredeen, 2004]

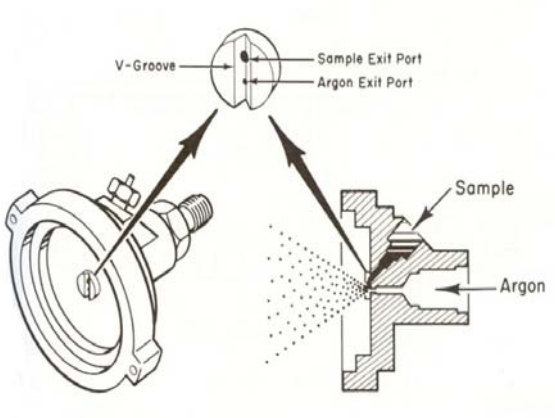

Figure 42 – V-groove nebuliser design
[source: Boss and Fredeen, 2004]

In the **V-groove nebuliser** the sample flows down a V-shaped groove that has a small hole in the centre for the high-speed nebulising gas (Ar) to intercept with the sample, shearing it into small droplets. The V-groove nebuliser is predominantly used for solutions containing high salt and particulate concentrations [Boss and Fredeen, 2004]. The torch arrangement shown in figure 41 is radial (side-on viewing) as opposed to axial (end-on viewing). The instrument used for analysis was equipped with a horizontal torch (axial). This has the advantage that no viewing height adjustments (optics) are required, as the radiation from elements emitted in all zones of the plasma will reach the optics.

The excitation and correlated decay processes result in a large number of emission lines from one individual element. This feature, on the one hand, allows for great flexibility when selecting a characteristic element line, but on the other hand, bears a large capacity for interferences of emissions lines that are too close in wavelength to be measured separately. The **optical system** of the instrument used (figure 43) is capable of analysing emissions from 166 – 785nm, which is realised via the arrangement of pre-optics, an **Echelle polychromator** and a camera/detector. The Echelle polychromator is designed to separate incident light into a large number of diffraction orders, 70 of which are used for data collection. It basically consists of an Echelle ruled grating with a cross dispersing prism forming a two-dimensional diffraction pattern across the focal plane.

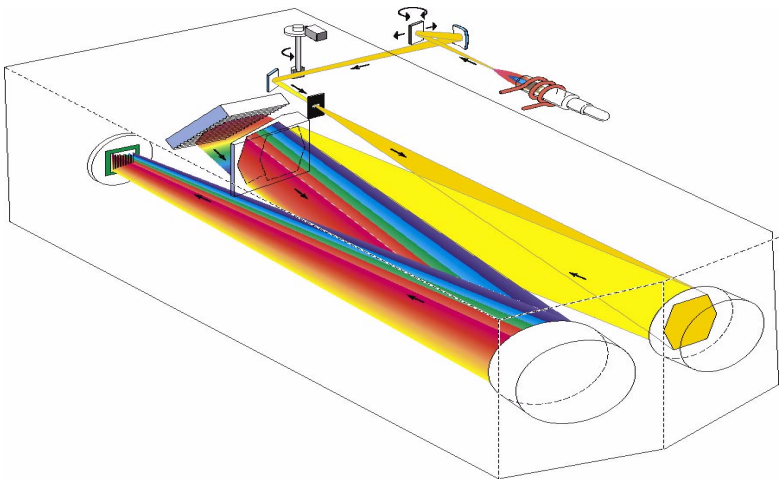

Figure 43 – Optical system consisting of pre-optics, Echelle polychromator and charge coupled device (CCD) detector [source: Skuins, 1998]

The camera assembly (**detector**) is mounted in that focal plane of the optics. It is a solid-state device made of radiation sensitive semiconductor picture elements (pixels), also called "**charge coupled device**" (CCD). The CCD is peltier cooled (-36°C) and made up of over 70,000 pixels that are spread across 70 non-linear arrays. That arrangement enables almost simultaneous detection of all emission lines and dramatically reduces overall analysis time (VARIAN, http://osiserver.varianinc.com, last accessed: 20.04.2007).
A particularly advantageous feature of the ICP-AES technique is its wide linear dynamic range (LDR), i.e. the range of concentrations from the detection limit to the upper limit. The upper limit of linear calibration is usually 10^4 to 10^6 times the detection limit for any particular emission line. There are two main advantages of the long linear dynamic range. Firstly, it simplifies calibration of the instrument, and secondly, less sample dilution is required.

4.4.2 ICP-AES Method of Analysis

The ICP-AES analysis was carried out on a VISTA AX instrument from VARIAN, depicted in figure 44. Prior to commencing with the measurements, several steps had to be taken in order to setup the instrument and analytes. After turning on the argon gas, the cooling system, which regulates the temperature of the coil and the arrangement around the plasma at 21°C, is switched on. As the CCD detector is peltier cooled (thermoelectric cooler), the plasma must not be ignited before the required temperature of around -36°C is reached on the detector.

Figure 44 – ICP-AES instrument used for analysis [source: Skujins, 1998]

4.4.2.1 Sample (SRM) Preparation

The ICP-AES technique was applied to detect and quantify the elements: **aluminium** (Al), **silicon** (Si), **calcium** (Ca), **iron** (Fe), **magnesium** (Mg), **sodium**

(Na), **titanium** (Ti) and **zinc** (Zn), first in the standard reference material (SRM1648) and afterwards in the Taiyuan samples. For most of the sample (SRM) preparation the procedure is identical to the one described for the ICP-MS technique (see section 4.3.2.2) and only the differences are pointed out in this section.

- The SRM1648 certified NIST values (appendix A) of the elements to be quantified were used to calculate the expected concentration (mg/l [ppm]) in the amount of SRM used for analysis in the 60ml of decomposition solution. The results are summarised in table E-1 in appendix E.

- The chosen concentration ranges, in mg/l, for the standards were: 0(only sample); 0.5; 1.0; 5.0; 10; 20, for all elements except:

Si: 0(only sample); 5; 10; 20; 40; 60. Single element stock standards [SESS] (1000mg/l) of the individual elements were again the basis for the standard preparations (see table 9).

Table 9 – Single element stock standard properties [data from manufacturer]

Element	Si	Al	Ca	Fe	Na	Zn	Mg	Ti
Conc. in mg/l	1000 ±1.0	1000 ±0.5	1000 ±0.5	1000 ±0.5	1000 ±0.5	1000 ±0.5	1000 ±2	1000 ±1
Matrix	1% HF, 2.5% HNO_3	2.5% HCl, 0.3% HNO_3	2.5% HNO_3	2.5% HNO_3	2.5% HNO_3	2.5% HNO_3	0.1% HNO_3	4.9% HCl, 0.2% HF

Table 10 – Standard preparation for ICP-AES

Element(s) Applied to:	Desired Standard Concentration in mg/l	Added Amount From Which Stock/Standard	Dilution Volume in ml
Al, Ca, Fe, Na, Ti, Mg, Zn	100	5.00ml from 1000mg/l	50
	50.0	12.5ml from 100mg/l	25
	10.0	6.25ml from 100mg/l	25
	5.00	1.25ml from 100mg/l	25
	2.50	0.625ml from 100mg/l	25
Si	300	7.50ml from 1000mg/l	25
	200	5.00ml from 1000mg/l	25
	100	12.5ml from 200mg/l	25
	50.0	12.5ml from 100mg/l	25
	25.0	6.25ml from 100mg/l	25

The standard concentrations produced are a factor 5 larger than the final analytical concentrations (standard addition), and the way of preparation is shown in table 10. For the calcium analysis, all samples were diluted by a factor of 10. Even though not particularly necessary, type 1 water was also used in all sample preparations for ICP-

AES. Standard addition was carried out in the same routine as mentioned in section 4.3.2.2. No dilutions were necessary and the washing acid mix was prepared according to the same procedure as described in appendix D-5 for ICP-MS analysis.

4.4.2.2 ICP-AES Analysis

The analysis of the SRM and samples was carried out with the aid of the computer software ICP Expert Vista Pro (version 4.0). Before starting with the analysis a so-called **torch alignment** needed to be performed, because a HF resistant torch was inserted into the instrument. Whenever the position of the torch is altered performing the torch alignment will ensure that the pre-optics of the ICP-AES instrument are adjusted to look at the optimum part of the plasma. For this purpose, a **5mg/l manganese solution** was prepared and its representative emission line at **257.610nm** was used to scan in and optimise the horizontal and vertical viewing positions. The reason for selecting this particular emission line is because it gives a representative viewing range scan for most elements (Skujins, 1998).
With the use of the **method editor**, provided by the software, a method is developed by selecting several emissions lines for each to be analysed element. The requirements of a suitable emission line are a high intensity and low interference with other elements present in the sample. The software graphically displays possible interfering lines and assigns a relative intensity to all included emission lines. Table 11 summarises the selected emission lines, their nature (atom or ion line) and relative intensities.

Table 11 – Selected emission lines of the analysed elements

Element	Type	Wavelength in nm	Relative Intensity
Si	Atom	251.611	49839.3
Al	Atom	394.401	7581.6
Ca	Ion	393.366	1930472.3
Fe	Ion	238.204	41015.0
Na	Atom	588.995	121539.5
Ti	Ion	334.941	298458.3
Mg	Atom	285.213	82150.0
Zn	Atom	213.857	42500.9

The sample flow rate was adjusted to be approximately 1ml/min. The standard reference material was analysed first and the best emission lines were chosen (table

11) with regard to the requirements mentioned above and the best recovery. Afterwards, the Taiyuan samples were analysed implementing the selected settings. LOD determination, as well as preparation and use of the washing acid mix were carried out analogous to section 4.3.2.3. The instrumental settings are summarised in table 12. At the end of each analysis, 10mg/l single element standards were run to check the exact wavelength location of the element peaks in the samples and to adjust the integration interval whenever necessary. A **fitted background** correction was applied for all data acquisition.

Table 12 – Instrumental settings for ICP-AES analysis

RF Power [W]	1000	Sample Uptake Delay [s]	30
Plasma Flow [l/min]	15	Pump Rate [rpm]	15
Auxiliary Flow [l/min]	1.5	Rinse Time [s]	0
Nebuliser Flow [l/min]	0.75	Replicates	5
Replicate Read Time [s]	1.0	Fast Pump	Yes
Instrument Stabilisation Delay [s]	15	Calibration	Standard Addition

4.5 Ion Chromatography (IC)

4.5.1 Theory, Components and Function

The ion chromatography (IC) is a form of liquid chromatography using ion-exchange resins to separate atomic or molecular ions based on their varying interactions with the resin. IC is the only technique that allows quantitative analysis of anions at the μg/l (ppb) level (NMSU, 2006). The minimum detection limits of both the analysed anions and cations are shown in table 13.

Table 13 – Minimum detection limits for anions and cations in IC [source: MEE, 2000]

Species:					
Anions		**MDL**	**Cations**		**MDL**
Fluoride	F^-	7	Sodium	Na^+	10
Chloride	Cl^-	25	Potassium	K^+	17
Nitrate	NO_3^-	30	Ammonium	NH_4^+	10
Sulphate	SO_4^{2-}	30	Calcium	Ca^{2+}	13

MDL: Minimum Detection Limit in μg/l (ppb)

As in all types of liquid chromatography, the solution (mobile phase) is forced through packed columns containing fine particles (solid, stationary phase) which allow high-resolution separation. The partitioning of the solutes between the mobile and the stationary phase gives rise to separation. The column is preceded by a so-called

guard column containing the same stationary phase, which serves to filter out impurities (dust, particles) that may degrade the rather expensive column.
The solution entering the column is called the **eluent**, while the emerging fluid is termed the **eluate** (Harris, 2003).

In Ion chromatography the **stationary phase** is an ion exchanger, such as resins made of amorphous particles of organic material. The retention of the solute ions is based on their attraction to charged sites bound to the resin. Anion exchangers contain positively charged groups on the stationary phase, whereas cation exchangers utilise negatively charged groups to attract oppositely charged solute ions. The **elution** process, i.e. the progression of the **mobile phase** through the column, is characterised by a competition between solvent and solute molecules for charged sites on the stationary phase (figure 45). Different solvents vary in the capability to elute a given solute from the stationary phase. The elution occurs when the solvent displaces the solute from the stationary phase and the eluent strength of any given solvent is greater, the more easily this displacement occurs.

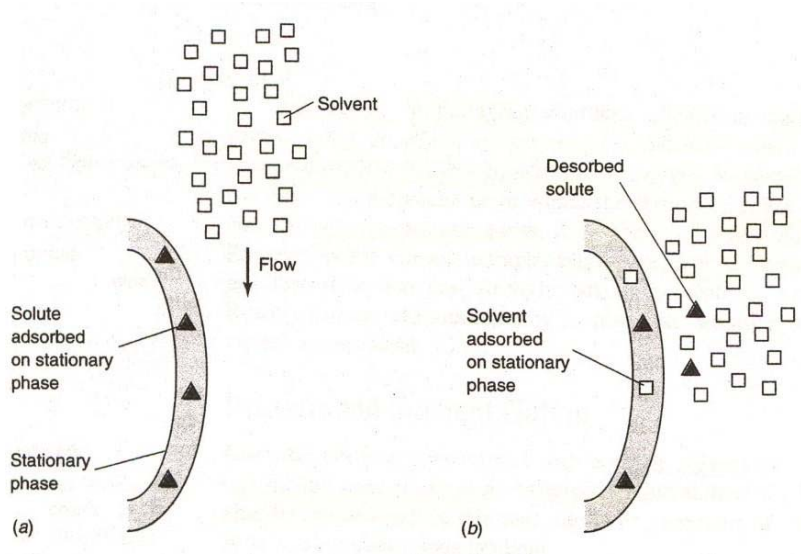

Figure 45 – Competition between solvent and solute for binding sites on stationary phase [source: Harris, 2003]

Figure 46 illustrates the structure of two different resins, one for anion exchange and another for cation exchange. This polystyrene resin is made by copolimerisation, cross-linking the styrene and divinylbenzene molecules. The benzene rings can be modified yielding the anion-exchange resin (ammonium groups – NR_3^+) and the

cation-exchange resin (sulphonate groups – SO_3^-) depicted in figure 46. The basic or acidic strength can be changed by altering the substituted groups.

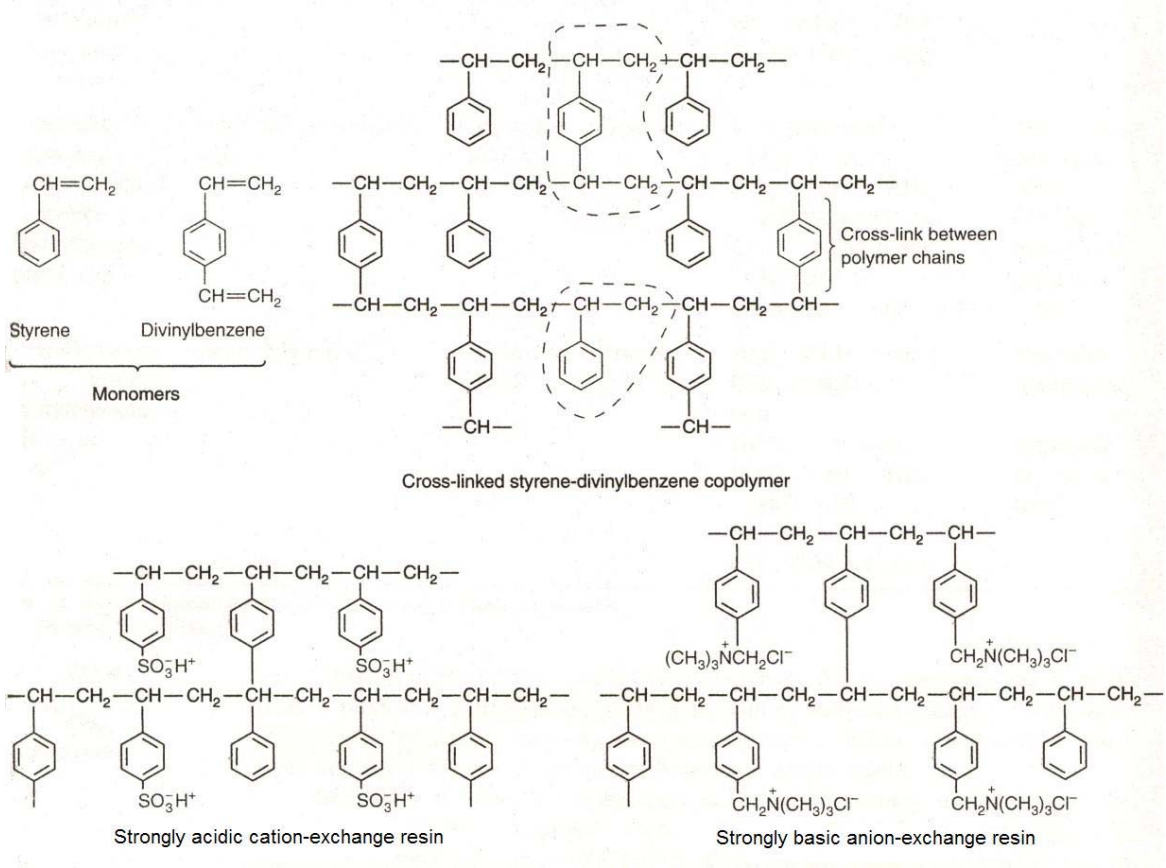

Figure 46 – Structure of styrene-divinylbenzene cross-linked ion exchange resin [source: Harris, 2003]

The particular type of ion chromatography applied in this work is called **suppressed-ion anion and cation chromatography**. The most important feature of this type of ion chromatography is the removal of unwanted electrolyte prior to conductivity detection. The mode of operation is illustrated in figure 47. In both cases in figure 47 (anion and cation chromatography) the solute peaks are obscured by the high conductivity of the eluent species (KOH, HCl). To solve this problem the solution is passed through a suppressor, in which cations are replaced by H^+ (anion chromatography) and anions by OH^- (cation chromatography), to produce a low conductivity species (Harris, 2003).

The **conductivity detector** detects sample ions based on their ability to conduct electricity. The sample and mobile phase pass between two electrodes, a conductivity cell. An electrical potential is established across the electrodes and the detector measures the energy necessary to move the different sample components and mobile phase through the electric field. A microprocessor analyses that

information and generates a chromatogram. Peak size and **retention time** (time it takes for the individual ion to eluate from the column) help identify the sample ions (Library for Science).

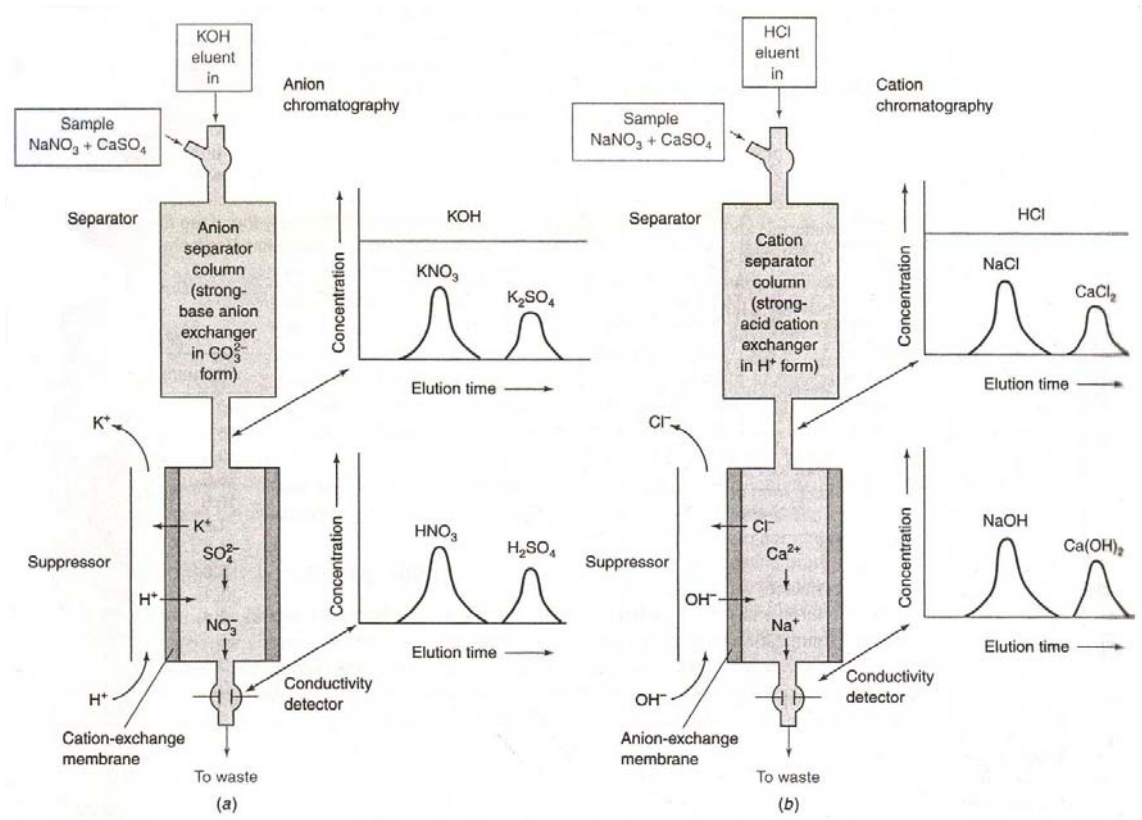

Figure 47 – Schematic of suppressed anion and cation chromatography [source: Harris, 2003]

4.5.2 Sample Preparation

The ion chromatography was applied for the analysis of aqueous samples of the common anions – fluoride [$\mathbf{F^-}$], chloride [$\mathbf{Cl^-}$], nitrate [$\mathbf{NO_3^-}$] and sulphate [$\mathbf{SO_4^{2-}}$] – as well as the common cations – sodium [$\mathbf{Na^+}$], potassium [$\mathbf{K^+}$], ammonium [$\mathbf{NH_4^+}$] and calcium [$\mathbf{Ca^{2+}}$].

In order to perform ion chromatographic analysis and to still have enough sample left for the carbonaceous matter determination, the quartz filter samples from Taiyuan needed to be cut reproducibly into two parts. This was done in a custom-made cutting mould with a scalpel (see figure 48). The diameter of the

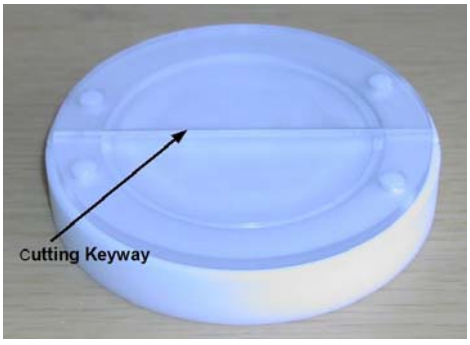

Figure 48 – Quartz filter cutting mould [picture mine]

mould was 90mm, yet due to the shrinkage of the quartz filters after pre-heating, it was not feasible to cut them exactly into half. Instead the filters were 'reproducibly' cut into a smaller and a larger part and the particle load on each piece was determined by measuring the exposed filter areas and under the assumption of a homogeneous particle loading. Calculating the average weight of the pieces is not useful as according to the manufacturer of the quartz filters, Pall Life Sciences, the weight distribution of the empty quartz filters, in g/cm², is not homogeneous, and the weight of each filter is rather variable. The filters were dried in a desiccator for 24h prior to cutting. The smaller half was then cut into small pieces with a pre-cleaned (ethanol) scissor and put into 100ml PP bottles for further treatment.
The Taiyuan quartz filter samples as well as 7 different amounts of SRM1648 in 100ml PP bottles were then **water extracted** and prepared for ion chromatography according to the following procedure, which was provided by Judy Chow and Steve Kohl from the Desert Research Institute (DRI), in Reno, USA:

1. To each sample, blank and SRM1648 were added 40ml of type 1 water with a pre-calibrated, 2-10ml automatic pipette. The amounts of SRM1648 used and the **total amount** of particles on the **whole** quartz filter are summarised in table 14.

Table 14 – Amount of SRM1648 for IC and total amount of particles collected on quartz filters

Standard Reference Material 1648							
Name	ICSRM1	ICSRM2	ICSRM3	ICSRM4	ICSRM5	ICSRM6	ICSRM7
Mass [mg]	1.8	7.0	3.5	5.3	7.8	8.5	11.5
Quartz Filter Samples - Taiyuan							
Name	Q1	Q3	Q5	Q7	Q9	Q11	Q13
Mass [mg]	30.0	12.9	14.9	19.7	10.9	6.8	5.0
Name	Q15	Q17	Q19	Q21	Q23		
Mass [mg]	7.8	7.9	9.2	10.4	6.9		

2. All bottles with analytes were immersed in water in an **ultrasound bath** [Branson 5510] (figure 49) for 60min at a temperature of about (19±2)°C. When the temperature was approaching 20°C, ice was added to bring it down to approximately 17°C.

Figure 49 – Ultrasound treatment [picture mine]

3. Each bottle was afterwards rigorously **shaken** for 100 times. According to Steve Kohl (DRI), the 60min treatment of the samples using a shaker did not significantly alter the extraction results.

4. In the **first filtration step**, each solution was passed through a 0.45μm particle filter with the aid of sterile 10ml syringes and pre-rinsed pieces of Teflon tubing. The solutions were slowly pressed through the filter which removed all larger particles. Each filter was only used for one individual sample and then discarded.

5. In the **second filtration step**, a Maxi-Clean IC-RP cartridge was applied to filter out hydrophobic components which may otherwise damage the ion chromatograph. Each cartridge was used several times, due to its high prize, yet was cleaned with 10ml of a 62mmol/l solution of methanesulfonic acid in between samples. The acid and concentration were selected because it is the mobile phase of the IC and there reaches a maximum concentration of 50mmol/l. The corresponding calculations can be found in appendix F-2.

All filtrated solutions were stored in a refrigerator until IC analysis.
Based on the results of preliminary, crude IC analysis of the SRM and samples, various concentration ranges for the standards have been selected both for the determination of anions as well as cations. **External standard calibration** was carried out due to the inferior effect of the matrix in IC and type 1 water was used at all times. The standards were prepared in different ways for cations than for anions.

Table 15 – Amounts of salts weighed into 1l glass flask for anion standards

Salts	Molar Mass of Salts in g/mol	Desired Concentration in μmol/l	Required Amount for Desired Concentration in g	Actual Amount Added in g	Actual Concentration in μmol/l*
NaF	41.99	8000	0.3360	0.3366	**8017**
NaCl	58.44	8000	0.4676	0.4769	**8160**
$NaNO_3$	84.99	16000	1.3600	1.3714	**16135**
Na_2SO_4	142.0	16000	2.2726	2.2061	**15531**

*) Concentration calculated by dividing the amount (in μg) in 1l by the molar mass of each salt

Cation standards were made from already available stock solutions, while the salts of the respective anions needed to be dried in the oven [Termaks® (max 250°C)] at 110°C for 2h, stored in a desiccator prior to use and transferred into 1l glass flasks in the adequate amounts [Sartorius® balance – 0.1mg] given in table 15.
The concentrations of the stock solutions from table 15 can be expressed in mg/l (ppm) by multiplying the actual amount added with the molar mass of the anion (i.e. F^-, Cl^-, NO_3^- and SO_4^{2-}) and dividing the result by 1000. The different standard concentrations for the individual ions are summarised in table 16 and the associated calculations are outlined in appendix F-2. The figures of the anion standards in table 16 are given this way because they were converted from μmol/l concentrations to mg/l. The original units used can also be found in appendix F-2.

Table 16 – External standard concentrations for IC

Anions – SRM1648				
Standards in mg/l	**F^-**	**Cl^-**	**NO_3^-**	**SO_4^{2-}**
Std 1	0.0190	0.181	0.625	9.32
Std 2	0.0952	0.362	1.88	28.0
Std 3	0.190	1.08	3.13	46.6
Std 4	0.286	1.81	5.00	55.9
Taiyuan Samples				
Std 1	0.0952	1.81	0.625	4.66
Std 2	0.190	5.42	2.50	9.32
Std 3	0.571	9.04	5.00	18.6
Std 4	0.952	14.5	7.50	28.0
Cations – SRM1648 and Taiyuan Samples				
Standards in mg/l	**Na^+**	**K^+**	**NH_4^+**	**Ca^{2+}**
Std 1	0.200	0.0100	0.500	1.00
Std 2	0.500	0.0500	1.00	5.00
Std 3	1.00	0.100	5.00	10.0
Std 4	4.00	0.300	10.0	15.0

4.5.3 IC Analysis

The above mentioned anions and cations were determined via the Dionex ICS-2000 ion chromatograph depicted in figure 50. It is the first totally integrated reagent free IC (RFIC) with an eluent generator for automated eluent delivery utilising a Dionex Elu-Gen® cartridge

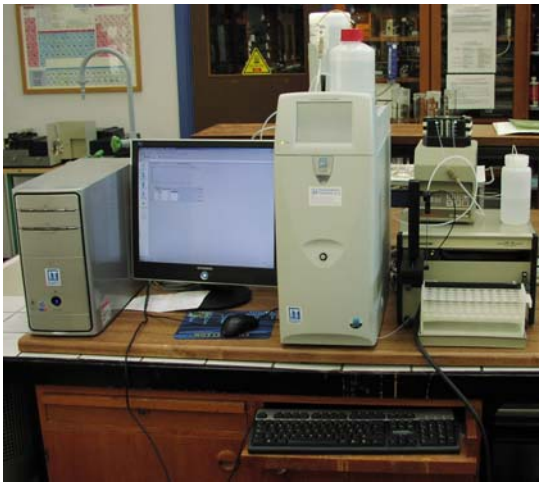

Figure 50 – Ion Chromatograph used for analysis [picture mine]

with methanesulfonic acid as the mobile phase. The standards, SRMs and samples are transferred into 5ml scintillation bottles and taken up by the instrument via a Gilson® auto-sampler. Sample and mobile phase pass through a guard column (particle filter to protect main column) and anion or cation exchange column [**types**: *anions* – Ion Pack AG18 3x50mm (guard), Ion Pack AS18 3x250mm anion exchanger (functionalised with quaternary ammonium groups ($-CH_2NR_3^+$) → strongly basic anion exchanger; *cations* – Ion Pack CG16 3x50mm (guard), Ion Pack CS16 3x250mm cation exchanger (functionalised with carboxylic acid groups ($-CO_2^-$) → weakly acidic cation exchanger)]. Prior to detection of the ionic species in the conductivity detector the solution passes through a Dionex CSRS Ultra II suppressor. With the aid of the Chromeleon® software, a gradient elution procedure and manufacturer compiled methods, defining important analysis parameters, are applied. The contents are shown in appendix F-3 and F-4. The computer software determines the total areas of the emerging ion peaks and by comparison with the results from the external standards generates the corresponding concentrations in the SRMs and samples.

4.6 Thermal/Optical Carbon Analysis

In order to determine the bulk organic and elemental carbon (OC/EC) compositions and ratios of atmospheric particulate matter collected on quartz fibre filters, the thermal/optical carbon analysis technique was carried out at the Norwegian Institute for Air Research (NILU).

4.6.1 Theory, Components and Function

The OC/EC fractions of the PM are measured via a thermal/optical carbon analyser (**TOA**) depicted in figure 51. This technique generally applies a temperature protocol to liberate carbonaceous material collected on the quartz filter pieces inserted and utilises optical and flame ionisation detection to determine type and quantity of the carbonaceous material.

A standard sized punch of 1.5cm² is taken from the quartz filter sample and put inside the quartz oven of the TOA. After purging the oven with helium (He), a stepped temperature ramp increases the temperature according to the settings of the used protocol to 870°C. This thermally desorbs the organic compounds and pyrolysis

products into a manganese dioxide (MnO_2) oxidising oven, where the carbon fragments are quantitatively converted to CO_2 gas. The helium stream transports the CO_2 gas out of the oxidising oven where it is mixed with hydrogen gas (H_2). The mixture then passes through a heated nickel catalyst where it is quantitatively converted to methane (CH_4). The generated methane is measured in the flame

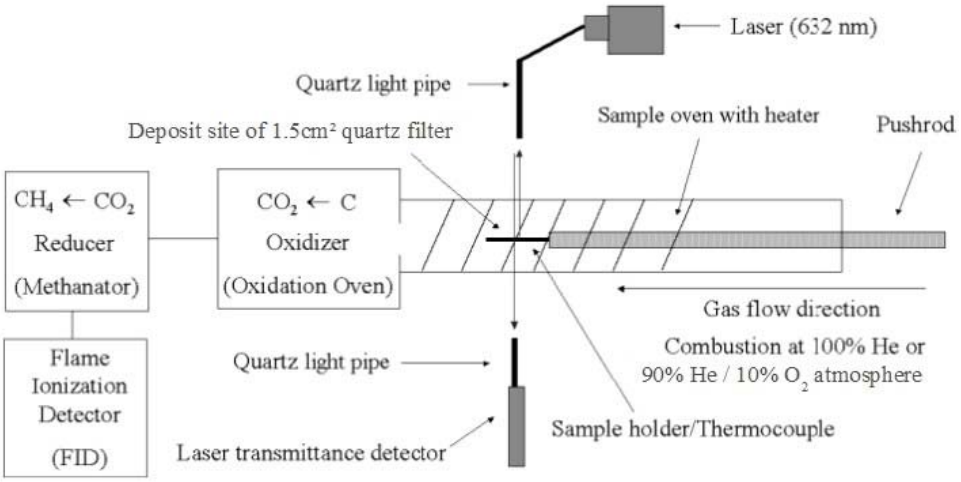

Figure 51 – Sketch of thermal/optical carbon analyser [source: adapted from Chow et al., 2004]

ionisation detector (FID). After the initial temperature ramp is completed the flow stream is switched to an oxidising helium/oxygen (90%/10%) carrier gas mixture. A second temperature ramp is initiated in this modified atmosphere and any elemental carbon and pyrolysed organic carbon is oxidised off the filter and detected in the same manner as mentioned above.

The overall method is characterised by three characteristic components determining its strength: **(1)** the optical detection and correction for elemental carbon, which is a strong absorber of light, especially in the red and infrared region, and pyrolised organic carbon, is done by incorporating a red light laser (He-Ne laser at 632.8nm). The laser beam passes through the filter that rests on the sample platform. The initial absorbance is recorded and monitored along the entire temperature program. Any charring of the organic carbon in the PM (**pyrolysis**) causes the laser transmittance to decrease (increase in absorbance) and the signal to fall. After changing from the helium to the He/O_2 atmosphere, all elemental and pyrolysed carbon is oxidised off (at sufficiently high temperatures, e.g. >350°C (Chow et al., 2004)) and the laser absorbance is eventually reduced to the background level.

The point in the laser monitoring protocol during oxidation, where the absorbance has returned to the initial value, is called the **split point**. All elemental carbon formed before this point is subtracted and termed pyrolytically formed elemental carbon, hence added to the organic carbon fraction. This correction method assumes equal absorption coefficients of elemental carbon and pyrolytically formed elemental carbon, which has proven to be satisfactory. Furthermore, it is assumed that charred organic carbon evolves before the original elemental carbon during oxidation.
(2) The FID has a very good sensitivity (10^{-12}g/s range) and a wide linear range (5-6 orders of magnitude) [detection limit ≈ 10cm³/m³, 10ppm].
(3) Finally, the incorporation of a fixed volume loop, used to inject an external standard at the end of every analysis, is another great advantage of this technique. The data acquired from the external standard is included in every data package and used along with the known carbon concentration in the loop to calculate the analytical results. This procedure results in a very stable, repeatable analytical method (Sunset Laboratory, 2000).

4.6.2 Protocols for Thermal/Optical Carbon Analysis

Unfortunately, matters are not very clear and unambiguous when it comes to the choice of any suitable and universally recognised protocol of analysis on the TOA. The most critical quantity prone to changes in any parameter is the split-point and associated EC/OC ratio in the sample analysed.
Methodological differences between OC and EC vary as a function of the **nature of the samples**, the **analysis protocol** and the applied **instrumentation**. Analysis protocols and instrumentation in turn vary with (a) temperature plateaus, (b) residence time at each plateau, (c) charring correction by light reflectance or transmittance, (d) optical monitoring configuration and wavelength, (e) combustion atmospheres, (f) temperature ramping rates, (g) carrier gas flow through or across the sample, (h) oven flush, (i) sample aliquot and size, (j) location of the temperature monitor relative to the sample, (k) oxidation and reduction catalysts, (l) evolved carbon detection method and (m) calibration standards. Moreover, different samples may react differently with various analysis protocols, thus giving rise to changes in the results. Sample biases include (a) non-uniform particle deposit on the filter, (b) particle deposits being too light or too dark, impairing charring correction, (c) organic vapour filter absorption and its charring during heating, (d) catalytic and oxidation

interactions between OC, EC and non-carbonaceous material in the sampled PM, and (e) changes in optical properties of the particles during thermal evolution (Chow et al., 2004).

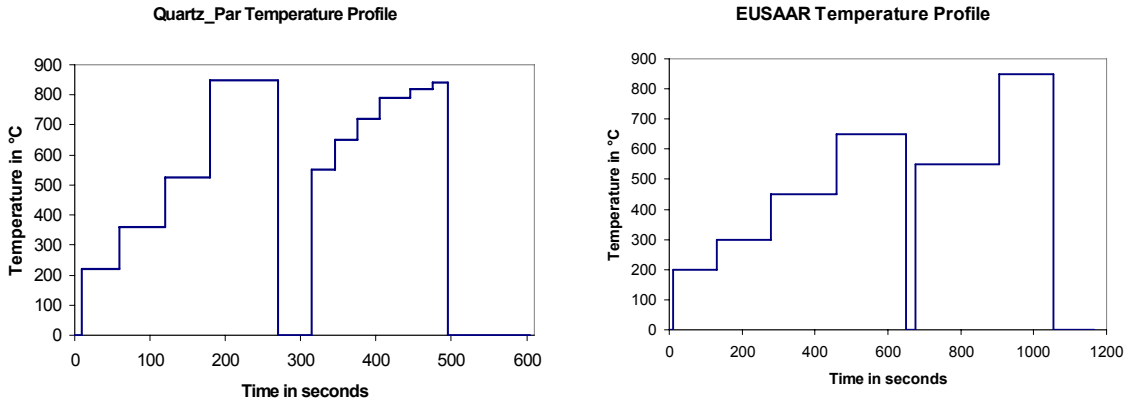

Figure 52 – Two analysis profiles applied; (left) NIOSH derived and (right) JRC-IMPROVE [source: NILU]

Two very well known and widely applied protocols are the **IMPROVE** (Interagency Monitoring of Protected Visual Environments) and the **NIOSH** (National Institute of Occupational Safety and Health). Chow et al. (2001) supplies ample information on the structure and contents of these protocols. During the analysis at NILU, two somewhat different analysis protocols were applied and their individual temperature-time characteristics are illustrated in figure 52. The one closely associated with the NIOSH protocol is called **quartz_par** or **NIOSH-derived**, while the other (new) analysis protocol is called **EUSAAR** or **JRC-IMPROVE** (Joint Research Centre) due to its derivation from the IMPROVE protocol. The exact protocols can be found in appendix G-1.

4.6.3 TOA Analytical Practise

Analysis of the carbonaceous fraction of the PM was carried out on a Sunset Laboratory OCEC carbon aerosol analyser (model 3) at NILU (see figure 53). Operation of the instrument is not too complicated and only few initial steps are necessary prior to analysis. The first of those is opening the individual gas valves and to adjust the gas flows according to the required ranges shown in table 17. After the air and hydrogen (H_2) gas valves were opened, the FID was ignited with a lighter. Two punches of 1.5cm² each were collected from empty quartz filters and run

through the quartz_par program for cleaning. One or both of the punches, depending on the carbon concentration range in the samples, are then used for carbon standardisation. For this purpose 20µl (automatic pipette) of several already prepared sucrose solutions of the concentrations 6.66µgC/20µl, 26.6µgC/20µl and 53.3µgC/20µl were used wherever suitable. These carbon standards served as a check-up of the instrument's performance and at the end of each analysis (day), an internal instrument parameter was adjusted, in order to match the external standardisation, done by the instrument, with the sucrose standard.

Table 17 – Gas settings at the TOA

Gas Type	Flow Rate Range in cm³/min
Air	280 – 300
H_2	55 – 60
He 1	54 – 58
He 2	12 – 15
He 3	67 – 70
He/O_2	12 – 15
Calib. Gas	10 – 15

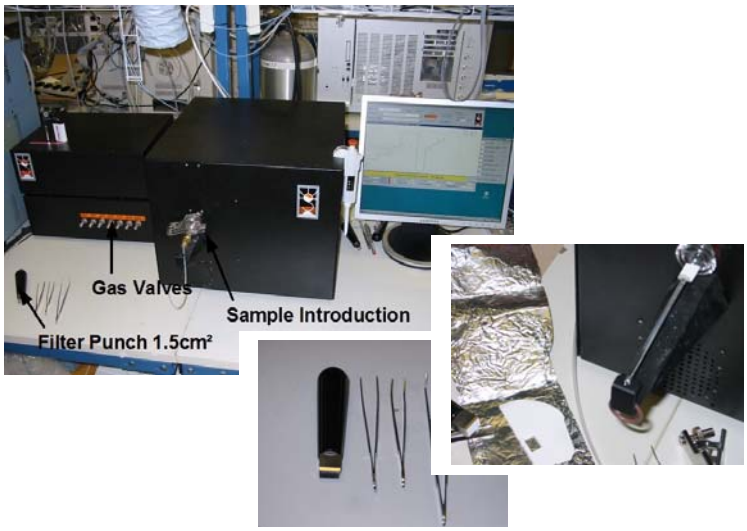

Figure 53 – TOA [picture mine]

Furthermore, the instrumental drift was determined by measuring the carbon standard again at the end of each analysis. Drifting up to ±10% was accepted.

The thermogram depicted in figure 54 serves as an example for the purpose of illustrating the different carbon fractions and their definitions.

The NIOSH protocol was used to generate the thermogram but the basic underlying principles are applicable to both of the protocols utilised in this work. The manner of assigning the evolution peaks to the carbon fractions has been discussed

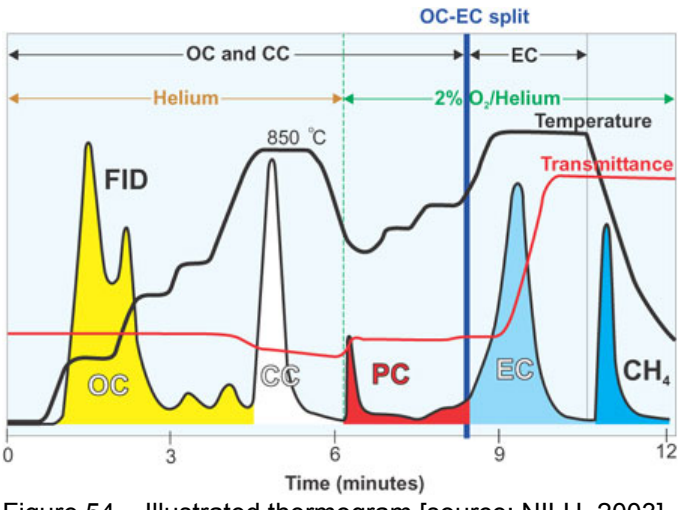

Figure 54 – Illustrated thermogram [source: NILU, 2003]

above. The methane (CH_4) peak is introduced by the internal calibration system and hence calibrates the FID. The carbonate carbon (CC) has not been considered in any of the analyses as its contribution was known to be insignificant (Yttri, pers. comm.). Thus peaks obtained during the 850°C temperature step in the quartz_par protocol were assigned to the OC fraction. The 12 thermograms from the actual Taiyuan samples can be found in the appendix K-2.

The TOA analysis was divided into three different parts:

1. The analysis protocol EUSAAR was tested on 52 $PM_{2.5}$ samples collected every week, for 24 hours, over the duration of one year (2005).
   The samples were collected at the rural site Birkenes [Aust-Agder county, southernmost Norway]. The results were then compared with data from the quartz_par protocol of the same samples.
2. In the second part a treatment of **positive artefacts** on the quartz filters was evaluated. Artefacts arise either from the adsorption of organic vapour (positive) or the evaporation of particle-bound organic compounds (negative). In order to determine the amount of positive artefacts a second quartz filter (**backup filter**) (collecting only OC_g) is arranged in series to the "main" sampling filter (collecting $OC_p + OC_g$). The gaseous fraction should equilibrate on both filters and can be accounted for by subtracting the organic fractions from each other ($OC_g + OC_p – OC_g = OC_p$) [p:particle; g:gas]. Backup filters were collected for three different size fractions (PM_1, $PM_{2.5}$ and PM_{10}) at the same site and time and at the same **filter face velocity** [airflow/exposed surface area of filter, in cm/s]. The theory was tested that the gaseous organic carbon content on the backup filters of all size fractions may yield similar results. Consequently, the analysis of merely one size fraction could suffice. The quartz_par protocol was used to analyse 13 day samples (collected from 9am till 9pm) of both PM_1 and $PM_{2.5}$ size fractions, from the 20th of June until the 4th of July 2006, at an urban site (Oslo), and 13 day samples of PM_1 and PM_{10} size fractions, collected over the same period of time at Hurdal [Akershus county], a rural site.
3. Finally, the Taiyuan samples were analysed using the quartz_par protocol.

5.0 Results and Discussion

The data obtained from the applied analytical techniques with regard of the atmospheric concentrations of each investigated PM component are presented and evaluated in this chapter.

5.1 Method Validation – Recoveries and Uncertainties

In order to determine the effectivity of the sample preparation procedure it is necessary to test the applied method against the expected results yielded from the analysis of the SRM1648.

5.1.1 ICP-MS and ICP-AES Analysis

Any method is only as good as the recovery of the known SRM constituents indicates. For ICP-MS and AES analysis the same sample preparation method was used (as described in the previous chapter) and the yielded recoveries (mean values and standard deviations of 7 replicates) are presented in figure 55. The data and calculations can be found in appendix H and appendix I. The elements calcium and silicon are not included as no certified NIST values were available.

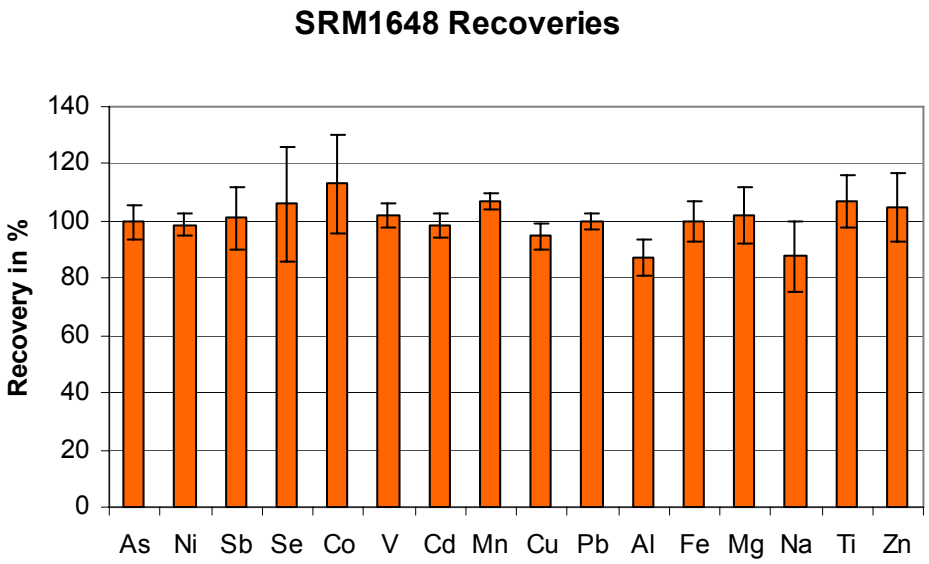

Figure 55 – SRM1648 recoveries for analysed by ICP-MS and ICP-AES analysis (error bars indicate the 95% confidence interval); Al, Fe, Mg, Na, Ti and Zn were analysed by ICP-AES, all other by ICP-MS

The values of the means, standard deviations and 95% confidence intervals can be found in the tables H-4 (ICP-MS) and I-4 (ICP-AES) in the appendix. Overall, the accuracy (proximity to the NIST reference value – here to 100%) and precision (standard deviation) of the method and detection techniques seem to be fairly good. Furthermore, the 95% confidence intervals (c.i.) include the reference value (100%) in all cases except for Al and Mn, an indication of satisfactory sample preparation. It was not possible to carry out a significance test between the means of the measured recoveries and the certified NIST means (t-test to check the probability of the zero hypothesis that both means are equal) because the number of replicates used to arrive at the NIST values was not provided.

The **maximum errors** of the atmospheric mass concentrations for each individual Taiyuan sample and element were calculated with aid of the following formula (Kuchling, 1999) and the results are summarised in tables 18 and 19.

$$\Delta c_a = \left(\left|\frac{\partial c_a}{\partial c_s}\cdot\Delta\bar{c}_s\right|\right)+\left(\left|\frac{\partial c_a}{\partial V_s}\cdot\Delta V_s\right|\right)+\left(\left|\frac{\partial c_a}{\partial t}\cdot\Delta t\right|\right) \quad with \quad c_a=\frac{c_s\cdot V_s}{\dot{V}\cdot t}$$

$$\Leftrightarrow \Delta c_a = \left(\left|\frac{V_s}{\dot{V}\cdot t}\cdot\Delta\bar{c}_s\right|\right)+\left(\left|\frac{c_s}{\dot{V}\cdot t}\cdot\Delta V_s\right|\right)+\left(\left|\frac{-c_s\cdot V_s}{\dot{V}\cdot t^2}\cdot\Delta t\right|\right)$$

Δc_a: maximal error of the atmospheric mass concentration

$\Delta\bar{c}_s$: 95% c.i. of mean of the solution concentration (tables H-4 and I-4)

ΔV_s: ±0.001l – estimated error of the decomposition solution volume

Δt: ±1min – estimated error of sampling time

$\dot{V}$: volume flow of the pumps (0.1m³/min)

t: sampling time (see table 2 – Teflon)

c_a: atmospheric mass concentration (tables H-7 and I-7 in the appendix)

c_s: element concentration in solution (table H-5 and I-5 in appendix)

V_s: decomposition volume (0.060l);

The maximum errors in the tables 18 and 19 are relative maximum errors ($\Delta c_a/c_a\cdot 100$ in %) of the measured atmospheric mass concentrations determined from the Taiyuan samples. The values can be found in tables H-7 and I-7 in the appendix. Since no certified NIST values for Si and Ca were available, the $\Delta\bar{c}_s$ value was estimated from the variance of the calibration graph, applying the formula:

$$s^2 = \frac{\sum_{i=1}^{n}(y_i - \hat{y}_i)^2}{n-2}$$ with s^2: variance; y_i: observed values; $\hat{y}_i$: predicted values from calibration graph; n-2 degrees of freedom (4);

This may be an underestimation of the actual error of the solution concentrations of Si and Ca in the samples. An estimated error of $\dot{V}$ was not included, as it was compensated for by a larger estimated error of t. The pumps were running very smoothly at nearly constant flow rate. Nevertheless, it took a little bit of time to reach the set value during start-up.

Table 18 – Relative maximum errors of atmospheric mass concentrations in % (ICP-MS)

Samples	As	Ni	Sb	Se	Co	V	Cd	Mn	Cu	Pb
T51	8	6	14	23	20	8	7	6	7	5
T53	8	5	14	23	20	8	7	5	7	7
T55	8	7	17	22	20	10	6	7	7	5
T57	9	7	18	23	20	8	10	5	11	5
T59	8	6	18	24	20	6	8	5	7	6
T61	10	9	14	23	20	8	7	6	8	9
T63	11	6	14	22	20	9	8	8	7	6
T65	10	6	14	24	20	6	7	7	12	6
T67	10	6	16	23	20	10	7	6	7	6
T69	11	8	13	25	20	6	8	7	8	9
T71	10	6	14	25	19	7	7	6	7	7
T73	8	10	14	22	20	7	7	8	8	7

Table 19 – Relative maximum errors of atmospheric mass concentrations in % (ICP-AES)

Samples	Al	Fe	Mg	Na	Ti	Zn	Si	Ca
T51	13	14	13	14	18	17	5	5
T53	13	9	12	14	18	16	7	9
T55	8	8	12	17	12	17	9	11
T57	9	12	12	16	13	17	7	6
T59	11	11	13	15	14	17	9	9
T61	13	10	13	17	18	16	11	19
T63	9	10	14	18	13	17	23	21
T65	8	10	13	19	18	17	14	11
T67	8	9	12	16	11	18	10	10
T69	10	13	12	14	13	13	7	11
T71	11	14	13	15	15	18	8	8
T73	10	10	14	14	12	15	11	12

Moreover, the limits of detection (**LOD**) and the method limits of detection (**MDL**) (see appendix H-1 for definitions) were calculated and can be found in the tables H-2 and I-2 in the appendix. The frequently stated requirement that the concentration of an element should be around 100 times above the LOD (Boss and Fredeen, 2004), to ensure accurate quantification, was not fulfilled for all samples due to the large differences in collected PM.

5.1.2 IC Analysis

No certified NIST values were available for the ions analysed via ion chromatography. Hence, no definite statements with regard to accuracy can be made. Nevertheless, the precision of the water extraction method and successive IC measurements was determined by analysing seven different amounts of SRM1648 (table 14) and calculating the standard deviation and 95% confidence interval. The results are shown in table J-18 in the appendix. The relative standard deviations are quite large, especially for sodium (55%), which may have its origin in an often observed sodium contamination of quartz fibre filters (Yttri, pers. comm.).
For all further considerations, only the three most important ions, in terms of detected quantity and environmental importance, ammonium (NH_4^+), sulphate (SO_4^{2-}) and nitrate (NO_3^-), will be dealt with.
The maximum error of the atmospheric mass concentrations (see tables J-7 and J-15) of the three mentioned ions was determined according to:

$$\Delta c_{a-IC} = \left(\left|\frac{\partial c_{a-IC}}{\partial c_{s-IC}} \cdot \Delta \bar{c}_{s-IC}\right|\right) + \left(\left|\frac{\partial c_{a-IC}}{\partial V_{s-IC}} \cdot \Delta V_{s-IC}\right|\right) + \left(\left|\frac{\partial c_{a-IC}}{\partial m_{tot}} \cdot \Delta m_{tot}\right|\right) + \left(\left|\frac{\partial c_{a-IC}}{\partial m_s} \cdot \Delta m_s\right|\right) + \left(\left|\frac{\partial c_{a-IC}}{\partial t} \cdot \Delta t\right|\right)$$

$$with \quad c_{a-IC} = \frac{c_{s-IC} \cdot V_{s-IC} \cdot m_{tot}}{\dot{V} \cdot t \cdot m_s}$$

$$\Leftrightarrow \Delta c_{a-IC} = \left(\left|\frac{V_{s-IC} \cdot m_{tot}}{\dot{V} \cdot t \cdot m_s} \cdot \Delta \bar{c}_{s-IC}\right|\right) + \left(\left|\frac{c_{s-IC} \cdot m_{tot}}{\dot{V} \cdot t \cdot m_s} \cdot \Delta V_{s-IC}\right|\right) + \left(\left|\frac{c_{s-IC} \cdot V_{s-IC}}{\dot{V} \cdot t \cdot m_s} \cdot \Delta m_{tot}\right|\right) + \left(\left|\frac{-c_{s-IC} \cdot V_{s-IC} \cdot m_{tot}}{\dot{V} \cdot t \cdot m_s^2} \cdot \Delta m_s\right|\right) + \left(\left|\frac{-c_{s-IC} \cdot V_{s-IC} \cdot m_{tot}}{\dot{V} \cdot t^2 \cdot m_s} \cdot \Delta t\right|\right)$$

$\Delta c_{a\text{-}IC}$: maximum error of atmospheric mass concentration of the ions

$\Delta \bar{c}_{s-IC}$: 95% c.i. of the concentrations of the ions in solution (table J-18)

$\Delta V_{s\text{-}IC}$: ±0.001l

Δm_{tot}: ±0.5mg – estimated error of total mass of PM on quartz filters

Δm_s: ±1mg – estim. error of the mass of PM on the small quartz filter pieces

$c_{s\text{-}IC}$: solution concentration of ions (see tables J-4 and J-11 in appendix)

$V_{s\text{-}IC}$: solution volume of water extraction (0.040l)

$\dot{V}$: volume flow (0.1m³/min)

t: sampling time (see table 2 – Quartz); Δt: ±1min

m_{tot}: total mass of PM on the quartz filters (table J-17)

m_s: mass of PM on small quartz filter pieces (table J-17)

The relative $\Delta c_{a\text{-}IC}$ values are shown in table 20.

Table 20 – Relative maximum errors of the ionic atmospheric mass concentrations in %

Samples	NH_4^+	SO_4^{2-}	NO_3^-
Q1	30	30	45
Q3	34	46	57
Q5	40	39	54
Q7	31	32	52
Q9	38	42	61
Q11	53	58	74
Q13	67	71	92
Q15	48	53	69
Q17	47	53	69
Q19	41	47	65
Q21	42	44	62
Q23	51	58	73

As can be seen from table 20, the relative maximum errors are very large. The reason for this is to a large part due to the cutting of the quartz filters, bearing large uncertainties in the determination of PM masses on each of the cut pieces. Appendix J-3 contains the associated calculations of the filter areas and masses. Since the masses were calculated from the exposed filter areas, the arbitrarily estimated values of Δm_{tot} and Δm_s, which may be even larger, will be the same for filters with both small and large amounts of PM, since the amount of collected PM on the same filter area varies for different sampling days. Furthermore, the term containing Δm_s in the maximum error formula has the largest impact. As a consequence, it seems to be rather advantageous to not cut the filters, both to reduce potential contaminations and to lower the maximum error.

5.1.3 Thermal/Optical Carbon Analysis

Maximum error considerations of the atmospheric mass concentrations of organic and elemental carbon were based on the following calculation:

$$\Delta c_{a-TOA} = \left(\left|\frac{\partial c_{a-TOA}}{\partial c_A}\cdot \Delta c_A\right|\right) + \left(\left|\frac{\partial c_{a-TOA}}{\partial A_{Tot}}\cdot \Delta A_{Tot}\right|\right) + \left(\left|\frac{\partial c_{a-TOA}}{\partial t}\cdot \Delta t\right|\right)$$

$$with \quad c_{a-TOA} = \frac{c_A \cdot A_{Tot}}{\dot{V}\cdot t}$$

$$\Leftrightarrow \Delta c_{a-TOA} = \left(\left|\frac{A_{Tot}}{\dot{V}\cdot t}\cdot \Delta c_A\right|\right) + \left(\left|\frac{c_A}{\dot{V}\cdot t}\cdot \Delta A_{Tot}\right|\right) + \left(\left|\frac{-c_A \cdot A_{Tot}}{\dot{V}\cdot t^2}\cdot \Delta t\right|\right)$$

$\Delta c_{a\text{-}TOA}$: maximum error of the OC, EC atmos. mass concentrations

Δc_A: ±5% – estimated error of the OC, EC mass per cm² filter area

ΔA_{Tot}: ±0.2cm² - estimated error of the total exposed quartz filter area

t: sampling time (see table 2 – Quartz); Δt: ±1min

$c_{a\text{-}TOA}$: atmospheric mass concentrations of OC, EC (see table K-3)

c_A: measured mass of OC, EC per cm² filter area (see table K-1)

A_{Tot}: total area of exposed quartz filter (table J-17)

$\dot{V}$: volume flow (0.1m³/min)

The maximum error of the total carbon atmospheric mass concentration is the sum of the maximum errors of the organic and elemental carbon. The 5% estimated error of Δc_a was half of the monitored instrumental drift. The relative maximum errors of each sample and carbonaceous specie are shown in table 21.

Table 21 – Relative maximum errors of OC, EC and TC in %

Samples	OC	EC	TC
Q1	6	6	6
Q3	6	6	6
Q5	6	6	6
Q7	6	6	6
Q9	6	6	6
Q11	6	6	6
Q13	6	6	6
Q15	6	6	6
Q17	6	6	6
Q19	6	6	6
Q21	6	6	6
Q23	6	6	6

All relative errors turned out to be ±6% of the measured atmospheric mass concentrations, as they are expressed with no decimal places. They seem to be comparatively small and perhaps too optimistic. Nevertheless, the errors are not directly influenced by the cutting of the filters.

5.2 Atmospheric Mass Concentrations and PM Composition of Taiyuan Samples

The atmospheric mass concentrations of bulk PM_{10} and all analysed components of the Taiyuan samples, as well as the compositional breakdown (mass closure) of the Taiyuan PM_{10}, are depicted in the following figures. As illustrated in figure 56, the two different filters show the same daily fluctuations along the graph but differ somewhat in the total amount of PM collected per day.

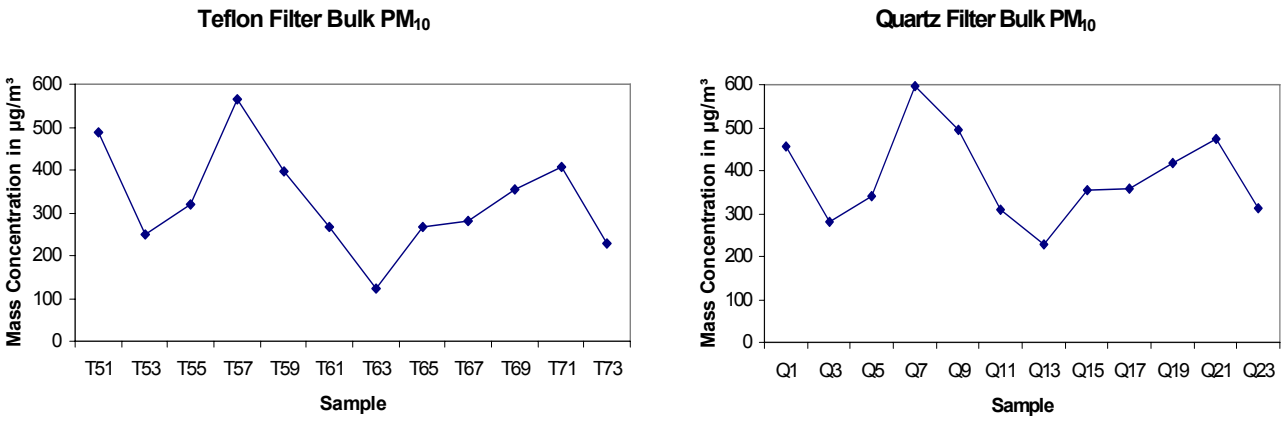

Figure 56 – Bulk PM_{10} atmospheric mass concentrations collected with Teflon and quartz filters

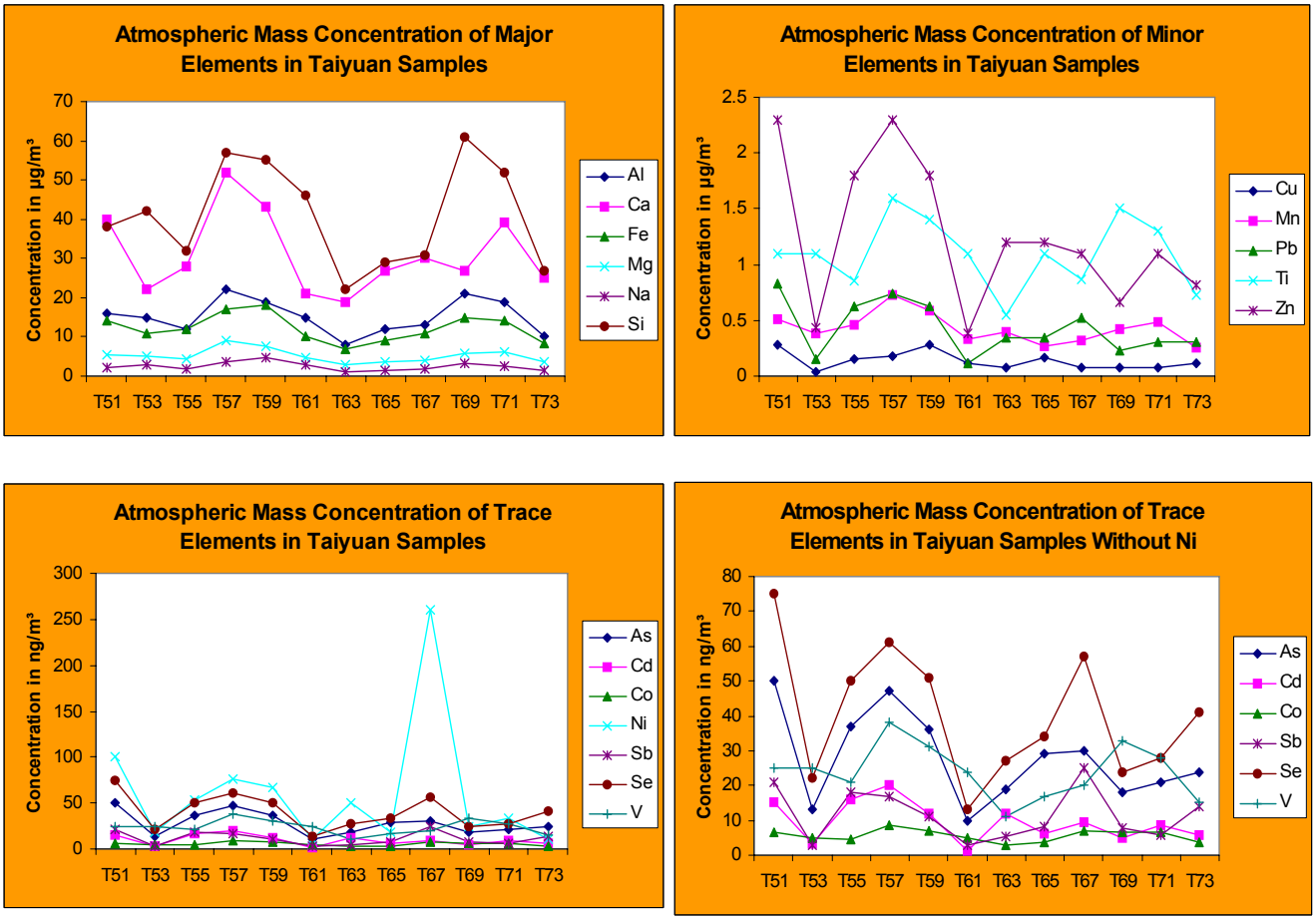

Figure 57 – Atmospheric mass concentrations of major, minor and trace elements

The mass concentrations were in general higher for the quartz filters (see table L-1 in the appendix). The atmospheric concentrations of the analysed elements are illustrated in figure 57 for each of the 12 sampling days (find data in tables H-7 and I-7 in the appendix). The elements are categorised into major, minor and trace elements according to their analysed concentrations in the Taiyuan air.

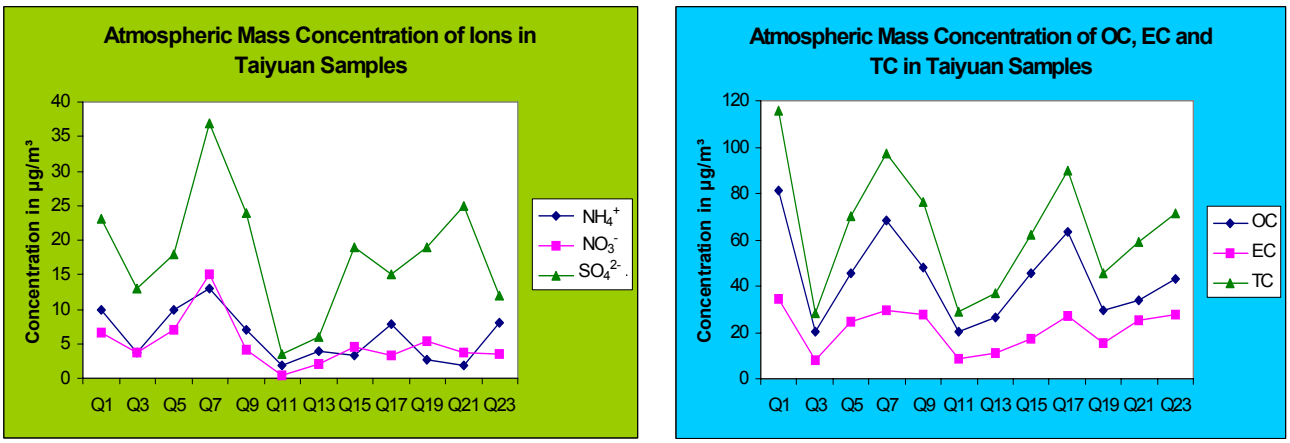

Figure 58 – Atmospheric mass concentrations of ions (left) and carbonaceous species (right)

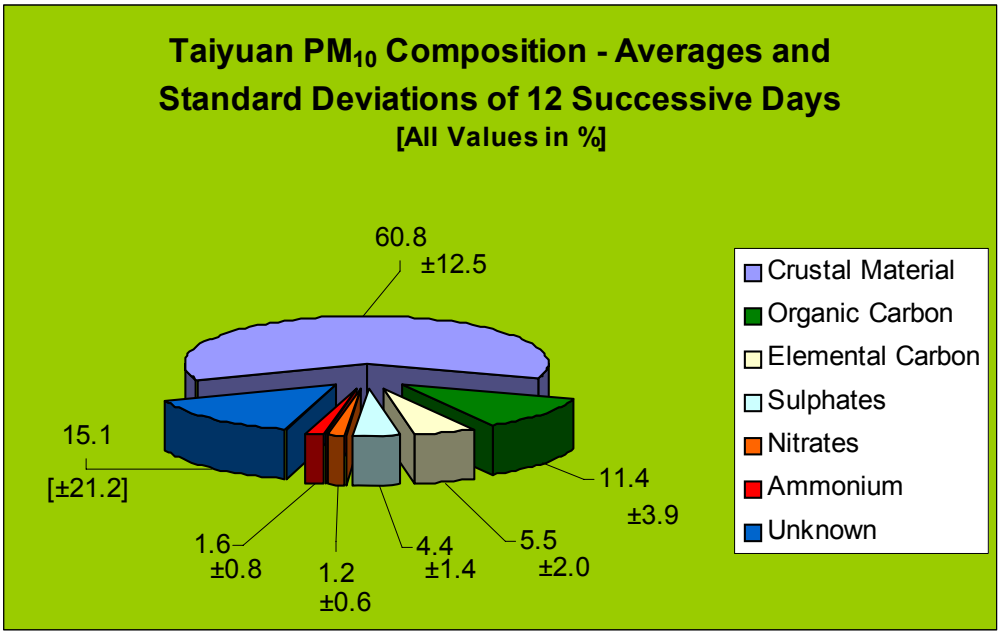

Figure 59 – Average composition of the Taiyuan PM_{10}

Figure 58 shows the variation of the atmospheric concentrations of the three most important ions and the organic species. Their data can be found in tables J-7, J-15 and K-3 in the appendix. The composition of the PM_{10} samples from Taiyuan is illustrated in figure 59 and presented as the averages and their standard deviations of the 12 days of sampling. The **crustal material** fraction was determined by choosing titanium's relative abundance in the earth's crust [0.57%] (Taylor, 1964), the actually measured amounts of Ti on the Teflon filters (m_{Ti} – table I-6), the total mass of PM_{10} on each filter (m_{PM10} – table 5) and the formula:

$$\%crustal\ Material = \frac{m_{Ti}}{m_{PM10} \cdot 0.083} \cdot 100\%,$$ averaged for all 12 sampling days.

This method ensures that not only the individual elements are included in this fraction but also elements (mostly oxygen) they are naturally bonded to, e.g. SiO_2, Al_2O_3, etc. It is important, though, that the selected reference element is to the least degree altered by anthropogenic sources and furthermore determined (ICP-MS) with reasonable accuracy and precision. All other fractions were determined by dividing their individual masses on the filters with the total masses of PM_{10} on the filters and multiplication with 100. The respective data can be found for: **organic and elemental carbon** (table K-2 and table L-1, quartz), **sulphates and nitrates** (J-6 and L-1, quartz) and **ammonium** (J-14 and L-1, quartz). The **unknown fraction** contains unanalysed elements, strongly bound water (Harrison et al., 2003) and a very large standard deviation that does not even include the maximum error of the individual components.

5.3 Discussion of Results from Taiyuan Sampling

In this chapter the obtained results from the 12 day sampling campaign in Taiyuan are investigated and discussed. However, it is important to note that several issues complicate the extraction of meaningful information. While generally the meteorological conditions (see table 22) can be used to explain variations in the atmospheric concentrations of the PM_{10}, such as the temperature and relative

Table 22 – Meteorological conditions during sampling in Taiyuan

Date	Sample Name	Highest Temp. in °C	Lowest Temp. in °C	Average Wind Speed In km/h	Wind Direction	Average Relative Humidity In %	Weather Phenomenon [no rain occurred]
17.03	Q1/T51	15.9	1	7.5	south	35	cloudy, haze
18.03	Q3/T53	11.8	2	9	south	27	sunny
19.03	Q5/T55	16.2	-3	6.5	east	32	haze
20.03	Q7/T57	18.9	4.3	6.5	west	27	haze
21.03	Q9/T59	14	2.8	6.5	south	30	cloudy, haze
22.03	Q11/T61	14.8	3.2	11.5	north	18	clear view
23.03	Q13/T63	14	1.9	7.4	east	24	light haze
24.03	Q15/T65	16.2	1	10.5	north	29	clear view
25.03	Q17/T67	18.2	-1.2	7.3	east	21	strong haze
26.03	Q19/T69	16	3.2	7.3	southwest	26	sunny
27.03	Q21/T71	16.3	3.8	13	southeast	33	“sand storm”
28.03	Q23/T73	14	-5.6	12	south	24	haze

[Data provided by the Environmental Monitoring Department of Taiyuan]

Humidity’s effect on the amount of particle bound water, particle number (particle growth increases with increasing humidity), surface area and size distribution; wind

speed, diluting the particle concentration and resuspending dust; wind direction (introducing PM from different sources) and the absence or presence of an inversion layer; these quantities do not seem to give a reasonable explanation for the variations observed.

Possible reasons are the rather unsuitable sampling location. The building is the lowest one of all surrounding structures, resulting in turbulent wind conditions and associated random fluctuations of the air masses reaching the samplers. The proximity to local dwellings and their respective chimney emissions, a massive construction site of a new university building and the thick layer of dust covering the actual sampling roof introduce such a variety of potential sources that assumptions based on the meteorological data could go into either direction. This makes it difficult to explain the sudden Ni pulse in sample T67 in figure 57, which could also be an ignorable outlier. Yet some correlations can be drawn: From table 22 it would make sense that the PM_{10} concentration on the 22nd of March would be the lowest, due to the high wind dilution, the very low humidity (smaller amount of water) and potential absence of an inversion layer, yet it is the following day the minimum is measured. Yet winds also mobilise dust, which will mostly add mass to the coarse fraction of the collected PM_{10}, thus increasing its value. It is interesting to note that the major elements and some minor and trace elements seem to at least reach the minimum on the same day as PM_{10}, while several elements (Zn, Pb, Se, Sb, As, Cd), as well as ammonium, nitrate, sulphate and the carbonaceous species, arrive at a minimum mass concentration on the 22nd of March (figures 57 and 58). A possible explanation is the impact of wind speed on the remobilisation of dust and soil, increasing the PM_{10} mass but not the mass of the mentioned exceptions. All the elements can be found in the mobilised dust and if none of them were enriched in their concentrations (see next chapter) all should ideally follow the PM_{10} minimum. Yet, as it turns out, the elements Zn, Pb, Se, Sb, As and Cd are significantly enriched by anthropogenic sources and are thus not coming from the mobilised dust but are rather found in the accumulation mode (see table 1), together with ammonium, sulphate, nitrate, OC and EC. As a result, the dilution effect of the wind and the minimum in relative humidity control their mass concentration.

5.3.1 Aerosol-Crust Enrichment Factors (EF)

The aerosol-crust enrichment factor (EF) of any element (X) is defined as:

$$EF = \frac{\left(X/Ti\right)_{Aerosol}}{\left(X/Ti\right)_{Crust}}$$

where Ti is the chosen crustal reference element [useful as there are relatively few pollution sources and it was determined in the samples with reasonable accuracy] and $(X/Ti)_{Crust}$ is the ratio of X and Ti in the earth's crust according to Taylor (1964). At most sites, EFs of about one half of all elements are around or below factors of three of unity, signifying that those elements originate from the crust (Rahn, 1999). Elements are regarded as being "enriched" when the EFs are considerably larger than 3, since the composition of the crust varies and Taylor's data was used as an approximation for this study. EFs most commonly differentiate **pollution derived** elements from **crustal elements**. Figure 60 shows the EFs of the elements determined in the Taiyuan PM_{10}. Presented are mean values of the 12 day sampling campaign. Individual values as well as standard deviations can be found in table 23. The relative standard deviations are large, especially for elements with EF>1, but do not change the overall picture of which element is enriched or not.

It is evident from figure 60 that the elements **Zn, As, Sb, Se, Cd** and **Pb** are enriched, presumably by anthropogenic activities, relative to Ti. This is particularly troublesome as some of them are the most toxic trace elements, i.e. As, Cd, Se and Pb. As and Se have long been understood to be tracer elements of coal combustion (Park and Kim, 2004; He et al., 2001). Pb is released during the combustion of coal and from cars still running on leaded fuel, which has officially been phased out. Cd is most commonly found in industrial workplaces, especially where ore is processed or smelted. Sb has several industrial sources, mostly smelters (U.S. Department of Labour, 2005). Waste incineration and smelters are dominant sources of Zn (Xie, 2002). Zn and Cu have also been reported to originate from wear of tires and breaks accumulating in street dust (Cyrys et al., 2003). However, according to Sager (1999), the trace elements As, Cd, Pb, Sb, Se and Zn can be more than 100-fold enriched in coals with respect to mean crust occurrence. The elements with EFs close to unity are predominantly derived from the crust. However, according to Xie et al. (2006), EFs of around 1 in coal-polluted areas do not necessarily indicate that these elements are merely of natural origin, as coal-derived fly ash particles tend to have a similar chemical composition.

Table 23 – Aerosol-crust enrichment factors of analysed elements [Ti as reference]

Samples	Al	Fe	Mg	Na	Zn	Si	Ca	As	Ni
T51	1.03	1.27	1.16	0.47	163	0.68	4.85	141	6.74
T53	0.99	1.05	1.17	0.64	34.2	0.80	2.88	38.7	1.33
T55	1.02	1.39	1.22	0.52	177	0.76	4.58	138	4.82
T57	0.98	1.09	1.39	0.59	120	0.74	4.54	95.4	3.71
T59	0.99	1.32	1.36	0.84	107	0.82	4.28	83.0	3.74
T61	1.00	0.99	1.09	0.68	29.2	0.88	2.76	30.0	0.78
T63	1.02	1.28	1.27	0.48	183	0.82	4.80	108	7.11
T65	0.74	0.84	0.84	0.36	89.6	0.53	3.35	83.9	1.22
T67	1.02	1.28	1.15	0.52	106	0.72	4.73	109	22.68
T69	0.97	1.02	0.98	0.55	35.2	0.83	2.48	39.1	1.24
T71	1.01	1.13	1.18	0.51	66.5	0.82	4.11	50.4	1.95
T73	0.97	1.14	1.17	0.46	91.6	0.74	4.66	106	1.08
mean	**0.98**	**1.15**	**1.16**	**0.55**	**100**	**0.76**	**4.00**	**85.3**	**4.70**
s	0.08	0.16	0.15	0.12	54	0.09	0.88	38.3	6.08
r.s.d. in %	**8**	**14**	**13**	**23**	**54**	**12**	**22**	**45**	**129**

Samples	Sb	Se	Co	V	Cd	Mn	Cu	Pb
T51	533	7621	1.31	0.93	382	2.73	26.1	336
T53	77.4	2379	1.10	1.00	84.4	2.16	3.81	64.2
T55	588	6785	1.25	1.04	538	3.29	18.4	341
T57	308	4454	1.25	1.02	361	2.80	11.7	215
T59	234	4241	1.19	0.96	251	2.59	21.4	206
T61	73.1	1403	1.05	0.95	36.5	1.85	11.5	48.5
T63	271	5643	1.25	0.87	599	4.44	13.6	290
T65	214	3591	0.80	0.65	157	1.48	15.7	144
T67	806	7446	1.85	0.95	312	2.22	8.42	272
T69	148	1816	1.04	0.94	98.5	1.71	5.57	70.4
T71	128	2473	1.12	0.91	189	2.22	6.00	107
T73	549	6413	1.14	0.89	221	2.18	17.5	190
mean	**327**	**4522**	**1.20**	**0.93**	**269**	**2.47**	**13.3**	**190**
s	236	2234	0.25	0.10	177	0.80	6.81	105
r.s.d. in %	**72**	**49**	**21**	**11**	**66**	**32**	**51**	**55**

[s: standard deviation; r.s.d is the relative standard deviation]

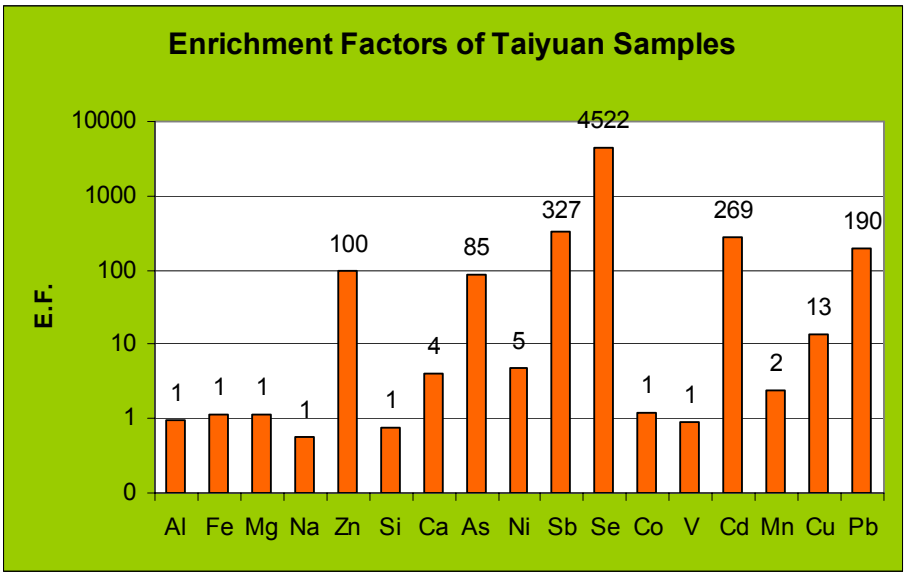

Figure 60 – Aerosol-Crust Enrichment Factors [Ti as reference]

Perhaps this could explain why Fe is not enriched despite the large iron and steel company located in Taiyuan, which may use coal as fuel in the process. Ca is slightly increased due to the large amount of construction sites (cement and associated lime ($CaCO_3$)). Co and V are presumably mostly of crustal origin. Their EFs are close to one and the most common other source is heavy oil combustion (Dzubay et al., 1988), which is not used in Taiyuan for heating and/or power generation (Xie, 2002).

Moreover, the little pollution influenced major elements Al and Mg have EFs close to 1 and therefore also could have been used as reference elements.
The crustal material clearly dominates the chemical composition of the Taiyuan PM_{10} aerosol (figure 59), which was also found by Xie (2002), who analysed five samples collected at the same location in late June. Generally, the absolute concentration of the crustal material varies with humidity, attaining higher contributions on dry days when soils are most easily suspended (Vasconcelos et al., 1994).

Due to Taiyuan's monsoonal climate, there was no precipitation during sampling, i.e. no wet deposition, which would have reduced bulk atmospheric PM_{10} concentrations, and no wet surfaces, which would have retained crustal material in soil and dust, occurred. Furthermore, the concentrations of pollution-derived elements will also fluctuate during the year, reaching a potential climax during heating season from November until April (Gongli et al., 2005), where the energy requirements and resulting fuel consumption will be highest.

5.3.2 Correlations and Source Apportionment

Correlation measurements are a very useful mathematical tool to determine the strength of a linear relationship between two quantitative variables. The correlation coefficient (R) is used as the indicator of the degree of correlation and is usually squared to express to what extent the observed variation of one variable is explained by the other. Tables 24 and 25 summarise correlation coefficients of the analysed entities. With the aid of the correlation coefficients careful interpretations of potential common sources are feasible. In general the assumption can be made that a high correlation coefficient (arbitrarily assigned: $R^2>0.80$) is a good indication of both quantities originating from the same source, whereas somewhat lower R^2 values may result if one or both of the quantities have several sources (confounding).

Table 24 – Correlation coefficients (R^2) of analysed elements

	Al	Fe	Mg	Na	Zn	Si	Ca	As	Ni	Sb	Se	Co	V	Cd	Mn	Cu	Pb
Al	1																
Fe	0.87	1															
Mg	0.88	0.87	1														
Na	0.76	0.75	0.80	1													
Zn	0.07	0.24	0.19	0.03	1												
Si	0.93	0.74	0.77	0.82	0.00	1											
Ca	0.53	0.71	0.73	0.36	0.58	0.31	1										
As	0.08	0.24	0.17	0.02	0.91	0.00	0.58	1									
Ni	0.00	0.02	0.00	0.01	0.10	0.03	0.07	0.16	1								
Sb	0.00	0.05	0.01	0.02	0.42	0.04	0.22	0.62	0.58	1							
Se	0.03	0.16	0.09	0.00	0.75	0.01	0.46	0.91	0.35	0.82	1						
Co	0.75	0.79	0.74	0.54	0.18	0.58	0.66	0.23	0.21	0.18	0.23	1					
V	0.97	0.85	0.90	0.79	0.07	0.91	0.51	0.08	0.00	0.00	0.03	0.75	1				
Cd	0.05	0.20	0.18	0.01	0.90	0.00	0.51	0.75	0.13	0.41	0.63	0.19	0.07	1			
Mn	0.52	0.66	0.73	0.44	0.54	0.38	0.72	0.39	0.01	0.05	0.24	0.51	0.56	0.60	1		
Cu	0.08	0.25	0.16	0.13	0.55	0.02	0.37	0.58	0.00	0.17	0.46	0.09	0.07	0.28	0.24	1	
Pb	0.06	0.24	0.15	0.02	0.94	0.00	0.54	0.95	0.24	0.64	0.91	0.24	0.06	0.84	0.43	0.54	1
Ti	0.92	0.77	0.81	0.70	0.05	0.85	0.48	0.07	0.01	0.00	0.01	0.63	0.90	0.03	0.40	0.10	0.04

[correlation coefficients greater than 0.80 are marked]

Table 25 – Correlation coefficients (R^2) of various compounds

	NH_4^+	NO_3^-	SO_4^{2-}	PM_{10}	OC	EC	Al	As	Ca
NH_4^+	1								
NO_3^-	0.56	1							
SO_4^{2-}	0.30	0.71	1						
PM_{10}	0.29	0.59	0.79	1					
OC	0.65	0.37	0.40	0.43	1				
EC	0.55	0.27	0.45	0.44	0.76	1			
Al	0.02	0.28	0.52	0.70	0.05	0.08	1		
As	0.74	0.54	0.53	0.50	0.87	0.71	0.08	1	
Ca	0.36	0.56	0.86	0.85	0.49	0.57	0.53	0.58	1

Elements which are apparently non-enriched (EF≈1) and highly correlated to each other are most likely of natural (crustal) origin, e.g. **Al**, **Fe**, **Si**, **Mg**, **Na**, **V**, **Ti** (table 24). They do not all have correlation coefficients higher than 0.80 with each other, but considering errors, are close enough. On the other hand, highly enriched elements that are closely correlated with each other can be assigned to a common anthropogenic source. The toxic trace metals are in this category, which includes **As**, **Se**, **Zn**, **Pb** and **Cd**. Even though As and Se are emitted from various anthropogenic sources, their presence is generally used as a marker for coal combustion resulting in an As/Se ratio of about 1, as it is found in aged coal combustion aerosols (Park and Kim, 2004). The average As/Se mass ratio on the Teflon filters of the 12 Taiyuan samples (**0.68±0.49** - 95% c.i. according to Gauss, see appendix L-2) indicates that both may have coal combustion as an important source, but there may be additional Se sources. The strong correlation of Se to Sb (0.82) seems to point towards the second possibility, perhaps the emission from smelters, which are common sources of Sb. The large correlations of As to Pb, Zn, and even to Cd (0.75) indicate coal-burning activities as the dominant source.

The investigated correlation between Al and As, Se and Zn, formulated by Xie (2006), could not be confirmed. The variability of emission sources close to the sampling location may be a possible explanation.

Daily atmospheric mass concentrations and correlation coefficients of the analysed ions: **ammonium**, **sulphate** and **nitrate**, are presented in figure 58 and table 25 respectively. They are all secondary pollutants, even though ammonium may be closest to its primary form (NH_3 – from predominantly agricultural activities), which is formed through gas-phase or droplet reactions in the atmosphere. Sulphur dioxide (SO_2) and nitrogen dioxides (NO_x) are precursors of sulphate and nitrate respectively. The effect of relative humidity on the amount of sulphate measured has been investigated by Vasconcelos et al. (1994), concluding that increasing humidity results in larger sulphate concentrations, most likely due to the aqueous pathways that promote sulphate formation. Regarding this finding, a certain trend can be perceived in figure 58, even though the R^2 value between relative humidity and atmospheric sulphate concentration is only 0.37, it explains part of the observed variation. Nitrate and sulphate are reasonably well correlated (0.71), which according to Mouli et al. (2006) assigns them to similar sources, because of their similar behaviour in the atmosphere and the co-emissions from coal burning of SO_2 and NO_x. Vehicle emissions are another wide-spread source of NO_x and eventually nitrate. Another source of sulphates may be gypsum ($CaSO_4$), which could be formed via sulphation of limestone during coal combustion (Xie et al., 2005) and would explain the strong correlation between Ca and SO_4^{2-} (0.86).

It is of interest (because of ammonia's neutralisation capacity) to ascertain which types of molecules of the ammonium-nitrate-sulphate system have been formed. According to thermodynamic calculations, the ammonium will first react with the available sulphate and only secondarily form ammonium nitrate (NH_4NO_3). To investigate which species dominates, the following calculations are carried out:

The collected masses of sulphate and ammonium on the quartz filters (tables J-6 and J-14) are transferred to equivalent masses. Table 26 summarises the results. Calculating the average ammonium-sulphate ratio yields a good indication of the prevailing compound(s). For the Taiyuan samples the ratio is (**1.0±0.8** – 95% c.i. according to Gauss, see appendix L-2), pointing to ammonium sulphate – **$(NH_4)_2SO_4$** – as the most likely form of sulphate and ammonium in the samples, despite the large standard deviation. Values at around 0.5 favour the formation of ammonium

bisulphate (NH_4HSO_4), while figures larger than one assign the remaining ammonium to be in the form of ammonium nitrate.

Table 26 – Equivalent masses of sulphate and ammonium

Sample	SO_4^{2-} [meq]	NH_4^+ [meq]
Q1	31.23	37.14
Q3	12.49	9.98
Q5	16.24	24.95
Q7	25.61	23.84
Q9	10.83	9.42
Q11	1.64	2.27
Q13	2.71	4.71
Q15	8.54	4.05
Q17	6.66	9.42
Q19	8.95	3.22
Q21	11.24	2.38
Q23	5.20	9.98
mean	**11.78**	**11.78**
s	8.86	11.04

The **carbonaceous fraction** accounts for on average 17% of the Taiyuan PM_{10} composition (figure 59). Their sources are manifold; such as coal combustion, vehicle emissions, meat cooking, backyard fires, etc., yet if a predominant source is responsible for the emission of major fractions of OC and EC, then their correlation to each other should be high, as their relative emission rates would be proportional to each other (Na et al., 2004). From figure 58 it becomes evident that the daily variations of OC and EC concentrations follow each other quite well. This apparent trend is confirmed by the relatively high correlation coefficient of 0.76 (table 25), indicating one dominant source. Further, the high correlation between As and OC (0.87) identifies coal combustion activities as the likely source.

5.3.3 Comparison with Other Results and Air Quality Standards

Even though great care should be taken, as the variability of daily PM_{10} (and included constituents) concentrations and the number of influencing parameters are very large, a comparison to a previous study carried out at the same location has been done. The analysis was conducted and Xie (2006) in the same laboratory, using the same instruments. The samples were collected during the period from 03rd of March till 16th of March 2004, which means the study finished when the present study began, only two years prior. The meteorological conditions were similar to this study, with perhaps somewhat lower winds, temperatures and one short (15min)

snow precipitation event. Only the results of the bulk PM_{10} concentration and of some trace elements can be compared. The comparison of the two studies is shown in table 27. The comparison was done statistically applying a two-sample t-test under the zero hypothesis that both means are equal and there is no difference between the results of the two studies.

Table 27 – Comparison with previous study at same location

		*Xie (2006)	This Study	t-value	P-value
		9 samples	12 samples		(one-sided)
PM_{10} [μg/m³]	mean	**553**	**385**	1.62	0.0759
	s	298	105		
Pb [μg/m³]	mean	**0.63**	**0.43**	1.41	0.0986
	s	0.38	0.24		
Zn [μg/m³]	mean	**1.3**	**1.3**	0.12	>0.5
	s	0.9	0.7		
As [ng/m³]	mean	**43.4**	**27.8**	1.57	0.0813
	s	27.6	12.8		
Se [ng/m³]	mean	**58.2**	**40.3**	1.14	0.144
	s	44.4	18.8		
Sb [ng/m³]	mean	**11.1**	**11.5**	0.1	>0.5
	s	9.6	7.3		

[*publication reference, not year of sampling (2004)] [this study data: tables H-7, I-7 and L-1]

To calculate the t-value the following formula was used: $$t = \frac{\left|\bar{x}_{Xie} - \bar{x}_{Mine}\right|}{\sqrt{\frac{s_{Xie}^2}{n_{Xie}} + \frac{s_{Mine}^2}{n_{Mine}}}}$$

[$\bar{x}_{Xie}, \bar{x}_{Mine}$: means; s_{Xie}^2, s_{Mine}^2: variances; n_{Xie}, n_{Mine}: number of samples in both studies]

The probabilities (P-values) were then determined by interpolation of the tabulated critical values of the t-distribution (Moore and McCabe, 2006). 8 degrees of freedom were chosen (as suggested in the literature), which is the smaller of n_{Xie}-1 and n_{Mine}-1. The P-values represent upper tail probabilities. Hence they need to be multiplied by two in order to arrive at two-sided confidence intervals. Even though none of the pairs of compared means can be said to be different according to the commonly required 95% confidence intervals (i.e. P-value of 0.025 and below), some trends can be observed. The P-values indicate the frequency of finding equal means in the collected data. The observed means are equal about 15% (PM_{10}), 20% (Pb), 16% (As) and 30% (Se) of the time and have smaller values at all other times, while no statistical change can be found for Zn and Sb. Optimistically, these results could be understood to indicate a decrease of atmospheric PM_{10}, As, Se and Pb pollution.

Another possibility is that the change was due to the two week sampling difference and associated rise in temperatures, which may pose smaller demands on heating. However, the former conclusion is in line with findings published in Aunan et al. (2006), stating that the air quality in Taiyuan has improved in recent years because of several governmental actions. However, the random emissions of several (mostly domestic) sources in the proximity of the sampling site will always cast a lot of doubt on trends from results gathered over such a short period of time as two weeks. **Cadmium**, also strongly enriched, has not been determined in previous sampling episodes at the Taiyuan location. Therefore, the obtained results in this study, as well as the bulk PM_{10} concentration, are compared to concentrations measured in several other cities. The data are collected in table 28.

Table 28 – Comparison of PM_{10} and Cd concentrations with other urban locations

Country	City	Population	Reference	Sampling Time	PM_{10} in $\mu g/m^3$	Cd in ng/m^3
India	Delhi	14 million	Balachandran et al. (2000)	Feb – May in 1998	**553** ±226	27±19
	New Delhi	14 million	Laakso et al. (2005)	one week autumn, 2002	**370**	
	Kolkata		Karar et al. (2007)	one year in 2004	**197** ±88	5±3
China	Beijing	11 million	Laakso et al. (2005)	one year 2000	**176**	
Finland	Helsinki	0.5 million	Laakso et al. (2005)	several years	**20**	
China	Taiyuan	2.9 million	Raw data provided by *EMD, Taiyuan	one year, 2005	**148** ±69	
			This study	12 days in March 2006	**385** ±105	9.5±5.6

[*EMD: Environmental Monitoring Department]

Generally speaking, these comparisons have very limited merit, as conditions are almost never comparable, such as time of year, duration of sampling, sampling location, emission sources, meteorological conditions, etc. Moreover, the very short sampling period of this study hardly represents the actual Taiyuan conditions. The annual average data provided by the EMD, Taiyuan, has been collected at a different (unknown) location. More meaningful is a comparison of the obtained results with internationally agreed upon air quality standards, which are usually selected to obviate detrimental health effects. Table 29 contains the most important air quality standards, issued by the WHO and SEPA, the state environmental protection agency of China. In 2005, WHO for the first time issued globally applicable air quality

standards, which targets, if achieved, would result in significant reductions in pollutant-related health risks.

Table 29 – Air quality standards for PM_{10} and cadmium

PM_{10}	Issuing Body	WHO, 2005		**Global**			
	Limit Values	**20μg/m³**		**50μg/m³**			
	Time Scale	annual mean		24h mean			
PM_{10}	Issuing Body	SEPA, 2006		**China**			
	Limit Values	Grade I		Grade II		Grade III	
		natural		residential, commercial, cultural		industrial areas	
		40μg/m³	**50μg/m³**	**100μg/m³**	**150μg/m³**	**150μg/m³**	**250μg/m³**
	Time Scale	annual	24h	annual	24h	annual	24h
Cd	Issuing Body	WHO, 2000		**Europe**			
	Limit Value	**5ng/m³**					
	Time Scale	annual mean					

As can be seen from table 29, the annual limit for cadmium lies just about 50% under the 12-day mean value found in this study, which indicates no gross exceedence, especially when transferring the given limit to a 24h mean (possible around 10ng/m³). This is good news, despite uncertainties, and may signify that cadmium pollution is not as big a threat as assumed. Nevertheless, all-year-round monitoring would be necessary to obtain a fuller emission profile and thus a clearer picture of the real situation. PM_{10} standards in China are much higher than the global guidelines proposed by WHO. The mean PM_{10} value of this study (385μg/m³) still exceeds even the grade III, 24h Chinese standard and lies by a factor of almost 8 above the WHO 24h average standard. However, the annual average of 148μg/m³ is just around the Chinese grade III limit. This should still give rise for great concern for the public health situation and compel China to move forward with countermeasures, which they have already started to implement. The result of this study seems to indicate a trend towards the better and, while a lot of work still needs to be done, is a beacon of hope for cleaner air, which everyone deserves.

5.4 Discussion of Results of Other TOA analyses

5.4.1 Comparison of the Thermal Protocols NIOSH-Derived and JRC-IMPROVE

The two thermal protocols (explained earlier) were applied to quartz filter samples collected at the rural site Birkenes, Norway, and compared with regard to the individual carbon fractions analysed [no data included in this study]. The reason for the development of a new, unified thermal protocol is partly because such a protocol does not exist yet [different protocols give different results for the OC, EC fractions] and partly because the already existing ones seem to have drawbacks, in particular the large amount of charring, which is to be decreased. In this early stage of protocol development the results obtained from the JRC-IMPROVE were compared to results from the NIOSH-derived (established) protocol on the same samples. The results are illustrated in figure 61.

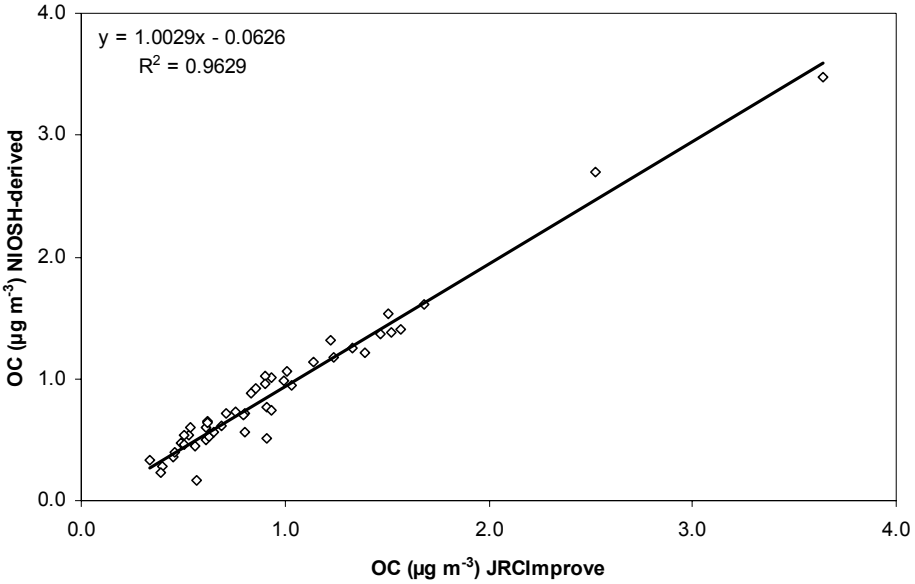

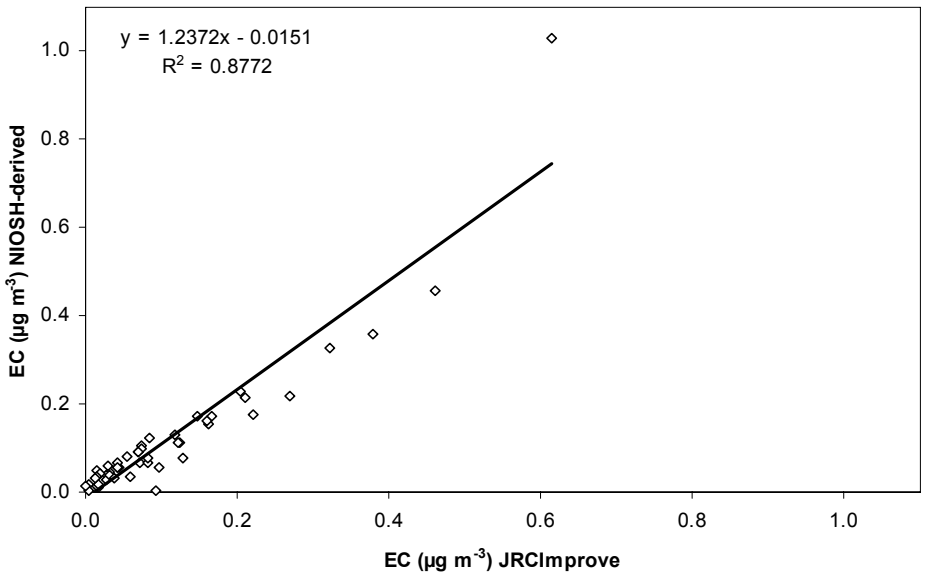

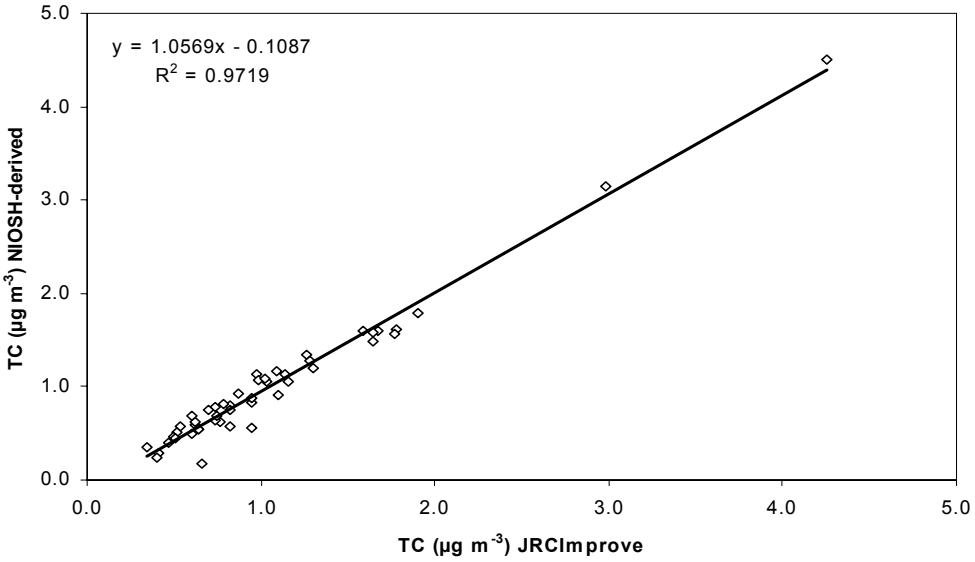

Figure 61 – Comparison of the JRC-IMPROVE protocol to the NIOSH-derived

The carbonaceous fractions determined with the JRC-IMPROVE protocol are surprisingly similar to the ones obtained from the NIOSH-derived protocol. The EC comparison could even be improved to a R^2 of 0.94 by removing the outlier. This should be good news but very frequently it occurred that the OC-EC split point was located on top of a large and narrow peak, which introduced the possibility of a large change in the assigned amounts of OC and EC with small changes in the location of the split point (see thermograms in appendix K-2: the black vertical line marks the OC-EC split point). The addition of several extra temperature steps between the 650°C and 850°C step might counteract this potential problem. Furthermore, a slightly increased transmittance was observed during the 650°C step prior to the introduction of oxygen. This could be due to the presence of mineral oxides that supply oxygen to neighbouring carbon particles at this temperature (Chow et al., 2001). This effect has already been reduced significantly by reducing the temperature from 850°C to 650°C. Perhaps it is necessary to further reduce the temperature in the pure helium atmosphere.

5.4.2 Backup Filter Results

The results of the backup-filter analysis of day samples (9am – 9pm) of different size fractions, collected in the same period at a rural and an urban site (Hurdal and Oslo) are summarised in table 30 by giving the ratio of the mean amount of gaseous OC on the backup filters, the Pearson correlation coefficients (r – indicating the direction and strength of the correlation) between the available size fraction [PM_1, $PM_{2.5}$, PM_{10}], and the percentage of gaseous backup filter OC compared to OC on the front filter. The goal was to identify the relationship of quartz backup filters for different size fractions when sampling at the same filter face velocity. The results show that there is not a very large difference in the mean amounts of gaseous organic carbon on the backup filters of the various size fractions and they are reasonably well correlated.

Table 30 – Backup filter comparison [OC on backup filter = TC]

	Oslo (urban)			Hurdal (rural)	
Ratio of Mean Amounts of Gaseous OC on Backup Filters	**$TC_{PM10}/TC_{PM2.5}$**	**TC_{PM10}/TC_{PM1}**	**$TC_{PM2.5}/TC_{PM1}$**	**TC_{PM10}/TC_{PM1}**	
	0.87±0.12	0.93±0.15	1.08±0.11	1.08±0.11	
Pearson Correlation Coefficients r	**$TC_{PM10}/TC_{PM2.5}$**	**TC_{PM10}/TC_{PM1}**	**$TC_{PM2.5}/TC_{PM1}$**	**TC_{PM10}/TC_{PM1}**	
	0.87	0.81	0.90	0.95	
Ratio OC Backup Filter to OC Front Filter in %	**PM_{10}**	**$PM_{2.5}$**	**PM_1**	**PM_{10}**	**PM_1**
	22±7	33±7	32±4	38±7	52±16

However, there seems to be a difference between the two sites with regard to the amount of vapour phase organic carbon adsorbed on the backup filters. While the amounts of OC on the front filters are almost the same for the same size fractions at both sites, the amount of vapour OC on the backup filters is significantly higher at the rural Hurdal site. Possible explanations are the failure to saturate the Oslo backup filters, and/or a different quality of vapour phase OC which adds more readily to the backup filters at Hurdal. These considerations may be subject of further studies.

6.0 Conclusion and Suggestions for Further Work

In conclusion it is important to stress that the findings obtained within this study do not represent the overall condition in Taiyuan for several reasons:

- All results were extracted out of merely 12 days of sampling
- The sampled air was “unpredictably” turbulent as the sampling location was lower than the surrounding buildings
- Local sources dominated and had partly the character of random emissions: large construction site of a new university building close by, a dust-covered roof as sampling location, the emissions of domestic backyard-fires and chimneys, all in close proximity.

Perhaps the collected results at this location could be considered a worst-case scenario. People may indeed sometimes be exposed to concentrations such as the ones measured, at certain hot-spots in the city. It may be wise to choose a more suitable location where more representative data could be collected.
Nevertheless, the obtained results were compared to previous data from the same site, which confirmed the dominating crustal material fraction in the Taiyuan PM_{10} aerosol and indicated a trend towards cleaner air, even though bulk atmospheric PM_{10} concentrations still significantly exceeded the Chinese grade III air quality standard for industrial areas [250$\mu g/m^3$]. Furthermore, correlation coefficients and enrichment factors were useful tools in the task of source apportionment and clearly pointed towards coal combustion activities as the main source of the anthropogenic emissions.

It would be desirable to collect air samples over a longer period of time, preferably over a year, to investigate seasonal variations and to obtain a fuller picture of the actual air quality. Deconvolution of the organic fraction both with regard to the presence and amount of potentially carcinogenic components, and useful tracer molecules, such as picenes for coal combustion, could be interesting future studies.

References

Agilent Technologies, 2005. ***ICP-MS: Inductively Coupled Plasma Mass Spectrometry – A Primer.*** Agilent Technologies, Inc., USA. 80pp.

Answers.com, 2006. Last accessed 18.01.2007. Available at http://www.answers.com/topic/taiyuan

Auffhammer, M., Ramanathan, V., and Vincent, J.R., 2006. ***Integrated Model Shows That Atmospheric Brown Clouds and Greenhouse Gases Have Reduced Rice Harvests in India.*** Proceedings of the National Academy of Sciences (PNAS), 103(52): 19668-72.

Aunan, K., Fang, J., Vennemo, H., Oye, K., and Seip, H.M., 2004. ***Co-Benefits of Climate Policy – Lessons Learned From a Study in Shanxi, China.*** Energy Policy, 32: 567-581.

Aunan, K., Mestl, E.S., Junghua, F., Yanhong, L., 2005. ***Household Fuel Use and Indoor Air Pollution in Shanxi.*** Workshop on masterplan against air pollution, Taiyuan, Shanxi.

Aunan, K., Fang, J., Hu, T., Seip, H.M., and Vennemo, H., 2006. ***Climate Change and Air Quality. Measures With Co-Benefits in China***. Environmental Science and Technology, 40(16): 4822-4829.

Baird, C., and Cann, M., 2005. ***Environmental Chemistry (3rd Edition).*** W. H. Freeman and Company, New York. 700pp.

Balachandran, S., Meena, B.R., and Khillare, P.S., 2000. ***Particle Size Distribution and its Elemental Composition in the Ambient Air In Delhi.*** Environment International, 26: 49-54.

Boss, C.B., and Fredeen, K.J., 2004. ***Concepts, Instrumentation and Techniques in Inductively Coupled Plasma Optical Emission Spectrometry.*** Perkin Elmer, Inc, USA. 124pp.

Brasseur, G., Orlando, J.J., and Tyndall, G.S., 1999. **Atmospheric Chemistry and Global Change.** Oxford University Press Inc, USA. 672pp.

Brimblecombe, P., 2002. ***Acid Drops*** – Inside Science (150). New Scientist, 2343.

China Population Information and Research Centre (CPIRC), 2007. Last accessed: 15.01.2007. Available at http://www.cpirc.org.cn/en/eindex.htm

Chow, J.C., Watson, J.G., Crow, D., Lowenthal, D.H., and Merrifield, T., 2001. ***Comparison of IMPROVE and NIOSH Carbon Measurements.*** Aerosol Science and Technology, 34: 23-34.

Chow, J.C., Watson, J.G., Chen, L.W.A., Arnott, W.P., and Moosmueller, H., 2004. ***Equivalence of Elemental Carbon by Thermal/Optical Reflectance and Transmittance with Different Temperature Protocols.*** Environmental Science and Technology, 38: 4414-4422.

Chow, J.C., Watson, J.G., Louie, P.K.K., Chen, L.W.A., and Sin, D., 2005. ***Comparison of $PM_{2.5}$ Carbon Measurement Methods in Hong Kong, China.*** Environmental Pollution, 137: 334-344.

Cyrys, J., Stölzel, M., Heinrich, J., Kreyling, W.G., Menzel, M., Wittmaack, K., Tuch, T., and Wichmann, H.E., 2003. ***Elemental Composition and Sources of Fine and Ultra-Fine Ambient Particles in Erfurt, Germany.*** The Science of the Total Environment, 305: 143-156.

Dockery, D.W., Pope, C.A., Xu, X., Spengler, J.D., Ware, J.H., Fay, M.E., Ferris, B.G., and Speizer, F.E., 1993. ***An Association Between Air Pollution and Mortality in Six U.S. Cities.*** New England Journal of Medicine, 329: 1753-1759.

Dzubay, T.G., Stevens, R.K., Gordon, G.E., Olmez, I., Sheffild, A.E., And Courtney, W.J., 1988. ***A Composite Receptor Model Applied to Philadelphia Aerosol.*** Environmental Science and Technology, 22:46-52.

EMPA – Materials Science and Technology. **Ambient Air.** Last accessed: 06.02.2007. Available at http://www.empa.ch/plugin/template/empa/*/29214/---/1=2

Energy Information Administration (EIA), 2003. ***China: Environmental Issues.*** Last accessed: 12.01.2007. Available at http://www.eia.doe.gov/emeu/cabs/chinaenv.pdf

Energy Information Administration (EIA), 2004. ***India: Environmental Issues.*** Last accessed: 12.01.2007. Available at http://www.eia.doe.gov/emeu/cabs/indiaenv.pdf

Environmental Protection Agency (EPA), 2006. ***Airborne Particulates.*** Queensland Government. Last accessed: 24.01.2007. Available at http://www.epa.qld.gov.au/environmental_management/air/air_quality_monitoring/air_pollutants/airborne_particulates

Food and Agriculture Administration of the United Nations (FAO), 2006. ***International Forum on Water Resources Management and Irrigation Modernisation.*** Last accessed: 17.01.2007. Available at http://www.fao.org/world/regional/rap/meetings/2006/Nov22/Nov22.htm

Gilmour, P.S., Brown, D.M., Lindsay, T.G., Beswick, P.W., MacNee, W., and Donaldson, K., 1996. ***Adverse Health Effects of PM_{10} Particles: Involvement of Iron in Generation of Hydroxyl Radical.*** ' Occupational Environmental Medicine, 53: 817-823.

Gongli, H., Ying, B., Liu, J., Gao, S., Shen, S., Balakrishna, K., Jin, Y., Liu, F., Tang, N., Shi, K., Baris, E., and Ezzati, M., 2005. ***Patterns of Household Concentrations of Multiple Indoor Air Pollutants in China.*** Environmental Science and Technology, 39: 991-998.

Guderian, R., 1985. ***Air Pollution by Photochemical Oxidants: Formation, Transport, Control and Effects on Plants***. Springer Verlag, N.Y.

Harris, D.C., 2003. ***Quantitative Chemical Analysis.*** W.H. Freeman and Company, USA. 744pp.

Harrison, R.M., 1999. ***Understanding our Environment.*** The Royal Society of Chemistry, Cambridge, UK. 445pp.

Harrison, R.M., Jones, A.M., and Lawrence, R.G., 2003. ***A Pragmatic Mass Closure Model for Airborne Particulate Matter at Urban Background and Roadside Sites.*** Atmospheric Environment, 37: 4927-4933.

He, B., Liang, L., and Jiang, G., 2001. ***Distribution of Arsenic and Selenium in Selected Chinese Coal Mines.*** The Science of the Total Environment, 296: 19-26.

Intergovernmental Panel on Climate Change (IPCC), 2001. ***Third Assessment Report – Technical Summary (Working Group I).*** Geneva. Last accessed: 05.02.2007. Available at http://www.ipcc.ch

Intergovernmental Panel on Climate Change (IPCC), 2007. ***Fourth Assessment Report – Technical Summary (Working Group I).*** Geneva. Last accessed: 15.05.2007. Available at http://www.ipcc.ch

Karar, K., and Gupta, A.K., 2007. ***Source Apportionment of PM_{10} at Residential and Industrial Sites of an Urban Region of Kolkata, India.*** Atmospheric Research, 84: 30-41.

Kingston, H.M., and Walter, P.J., 1998. ***The Art and Science of Microwave Sample Preparations for Trace and Ultra-trace Elemental Analysis.*** Wiley-VCH, Inc. Chapter 2.

Kuchling, H., 1999. ***Taschenbuch der Physik.*** Fachbuchverlag Leipzig. 708pp.

Laakso, L., Koponen, I.K., Mönkkönen, P., Kulmala, M., Kerminen, V.M., Wehner, B., Wiedensohler, A., Wu, Z., and Hu, M., 2006. ***Aerosol Particles in the Developing World; a Comparison Between New Delhi in India and Beijing in China***. Water, Air and Soil Pollution, 173: 5-20.

Lee, J., and Manning, L., 1995. ***Environmental Lung Disease –*** Inside Science (84). New Scientist, 1995.

Library for Science. ***Electrical Conductivity Detector***. Last accessed: 03.04.2007. Available at http://www.chromatography-online.org/topics/electrical/conductivity/detector.html

Lundgren, D.A., Hausknecht, B.J., and Burton, R.M., 1984. ***Large Particle Size Distribution in Five U.S. Cities and the Effect on a New Ambient Particulate Matter Standard (PM_{10}).*** Aerosol Science and Technology, 467-473.

Lundgren, D.A., and Burton, R.M., 1995. ***Effect of Particle Size Distribution on the Cut Point Between Fine and Coarse Ambient Mass Fractions.*** Inhalation Toxicology, 7: 131-148.

Maynard, R., 2004. ***Key Airborne Pollutants – The Impact on Health.*** Science of the Total Environment, 334-335: 9-13.

Materials Evaluation and Engineering (MEE), 2000. ***Handbook of Analytical Methods – Ion Chromatography.*** Materials Evaluation and Engineering, Inc. Last accessed: 03.04.2007. Available at http://www.mee-inc.com/ion.html

Menon, S., Hansen, J., Nazarenko, L., and Luo, Y., 2002. ***Climate Effects of Black Carbon Aerosols in China and India.*** Science, 297: 2250-53.

Merefield, J., 2002. ***Dust to Dust*** – Inside Science (153). New Scientist, 2361.

Mestl, H.E.S., and Fang, J., 2003. ***Air Quality Estimates in Taiyuan, Shanxi Province, China.*** CICERO Report 2003:01.

Moore, D.S., and McCabe, G.P., 2006. ***Introduction to the Practice of Statistics.*** W.H. Freeman and Company, New York. 883pp.

Mouli, P.C., Mohan, S.V., and Reddy, S.J., 2006. ***Chemical Composition of Atmospheric Aerosol (PM_{10}) at a Semi-Arid Urban Site: Influence of Terrestrial Sources.*** Environmental Monitoring and Assessment, 117: 291-305.

Na, K., Sawant, A.A., Song, C., and Cocker, D.R. III, 2004. ***Primary and Secondary Carbonaceous Species in the Atmosphere of Western Riverside County, California.*** Atmospheric Environment, 38: 1345-1355.

National Institute of Standards and Technology (NIST), 1998. ***Standard Reference Material 1648 – Certificate of Analysis.*** NIST Last accessed: 09.03.2007. Available at https://srmors.nist.gov/view_cert.cfm?srm=1648

New Mexico State University (NMSU), 2006. ***Teaching Laboratory Instrument – Ion Chromatography.***
Last accessed: 03.04.2007.
Available at http://www.chemistry.nmsu.edu/Instrumentation/IC.html

Norwegian Institute for Air Research (NILU), 2003. ***Understanding Particles.***
NILU Report (03.01.2003).
Last accessed: 07.05.07.
Available at
http://www.nilu.no/index.cfm?ac=topics&text_id=8773&folder_id=7358&view=text&crit=carbon,analyser

Park, S.S., and Kim, Y.J., 2004. ***$PM_{2.5}$ Particles and Size-Segregated ionic Species Measured During Fall Season in Three Urban Sites in Korea.*** Atmospheric Environment, 38:1459-1471.

Pope III, C.A., Burnett, R.T., Thun, M.J., Calle, E.E., Krewski, D., Ito, K., and Thurston, G.D., 2002. ***Lung Cancer, Cardiopulmonary Mortality, and Long-Term Exposure to Fine Particulate Air Pollution.***
The Journal of the American Medical Association, 287(9): 1132-1141.

Pope III, C.A., 2004. ***Air Pollution and Health – Good News and Bad.***
New England Journal of Medicine, 351: 1132-1134.

Pope III, C.A., Burnett, T., Thurston, G.D., Thun, M.J., Calle, E.E., Krewski, D., and Godleski, J.J., 2004. ***Cardiovascular Mortality and Long-Term Exposure to Particulate Air Pollution.***
Journal of the American Heart Association, 109: 71-77.

Province View – China, 2004. ***Shanxi Province.***
Last accessed: 17.01.2007.
Available at
http://www.china.org.cn/english/features/ProvinceView/156508.htm

Quaschning, V., 1999. ***Regenerative Energiesysteme.*** Carl Hanser Verlag, München. 270pp.

Rahn, K.A., 1999. ***A Graphical Technique for Determining Major Components in a Mixed Aerosol. I. Descriptive Aspects.***
Atmospheric Environment, 33:1441-1455.

Ravilious, K., 2006. ***Brown Haze Over India Harming Rice Harvest.***
New Scientist (04.12.2006), special report. Last accessed: 31.05.2007.
Available at
http://environment.newscientist.com/channel/earth/dn10722-brown-haze-over-india-harming-rice-harvest.html

Roberts, T.M., 1987. ***Effects of Air Pollution on Agriculture and Forestry.***
CEGB Research, August 1987, 39-52.

Sager, M., 1999. ***Environmental Aspects of Trace Elements in Coal Combustion.*** Toxicological and Environmental Chemistry, 71: 159-183.

Seaton, A., MacNee, W., Donaldson, K., and Godden, D., 1995. ***Particulate Air Pollution and Acute Health Effects.*** Lancet, 345: 176-178.

Seinfeld, J.H., and Pankow, J.F., 2003. ***Organic Atmospheric Particulate Material.*** Annu. Rev. Phys. Chem., 54:121-140.

Skramstad, A.M., Dep. of Chemistry, Univ. of Oslo, PO Box 1033, 0315 Oslo.

Skujins, S., 1998. ***A Short Guide to VISTA Series ICP-AES Operation.*** Varian International AG, Zug, Switzerland.

State Environmental Protection Administration (SEPA), 2000. ***Report on the State of the Environment in China 1999.*** Last accessed: 15.01.2007. Available at http://www.zhb.gov.cn/english/SOE/soechina1999/air/air.htm

State Environmental Protection Administration, China (SEPA), 2005. ***Report on the State of the Environment in China.*** Last accessed: 10.05.2007. Available at http://english.sepa.gov.cn/ghjh/hjzkgb/200701/P020070118528407141643.pdf

SEPA, 2006. ***Emission Standards for Pollutants from Coal Industry.*** Last accessed: 24.05.2007. Available at http://english.sepa.gov.cn/kjbz/hjbz/

Steven, F.M., Lynn, M.R., Mary, K.G., and Satish, C.B.M., 2004. ***Organic Aerosol Growth Mechanisms and Their Climate-Forcing Implications***. Science, 306: 1921-1924.

Sunset Laboratory, 2000. ***Thermal/Optical Carbon Analyser***. A Guide to Running and Maintaining the Sunset Laboratory OCEC Analyser. Version 6.2. Sunset Laboratory Inc.

Taylor, S.R., 1964. ***Abundance of Chemical Elements in the Continental Crust: A new Table***. Geochimica et Cosmochimica Acta, 28: 1273-1285.

Tong, S.T.Y., 1991. ***The Retention of Copper and Lead Particulate Matter in Plant Foliage and Forest Soil.*** Environment International, 17: 31-37.

The Guardian, 2003. ***Global Warming is now a Weapon of Mass Destruction.*** John Houghton, July 28. Last accessed: 12.02.2007. Available at http://politics.guardian.co.uk/green/comment/0,9236,1007302,00.html

U.S. Department of Labour, 2005. Occupational Safety and Health Administration. ***Toxic Metals – Cadmium, Antimony.*** Last accessed: 19.05.2007. Available at http://www.osha.gov/SLTC/metalsheavy/index.html

U.S. Environmental Protection Agency, 1979. ***Protecting Visibility: an EPA Report to Congress.*** Research Triangle Park, NC: Office of Air Quality Planning and Standards; EPA report no. EPA-450/5-79-008.

U.S. Environmental Protection Agency, 2004. ***Air Quality Criteria for Particulate Matter.*** Volume I. Last accessed: 24.01.2007 Available at http://cfpub.epa.gov/ncea/cfm/partmatt.cfm

U.S. Environmental Protection Agency – National Centre for Environmental Assessment, 1997. ***Exposure Factors Handbook.*** Last accessed: 11.01.2007. Available at http://www.epa.gov/ncea/pdfs/efh/front.pdf

Vasconcelos, L.A., Macias, E.S., and White, W.H., 1994. ***Aerosol Composition as a Function of Haze and Humidity Levels in the Southwestern U.S.*** Atmospheric Environment, 28(22): 3679-3691.

Walker, M., 2006. ***China Struggling to Catch its Breath.*** New Scientist, 2549.

Watson, J.G., and Chow, J.C., 1994. ***Clear Sky Visibility as a Challenge for Society.*** Annual Review of Energy and the Environment, 19: 241-266.

Wayne, R.P., 2000. ***Chemistry of Atmospheres.*** Oxford University Press, 382-83.

Whitby, K.T., 1978. ***The Physical Characteristics of Sulphur Aerosols.*** Atmos. Environ. 12: 135-159.

Whittaker, A., BéruBé, K., Jones, T., Maynard, R., and Richards, R., 2004. ***Killer Smog of London, 50 Years on: Particle Properties and Oxidative Capacity.*** Science of the Total Environment, 334-335: 435-445.

Woodwell, G.M., 1970. ***Effects of Pollution on the Structure and Physiology of Ecosystems.*** Science, 168: 429-433.

World Health Organisation (WHO), 2000. ***Air Quality Guidelines for Europe.*** Copenhagen, Denmark. Last accessed: 24.05.2007. Available at http://www.euro.who.int/document/e71922.pdf

WHO, 2002. ***World Health Report 2002: Reducing Risk, Promoting Healthy Life.*** Geneva. Chapter 4. Last accessed: 12.01.2007. Available at http://www.who.int/whr/2002/en/whr02_ch4.pdf

WHO, 2005. ***WHO Air Quality Guidelines Global Update 2005.*** Bonn, Germany. Last accessed: 24.05.2007. Available at http://www.euro.who.int/Document/E87950.pdf

Xie, R., 2002. ***Characterisation and Apportionment of Particulate Matter (PM_{10}) in two Chinese Cities.*** Department of Chemistry, University Oslo.

Xie, R., Seip, H.M., Wibetoe, G., Nori, S., McLeod, C.W., and Larssen, S., 2006. ***Heavy Coal Combustion as the Dominant Source of Particulate Pollution in Taiyuan, China, corroborated by High Concentrations of Arsenic and Selenium in PM_{10}.*** Science of the Total Environment, not published yet.

Yi, H., Hao, J., and Tang, X., 2007. ***Atmospheric Environmental Protection in China: Current Status, Developmental Trend and Research Emphasis.*** Energy Policy, 35: 907-915.

Youngs, W.D., Rutzke, M., Gutenmann, W.H., and Lisk, D.J., 1993. ***Nickel and Vanadium in Foliage in the Vicinity of an Oil-Fired Power Plant.*** Chemosphere, 27(7): 1269-1272.

Yttri, K.E., Norwegian Institute for Air Research, PO Box 100, 2027 Kjeller.

Zhao, C., Tie, X., and Lin, Y., 2006. ***A Possible Positive Feedback of Reduction Of Precipitation and Increase in Aerosols Over Eastern Central China.*** Geophysical Research Letters, 33, L11814.

Zhao, Y., Wang, S., Aunan, K., Seip, H.M., and Hao, J., 2006. ***Air Pollution and Lung Cancer Risks in China – a Meta Analysis.*** Science of the Total Environment, 366: 500-513.

Appendix Overview

	Page
Appendix A	
NIST Data	116
Appendix B	
B-1 Volatilisation of elements in four acids	119
B-2 Precipitation of elements in four acids	120
B-3 Microwave decomposition program – temperature/pressure curves	121
Appendix C	
C-1 Preparation of the daily test solution for ICP-MS	122
Appendix D	
ICP-MS info - colour tables of LODs and all isotopes	123
D-1 Calculation of volumetric element concentrations in SRM	125
D-2 Calculation of required amount of 10mg/l and 1mg/l stocks for std. preparation	127
D-3 Determination of HF load on the instrument	127
D-4 Dilutions carried out for ICP-MS analysis	127
D-5 Preparation of the washing acid mix solution	128
Appendix E	
ICP-AES info – colour table of LODs and characteristic wavelengths	129
E-1 Calculation of volumetric element concentrations in SRM for ICP-AES	131
Appendix F	
F-1 Preparation of methanesulfonic acid for filtration	132
F-2 Calculations regarding external standards for IC	132
F-3 Gradient elution data for anion and cation exchange	135
F-4 IC methods of analysis for anions and cations	136
Appendix G	
G-1 Contents of the quartz_par and EUSAAR TOA protocols	138
Appendix H	
H-1 Elaboration of ICP-MS data	143
Appendix I	
I-1 Elaboration of ICP-AES data	151
Appendix J	
J-1 Results of IC analysis of solutions – Anions	156
J-2 Results of IC analysis of solutions – Cations	159
J-3 PM quantifications on cut quartz filters	162
J-4 Error assessment of solution concentrations of all analysed ions	164
Appendix K	
K-1 Thermal/optical carbon analysis of Taiyuan samples	165
K-2 Thermograms of Taiyuan samples	166
Appendix L	
L-1 Bulk PM_{10} concentrations of Taiyuan samples on Teflon and quartz filters	179
L-2 Gauss' error progression law	179

Appendix A

National Institute of Standards & Technology

Certificate of Analysis

Standard Reference Material® 1648

Urban Particulate Matter

This Standard Reference Material (SRM) is intended primarily for use as a control material and in the evaluation of methods used in the analysis of atmospheric particulate matter and materials with a similar matrix. It consists of 2 g of natural atmospheric particulate matter collected in an urban location. While not represented to be typical of the area in which it was collected, its use should typify the analytical problems of atmospheric samples obtained from industrialized urban areas.

The certified values expressed in mass fraction, for the constituent elements are shown in Table 1. Noncertified values expressed in mass fraction, are given for information only in Table 2. The analytical methods used in the characterization of this SRM are shown in Table 3. The certified values are based on measurements of 6 to 30 samples by each of the analytical methods indicated.

NOTICE AND WARNING TO USERS

Expiration of Certification: The certification of SRM 1648 is valid, within the measurement uncertainty (ies) specified, until **31 December 2008**, provided the SRM is handled in accordance with instructions given in this certificate (see Instructions for Use). This certification is nullified if the SRM is damaged, contaminated, or modified.

Maintenance of SRM Certification: NIST will monitor this SRM over the period of its certification. If substantive technical changes occur that affect the certification before the expiration of this certificate, NIST will notify the purchaser. Return of the attached registration card will facilitate notification.

Instructions for Use: This material may contain a number of chemicals of unknown toxicities. Therefore, the utmost caution and care must be exercised in its use. A minimum of 100 mg of the dried material (See Instructions for Drying) should be used for any analytical determination to be related to the certified values of this certificate. When not in use, this material should be kept in its original bottle and stored at temperatures between 10 °C to 30 °C. It should not be exposed to intense sources of radiation, including ultraviolet lamps or sunlight. Ideally, the bottle should be kept in a desiccator in the recommended temperature range.

Instructions for Drying: The certified concentrations are reported on a "dry-weight" basis. This material should be dried at 105 °C for 8 h before use because concentrations determined on undried samples must therefore be adjusted for the moisture content.

The technical and support aspects involved in the original preparation, certification, and issuance of this SRM were coordinated through the Standard Reference Materials Program by T.E. Gills. Measurement activities for revision of this certificate were coordinated through the Standard Reference Materials Program by B.S. MacDonald.

Gaithersburg, MD 20899
Certificate Issue Date: 28 April 1998

Thomas E. Gills, Chief
Standard Reference Materials Program

11/16/78 (original certificate date); 5/11/82 (additional certification update); 6/30/91 (editorial)
*This revision reports a change in the certified value of vanadium, the addition of the manganese certified value, the subsequent removal of the manganese information value, and change in expiration date.

Statistical analysis of the revised certification data for manganese and vanadium was performed by K.R. Eberhardt of the NIST Statistical Engineering Division.

Homogeneity Assessment: Randomly selected bottles were used for the analytical measurements. Each analyst examined at least 6 bottles. No correlation was found between measured values and the bottling sequence. Also, the results of measurements of samples from different bottles were not significantly different from the measurements of replicate samples from single bottles. Accordingly, all bottles of this SRM have been assigned the same certified values of constituent elements.

Source and Preparation of Material: This SRM was prepared from urban particulate matter collected in the St. Louis, MO area in a baghouse specially designed for this purpose. The material was collected over a period in excess of 12 months and, therefore, is a time-integrated sample. The material was removed from the filter bags, combined in a single lot, screened through a fine mesh sieve to remove extraneous materials and thoroughly blended in a v-blender. The material was then packaged into sequentially numbered bottles.

Table 1. Certified Values of Constituent Elements

Major Constituents

Element	Content Mass Fraction, in %
Aluminum	3.42 ± 0.11
Iron	3.91 ± 0.10
Potassium	1.05 ± 0.01

Minor Constituents

Element	Content Mass Fraction, in %
Lead	0.655 ± 0.008
Sodium	0.425 ± 0.002
Zinc	0.476 ± 0.014

Trace Constituents

Element	Content mg/kg
Arsenic	115 ± 10
Cadmium	75 ± 7
Chromium	403 ± 12
Copper	609 ± 27
Manganese	786 ± 17

Element	Content mg/kg
Nickel	82 ± 3
Selenium	27 ± 1
Uranium	5.5 ± 0.1
Vanadium	127 ± 7

[a] The uncertainties of the certified values, except those noted, include errors associated with both measurement and material variability. They represent the 95 % tolerance limits for individual subsamples, i.e., 95 % of the subsamples from a single unit of this SRM would be expected to have a composition within the indicated range of values 95 % of the time.

[b] The indicated constituent was certified as a part of the NIST update certification program, in August 1991. The value for each indicated constituent is the "best value" based on all measurement methods used and the associated uncertainty is expressed as the standard error considering variability within and between analytical methods.

[c] The uncertainty in the certified value is calculated as $U = ku + B$ where u is the combined standard uncertainty calculated according to the ISO Guide [1] and k is a coverage factor. The additional quantity, B, is an allowance for the differences between methods of analysis and is taken to be equal to the difference between the most discrepant method value and the certified value. The expanded uncertainty (U) given is intended to approximate the 95 % level of confidence.

Table 2. Noncertified Values for Constituent Elements

Major Constituents		Minor Constituents	
Element	Content Mass Fraction, in %	Element	Content Mass Fraction, in %
Sulfur	5.0	Chlorine	0.45
Magnesium	0.8	Titanium	0.40

Trace Constituents

Element	Content mg/kg	Element	Content mg/kg
Antimony	45	Iodine	20
Barium	737	Lanthanum	42
Bromine	500	Rubidium	52
Cerium	55	Samarium	4.4
Cesium	3	Scandium	7
Cobalt	18	Silver	6
Europium	0.8	Thorium	7.4
Hafnium	4.4	Tungsten	4.8
Indium	1.0		

Table 3. Methods of Analysis

Element	Methods	Element	Methods
Aluminum	DCPAES, NAA	Lead	AAS, IDMS, POL
Antimony	NAA	Magnesium	NAA
Arsenic	NAA, SPECTR	Manganese	AAS, NAA, DCPAES
Barium	NAA	Nickel	AAS, IDMS, POL
Bromine	NAA	Potassium	AAS
Cadmium	AAS, IDMS, NAA, POL	Rubidium	NAA
Cerium	NAA	Samarium	NAA
Cesium	NAA	Scandium	NAA
Chlorine	NAA	Selenium	AAS, NAA, FES
Chromium	IDMS, NAA	Sodium	AAS, NAA, FES
Cobalt	NAA	Silver	NAA
Copper	AAS, IDMS, SPECTR	Sulfur	IC
Europium	NAA	Thorium	NAA
Hanfium	NAA	Titanium	NAA
Indium	NAA	Tungsten	NAA
Iodine	NAA, PAA	Uranium	IDMS
Iron	AAS, IDMS, NAA, SPECTR	Vanadium	NAA
Lanthanum	NAA	Zinc	AAS, IDMS, NAA, POL

Methods

AAS	Atomic Absorption Spectrometry	FES	Flame Emission Spectrometry
DCPAES	DC Plasma Atomic Emission Spectrometry	NAA	Neutron Activation Analysis
IC	Ion Chromatography	PAA	Photon Activation Analysis
IDMS	Isotope Dilution Thermal Ionization Spectrometry	POL	Polarography
		SPECTR	Spectrophotometry

Appendix B

B-1 Volatility of elements in four acids [microwave decomposition]

[source: Kingston and Walter, 1998]

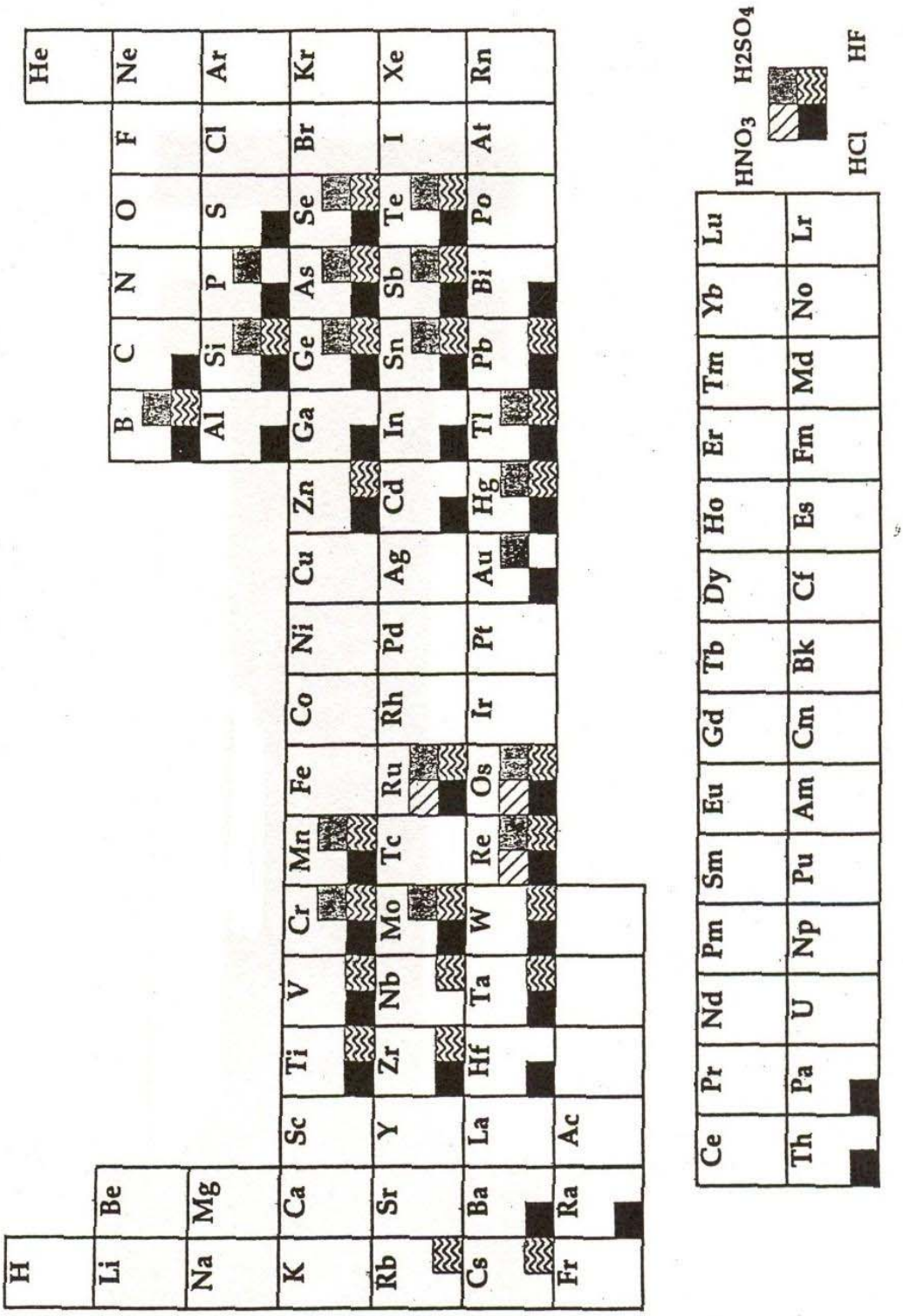

B-2 Precipitation of elements in four acids [microwave decomposition]

[source: Kingston and Walter, 1998]

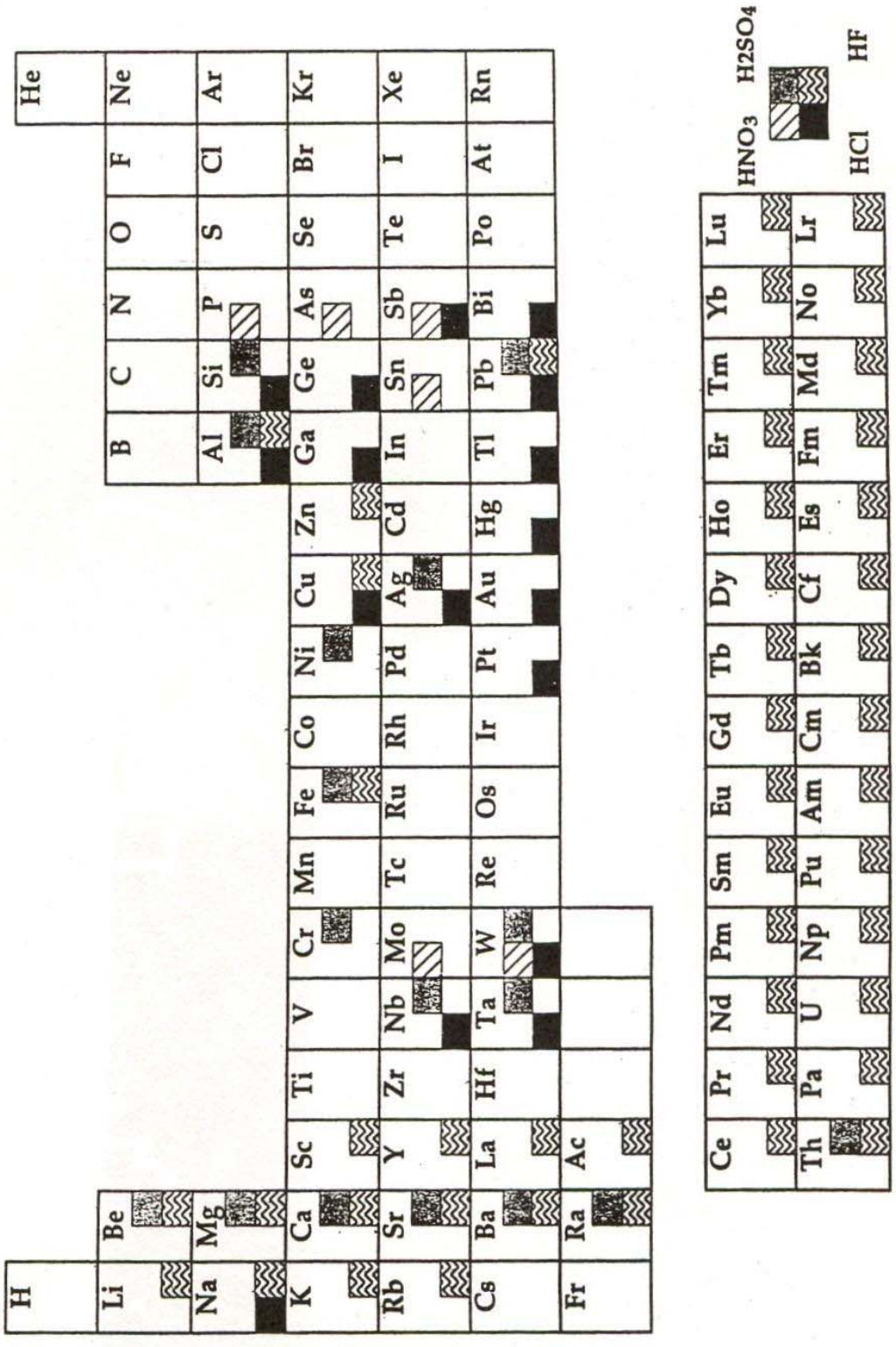

B-3 Microwave decomposition program – temperature/pressure curves

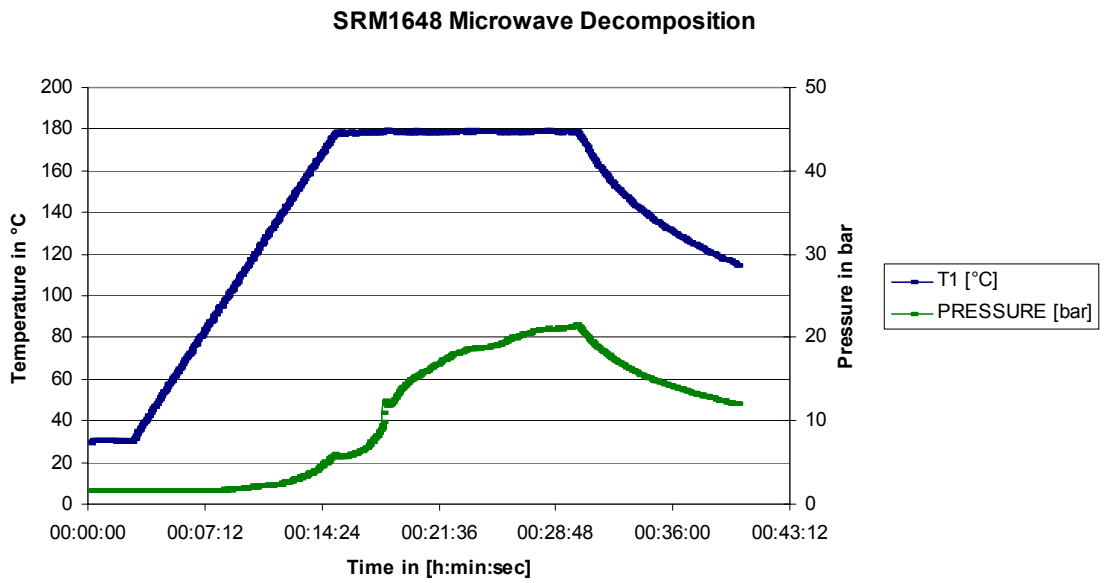

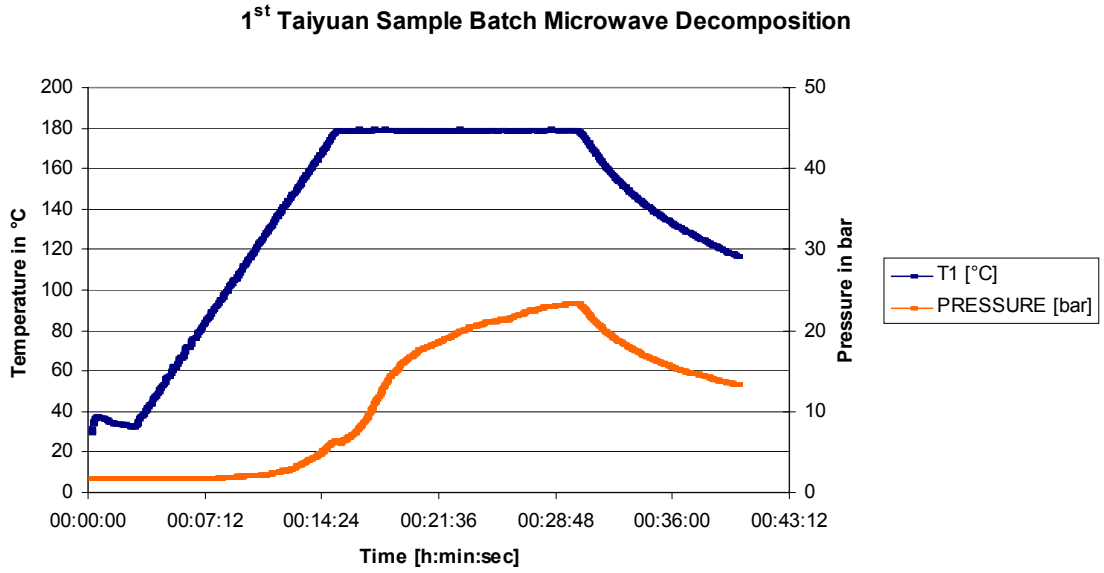

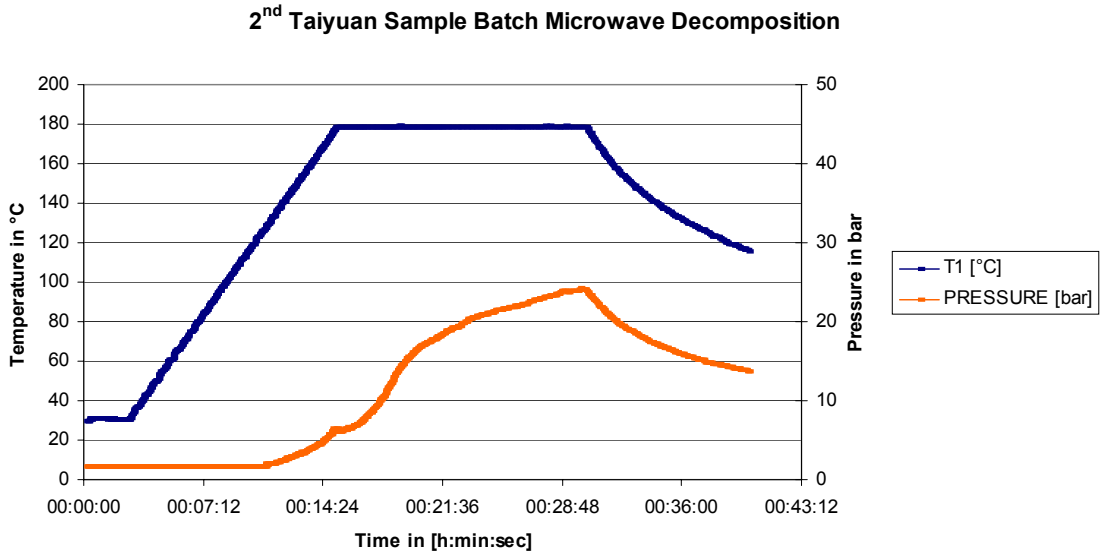

Appendix C

C-1 Preparation of the daily test solution for ICP-MS

A daily test solution was prepared containing Mg, Cu, Cd, Pb, Sc, Rh, Tl, Ce, Tb, Ba and Ge in the concentration of 10ng/ml. This was done in two steps:

1. 5ml of each of the above mentioned single element standards (1000μg/ml) were transferred into a 1000ml glass flask resulting in a solution with the concentration of 5μg/ml. This solution was already prepared and only the second step needed to be carried out.

2. 2ml of the 5μg/ml solution was transferred into a 1000ml volumetric glass flask to obtain the desired concentration of 10ng/ml.

Appendix D


The ELAN® Series of ICP-Mass Spectrometers
Simplifying Ultratrace Analysis
Zn — Atomic Number, Symbol
Isotopic Abundance
Most Abundant Isotope
Detection Limit Ranges
<0.1–1 ppt
1-10 ppt
10-100 ppt
0.1-1 ppb
1-10 ppb
PerkinElmerSCIEX
instruments

Relative Abundance of the Natural Isotopes

Isotope		%		%		%	Isotope		%		%		%		%	Isotope		%		%		%	Isotope		%		%		%
1	H	99.985					61					Ni	1.140	121					Sb	57.36	181	Ta	99.988				
2	H	0.015					62					Ni	3.634	122	Sn	4.63	Te	2.603			182			W	26.3		
3			He	0.000137			63	Cu	69.17					123			Te	0.908	Sb	42.64	183			W	14.3		
4			He	99.999863			64			Zn	48.6	Ni	0.926	124	Sn	5.79	Te	4.816	Xe	0.10	184	Os	0.02	W	30.67		
5							65	Cu	30.83					125			Te	7.139			185					Re	37.40
6					Li	7.5	66			Zn	27.9			126			Te	18.95	Xe	0.09	186	Os	1.58	W	28.6		
7					Li	92.5	67			Zn	4.1			127	I	100					187	Os	1.6			Re	62.60
8							68			Zn	18.8			128			Te	31.69	Xe	1.91	188	Os	13.3				
9	Be	100					69					Ga	60.108	129					Xe	26.4	189	Os	16.1				
10			B	19.9			70	Ge	21.23	Zn	0.6			130	Ba	0.106	Te	33.80	Xe	4.1	190	Os	26.4			Pt	0.01
11			B	80.1			71					Ga	39.892	131					Xe	21.2	191			Ir	37.3		
12					C	98.90	72	Ge	27.66					132	Ba	0.101			Xe	26.9	192	Os	41.0			Pt	0.79
13					C	1.10	73	Ge	7.73					133			Cs	100			193			Ir	62.7		
14	N	99.643					74	Ge	35.94	Se	0.89			134	Ba	2.417			Xe	10.4	194					Pt	32.9
15	N	0.366					75					As	100	135	Ba	6.592					195					Pt	33.8
16			O	99.762			76	Ge	7.44	Se	9.36			136	Ba	7.854	Ce	0.19	Xe	8.9	196	Hg	0.15			Pt	25.3
17			O	0.038			77			Se	7.63			137	Ba	11.23					197			Au	100		
18			O	0.200			78	Kr	0.35	Se	23.78			138	Ba	71.70	Ce	0.25	La	0.0902	198	Hg	9.97			Pt	7.2
19					F	100	79					Br	50.69	139					La	99.9098	199	Hg	16.87				
20	Ne	90.48					80	Kr	2.25	Se	49.61			140			Ce	88.48			200	Hg	23.10				
21	Ne	0.27					81					Br	49.31	141					Pr	100	201	Hg	13.18				
22	Ne	9.25					82	Kr	11.6	Se	8.73			142	Nd	27.13	Ce	11.08			202	Hg	29.86				
23			Na	100			83	Kr	11.5					143	Nd	12.18					203					Tl	29.524
24					Mg	78.99	84	Kr	57.0	Sr	0.56			144	Nd	23.80	Sm	3.1			204	Hg	6.87	Pb	1.4		
25					Mg	10.00	85					Rb	72.165	145	Nd	8.30					205					Tl	70.476
26					Mg	11.01	86	Kr	17.3	Sr	9.86			146	Nd	17.19					206			Pb	24.1		
27	Al	100					87			Sr	7.00	Rb	27.835	147			Sm	15.0			207			Pb	22.1		
28			Si	92.23			88			Sr	82.58			148	Nd	5.76	Sm	11.3			208			Pb	52.4		
29			Si	4.67			89					Y	100	149			Sm	13.8			209	Bi	100				
30			Si	3.10			90	Zr	51.45					150	Nd	5.64	Sm	7.4			210						
31					P	100	91	Zr	11.22					151					Eu	47.8	211						
32	S	95.02					92	Zr	17.15	Mo	14.84			152	Gd	0.20	Sm	26.7			212						
33	S	0.75					93					Nb	100	153					Eu	52.2	213						
34	S	4.21					94	Zr	17.38	Mo	9.25			154	Gd	2.18	Sm	22.7			214						
35			Cl	75.77			95			Mo	15.92			155	Gd	14.80					215						
36	S	0.02			Ar	0.337	96	Zr	2.80	Mo	16.68	Ru	5.52	156	Gd	20.47	Dy	0.06			216						
37			Cl	24.23			97			Mo	9.55			157	Gd	15.65					217						
38					Ar	0.063	98			Mo	24.13	Ru	1.88	158	Gd	24.84	Dy	0.10			218						
39	K	93.2581					99					Ru	12.7	159					Tb	100	219						
40	K	0.0117	Ca	96.941	Ar	99.600	100			Mo	9.63	Ru	12.6	160	Gd	21.86	Dy	2.34			220						
41	K	6.7302					101					Ru	17.0	161			Dy	18.9			221						
42			Ca	0.647			102	Pd	1.02			Ru	31.6	162	Er	0.14	Dy	25.5			222						
43			Ca	0.135			103			Rh	100			163			Dy	24.9			223						
44			Ca	2.086			104	Pd	11.14			Ru	18.7	164	Er	1.61	Dy	28.2			224						
45					Sc	100	105	Pd	22.33					165					Ho	100	225						
46	Ti	8.0	Ca	0.004			106	Pd	27.33	Cd	1.25			166	Er	33.6					226						
47	Ti	7.3					107					Ag	51.839	167	Er	22.95					227						
48	Ti	73.8	Ca	0.187			108	Pd	26.46	Cd	0.89			168	Er	26.8	Yb	0.13			228						
49	Ti	5.5					109					Ag	48.161	169					Tm	100	229						
50	Ti	5.4	V	0.250	Cr	4.345	110	Pd	11.72	Cd	12.49			170	Er	14.9	Yb	3.05			230						
51			V	99.750			111			Cd	12.80			171			Yb	14.3			231	Pa	100				
52					Cr	83.789	112	Sn	0.97	Cd	24.13			172			Yb	21.9			232	Th	100				
53					Cr	9.501	113			Cd	12.22	In	4.3	173			Yb	16.12			233						
54	Fe	5.8			Cr	2.365	114	Sn	0.65	Cd	28.73			174			Yb	31.8	Hf	0.162	234	U	0.0055				
55			Mn	100			115	Sn	0.34			In	95.7	175	Lu	97.41					235	U	0.7200				
56	Fe	91.72					116	Sn	14.53	Cd	7.49			176	Lu	2.59	Yb	12.7	Hf	5.206	236						
57	Fe	2.2					117	Sn	7.68					177					Hf	18.606	237						
58	Fe	0.28			Ni	68.077	118	Sn	24.23					178					Hf	27.297	238	U	99.2745				
59			Co	100			119	Sn	8.59					179					Hf	13.629							
60					Ni	26.223	120	Sn	32.59	Te	0.096			180	Ta	0.012	W	0.13	Hf	35.100							

"Isotopic Compositions of the Elements 1989," Pure Appl. Chem., Vol. 63, No. 7, pp. 991-1002, 1991. © 1991 IUPAC.

PerkinElmer Instruments
710 Bridgeport Avenue, Shelton, CT 06484 USA
Tel: 800-762-4000 or (+1) 203-925-4600
www.perkinelmer.com/instruments

PerkinElmerSCIEX
instruments

D-1 Calculation of volumetric element concentrations in SRM

- With the use of the individual NIST value of the certified element concentration in 1kg of standard reference material 1648 (see appendix A) example **As**: NIST concentration – **115 mg (As)/kg (SRM)**
- The actual amount of SRM used for decomposition, e.g. **15mg**
- And the total volume of liquid in which it was dissolved in: **60ml**

→ The volumetric concentration of As can be calculated according to:

$$c_{As} = \frac{115 \cdot 10^{3}\,\mu g(As) \cdot 15 \cdot 10^{-6}\,kg(SRM)}{kg(SRM) \cdot 60 \cdot 10^{-3}\,l} = 28.75\,\frac{\mu g(As)}{l} = \underline{28.75\,ppb}$$

This concentration does not account for the water content and thus needs to be adjusted. The water content was determined to be 3.36% and the corrected results are shown in table D-1 on the next page.

Seven different amounts of SRM1648 have been prepared leading to the seven different solution concentrations for each element in table D-1. The order, according to the names of the SRM1648 samples shown in table 5, is:

2SRM4
2SRM3
2SRM2
2SRM1
2SRM5
2SRM6
2SRM7

Table D-1 – Determination of volumetric concentrations of SRM1648 for ICP-MS

Element and relative abundance	NIST conc. in mg/kg	Amount SRM used in mg	Amount corrected for water in mg	Solution conc. in μg/l	Element and relative abundance	NIST conc. in mg/kg	Amount SRM used in mg	Amount corrected for water in mg	Solution conc. in μg/l
V[51]	127	3.00	2.90	**6.14**	**As[75]**	115	3.00	2.90	**5.56**
99,75%	127	5.70	5.51	**11.7**	**100%**	115	5.70	5.51	**10.6**
	127	8.70	8.41	**17.8**		115	8.70	8.41	**16.1**
	127	11.0	10.6	**22.5**		115	11.0	10.6	**20.4**
	127	12.1	11.7	**24.8**		115	12.1	11.7	**22.4**
	127	15.3	14.8	**31.3**		115	15.3	14.8	**28.3**
	127	33.3	32.2	**68.1**		115	33.3	32.2	**61.7**
Mn[55]	786	3.00	2.90	**38.0**	**Se[77]**	27	3.00	2.90	**1.30**
100%	786	5.70	5.51	**72.2**	**7,63%**	27	5.70	5.51	**2.48**
	786	8.70	8.41	**110**		27	8.70	8.41	**3.78**
	786	11.0	10.6	**139**		27	11.0	10.6	**4.78**
	786	12.1	11.7	**153**		27	12.1	11.7	**5.26**
	786	15.3	14.8	**194**		27	15.3	14.8	**6.65**
	786	33.3	32.2	**422**		27	33.3	32.2	**14.5**
Co[59]	18	3.00	2.90	**0.87**	**Cd[111]**	75	3.00	2.90	**3.62**
100%	18	5.70	5.51	**1.65**	**12,80%**	75	5.70	5.51	**6.89**
	18	8.70	8.41	**2.52**		75	8.70	8.41	**10.5**
	18	11.0	10.6	**3.19**		75	11.0	10.6	**13.3**
	18	12.1	11.7	**3.51**		75	12.1	11.7	**14.6**
	18	15.3	14.8	**4.44**		75	15.3	14.8	**18.5**
	18	33.3	32.2	**9.65**		75	33.3	32.2	**40.2**
Ni[60]	82	3.00	2.90	**3.96**	**Sb[121]**	45	3.00	2.90	**2.17**
26,22%	82	5.70	5.51	**7.53**	**57,36%**	45	5.70	5.51	**4.13**
	82	8.70	8.41	**11.5**		45	8.70	8.41	**6.31**
	82	11.0	10.6	**14.5**		45	11.0	10.6	**7.97**
	82	12.1	11.7	**16.0**		45	12.1	11.7	**8.77**
	82	15.3	14.8	**20.2**		45	15.3	14.8	**11.1**
	82	33.3	32.2	**44.0**		45	33.3	32.2	**24.1**
Cu[63]	609	3.00	2.90	**29.4**	**Pb[208]**	$655•10^1$	3.00	2.90	**316**
69.17%	609	5.70	5.51	**55.9**	**52,4%**	$655•10^1$	5.70	5.51	**601**
	609	8.70	8.41	**85.3**		$655•10^1$	8.70	8.41	**918**
	609	11.0	10.6	**108**		$655•10^1$	11.0	10.6	**$116•10^1$**
	609	12.1	11.7	**119**		$655•10^1$	12.1	11.7	**$128•10^1$**
	609	15.3	14.8	**150**		$655•10^1$	15.3	14.8	**$161•10^1$**
	609	33.3	32.2	**327**		$655•10^1$	33.3	32.2	**$351•10^1$**

D-2 Calculation of required amount of 10mg/l and 1mg/l stocks for standard preparation

By using the formula: $c_1 \cdot V_1 = c_2 \cdot V_2 \quad \Leftrightarrow \quad V_1 = \frac{c_2 \cdot V_2}{c_1}$

with: V_1,V_2 – needed volume from element stock, 100ml and
c_1,c_2 – desired standard concentration, element stock concentration,

the required amounts (see table 7) of each stock solution, to obtain the desired standard concentration, can be determined.

D-3 Determination of HF load on the instrument

The instrumental parts which are in contact with the sample are considered HF resistant up to a certain level. The maximum acceptable percentage of HF was set to 10%.

The HF concentration in the decomposed samples (SRM) can be calculated as follows: **4ml** of HF in **24ml** of the decomposition acid mixture

xml of HF in **10ml** added for each individual decomposition

→ **x = 1.67ml** of concentrated (40%) HF in 60ml of total sample (SRM) decomposition solution

→ 2.8% concentrated HF

[1.1% HF, as conc. HF = 40%]

After accounting for the dilution factor introduced by the standard addition procedure (4/5), the actual figures decrease to: → **2.2% concentrated HF**

[0.90% HF]

D-4 Dilutions carried out for ICP-MS analysis

A few samples (SRM) were diluted in order for them to fall within the selected standard concentration range. The applied dilution caused the acid concentration to fall and was accounted for by the addition of nitric acid. The initial HNO_3 concentration after decomposition in 60ml of solution was approximately 9%. Table D-2 summarises the procedure but only includes instances where dilutions have been carried out. For the determination of the elements **As[75]**, **Ni[60]**, **Sb[121]**, **Se[77]**, **V[51]**, **Cd[111]** and **Co[59]**, where no dilutions were applied, the

representative samples **2SRM5** and **T69** were selected for the analysis of the standard reference material and samples respectively.

Table D-2 – Dilutions performed for ICP-MS analysis

Determined Element(s)	SRM or Sample	Dilution Factor	Samples (SRM) Applied to	Amounts Mixed [ml] of		
				SRM/Sample	Nitric Acid	Type 1 H_2O
Pb	Sample	5	T59*	6.00	1.50	22.5
Pb	Sample	5	All others	2.00	0.50	7.50
Pb	SRM	20	2SRM3*	2.00	2.00	36.0
Pb	SRM	20	All others except	1.00	1.00	18.0
Pb	SRM	30	2SRM7	1.00	1.50	27.5
Cu, Mn	Sample	10	T59*	3.00	1.50	25.5
Cu, Mn	Sample	10	All others	1.00	0.50	8.50
Cu, Mn	SRM	10	2SRM3*	3.00	1.50	25.5
Cu, Mn	SRM	10	All others	1.00	0.50	8.50

*) Indicates the representative sample (SRM)

D-5 Preparation of the washing acid mix solution

A washing solution containing a slightly stronger acid matrix than all samples was used to clean the system from potential contaminations, deposited substances and to eliminate a possible memory effect.

The solution was prepared in a 100ml volumetric flask made of PP because of the HF content. The following calculation illustrates how the solution was obtained.

10ml of acid mixture (5+1 HNO_3 – HF) in **60ml** for all samples, etc.

xml of acid mixture in **100ml** for the washing sol.

→ x = 16.667ml of acid mixture needed to achieve the same concentration as in the samples

With consideration of the standard addition procedure, a dilution factor of 1.25 Is introduced, changing the actual amount of acid matrix to: **x = 13.334ml**

A slightly larger amount was applied when non-diluted samples (SRM) were analysed [13.5ml] and in case of analysis of diluted samples (SRM), the volume of acid added to the washing solution was reduced by the given dilution factor.

Appendix E

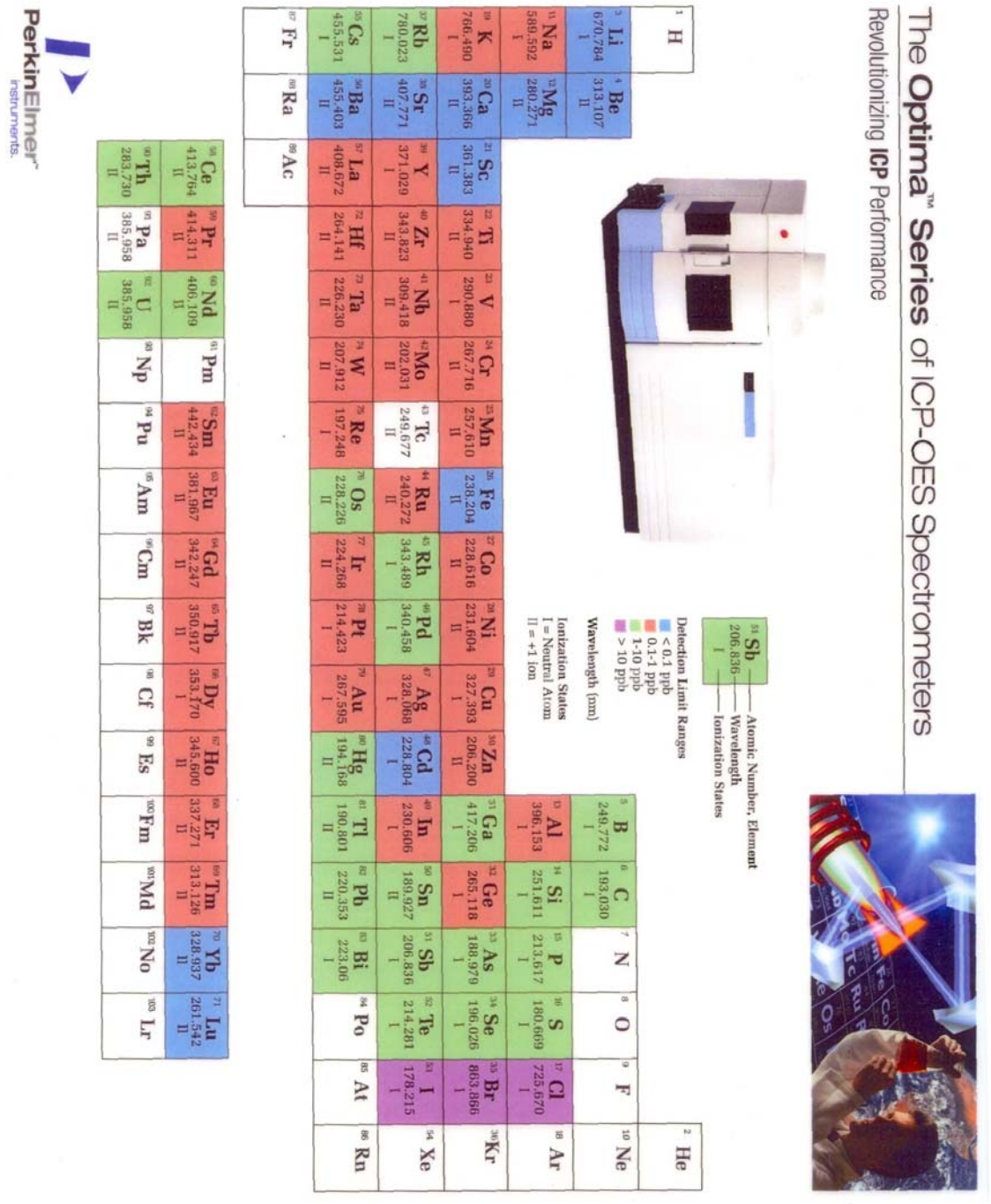
The Optima™ Series of ICP-OES Spectrometers
Revolutionizing ICP Performance
51 Sb 206.836 I
Atomic Number, Element
Wavelength
Ionization States
Detection Limit Ranges
< 0.1 ppb
0.1-1 ppb
1-10 ppb
> 10 ppb
Wavelength (nm)
Ionization States
I = Neutral Atom
II = +1 ion
PerkinElmer instruments.

Selected Wavelengths (Relative Intensities Normalized to Preferred Wavelength)

Analyte	Wave Lengths (nm)	Relative Sensitivity	Ionization State
Ag	328.068	1.00	I
	338.289	0.48	I
	243.778	0.02	II
Al	396.153	1.00	I
	308.215	0.36	I
	394.401	0.50	I
As	188.979	1.00	I
	193.696	2.76	I
	197.197	2.05	I
Au	267.595	1.00	I
	242.795	0.77	I
	208.209	0.22	II
B	249.667	1.00	I
	249.772	0.20	I
	208.889	0.42	I
Ba	233.527	1.00	II
	455.403	9.33	II
	493.408	2.87	II
Be	313.107	1.00	II
	313.042	1.53	II
	234.861	0.74	I
Bi	223.061	1.00	I
	190.171	0.07	II
	306.766	1.08	I
Br	863.866	1.00	I
	700.570		I
C	193.030	1.00	I
	247.856	0.45	I
Ca	317.933	1.00	II
	393.366	84	II
	227.546	0.003	I
Cd	228.802	1.00	I
	214.440	1.13	II
	226.502	0.93	II
Ce	413.764	1.00	II
	418.660	1.75	II
	413.380	1.35	II
Cl	725.670	1.00	I
	782.139	0.01	I
Co	228.616	1.00	II
	238.892	1.11	II
	230.786	0.98	II
Cr	267.716	1.00	II
	205.560	0.49	II
	283.563	1.31	II
Cs	455.531	1.00	I
	459.320	0.21	I
Cu	327.393	1.00	I
	324.752	1.98	I
	224.700	0.78	II
Dy	353.170	1.00	II
	394.468	0.46	II
	396.839	0.33	II
Er	337.271	1.00	II
	349.910	0.87	II
	339.200	0.30	II
Eu	381.967	1.00	II
	412.970	0.41	II
	393.048	0.40	II
Fe	238.204	1.00	II
	239.562	0.81	II
	259.939	1.55	II
Ga	417.206	1.00	I
	294.364	0.86	I
	209.134	0.04	I
Gd	342.247	1.00	II
	336.223	0.78	II
	335.047	0.78	II
Ge	209.426	1.00	I
	265.118	1.74	I
	206.866	0.87	I
Hf	277.336	1.00	II
	232.247	0.59	II
	264.141	0.87	II
Hg	253.652	1.00	II
	404.656	0.12	I
	435.835	0.06	I
Ho	345.600	1.00	II
	339.898	0.50	II
	347.426	0.33	II
I	178.215	1.00	I
	206.188	1.56	I
	182.976	0.62	I
In	230.606	1.00	II
	325.609	1.06	I
	303.936	0.65	I
Ir	205.222	1.00	I
	224.268	3.13	II
	208.882	0.58	I
K	766.490	1.00	I
	404.721	0.001	I
	769.896	0.60	I
La	408.672	1.00	II
	379.478	0.71	II
	407.735	0.52	II
Li	670.784	1.00	I
	610.362	0.09	I
	460.286	0.004	I
Lu	261.542	1.00	II
	291.139	0.25	II
	219.554	0.07	II
Mg	285.213	1.00	I
	279.077	0.04	II
	280.271	4.67	II
Mn	257.610	1.00	II
	259.372	0.83	II
	260.568	0.59	II
Mo	202.031	1.00	II
	203.845	0.65	II
	204.597	0.65	II
Na	589.592	1.00	I
	330.237	0.03	I
	588.995	1.95	I
Nb	309.418	1.00	II
	313.079	0.82	II
	269.706	0.57	II
Nd	406.109	1.00	II
	401.225	1.43	II
	430.358	1.13	II
Ni	231.604	1.00	II
	221.648	2.04	II
	232.003	1.30	I
Os	228.226	1.00	II
	225.585	1.45	II
	189.900	0.33	II
P	213.617	1.00	I
	214.914	0.46	I
	178.221	0.68	I
Pb	220.353	1.00	II
	217.000	0.38	I
	261.418	0.38	I
Pd	340.458	1.00	I
	363.470	0.85	I
	324.270	0.46	I
Pr	390.844	1.00	II
	414.311	0.89	II
	422.293	1.24	II
Pt	265.945	1.00	I
	214.423	1.57	II
	299.797	0.64	I
Rb	780.023	1.00	I
	420.185	0.001	I
Re	197.248	1.00	II
	227.525	1.74	II
	204.908	0.09	I
Rh	343.489	1.00	I
	233.477	0.88	II
	346.204	0.79	I
Ru	240.272	1.00	II
	349.894	0.65	I
	279.535	0.27	II
S	181.975	1.00	I
	180.669	2.38	I
	182.563	1.72	I
Sb	206.836	1.00	I
	217.582	0.83	I
	231.146	0.68	I
Sc	361.383	1.00	II
	357.253	0.78	II
	424.683	0.52	II
Se	196.026	1.00	I
	203.985	0.74	I
Si	251.611	1.00	I
	212.412	0.22	I
	288.158	0.73	I
Sm	359.260	1.00	II
	442.434	0.69	II
	388.529	0.86	II
Sn	189.927	1.00	I
	235.485	1.34	I
	283.998	2.22	I
Sr	407.771	1.00	II
	421.552	0.70	II
	460.773	0.01	I
Ta	226.230	1.00	II
	240.063	1.45	II
	233.198	0.70	II
Tb	350.917	1.00	II
	384.873	0.37	II
Te	214.281	1.00	I
	238.578	0.29	I
	226.555	0.04	I
Th	283.730	1.00	II
	401.913	1.05	II
	339.204	0.65	II
Ti	334.940	1.00	II
	336.121	0.59	II
	337.279	0.49	II
Tl	190.801	1.00	II
	276.787	0.59	I
	351.924	0.49	I
Tm	313.126	1.00	II
	346.220	1.17	II
U	385.958	1.00	II
	367.007	0.92	II
	409.014	0.72	II
V	290.880	1.00	II
	310.230	1.21	II
	309.310	1.57	II
W	207.912	1.00	II
	224.876	0.72	II
	239.708	1.15	II
Y	371.029	1.00	II
	324.227	0.47	II
	360.073	0.76	II
Yb	328.937	1.00	II
	369.419	1.05	II
	289.138	0.21	II
Zn	206.200	1.00	II
	213.857	4.44	I
	202.548	1.41	II
Zr	343.823	1.00	II
	339.197	1.21	II
	257.139	0.44	II

PerkinElmer Instruments
710 Bridgeport Avenue, Shelton, CT 06484 USA
Tel: 800-762-4000 or (+1) 203-925-4600
www.perkinelmer.com/instruments

Printed in U.S.A. KG120103 D-6592

PerkinElmer instruments.

E-1 Calculation of volumetric element concentrations in SRM for ICP-AES

The way of calculating the table data follows the procedure outlined in D-1. Silicon is not mentioned in table F-1 as there was no certified NIST value available.

Table E-1 – Determination of volumetric concentrations of SRM1648 for ICP-AES

Element	NIST conc. in g/kg	Amount SRM used in mg	Amount corrected for water in mg	Solution conc. in mg/l	Element	NIST conc. in g/kg	Amount SRM used in mg	Amount corrected for water in mg	Solution conc. in mg/l
	34.2	3.00	2.90	**1.65**		4.76	3.00	2.90	**0.23**
	34.2	5.70	5.51	**3.14**		4.76	5.70	5.51	**0.44**
	34.2	8.70	8.41	**4.79**		4.76	8.70	8.41	**0.67**
Al	34.2	11.0	10.6	**6.06**	**Zn**	4.76	11.0	10.6	**0.84**
	34.2	12.1	11.7	**6.67**		4.76	12.1	11.7	**0.93**
	34.2	15.3	14.8	**8.43**		4.76	15.3	14.8	**1.17**
	34.2	33.3	32.2	**18.34**		4.76	33.3	32.2	**2.55**
	39.1	3.00	2.90	**1.89**		8	3.00	2.90	**0.39**
	39.1	5.70	5.51	**3.59**		8	5.70	5.51	**0.73**
	39.1	8.70	8.41	**5.48**		8	8.70	8.41	**1.12**
Fe	39.1	11.0	10.6	**6.93**	**Mg**	8	11.0	10.6	**1.42**
	39.1	12.1	11.7	**7.62**		8	12.1	11.7	**1.56**
	39.1	15.3	14.8	**9.64**		8	15.3	14.8	**1.97**
	39.1	33.3	32.2	**20.97**		8	33.3	32.2	**4.29**
	4.25	3.00	2.90	**0.21**		4	3.00	2.90	**0.19**
	4.25	5.70	5.51	**0.39**		4	5.70	5.51	**0.37**
	4.25	8.70	8.41	**0.60**		4	8.70	8.41	**0.56**
Na	4.25	11.0	10.6	**0.75**	**Ti**	4	11.0	10.6	**0.71**
	4.25	12.1	11.7	**0.83**		4	12.1	11.7	**0.78**
	4.25	15.3	14.8	**1.05**		4	15.3	14.8	**0.99**
	4.25	33.3	32.2	**2.28**		4	33.3	32.2	**2.15**

Appendix F

F-1 Preparation of methanesulfonic acid for filtration

The mobile phase of the IC reaches a maximum of 50mmol/l methanesulfonic acid (MSA). In order to clean the Maxi-Clean IC-RP cartridge used for sample filtration, a methanesulfonic acid solution slightly stronger was prepared and determined according to the following calculations:

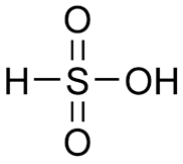

Methanesulfonic Acid

- Amount of MSA needed to obtain 50mmol/l solution:

$$V = \frac{n \cdot M}{\rho} = \frac{50 \cdot 10^{-3} mol \cdot 96.11 g \cdot ml}{1.481 g \cdot mol} = \underline{3.24 ml}$$ of MSA in 1liter solution

With n: number of moles ρ: density of MSA

M: molar mass V: volume

The volume (V) was calculated for 50mmol

- To obtain a higher concentration for filtration, 4ml of MSA in 1l solution were chosen and a solution of 0.4ml in a 100ml flask was prepared. This results in a concentration of 61.6mmol/l

F-2 Calculations regarding external standards for IC

The various standards for IC analysis were generated in two different ways according to the nature of the ions. Furthermore, in the case of the anion standards, which were prepared in μmol/l units, the actually prepared concentrations in the basic stock solutions were initially set equal to the desired, round concentrations (see table 15). They have afterwards been corrected for and included in the calculations leading to the results shown in table 16.

Table F-1 External standard preparation for anions of the SRM1648

F^-				
Standard Concentrations in μmol/l	1	5	10	15
V_1 in ml of c_1	0.125	0.625	1.25	1.875
c_1 in μmol/l	800	800	800	800
Cl^-				
Standard Concentrations in μmol/l	5	10	30	50
V_1 in ml of c_1	0.625	1.25	3.75	6.25
c_1 in μmol/l	800	800	800	800
NO_3^-				
Standard Concentrations in μmol/l	10	30	50	80
V_1 in ml of c_1	0.625	1.875	3.125	5.00
c_1 in μmol/l	1600	1600	1600	1600
SO_4^{2-}				
Standard Concentrations in μmol/l	100	300	500	600
V_1 in ml of c_1	0.625	1.875	3.125	3.75
c_1 in μmol/l	16000	16000	16000	16000

The different stock solutions, indicated by the concentrations [c_1], were either the original ones (table 15), or diluted from them by a factor of 10.

Table F-2 – External standard preparation for anions of the Taiyuan samples

F^-				
Standard Concentrations in μmol/l	5	10	30	50
V_1 in ml of c_1	0.625	1.25	3.75	6.25
c_1 in μmol/l	800	800	800	800
Cl^-				
Standard Concentrations in μmol/l	50	150	250	400
V_1 in ml of c_1	6.25	1.875	3.125	5.00
c_1 in μmol/l	800	8000	8000	8000
NO_3^-				
Standard Concentrations in μmol/l	10	40	80	120
V_1 in ml of c_1	0.625	2.50	5.00	7.50
c_1 in μmol/l	1600	1600	1600	1600
SO_4^{2-}				
Standard Concentrations in μmol/l	50	100	200	300
V_1 in ml of c_1	3.125	0.625	1.25	1.875
c_1 in μmol/l	1600	16000	16000	16000

a) **Anions**:

Two different sets of standards were prepared for anion analysis, one for the SRM1648 and another one for the Taiyuan samples.

With the aid of the formula from D-2: $V_1 = \frac{100ml \cdot c_2}{c_1}$

V_1: needed volume from concentration c_1; c_2: desired concentration in 100ml, the necessary volumes of the individual stocks can be calculated (see tables F-1 and F-2 above).

b) **Cations**:

The cation standards and their preparation from the stock solutions are summarised in table F-3 below. Similar to the anion standards, the cation standards were made in 100ml glass flasks.

Table F-3 – External standard preparation for cations of both SRM1648 and Taiyuan samples

Na^+				
Standard Concentrations in mg/l	0.200	0.500	1.00	4.00
V_1 in ml of c_1	0.200	0.500	1.00	4.00
c_1 in mg/l	100	100	100	100
K^+				
Standard Concentrations in mg/l	0.0100	0.0500	0.100	0.300
V_1 in ml of c_1	0.500	2.50	5.00	15.0
c_1 in mg/l	2.00	2.00	2.00	2.00
NH_4^+				
Standard Concentrations in mg/l	0.500	1.00	5.00	10.0
V_1 in ml of c_1	0.500	1.00	5.00	10.0
c_1 in mg/l	100	100	100	100
Ca^{2+}				
Standard Concentrations in mg/l	1.00	5.00	10.0	15.0
V_1 in ml of c_1	1.00	5.00	10.0	15.0
c_1 in mg/l	100	100	100	100

The utilised stock solutions [c_1] have either already been made recently, or were diluted from them.

F-3 Gradient elution data for anion and cation exchange

As opposed to isocratic elution (i.e. one solvent or constant solvent mixture), the gradient elution is applied to provide sufficiently rapid elution. The following figures F-1 and F-2 display the gradient elution for anions (a) and cations (b).

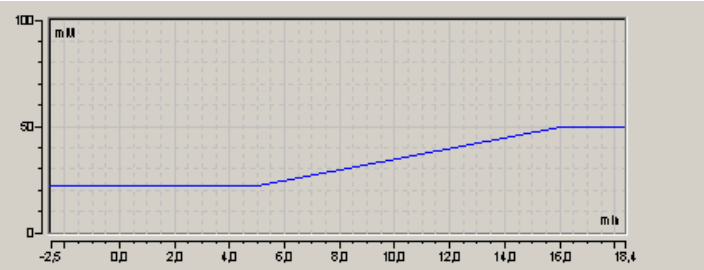

	Retention [min]	Concentration	Curve
1	-2,500	22,00	
2	5,000	22,00	5
3	16,000	50,00	5
4	18,000	50,00	5

Figure F-1 – Gradient elution, anions [concentrations in mmol/l]

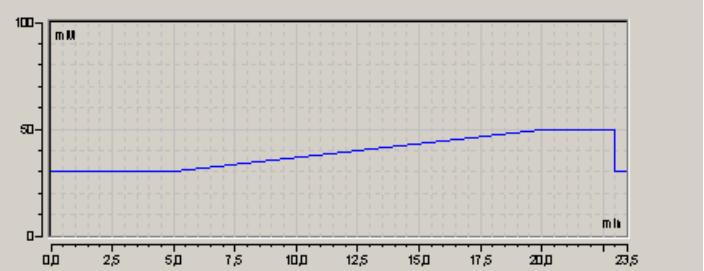

	Retention [min]	Concentration	Curve
1	0,000	30,00	
2	0,000	30,00	
3	5,000	30,00	
4	20,000	50,00	
5	23,000	50,00	

Figure F-2 – Gradient elution, cations [concentrations in mmol/l]

F-4 IC methods of analysis for anions and cations

The used methods in the IC analysis are shown below. Both methods were recommended by the manufacturer and contain optimised parameters.

a) Method of Analysis – CS16 Gradient - Cations

	Data_Collection_Rate =	10.0 [Hz]
	CellTemperature.Nominal =	30.0 [°C]
	ColumnTemperature.Nominal =	40.0 [°C]
	Suppressor_Type =	CSRS_2mm
	Suppressor_Current =	54 [mA]
	Pressure.LowerLimit =	200 [psi]
	Pressure.UpperLimit =	3000 [psi]
	%A.Equate =	"%A"
	Pump_ECD_Relay_1.State	Closed
	CR_TC =	On
	Flow =	0.36 [ml/min]
0.000	Autozero	
	Concentration =	30.00 [mM]
	Inject	
	ECD_1.AcqOn	
	Pump_ECD_Relay_1.State	Open
	Concentration =	30.00 [mM]
0.500	LoadPosition	
5.000	Concentration =	30.00 [mM]
20.000	Concentration =	50.00 [mM]
23.000	Concentration =	50.00 [mM]
	Concentration =	30.00 [mM]
23.400	ECD_1.AcqOff	
	End	

[mM = mmol/l]

b) Method of Analysis – AS18 Gradient – Anions

	LoadPosition	
	Pressure.LowerLimit =	200 [psi]
	Pressure.UpperLimit =	3000 [psi]
	%A.Equate =	"%A"
	CR_TC =	Off
	Data_Collection_Rate =	5.0 [Hz]
	CellTemperature =	35.0 [°C]
	ColumnTemperature =	30.0 [°C]
	Suppressor_Type =	ASRS_4mm
	Suppressor_Current =	100 [mA]
	Flow =	1.00 [ml/min]
-2.500	Concentration =	22.00 [mM]
	Curve =	5
-1.300	Pump_ECD_Relay_1.Closed	
0.000	Inject	
	ECD_1.AcqOn	
	Pump_ECD_Relay_1.Open	
0.5	LoadPosition	
5.000	Concentration =	22.00 [mM]
	Curve =	5
16.000	Concentration =	50.00 [mM]
	Curve =	5
18.000	ECD_1.AcqOff	
	Concentration =	50.00 [mM]
	Curve =	5
	End	

Appendix G

G-1 Contents of the quartz_par and EUSAAR TOA protocols

a) *Quartz_par analysis protocol*

Purge for 10s with blower off

Helium, 10s, 1°C
'start ramping the temperature'
Helium, 60s, 220°C
Helium, 60s, 360°C
Helium, 60s, 525°C
Helium, 90s, 850°C
'let the oven cool before starting elemental'
Helium, 45s, 0°C
'elemental'
Oxygen, 30s, 550°C
Oxygen, 30s, 650°C
Oxygen, 30s, 720°C
Oxygen, 40s, 790°C
Oxygen, 30s, 820°C
Oxygen, 20s, 840°C
CalibrationOx, 110s, 0°C
'end'

b) *EUSAAR analysis protocol*

Helium, 10s, 1°C
'start ramping the temperature'
Helium, 120s, 200°C
Helium, 150s, 300°C
Helium, 180s, 450°C
Helium, 180s, 650°C
'let the oven cool before elemental'
Helium, 25s, 0°C
'elemental'
Oxygen, 240s, 550°C
Oxygen, 150s, 850°C
CalibrationOx, 110s, 0°C
'end'

Appendix H

Table H-1 – ICP-MS analysis instrumental data

Standard, SRM, Sample or Blank Name	Elements	Analyte Flow Rate in ml/min	No of Replicates	Average Intensity	Standard Deviation	Rel. Standard Deviation in %
Standard Reference Material SRM1648						
BlankSRM	As	1.09	3	899	44	4.9
	Ni			440	42	9.5
	Sb			565	32	5.7
	Se			48	12	25
	V			135	12	8.8
	Cd			68	2	2.9
	Co			787	22	2.8
SRM5ppb	As	1.09	3	9798	108	1.1
	Ni			20660	104	0.5
	Sb			25431	345	1.4
	Se			264	31	12
	V			100758	772	0.8
	Cd			11240	177	1.6
	Co			42605	154	0.4
SRM10ppb	As	1.09	3	11779	181	1.5
	Ni			25515	337	1.3
	Sb			32367	221	0.7
	Se			404	13	3.2
	V			120484	1011	0.8
	Cd			14381	147	1.0
	Co			66397	522	0.8
SRM30ppb	As	1.09	3	19915	227	1.1
	Ni			49109	501	1.0
	Sb			79939	638	0.8
	Se			961	31	3.2
	V			195923	4511	2.3
	Cd			28116	18	0.1
	Co			172450	700	0.4
SRM50ppb	As	1.09	3	27815	407	1.5
	Ni			72145	472	0.7
	Sb			123930	1024	0.8
	Se			1506	21	1.4
	V			274065	1277	0.5
	Cd			41097	326	0.8
	Co			277811	2899	1.0
SRM80ppb	As	1.09	3	39328	415	1.1
	Ni			105996	1282	1.2
	Sb			185219	2271	1.2
	Se			2330	71	3.0
	V			386224	846	0.2
	Cd			60842	467	0.8
	Co			430229	1473	0.3
2SRM5 (representative Sample)	As	1.09	3	7289	166	2.3
	Ni			14651	193	1.3
	Sb			15161	233	1.5
	Se			109	16	15
	V			80318	577	0.7
	Cd			7757	160	2.1
	Co			16578	255	1.5
2SRM1	As	1.09	3	6065	155	2.6
	Ni			13458	178	1.3
	Sb			13633	197	1.4
	Se			95	19	20
	V			69529	420	0.6
	Cd			7290	81	1.1
	Co			13428	273	2.0
2SRM2	As	1.09	3	4800	142	3.0
	Ni			9864	222	2.3
	Sb			10396	77	0.7
	Se			82	13	16
	V			54307	1017	1.9
	Cd			5142	62	1.2
	Co			10286	224	2.2
2SRM3	As	1.09	3	3074	135	4.4
	Ni			6699	124	1.9
	Sb			6464	106	1.6
	Se			57	18	32
	V			35711	904	2.5
	Cd			3452	17	0.5
	Co			7880	41	0.5
2SRM4	As	1.09	3	1701	54	3.2
	Ni			3833	54	1.4
	Sb			4661	120	2.6
	Se			43	15	35
	V			20561	100	0.5
	Cd			2005	88	4.4
	Co			5339	127	2.4
2SRM6	As	1.09	3	9713	263	2.7
	Ni			17902	496	2.8
	Sb			19167	100	0.5
	Se			162	15	9.3

	V			97008	486	0.5	
	Cd			9682	150	1.5	
	Co			19493	474	2.4	
Standard, SRM, Sample or Blank Name	**Elements**	**Analyte Flow Rate in ml/min**	**No of Replicates**	**Average Intensity**	**Standard Deviation**	**Rel. Standard Deviation in %**	
2SRM7	As	1.09	3	20530	302	1.5	
	Ni			38789	603	1.6	
	Sb			40598	118	0.3	
	Se			314	18	5.7	
	V			202592	2897	1.4	
	Cd			20476	90	0.4	
	Co			41288	394	1.0	
SRM30ppb repeated as a drift check	As	1.09	3	19048	163	0.9	-4.6% drift
	Ni			47657	622	1.3	-3.0% drift
	Sb			77844	291	0.4	-2.7% drift
	Se			970	18	1.9	+0.9% drift
	V			188132	1301	0.7	-4.1% drift
	Cd			27073	303	1.1	-3.9% drift
	Co			167891	1182	0.7	-2.7% drift
2SRMblank	Mn	0.97	3	140	6	4.3	
	Cu			1711	18	1.1	
SRM5ppb	Mn	0.97	3	46290	1848	4.0	
	Cu			17418	187	1.1	
SRM10ppb	Mn	0.97	3	67518	1286	1.9	
	Cu			26098	429	1.6	
SRM30ppb	Mn	0.97	3	147176	1487	1.0	
	Cu			62033	643	1.0	
SRM50ppb	Mn	0.97	3	224518	1485	0.7	
	Cu			96061	1067	1.1	
SRM80ppb	Mn	0.97	3	351707	1137	0.3	
	Cu			150076	1463	1.0	
2SRM3 (representative sample)	Mn	0.97	3	25192	291	1.2	
	Cu			7894	196	2.5	
2SRM1	Mn	0.97	3	49653	507	1.0	
	Cu			14222	309	2.2	
2SRM2	Mn	0.97	3	36559	156	0.4	
	Cu			10748	124	1.2	
2SRM4	Mn	0.97	3	14116	384	2.7	
	Cu			4213	185	4.4	
2SRM5	Mn	0.97	3	52064	351	0.7	
	Cu			15304	579	3.8	
2SRM6	Mn	0.97	3	66181	1129	1.7	
	Cu			20924	256	1.2	
2SRM7	Mn	0.97	3	143827	78	0.1	
	Cu			45033	681	1.5	
SRM30ppb repeated as drift check	Mn	0.97	3	148423	1024	0.7	+0.8% drift
	Cu			62127	537	0.9	+0.2% drift
2SRMblank	Pb	0.92	3	340	77	23	
SRM10ppb	Pb	0.92	3	104306	4028	3.9	
SRM30ppb	Pb	0.92	3	169834	1976	1.2	
SRM50ppb	Pb	0.92	3	238755	970	0.4	
SRM80ppb	Pb	0.92	3	321671	3134	1.0	
SRM100ppb	Pb	0.92	3	379530	11270	3.0	
2SRM3 (represent. Sample)	Pb	0.92	3	74534	476	0.6	
2SRM1	Pb	0.92	3	144579	1042	0.7	
2SRM2	Pb	0.92	3	107873	1177	1.1	
2SRM4	Pb	0.92	3	33717	857	2.5	
2SRM5	Pb	0.92	3	152217	2734	1.8	
2SRM6	Pb	0.92	3	197784	6789	3.4	
2SRM7	Pb	0.92	3	281155	6680	2.4	
SRM50ppb drift check	Pb	0.92	3	234366	4603	2.0	-1.9% drift
Taiyuan Samples							
Standard, SRM, Sample or Blank Name	**Elements**	**Analyte Flow Rate in ml/min**	**No of Replicates**	**Average Intensity**	**Standard Deviation**	**Rel. Standard Deviation in %**	
T54 (blank)	As	1.02	5	508	14	2.8	
	Ni			562	27	4.8	
	Sb			914	39	4.3	
	Se			45	7	16	
	V			259	13	5.0	
	Cd			17	2	12	
	Co			232	9	3.9	
T74 (blank)	As	1.02	5	112	31	28	
	Ni			376	35	9.3	
	Sb			340	29	8.5	
	Se			53	7	13	
	V			229	19	8.3	
	Cd			28	6	21	
	Co			291	16	5.5	
5ppb	As	1.02	5	5460	94	1.7	
	Ni			17304	164	0.9	
	Sb			16465	133	0.8	
	Se			428	19	4.4	
	V			75733	712	0.9	
	Cd			4691	58	1.2	
	Co			40707	338	0.8	
10ppb	As	1.02	5	7271	203	2.8	
	Ni			22730	309	1.4	
	Sb			23039	117	0.5	
	Se			577	20	3.5	
	V			94872	984	1.0	

	Cd			7669	98	1.3
	Co			63461	564	0.9
Standard, SRM, Sample or Blank Name	**Elements**	**Analyte Flow Rate in ml/min**	**No of Replicates**	**Average Intensity**	**Standard Deviation**	**Rel. Standard Deviation in %**
30ppb	As	1.02	5	15094	178	1.2
	Ni			44946	333	0.7
	Sb			67698	782	1.2
	Se			1115	52	4.7
	V			169886	2194	1.3
	Cd			20423	204	1.0
	Co			166184	1962	1.2
50ppb	As	1.02	5	23268	260	1.1
	Ni			67686	869	1.3
	Sb			111189	384	0.3
	Se			1668	51	3.1
	V			247371	2098	0.8
	Cd			33369	407	1.2
	Co			270264	4119	1.5
80ppb	As	1.02	5	35065	436	1.2
	Ni			99924	727	0.7
	Sb			174284	2810	1.6
	Se			2524	87	3.4
	V			362568	5840	1.6
	Cd			52515	733	1.4
	Co			418423	5524	1.3
T69 (representative sample)	As	1.02	5	3390	86	2.5
	Ni			11801	284	2.4
	Sb			7335	78	1.1
	Se			284	33	12
	V			55390	188	0.3
	Cd			1407	36	2.6
	Co			14902	387	2.6
T51	As	1.02	5	17738	147	0.8
	Ni			97111	826	0.9
	Sb			39494	637	1.6
	Se			1841	38	2.1
	V			83508	743	0.9
	Cd			8454	152	1.8
	Co			28748	789	2.7
T53	As	1.02	5	3329	88	2.6
	Ni			12659	343	2.7
	Sb			3947	116	2.9
	Se			372	11	3.0
	V			58924	1072	1.8
	Cd			1227	34	2.8
	Co			15550	236	1.5
T55	As	1.02	5	8797	154	1.8
	Ni			34834	325	0.9
	Sb			21907	190	0.9
	Se			817	29	3.5
	V			46541	289	0.6
	Cd			5993	174	2.9
	Co			13832	242	1.7
T57	As	1.02	5	8423	179	2.1
	Ni			37278	538	1.4
	Sb			15988	436	2.7
	Se			745	35	4.7
	V			63440	1569	2.5
	Cd			5547	77	1.4
	Co			18974	222	1.2
T59	As	1.02	5	4355	63	1.4
	Ni			21839	255	1.2
	Sb			7137	147	2.1
	Se			411	30	7.3
	V			34869	461	1.3
	Cd			2258	40	1.8
	Co			10542	233	2.2
T61	As	1.02	5	1383	122	8.8
	Ni			3637	59	1.6
	Sb			2029	56	2.8
	Se			103	13	13
	V			26991	396	1.5
	Cd			233	14	6.0
	Co			7286	191	2.6
T63	As	1.02	5	2367	153	6.5
	Ni			16663	207	1.2
	Sb			3441	57	1.7
	Se			217	11	5.1
	V			12550	296	2.4
	Cd			2126	72	3.4
	Co			4395	122	2.8
T65	As	1.02	5	5254	221	4.2
	Ni			8569	108	1.3
	Sb			7817	89	1.1
	Se			417	23	5.5
	V			28495	598	2.1
	Cd			1658	45	2.7
	Co			8515	210	2.5
T67	As	1.02	5	7229	134	1.9
	Ni			169489	2228	1.3
	Sb			30944	267	0.9
	Se			927	41	4.4
	V			44215	877	2.0
	Cd			3571	49	1.4

	Co			21075	339	1.6	
Standard, SRM, Sample or Blank Name	**Elements**	**Analyte Flow Rate in ml/min**	**No of Replicates**	**Average Intensity**	**Standard Deviation**	**Rel. Standard Deviation in %**	
T71	As	1.02	5	3801	37	1.0	
	Ni			16231	309	1.9	
	Sb			5615	208	3.7	
	Se			338	18	5.3	
	V			47000	658	1.4	
	Cd			2384	50	2.1	
	Co			14278	283	2.0	
T73	As	1.02	5	4463	140	3.1	
	Ni			5130	77	1.5	
	Sb			13298	99	0.7	
	Se			496	31	6.3	
	V			25663	281	1.1	
	Cd			1592	64	4.0	
	Co			8150	177	2.2	
50ppb repeated for drift check	As	1.02	5	22057	311	1.4	-5.5% drift
	Ni			64648	843	1.3	-4.7% drift
	Sb			106593	1091	1.0	-4.3% drift
	Se			1608	51	3.2	-3.7% drift
	V			235457	1804	0.8	-5.1% drift
	Cd			32399	251	0.8	-3.0% drift
	Co			258023	2606	1.0	-4.7% drift
T54 (blank)	Mn	0.97	5	586	25	4.3	
	Cu			537	26	4.8	
T74 (blank)	Mn	0.97	5	532	17	3.2	
	Cu			610	28	4.6	
5ppb	Mn	0.97	5	91719	2169	2.4	
	Cu			22634	127	0.6	
10ppb	Mn	0.97	5	113981	2451	2.2	
	Cu			31253	731	2.3	
30ppb	Mn	0.97	5	196271	3443	1.8	
	Cu			66182	1020	1.5	
50ppb	Mn	0.97	5	279005	2308	0.8	
	Cu			100333	1802	1.8	
80ppb	Mn	0.97	5	403838	5066	1.3	
	Cu			152375	1952	1.3	
T59 (representative sample)	Mn	0.97	5	71601	1161	1.6	
	Cu			14232	346	2.4	
T51	Mn	0.97	5	187589	1499	0.8	
	Cu			43097	759	1.8	
T53	Mn	0.97	5	96490	1880	1.9	
	Cu			4123	131	3.2	
T55	Mn	0.97	5	112888	584	0.5	
	Cu			15271	217	1.4	
T57	Mn	0.97	5	133416	1919	1.4	
	Cu			13398	163	1.2	
T61	Mn	0.97	5	39881	761	1.9	
	Cu			5977	131	2.2	
T63	Mn	0.97	5	49036	904	1.8	
	Cu			3631	79	2.2	
T65	Mn	0.97	5	49037	726	1.5	
	Cu			12553	359	2.9	
T67	Mn	0.97	5	78664	1145	1.5	
	Cu			7194	202	2.8	
T69	Mn	0.97	5	76687	1320	1.7	
	Cu			6012	44	0.7	
T71	Mn	0.97	5	87296	2004	2.3	
	Cu			5683	43	0.8	
T73	Mn	0.97	5	48313	857	1.8	
	Cu			9328	94	1.0	
30ppb repeated for drift check	Mn	0.97	5	196424	3829	1.9	+0.1% drift
	Cu			65425	1415	2.2	-1.2% drift
T54 (blank)	Pb	1.0	5	571	20	3.5	
T74 (blank)	Pb	1.0	5	821	67	8.2	
10ppb	Pb	1.0	5	190623	2749	1.4	
30ppb	Pb	1.0	5	265469	5273	2.0	
50ppb	Pb	1.0	5	351356	3492	1.0	
80ppb	Pb	1.0	5	477178	11770	2.5	
100ppb	Pb	1.0	5	560719	5543	1.0	
T59 (representative sample)	Pb	1.0	5	148931	1291	0.9	
T51	Pb	1.0	5	603485	11020	1.8	
T53	Pb	1.0	5	75054	1172	1.6	
T55	Pb	1.0	5	305796	5968	2.0	
T57	Pb	1.0	5	267838	4745	1.8	
T61	Pb	1.0	5	27244	266	1.0	
T63	Pb	1.0	5	83750	1399	1.7	
T65	Pb	1.0	5	124180	1995	1.6	
T67	Pb	1.0	5	251484	7129	2.8	
T69	Pb	1.0	5	82416	1823	2.2	
T71	Pb	1.0	5	109265	1468	1.3	
T73	Pb	1.0	5	110039	783	0.7	
50ppb repeated for drift check	Pb	1.0	5	355386	4025	1.1	+1.1% drift

The average values of the two blanks have already been subtracted from the intensities of the samples!

H-1 Elaboration of ICP-MS data

The data obtained from the instrumental analysis of the Taiyuan samples and SRMs is summarised in table H-1. Mean values (averages), standard deviations and relative standard deviations are calculated according to the following formulas:

Arithmetic Mean: $$\bar{x} = \sum_{i=1}^{n} x_i$$

Standard Deviation: $$s = \sigma = \sqrt{\frac{\sum_{i=1}^{n} (x_i - \bar{x})^2}{n-1}}$$

Relative St. Deviation: $$RSD = \frac{\sigma}{\bar{x}} \cdot 100(\%)$$

[n=number of replicates]

The instrumental detection limits [**LOD –** the lowest concentration at which one can be relatively certain that an element is present in the sample (Boss and Fredeen, 2004)] and method detection limits (**MDL**) are shown in table H-2 and determined as follows: The blank method is used to obtain the LOD value for each element. This means that a blank (acid mixture) is aspirated and analysed 10 times. The standard deviation of these 10 repeats is then multiplied by 3 (corresponding to a probability of 99.7% that the signal is detected). The MDL values are obtained by calculating backwards from the LOD to the solid mass concentration in the PM. This is a rather crude approximation which assumes the absence of matrix effects and other potential errors in the process of sample dissolution (decomposition). The MDL values are calculated for the smallest amount of sample used, according to:

$$MDL = \frac{LOD \cdot V_s}{m_{PM}} \qquad \text{[in μg (element) per g (PM)]}$$

[$V_s = 60 \cdot 10^{-3}$l; SRM: m_{PM}=3.0mg; Sample: m_{PM}=2.7mg]

Table H-2 – ICP-MS LOD and MDL values of the elements in SRM1648 and Taiyuan samples

	As	Ni	Sb	Se	V	Cd	Co	Mn	Cu	Pb
SRM1648										
LOD [μg/l]	0.07	0.09	0.01	0.40	0.01	0.02	0.01	0.01	0.03	0.01
MDL [μg/g]	1	2	0.2	8	0.2	0.4	0.2	0.2	0.6	0.2
Taiyuan Samples										
LOD [μg/l]	0.12	0.06	0.01	0.26	0.01	0.01	0.01	0.02	0.04	0.02
MDL [μg/g]	3	1	0.2	6	0.2	0.2	0.2	0.4	0.9	0.4

a) SRM1648

The data from table H-1 yields the following calibration graphs for the elements in the standard reference material (figure H-1), their solution concentrations (table H-3) and corresponding NIST recoveries (see table H-4).

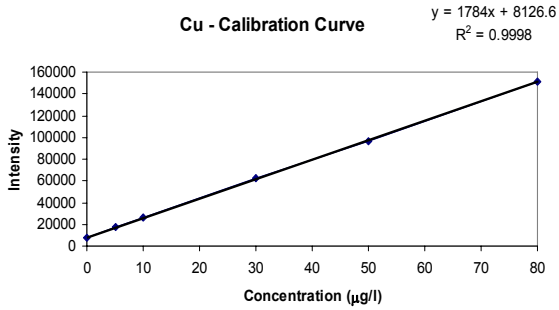

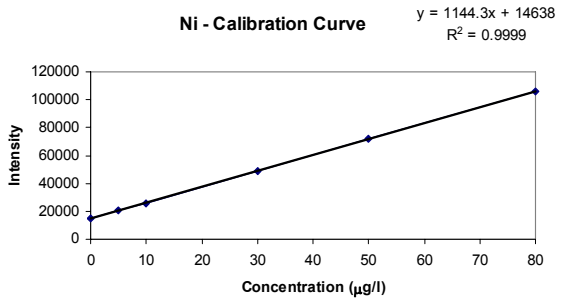

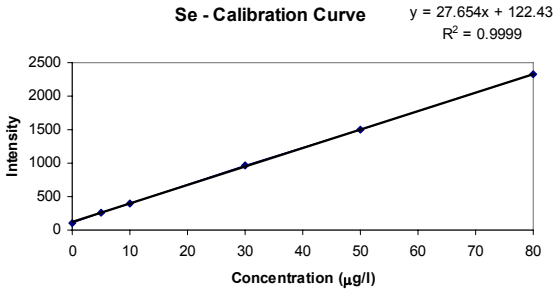

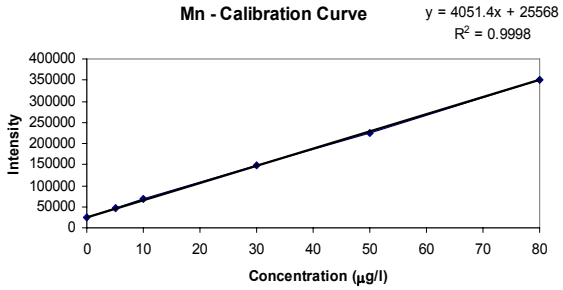

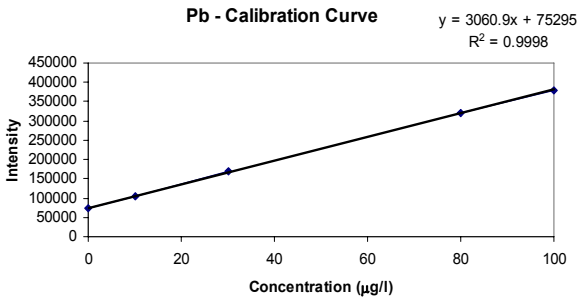

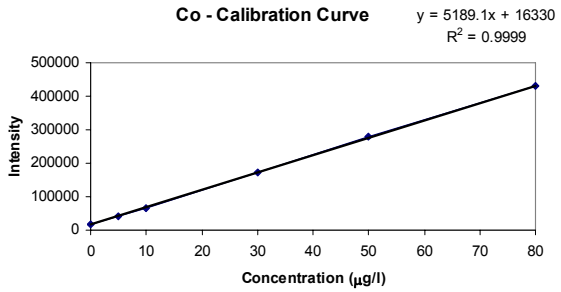

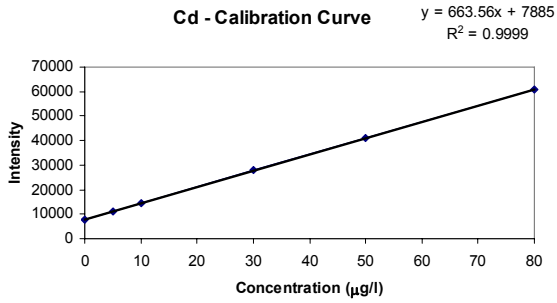

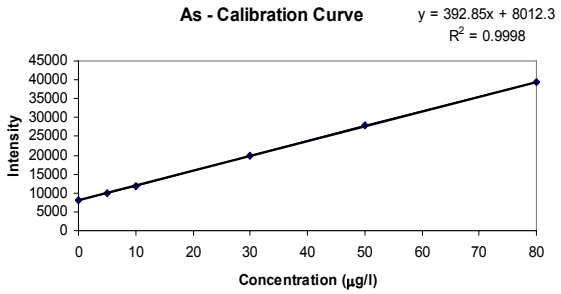

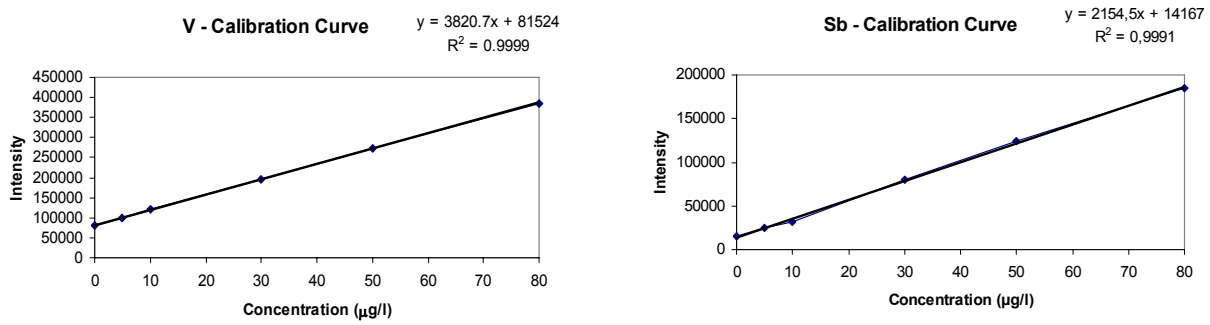

Figure H-1 – Calibration graphs of ICP-MS analysis of SRM1648

Table H-3 – ICP-MS Element concentrations in solution of SRM

	Element Concentrations in µg/l									
SRM	**As**	**Ni**	**Sb**	**Se**	**Co**	**V**	**Cd**	**Mn**	**Cu**	**Pb**
2SRM1	19.3	14.7	7.9	4.3	3.2	22.7	13.7	153	99.6	1181
2SRM2	15.3	10.8	6.0	3.7	2.5	17.8	9.7	113	75.3	881
2SRM3	9.8	7.3	3.8	2.6	1.9	11.7	6.5	77.7	55.3	609
2SRM4	5.4	4.2	2.7	1.9	1.3	6.7	3.8	43.6	29.5	330
2SRM5	23.2	16.0	8.8	4.9	4.0	26.3	14.6	161	107	1243
2SRM6	30.9	19.6	11.1	7.3	4.7	31.7	18.2	204	147	1615
2SRM7	65.3	42.4	23.6	14.2	9.9	66.3	38.6	444	316	3445

[all concentrations are already dilution corrected]

Table H-4 – ICP-MS recoveries of the NIST values

	Element Recoveries in %									
SRM	**As**	**Ni**	**Sb**	**Se**	**Co**	**V**	**Cd**	**Mn**	**Cu**	**Pb**
2SRM1	95.0	101	99.2	89.8	101	101	103	110	92.4	102
2SRM2	95.0	93.8	95.6	97.8	98.3	99.8	92.2	102	88.2	96.0
2SRM3	92.8	97.2	90.6	104	115	100	94.4	108	98.9	101
2SRM4	97.3	106	125	150	148	110	104	115	100	104
2SRM5	104	100	100	93.5	114	106	99.9	105	90.3	97.4
2SRM6	109	96.8	100	110	110	101	98.6	105	97.7	100
2SRM7	106	96.3	97.6	98.0	103	97.3	95.9	105	96.6	98.0
$\bar{x}$ **in %**	**99.8**	**98.7**	**101**	**106**	**113**	**102**	**98.4**	**107**	**94.9**	**99.8**
s in %	±6.4	±4.2	±12	±22	±18	±4	±4.8	±3	±5.0	±3.1
95% c.i. in %	±5.9	±3.9	±11	±20	±17	±4	±4.4	±3	±4.6	±2.9

The 95% confidence interval (c.i.) was obtained by assuming a t-distribution of the data (which makes sense as the population standard deviation σ was estimated via the observed standard deviation s) with k=n-1 [n: number of replicates, i.e. 7] degrees of freedom and the resulting Student t factor of 2.447 (95% c.i.) (Moore and McCabe, 2006).

$$c.i. = \pm t \cdot \frac{s}{\sqrt{n}} = \pm 2.447 \cdot \frac{s}{\sqrt{7}}$$

b) Taiyuan Samples

The calibration graphs of the Taiyuan samples are depicted in figure H-2, their solution concentrations can be found in table H-5, their mass on the Teflon filter in table H-6 and the atmospheric concentrations are gathered in table H-7.

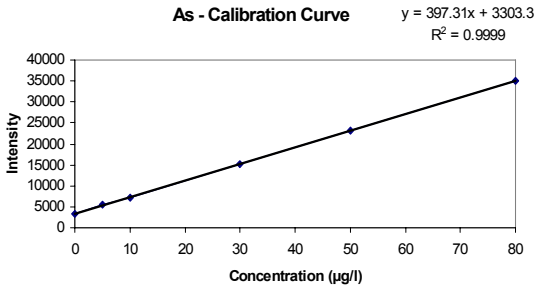

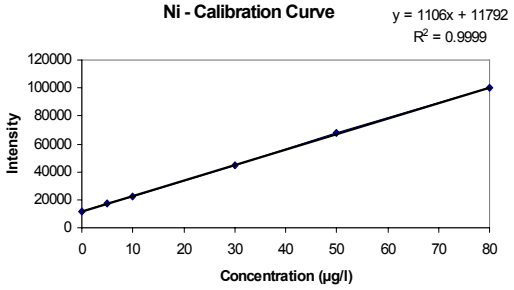

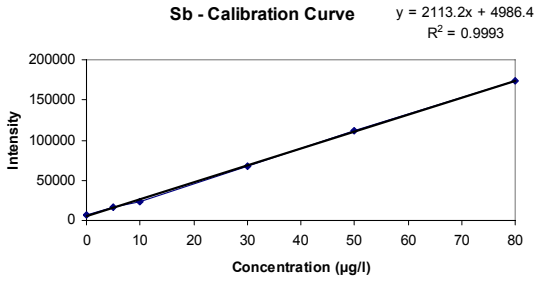

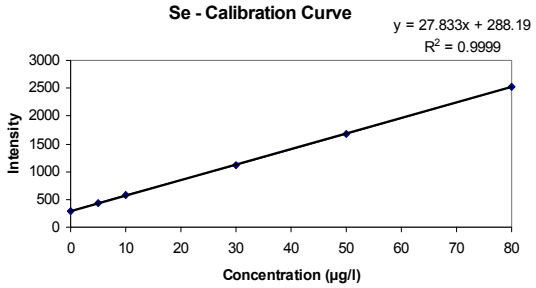

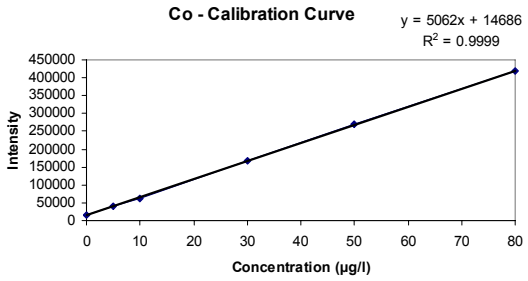

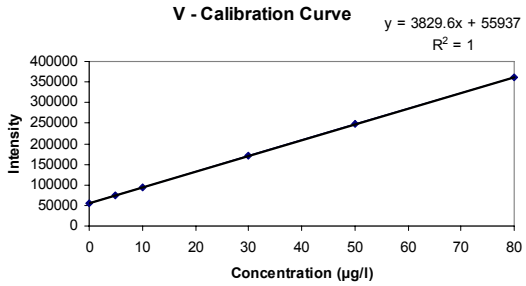

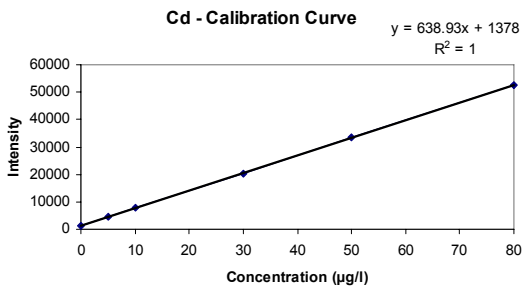

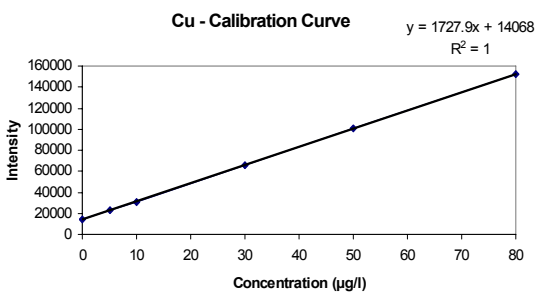

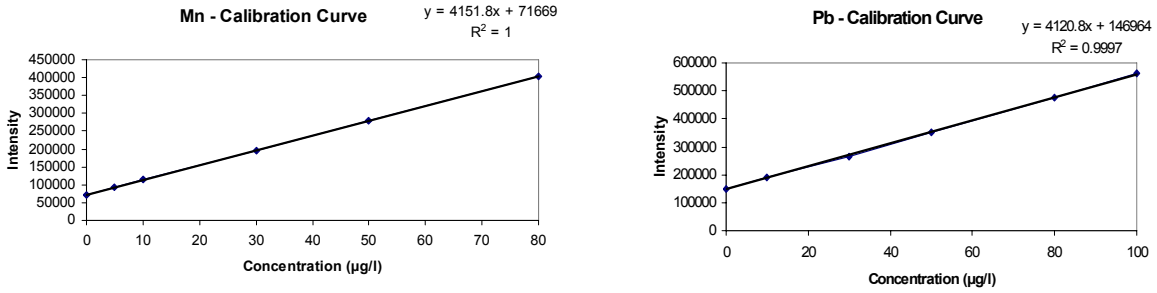

Figure H-2 – Calibration graphs of ICP-MS analysis of Taiyuan samples

Table H-5 – ICP-MS element concentration in solution of Taiyuan samples

	Element Concentrations in µg/l									
Samples	**As**	**Ni**	**Sb**	**Se**	**Co**	**V**	**Cd**	**Mn**	**Cu**	**Pb**
T51	55.2	110	23.2	82.9	7.1	27.3	16.6	565	312	915
T53	9.9	14.2	2.2	16.9	3.9	19.2	2.4	291	29.8	114
T55	27.1	39.3	12.8	36.9	3.4	15.2	11.7	340	110	464
T57	25.9	42.0	9.3	33.6	4.7	20.7	10.9	402	96.9	406
T59	13.1	24.6	4.1	18.6	2.6	11.4	4.4	216	103	226
T61	3.7	4.0	1.0	4.8	1.8	8.8	0.50	120	43.2	41.5
T63	6.8	18.7	1.9	9.9	1.1	4.1	4.2	148	26.3	127
T65	15.9	9.6	4.5	18.9	2.1	9.3	3.3	148	90.8	189
T67	22.1	191	18.1	41.8	5.2	14.4	7.0	237	52.0	382
T69	10.0	13.2	4.2	12.9	3.7	18.1	2.8	231	43.5	125
T71	11.3	18.2	3.2	15.4	3.5	15.3	4.7	263	41.1	166
T73	13.4	5.7	7.7	22.5	2.0	8.4	3.1	145	67.5	167

[all concentrations are already dilution corrected]

The atmospheric mass concentrations of the elements in the PM are obtained by the following formula:

$$c_a = \frac{c_s \cdot V_s}{\dot{V} \cdot t}$$

and C_a : mass concentration in the atmosphere

C_s : solution concentration (table H-5)

V_s : 60ml (decomposition volume)

$\dot{V}$: sampled air volume flow (0.1 m³/min)

t : sampling duration (min)

Table H-6 – Sampled element mass on each Teflon filter

	Mass of Each Element on Teflon Filter in μg									
Samples	**As**	**Ni**	**Sb**	**Se**	**Co**	**V**	**Cd**	**Mn**	**Cu**	**Pb**
T51	3.3	6.6	1.4	5.0	0.43	1.6	1.0	34	19	55
T53	0.59	0.85	0.13	1.0	0.23	1.2	0.14	17	1.8	6.8
T55	1.6	2.4	0.77	2.2	0.20	0.91	0.70	20	6.6	28
T57	1.6	2.5	0.56	2.0	0.28	1.2	0.65	24	5.8	24
T59	0.79	1.5	0.25	1.1	0.16	0.68	0.26	13	6.2	14
T61	0.22	0.24	0.060	0.29	0.11	0.53	0.030	7.2	2.6	2.5
T63	0.41	1.1	0.11	0.59	0.066	0.25	0.25	8.9	1.6	7.6
T65	0.95	0.58	0.27	1.1	0.13	0.56	0.20	8.9	5.5	11
T67	1.3	11	1.1	2.5	0.31	0.86	0.42	14	3.1	23
T69	0.60	0.79	0.25	0.77	0.22	1.1	0.17	14	2.6	7.5
T71	0.68	1.1	0.19	0.92	0.21	0.92	0.28	16	2.5	10
T73	0.80	0.34	0.46	1.4	0.12	0.50	0.19	8.7	4.1	10
mean	**1.07**	**2.42**	**0.46**	**1.57**	**0.21**	**0.86**	**0.36**	**15**	**5.12**	**17**
s	0.83	3.21	0.43	1.27	0.10	0.38	0.28	8	4.72	14
r.s.d (%)	**77**	**133**	**92**	**81**	**49**	**44**	**80**	**50**	**92**	**87**

[figures determined by multiplying values from table H-5 with $V_s=60\cdot10^{-3}$l]

Table H-7 – Atmospheric mass concentrations of the elements determined with ICP-MS

		Element Mass Concentration in the Atmosphere									
Samples	t [min]	**As [ng/m³]**	**Ni [ng/m³]**	**Sb [ng/m³]**	**Se [ng/m³]**	**Co [ng/m³]**	**V [ng/m³]**	**Cd [ng/m³]**	**Mn [μg/m³]**	**Cu [μg/m³]**	**Pb [μg/m³]**
T51	660	50	100	21	75	6.5	25	15	0.51	0.28	0.83
T53	460	13	19	2.9	22	5.1	25	3.1	0.38	0.039	0.15
T55	440	37	54	18	50	4.6	21	16	0.46	0.15	0.63
T57	330	47	76	17	61	8.5	38	20	0.73	0.18	0.74
T59	220	36	67	11	51	7.1	31	12	0.59	0.28	0.62
T61	220	10	11	2.7	13	4.9	24	1.4	0.33	0.12	0.11
T63	220	19	51	5.2	27	3.0	11	12	0.40	0.072	0.35
T65	330	29	18	8.2	34	3.8	17	6.0	0.27	0.17	0.34
T67	440	30	261	25	57	7.1	20	9.5	0.32	0.071	0.52
T69	330	18	24	7.6	24	6.7	33	5.1	0.42	0.079	0.23
T71	330	21	33	5.8	28	6.4	28	8.5	0.48	0.075	0.30
T73	330	24	10	14	41	3.6	15	5.6	0.26	0.12	0.30
	mean	**28**	**60**	**12**	**40**	**5.6**	**24**	**9.5**	**0.43**	**0.14**	**0.43**
	s	13	69	7.3	19	1.7	8	5.6	0.14	0.08	0.24
	r.s.d	46	115	64	47	30	32	59	32	59	55

Appendix I

Table I-1 – ICP-AES analysis instrumental data

Standard, SRM, Sample or Blank Name	Elements	Analyte Flow Rate in ml/min	No of Replicates	Average Intensity	Standard Deviation	Rel. Standard Deviation in %
Standard Reference Material SRM1648						
BlankSRM	Al	1.0	5	159	16	9.8
	Fe			28	5	17
	Mg			100	9	9.1
	Na			1689	125	7.4
	Ti			167	17	10
	Zn			26	5	18
0.5ppm	Al	1.0	5	6458	68	1.1
	Fe			5695	35	0.6
	Mg			5010	58	1.2
	Na			40740	404	1.0
	Ti			13968	101	0.7
	Zn			991	14	1.5
1.0ppm	Al	1.0	5	6925	52	0.7
	Fe			5963	52	0.9
	Mg			6188	25	0.4
	Na			55598	393	0.7
	Ti			19109	117	0.6
	Zn			1304	17	1.3
5.0ppm	Al	1.0	5	10162	91	0.9
	Fe			8047	91	1.1
	Mg			14655	106	0.7
	Na			177396	1621	0.9
	Ti			56305	614	1.1
	Zn			3540	36	1.0
10ppm	Al	1.0	5	15425	260	1.7
	Fe			11166	36	0.3
	Mg			27780	119	0.4
	Na			380847	1819	0.5
	Ti			111518	821	0.7
	Zn			6855	31	0.4
20ppm	Al	1.0	5	25294	240	0.9
	Fe			16596	171	1.0
	Mg			50796	352	0.7
	Na			777556	7614	1.0
	Ti			205479	1529	0.7
	Zn			12305	115	0.9
2SRM6 (representative sample)	Al	1.0	5	5927	83	1.4
	Fe			4968	68	1.4
	Mg			3912	52	1.3
	Na			25343	206	0.8
	Ti			9120	94	1.0
	Zn			664	15	2.3
2SRM1	Al	1.0	5	4189	67	1.6
	Fe			3334	70	2.1
	Mg			2480	53	2.1
	Na			15467	245	1.6
	Ti			5782	90	1.6
	Zn			405	10	2.4
2SRM2	Al	1.0	5	2980	55	1.8
	Fe			2407	27	1.1
	Mg			1708	31	1.8
	Na			11100	151	1.4
	Ti			4246	49	1.2
	Zn			293	8	2.8
2SRM3	Al	1.0	5	2025	48	2.4
	Fe			1584	24	1.5
	Mg			1236	16	1.3
	Na			7999	85	1.1
	Ti			2855	46	1.6
	Zn			195	7	3.8
2SRM4	Al	1.0	5	1279	32	2.5
	Fe			904	17	1.9
	Mg			802	14	1.8
	Na			5600	116	2.1
	Ti			1717	33	1.9
	Zn			128	11	8.9
2SRM5	Al	1.0	5	4160	21	0.5
	Fe			3176	46	1.4
	Mg			2510	44	1.7
	Na			15225	127	0.8
	Ti			5685	59	1.0
	Zn			399	17	4.3
2SRM7	Al	1.0	5	12022	89	0.7
	Fe			8960	64	0.7
	Mg			7174	126	1.8
	Na			46268	501	1.1
	Ti			15940	152	1.0
	Zn			1083	23	2.1
Drift check not done – ran out of sample						

Standard, SRM, Sample or Blank Name	Elements	Analyte Flow Rate in ml/min	No of Replicates	Average Intensity	Standard Deviation	Rel. Standard Deviation in %
Taiyuan Samples						
T54 (blank)	Al	0.95	5	129	27	21
	Fe			36	6	17
	Mg			86	3	3.7
	Na			2171	90	4.1
	Ti			122	11	9.2
	Zn			13	6	42
T74 (blank)	Al	0.95	5	236	16	6.6
	Fe			78	6	8.2
	Mg			268	8	2.9
	Na			2611	82	3.2
	Ti			569	15	2.6
	Zn			48	5	9.7
0.5ppm	Al	0.95	5	6041	65	1.1
	Fe			3639	52	1.4
	Mg			5316	42	0.8
	Na			44766	369	0.8
	Ti			10617	91	0.9
	Zn			754	22	2.9
1.0ppm	Al	0.95	5	6623	95	1.4
	Fe			4104	39	1.0
	Mg			6743	47	0.7
	Na			62573	584	0.9
	Ti			16858	193	1.1
	Zn			1188	14	1.2
5.0ppm	Al	0.95	5	10365	89	0.9
	Fe			7052	67	0.9
	Mg			16850	89	0.5
	Na			204784	1761	0.9
	Ti			62007	482	0.8
	Zn			4268	31	0.7
10ppm	Al	0.95	5	16582	179	1.1
	Fe			11644	166	1.4
	Mg			32867	343	1.0
	Na			431365	4287	1.0
	Ti			129928	1077	0.8
	Zn			9000	94	1.0
20ppm	Al	0.95	5	27583	384	1.4
	Fe			19394	264	1.4
	Mg			60684	748	1.2
	Na			879433	10735	1.2
	Ti			247370	3127	1.3
	Zn			16936	218	1.3
T65 (representative sample)	Al	0.95	5	5641	35	0.6
	Fe			3237	50	1.6
	Mg			4192	35	0.8
	Na			25348	272	1.1
	Ti			5409	68	1.3
	Zn			408	13	3.2
T51	Al	0.95	5	16226	126	0.8
	Fe			10105	118	1.2
	Mg			11906	135	1.1
	Na			68719	794	1.2
	Ti			11277	145	1.3
	Zn			1539	20	1.3
T53	Al	0.95	5	10175	74	0.7
	Fe			5483	61	1.1
	Mg			7894	28	0.4
	Na			61775	366	0.6
	Ti			7346	40	0.6
	Zn			213	10	4.6
T55	Al	0.95	5	8049	39	0.5
	Fe			5522	53	1.0
	Mg			6268	28	0.4
	Na			38115	123	0.3
	Ti			5637	21	0.4
	Zn			835	5	0.6
T57	Al	0.95	5	10753	130	1.2
	Fe			6009	72	1.2
	Mg			9919	99	1.0
	Na			60331	712	1.2
	Ti			7845	78	1.0
	Zn			784	12	1.5
T59	Al	0.95	5	6281	48	0.8
	Fe			4235	47	1.1
	Mg			5657	36	0.6
	Na			49817	360	0.7
	Ti			4508	36	0.8
	Zn			409	12	2.8
T61	Al	0.95	5	4979	49	1.0
	Fe			2491	31	1.2
	Mg			3526	28	0.8
	Na			31329	257	0.8
	Ti			3512	34	1.0
	Zn			89	6	6.7
T63	Al	0.95	5	2597	27	1.0
	Fe			1635	25	1.6
	Mg			2118	23	1.1
	Na			11300	109	1.0
	Ti			1820	11	0.6

	Zn			280	8	2.9
T67	Al	0.95	5	8288	89	1.1
	Fe			5271	55	1.0
	Mg			6095	63	1.0
	Na			39377	423	1.1
	Ti			5836	32	0.5
	Zn			514	9	1.7
Standard, SRM, Sample or Blank Name	**Elements**	**Analyte Flow Rate in ml/min**	**No of Replicates**	**Average Intensity**	**Standard Deviation**	**Rel. Standard Deviation in %**	
T69	Al	0.95	5	9928	67	0.7	
	Fe			5282	31	0.6	
	Mg			6620	20	0.3	
	Na			52222	343	0.7	
	Ti			7382	32	0.4	
	Zn			218	7	3.3	
T71	Al	0.95	5	9190	45	0.5	
	Fe			5150	36	0.7	
	Mg			6975	37	0.5	
	Na			42470	234	0.6	
	Ti			6437	57	0.9	
	Zn			362	23	6.3	
T73	Al	0.95	5	4937	33	0.7	
	Fe			2924	31	1.0	
	Mg			3898	41	1.0	
	Na			22102	194	0.9	
	Ti			3596	52	1.4	
	Zn			278	7	2.6	
10ppm repeated for drift check	Al	0.95	5	16443	173	1.1	-0.8% drift
	Fe			11246	80	0.7	-3.5% drift
	Mg			32299	305	0.9	-1.8% drift
	Na			421225	4126	1.0	-2.4% drift
	Ti			125424	1293	1.0	-3.6% drift
	Zn			8746	91	1.0	-2.9% drift
T54 (blank)	Si	1.02	5	162	5	3.3	
	Ca			12890	139	1.1	
T74 (blank)	Si	1.02	5	166	9	5.6	
	Ca			22289	245	1.1	
5ppm	Si	1.02	5	1417	17	1.2	
0.5ppm	Ca	1.02	5	323703	1299	0.40	
10ppm	Si	1.02	5	1856	24	1.3	
1.0ppm	Ca	1.02	5	362043	4492	1.2	
20ppm	Si	1.02	5	2618	36	1.4	
5.0ppm	Ca	1.02	5	1.06E+06	6870	0.65	
40ppm	Si	1.02	5	4032	52	1.3	
10ppm	Ca	1.02	5	2.93E+06	35967	1.2	
60ppm	Si	1.02	5	5212	66	1.3	
20ppm	Ca	1.02	5	4.82E+06	39850	0.83	
T59 (representative sample)	Si	1.02	5	1121	13	1.2	
	Ca			294646	2125	0.68	
T51	Si	1.02	5	2297	22	0.9	
	Ca			826903	5915	0.70	
T53	Si	1.02	5	1780	20	1.1	
	Ca			320656	2114	0.63	
T55	Si	1.02	5	1285	17	1.3	
	Ca			390526	997	0.24	
T57	Si	1.02	5	1732	21	1.2	
	Ca			537150	4346	0.78	
T61	Si	1.02	5	940	7	0.8	
	Ca			148332	961	0.58	
T63	Si	1.02	5	448	11	2.5	
	Ca			132150	1480	0.99	
T65	Si	1.02	5	874	7	0.8	
	Ca			276419	2747	0.93	
T67	Si	1.02	5	1253	17	1.3	
	Ca			416476	868	0.20	
T69	Si	1.02	5	1849	16	0.9	
	Ca			275809	1002	0.34	
T71	Si	1.02	5	1582	15	0.9	
	Ca			401523	3465	0.83	
T73	Si	1.02	5	805	15	1.9	
	Ca			256665	1159	0.42	
10ppm repeated for drift check	Si	1.02	5	1758	7	0.4	-5.6% drift
	Ca			2.85E+06	23650	0.83	-2.7% drift

The average values from the two blanks have already been subtracted from the intensities of the samples!

I-1 Elaboration of ICP-AES data

The procedure is analogous to the one followed in appendix H for the ICP-MS data. Moreover, the same PM masses are used to determine the MDL values as in appendix H (SRM: 3.0mg; Sample: 2.7mg).

Table I-2 - ICP-AES LOD and MDL values of the elements in SRM1648 and Taiyuan samples

	Al	Fe	Mg	Na	Ti	Zn	Ca	Si
SRM1648								
LOD [mg/l]	0.02	0.04	0.01	0.01	0.01	0.03		
MDL [mg/g]	0.4	0.8	0.2	0.2	0.2	0.6		
Taiyuan Samples								
LOD [mg/l]	0.04	0.02	0.005	0.01	0.002	0.02	0.08	0.35
MDL [mg/g]	0.9	0.4	0.1	0.2	0.04	0.4	2	8

a)SRM1648

The data from table I-1 yields the following calibration graphs for the elements in the standard reference material (figure I-1), their solution concentrations (table I-3) and corresponding NIST recoveries (see table I-4).

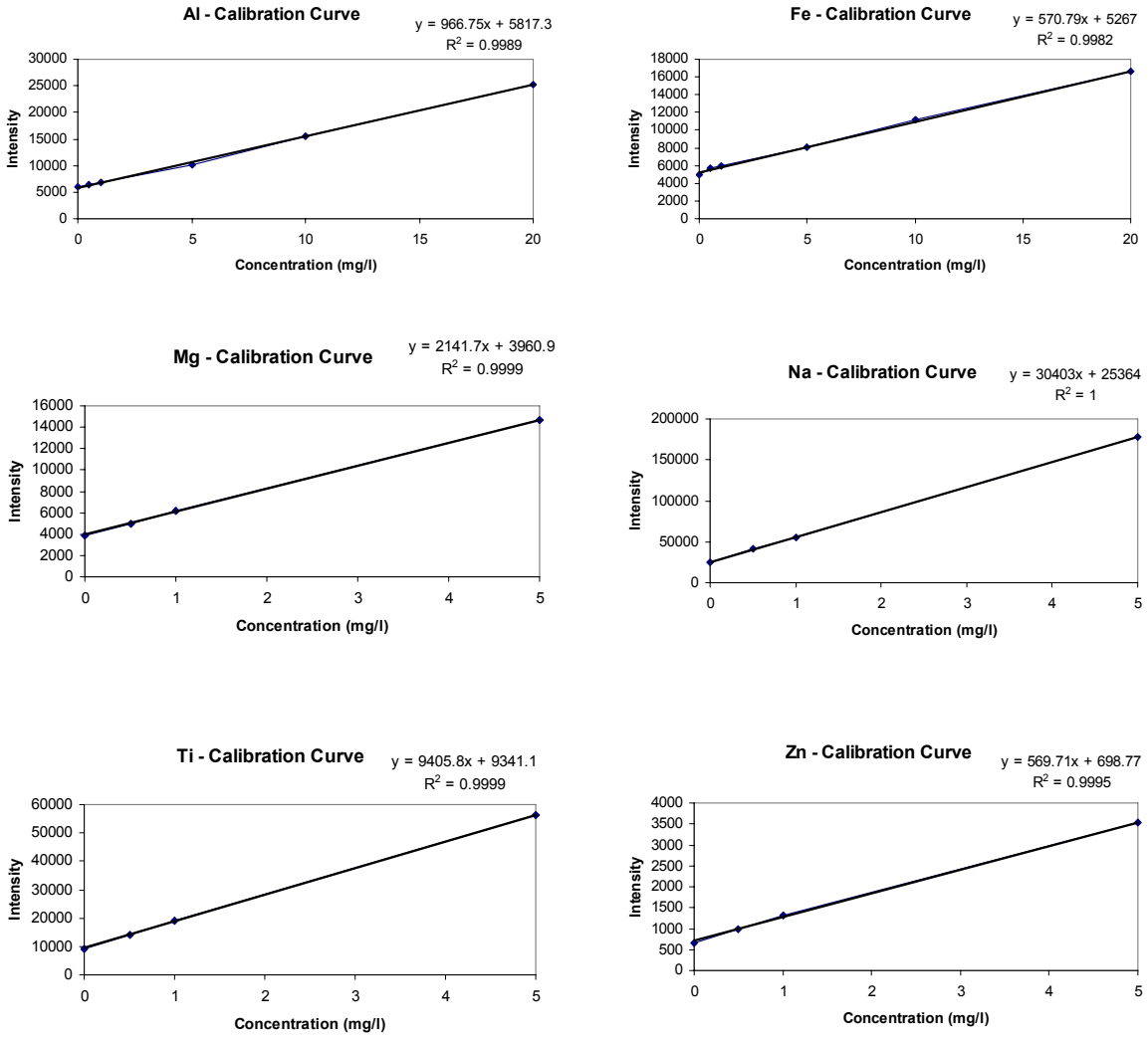

Figure I-1 - Calibration graphs of ICP-AES analysis of SRM1648

Table I-3 – ICP-AES Element concentrations in solution of SRM

	Element Concentrations in mg/l					
SRM	**Al**	**Fe**	**Mg**	**Na**	**Ti**	**Zn**
2SRM1	5.42	7.30	1.45	0.64	0.77	0.89
2SRM2	3.85	5.27	1.00	0.46	0.56	0.64
2SRM3	2.62	3.47	0.72	0.33	0.38	0.43
2SRM4	1.65	1.98	0.47	0.23	0.23	0.28
2SRM5	5.38	6.95	1.47	0.63	0.76	0.88
2SRM6	7.66	10.88	2.28	1.04	1.21	1.46
2SRM7	15.54	19.62	4.19	1.90	2.12	2.38

Table I-4 – ICP-AES recoveries of the NIST values

	Element Recoveries in %					
SRM	**Al**	**Fe**	**Mg**	**Na**	**Ti**	**Zn**
2SRM1	89.4	105	102	84.8	108	106
2SRM2	80.5	96.2	89.0	76.1	101	95.9
2SRM3	83.4	96.6	98.8	84.3	103	97.0
2SRM4	100	105	120	110	120	122
2SRM5	80.7	91.3	93.9	75.4	96.9	94.1
2SRM6	90.9	113	116	99.2	122	124
2SRM7	84.8	93.6	97.6	83.4	98.5	93.2
$\bar{x}$ in %	**87.1**	**100**	**102**	**87.6**	**107**	**105**
s in %	±7.0	±7.7	±11	±13	±10	±13
95% c.i. in %	±6.5	±7.1	±10	±12	±9.2	±12

[95% confidence interval determined as in appendix H-1]

b) Taiyuan samples

The calibration graphs of the Taiyuan samples are depicted in figure I-2, their solution concentrations can be found in table I-5, their mass on the Teflon filter in table I-6 and the atmospheric concentrations are gathered in table I-7. Some standard concentrations in the calibration graphs that lay outside the range of the actual sample concentrations have been deleted to increase the correlation coefficient.

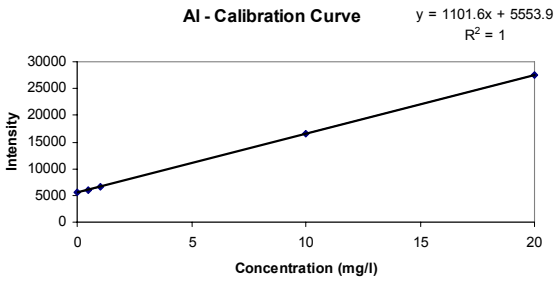

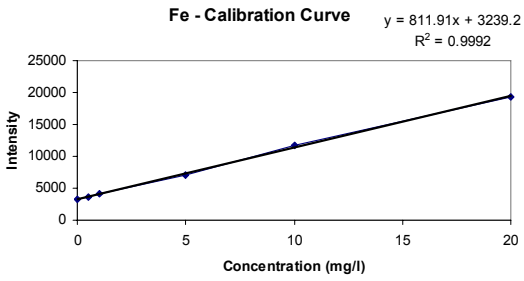

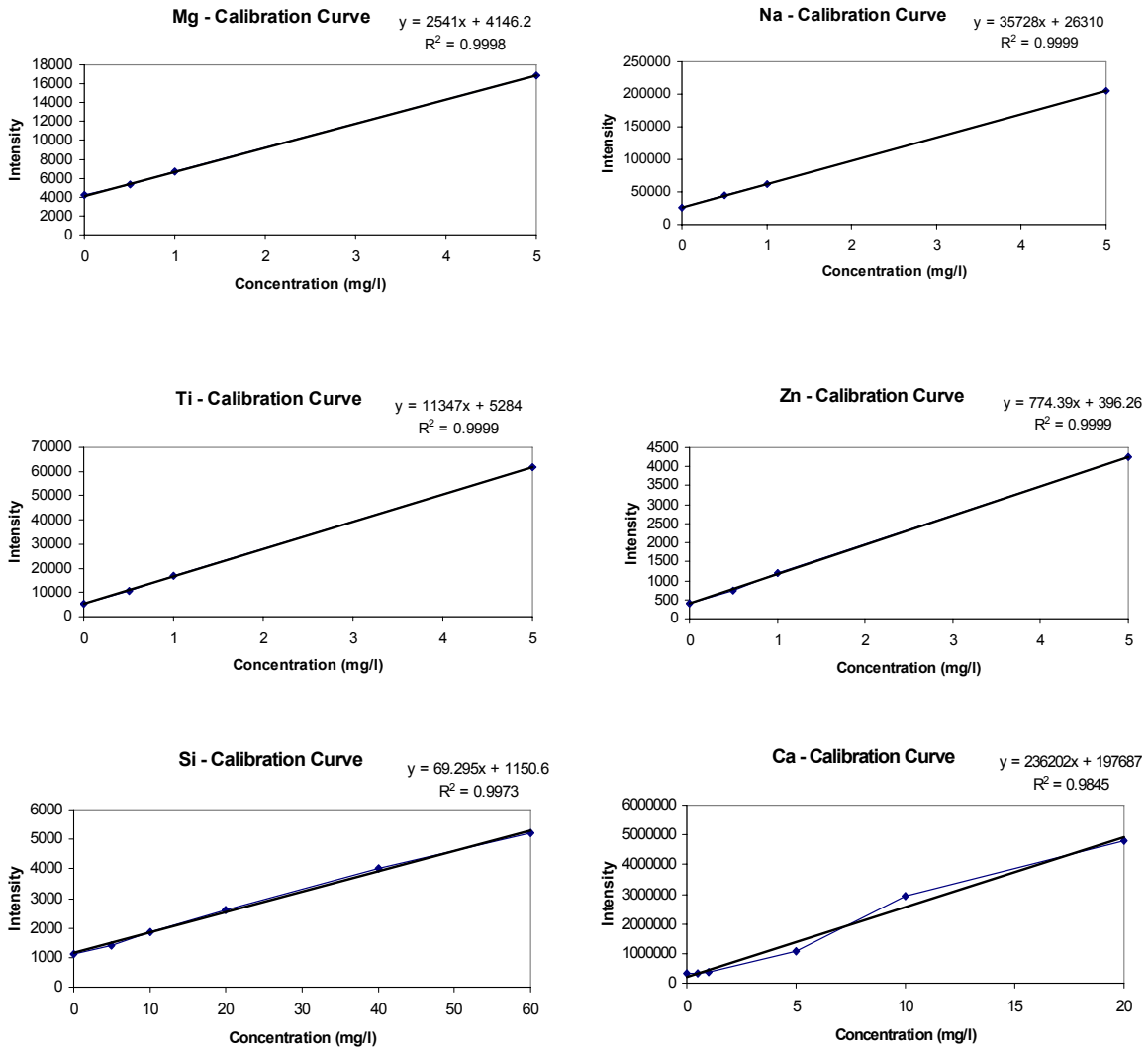

Figure I-2 – Calibration graphs of ICP-AES analysis of Taiyuan samples

Table I-5 – ICP-AES element concentration in solution of Taiyuan samples

	Element Concentrations in mg/l							
Samples	**Al**	**Fe**	**Mg**	**Na**	**Ti**	**Zn**	**Si**	**Ca**
T51	18.4	15.6	5.86	2.40	1.24	2.48	41.5	43.8
T53	11.6	8.44	3.88	2.16	0.81	0.34	32.1	17.0
T55	9.13	8.50	3.08	1.33	0.62	1.35	23.2	20.7
T57	12.2	9.25	4.88	2.11	0.86	1.27	31.3	28.4
T59	7.13	6.52	2.78	1.74	0.50	0.66	20.3	15.6
T61	5.65	3.83	1.73	1.10	0.39	0.14	17.0	7.85
T63	2.95	2.52	1.04	0.40	0.20	0.45	8.12	6.99
T65	6.40	4.98	2.06	0.89	0.60	0.66	15.8	14.6
T67	9.40	8.12	3.00	1.38	0.64	0.83	22.7	22.0
T69	11.3	8.13	3.26	1.83	0.81	0.35	33.4	14.6
T71	10.4	7.93	3.43	1.49	0.71	0.58	28.6	21.3
T73	5.60	4.50	1.92	0.77	0.40	0.45	14.6	13.6

Table I-6 – Sampled element mass on each Teflon filter

	Mass of Each Element on Teflon Filter							
Samples	**Al [mg]**	**Fe [mg]**	**Mg [mg]**	**Na [μg]**	**Ti [μg]**	**Zn [μg]**	**Si [mg]**	**Ca [mg]**
T51	1.1	0.94	0.35	144	74	149	2.5	2.6
T53	0.70	0.51	0.23	130	49	20	1.9	1.0
T55	0.55	0.51	0.18	80	37	81	1.4	1.2
T57	0.73	0.56	0.29	127	52	76	1.9	1.7
T59	0.43	0.39	0.17	104	30	40	1.2	0.94
T61	0.34	0.23	0.10	66	23	8.4	1.0	0.47
T63	0.18	0.15	0.062	24	12	27	0.49	0.42
T65	0.38	0.30	0.12	53	36	40	0.95	0.88
T67	0.56	0.49	0.18	83	38	50	1.4	1.3
T69	0.68	0.49	0.20	110	49	21	2.0	0.88
T71	0.62	0.48	0.21	89	43	35	1.7	1.3
T73	0.34	0.27	0.12	46	24	27	0.88	0.81

[figures obtained by multiplying the values from table I-5 with $V_s=60\cdot10^{-3}$l]

Table I-7 – Atmospheric mass concentrations of the elements determined with ICP-AES

		Atmospheric mass concentrations in μg/m³							
Samples	t [min]	**Al**	**Fe**	**Mg**	**Na**	**Ti**	**Zn**	**Si**	**Ca**
T51	660	16	14	5.3	2.2	1.1	2.3	38	40
T53	460	15	11	5.1	2.8	1.1	0.44	42	22
T55	440	12	12	4.2	1.8	0.85	1.8	32	28
T57	330	22	17	8.9	3.8	1.6	2.3	57	52
T59	220	19	18	7.6	4.8	1.4	1.8	55	43
T61	220	15	10	4.7	3.0	1.1	0.38	46	21
T63	220	8.1	6.9	2.8	1.1	0.55	1.2	22	19
T65	330	12	9.1	3.8	1.6	1.1	1.2	29	27
T67	440	13	11	4.1	1.9	0.87	1.1	31	30
T69	330	21	15	5.9	3.3	1.5	0.66	61	27
T71	330	19	14	6.2	2.7	1.3	1.1	52	39
T73	330	10	8.2	3.5	1.4	0.73	0.82	27	25
	mean	**15**	**12**	**5.2**	**2.5**	**1.1**	**1.3**	**41**	**31**
	s	4	3	1.8	1.1	0.3	0.7	13	10
	r.s.d	29	28	34	43	28	53	32	32

[concentrations have been determined according to same formula as in appendix H-1b]

Appendix J

J-1 Results of IC analysis of solutions - Anions

The data retrieved from the IC analysis is expressed in μS*min and corresponds to the area under each detected peak in the spectrogram. Table J-1 contains the blank values for both the Taiyuan samples (three blank averages) and the SRM1648 (one blank), which were subtracted from the instrumental data of the samples (summarised in table J-2) and finally converted to mg/l quantities with the aid of the calibration graphs of figure J-1. For the anion analysis, two sets of standards needed to be prepared (see table 16, also for standard concentrations) and the corresponding values are given in table J-3. The resulting anion concentrations in the Taiyuan samples and SRMs are shown in table J-4.

Table J-1 – Blank values for anions of Taiyuan Samples and SRM [sample blanks: Q6, Q12, Q22]

Taiyuan Samples					**SRM1648**			
Anions	**F^-**	**Cl^-**	**SO_4^{2-}**	**NO_3^-**	**F^-**	**Cl^-**	**SO_4^{2-}**	**NO_3^-**
Area [μS*min]	0.010	0.016	0.43	0.058	0.014	0.0080	0.784	0.091
s.d. [μS*min]	±0.009	±0.001	±.039	±0.059	only one blank			

[s.d. – standard deviation]

Table J-2 – Blank corrected peak area results from anions of Taiyuan samples and SRM

	Areas in μS*min					Areas in μS*min			
Sample Names	**F^-**	**Cl^-**	**SO_4^{2-}**	**NO_3^-**	**SRM Names**	**F^-**	**Cl^-**	**SO_4^{2-}**	**NO_3^-**
Q1	0.395	3.87	4.30	0.909					
Q3	0.093	1.11	1.65	0.340					
Q5	0.188	2.96	2.18	0.636					
Q7	0.250	3.12	3.42	1.05	**ICSRM1**	0.022	0.038	2.44	0.220
Q9	0.106	1.67	1.43	0.186	**ICSRM2**	0.039	0.158	6.20	0.406
Q11	0.019	0.500	0.211	0.018	**ICSRM3**	0.032	0.081	4.11	0.249
Q13	0.048	0.801	0.349	0.090	**ICSRM4**	0.043	0.162	6.64	0.429
Q15	0.088	0.612	1.14	0.201	**ICSRM5**	0.052	0.195	7.98	0.476
Q17	0.073	0.946	0.893	0.143	**ICSRM6**	0.045	0.195	7.61	0.437
Q19	0.070	0.846	1.18	0.235	**ICSRM7**	0.074	0.304	12.0	0.636
Q21	0.087	1.02	1.51	0.166					
Q23	0.067	1.17	0.698	0.158					

Table J-3 – Peak areas for anion standards of Taiyuan samples and SRM

	Areas in μS*min					Areas in μS*min			
Sample Standards	**F^-**	**Cl^-**	**SO_4^{2-}**	**NO_3^-**	**SRM Standards**	**F^-**	**Cl^-**	**SO_4^{2-}**	**NO_3^-**
Std 1	0.040	0.538	1.04	0.114	**SRMSt 1**	0.007	0.050	2.12	0.084
Std 2	0.076	1.624	2.10	0.400	**SRMSt 2**	0.036	0.092	6.43	0.275
Std 3	0.270	2.71	4.24	0.832	**SRMSt 3**	0.076	0.305	10.8	0.482
Std 4	0.464	4.34	6.33	1.27	**SRMSt 4**	0.125	0.536	13.0	0.788

[(0/0) included as no detectable anions in water blank]

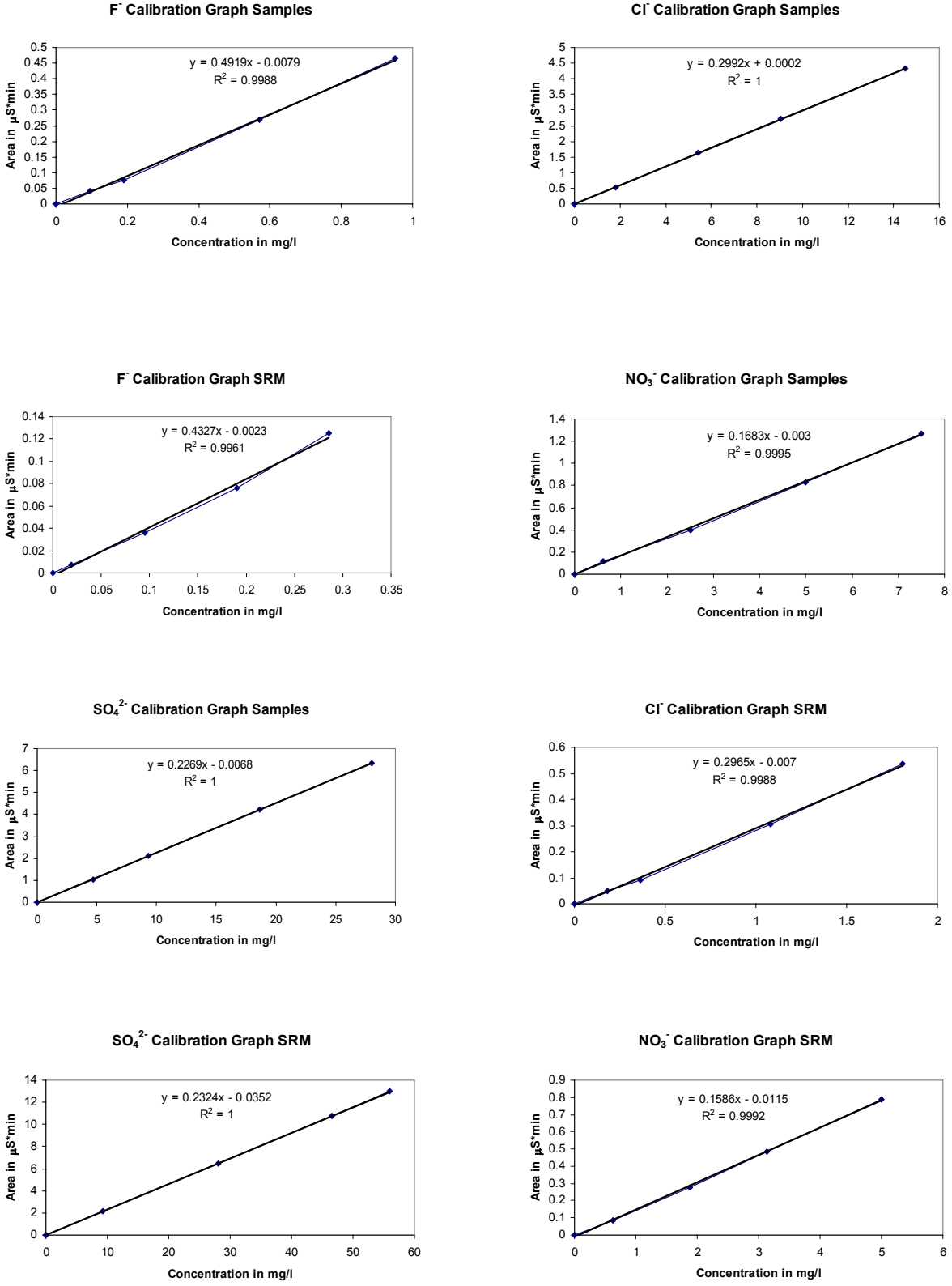

Figure J-1 – Anion calibration graphs for Taiyuan samples and SRM

Table J-4 – Anion concentrations in solution from Taiyuan samples and SRM

	Sample Concentrations in mg/l					SRM Concentrations in mg/l			
Sample Names	**F^-**	**Cl^-**	**SO_4^{2-}**	**NO_3^-**	**SRM Names**	**F^-**	**Cl^-**	**SO_4^{2-}**	**NO_3^-**
Q1	0.818	12.9	19.0	5.42					
Q3	0.204	3.70	7.31	2.04					
Q5	0.397	9.91	9.65	3.80					
Q7	0.524	10.4	15.1	6.28	**ICSRM1**	0.056	0.150	10.7	1.46
Q9	0.231	5.58	6.33	1.13	**ICSRM2**	0.096	0.558	26.8	2.63
Q11	0.056	1.67	0.961	0.123	**ICSRM3**	0.078	0.297	17.8	1.64
Q13	0.113	2.68	1.57	0.555	**ICSRM4**	0.105	0.569	28.7	2.78
Q15	0.195	2.05	5.04	1.21	**ICSRM5**	0.125	0.682	34.5	3.07
Q17	0.164	3.16	3.97	0.868	**ICSRM6**	0.109	0.681	32.9	2.83
Q19	0.158	2.83	5.21	1.41	**ICSRM7**	0.177	1.05	51.7	4.09
Q21	0.193	3.39	6.67	1.00					
Q23	0.152	3.92	3.11	0.959					

Instrumental drift was monitored via re-measuring of the standard 3 at the end of each analysis and the results are summarised in table J-5 for the analysis of the Taiyuan samples and the SRMs.

Table J-5 – Instrumental drift for anion analysis

Instrumental Drift – Anion Analysis				
Type	**F^-**	**Cl^-**	**SO_4^{2-}**	**NO_3^-**
Taiyuan Samples	+8.5%	+1.3%	+1.3%	-1.6%
SRM1648	-7.0%	-7.4%	-11%	-7.8%

The individual **masses on the whole quartz filter** of each anion and their **atmospheric mass concentrations** are collected in table J-6 and J-7 and are calculated according to the following formula:

$$m_{F-IC} = \frac{c_{s-IC} \cdot V_{s-IC} \cdot m_{tot}}{m_s}$$

with $m_{F\text{-}IC}$: mass of ion on whole filter

$c_{s\text{-}IC}$: solution concentration (table J-4)

$V_{s\text{-}IC}$: solution volume [**40ml**]

m_{tot}, m_s : total mass of PM (table J-13) and mass of PM on small quartz filter piece (table J-13) respectively

The above formula allows the determination of the total mass of each individual ion on the whole quartz filter. This is necessary for the calculation of the atmospheric mass concentrations.

Table J-6 – Anion masses on whole filter [$m_{F\text{-}IC}$]

	Mass of Each Anion on Whole Quartz Filter			
Sample	**F^- [µg]**	**Cl^- [mg]**	**SO_4^{2-} [mg]**	**NO_3^- [mg]**
Q1	67	1.1	1.5	0.44
Q3	17	0.31	0.60	0.17
Q5	32	0.81	0.78	0.31
Q7	43	0.85	1.23	0.51
Q9	19	0.46	0.52	0.093
Q11	4.6	0.14	0.079	0.010
Q13	9.4	0.22	0.13	0.045
Q15	16	0.17	0.41	0.099
Q17	13	0.26	0.32	0.071
Q19	13	0.23	0.43	0.12
Q21	16	0.28	0.54	0.081
Q23	13	0.32	0.25	0.079

Table J-7 – Anion mass concentrations in the atmosphere

		Anion Mass Concentrations in the Atmosphere in µg/m³			
Sample	t [min]	**F^-**	**Cl^-**	**SO_4^{2-}**	**NO_3^-**
Q1	660	1.0	16	23	6.7
Q3	460	0.37	6.7	13	3.7
Q5	440	0.73	18	18	7.0
Q7	330	1.3	26	37	15
Q9	220	0.87	21	24	4.2
Q11	220	0.21	6.2	3.6	0.46
Q13	220	0.42	10	5.9	2.1
Q15	220	0.73	7.6	19	4.5
Q17	220	0.61	12	15	3.2
Q19	220	0.59	11	19	5.3
Q21	220	0.71	13	25	3.7
Q23	220	0.57	15	12	3.6

[obtained by dividing values of table J-6 with (0.1·t in m³)]

J-2 Results of IC analysis of solutions - Cations

Analogous to the anion analysis, the cation concentrations in the solutions of the Taiyuan samples and SRMs were determined and the results are gathered in the following tables and figure. Only one set of standards was necessary for the calibration and the magnesium cations needed to be analysed separately and at a later stage, due to a defect in the instrument only affecting magnesium in the cooperate analysis.

Table J-8 – Blank values for cations of Taiyuan samples and SRM [sample blanks: Q6, Q12, Q22]

Taiyuan Samples					**SRM1648**			
Anions	**Na^+**	**NH_4^+**	**K^+**	**Ca^{2+}**	**Na^+**	**NH_4^+**	**K^+**	**Ca^{2+}**
Area [µS*min]	0.513	0.005	0.014	0.09	1.639	0.005	0.024	0.256
s.d. [µS*min]	±0.282	±0.001	±0.004	±0.03	only one blank			

Table J-9 – Blank corrected peak area results from cations of Taiyuan samples and SRM

	Areas in μS*min					Areas in μS*min			
Sample Names	**Na^+**	**NH_4^+**	**K^+**	**Ca^{2+}**	**SRM Names**	**Na^+**	**NH_4^+**	**K^+**	**Ca^{2+}**
Q1	1.13	3.35	1.46	9.26					
Q3	1.24	0.942	0.255	5.34					
Q5	1.03	2.28	0.794	5.45					
Q7	3.19	2.18	0.829	7.42	**ICSRM1**	1.64	0.287	0.113	2.19
Q9	2.18	0.852	0.304	4.55	**ICSRM2**	2.12	1.33	0.337	8.17
Q11	0.568	0.025	0.048	3.33	**ICSRM3**	2.05	0.590	0.191	4.21
Q13	0.472	0.519	0.186	2.46	**ICSRM4**	2.08	1.22	0.332	7.62
Q15	2.26	0.461	0.173	3.53	**ICSRM5**	2.23	1.54	0.393	9.38
Q17	0.688	0.949	0.310	3.42	**ICSRM6**	2.47	1.68	0.428	10.0
Q19	2.49	0.391	0.197	3.51	**ICSRM7**	3.13	2.23	0.579	14.0
Q21	2.26	0.318	0.135	4.70					
Q23	0.533	0.963	0.287	3.27					

Table J-10 – Peak areas for cation standards of Taiyuan samples and SRM

	Areas in μS*min				
Sample and SRM Standards	**Na^+**	**NH_4^+**	**K^+**	**Ca^{2+}**	**Blank at 0mg/l**
Std 1	0.144	0.265	0.033	0.820	0.002
Std 2	0.361	0.553	0.210	4.25	0.002
Std 3	0.720	2.28	0.436	8.43	0.002
Std 4	3.04	3.92	1.35	12.7	0.011

[for corresponding mg/l concentrations see table 16]

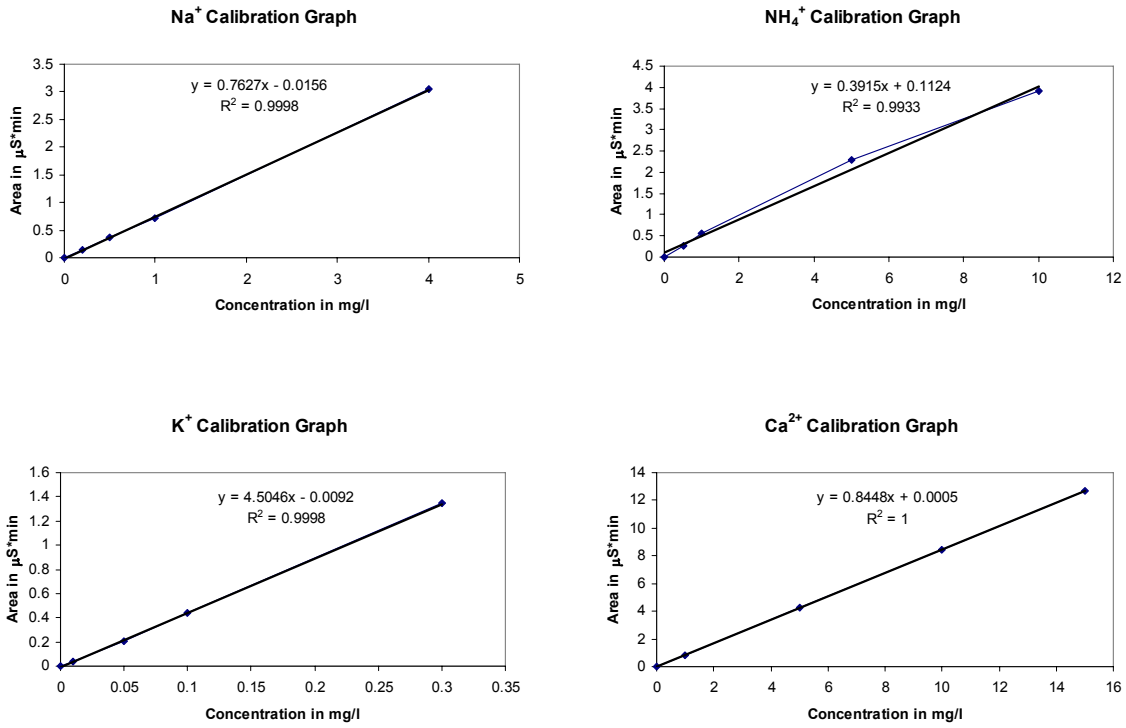

Figure J-2 – Cation calibration graphs for Taiyuan samples and SRM

Table J-11 – Cation concentrations in solution of Taiyuan samples and SRM

	Sample Concentrations in mg/l					SRM Concentrations in mg/l			
Sample Names	**Na^+**	**NH_4^+**	**K^+**	**Ca^{2+}**	**SRM Names**	**Na^+**	**NH_4^+**	**K^+**	**Ca^{2+}**
Q1	1.50	8.27	0.327	11.0					
Q3	1.65	2.12	0.059	6.32					
Q5	1.37	5.55	0.178	6.45					
Q7	4.20	5.28	0.186	8.78	**ICSRM1**	1.64	0.287	0.113	2.19
Q9	2.88	1.89	0.069	5.38	**ICSRM2**	2.12	1.33	0.337	8.17
Q11	0.766	]0;0.5[*	0.013	3.94	**ICSRM3**	2.05	0.590	0.191	4.21
Q13	0.639	1.04	0.043	2.91	**ICSRM4**	2.08	1.22	0.332	7.62
Q15	2.98	0.890	0.041	4.17	**ICSRM5**	2.23	1.54	0.393	9.38
Q17	0.923	2.14	0.071	4.05	**ICSRM6**	2.47	1.68	0.428	10.0
Q19	3.28	0.712	0.046	4.16	**ICSRM7**	3.13	2.23	0.579	14.0
Q21	2.99	0.525	0.032	5.56					
Q23	0.719	2.17	0.066	3.87					

*)Negative result due to regression line – interval for value given – highest one was chosen in all following considerations

Table J-12 – Instrumental drift for cation analysis

Instrumental Drift – Cation Analysis				
Type	**Na^+**	**NH_4^+**	**K^+**	**Ca^{2+}**
Taiyuan Samples	+0.83%	-1.3%	-3.6%	+1.4%
SRM1648	+0.41%	+1.1%	0.0%	+3.2%

The average retention times of the cations and anions are summarised in table J-13.

Table J-13 – Retention times of the analysed cations and anions

	F^-	**Cl^-**	**SO_4^{2-}**	**NO_3^-**	**Na^+**	**NH_4^+**	**K^+**	**Ca^{2+}**
Retention time [min]	3.19	4.95	9.43	10.4	7.38	9.14	13.1	20.9
Stand. Deviation [min]	±0.01	±0.004	±0.06	±0.02	±0.004	±0.04	±0.1	±0.2

Cation masses on the whole quartz filter and atmospheric concentrations have been obtained in the same way as described in appendix J-1 and the results are shown in tables J-14 and J-15.

Table J-14 – Cation masses on whole filter [$m_{F\text{-}IC}$]

	Mass of Each Cation on Whole Quartz Filter			
Sample	**Na^+ [mg]**	**NH_4^+ [mg]**	**K^+ [µg]**	**Ca^{2+} [mg]**
Q1	0.12	0.67	27	0.89
Q3	0.14	0.18	4.9	0.52
Q5	0.11	0.45	15	0.52
Q7	0.34	0.43	15	0.71
Q9	0.24	0.17	5.7	0.44
Q11	0.063	0.041	1.1	0.32
Q13	0.052	0.085	3.5	0.24
Q15	0.24	0.073	3.4	0.34
Q17	0.075	0.17	5.8	0.33
Q19	0.27	0.058	3.8	0.34
Q21	0.24	0.043	2.6	0.45
Q23	0.059	0.18	5.4	0.32

Table J-15 – Cation mass concentrations in the atmosphere

		Cation Mass Concentrations in the Atmosphere in μg/m³			
Sample	t [min]	**Na^+**	**NH_4^+**	**K^+**	**Ca^{2+}**
Q1	660	1.9	10	0.40	14
Q3	460	3.0	3.8	0.11	11
Q5	440	2.5	10	0.33	12
Q7	330	10	13	0.46	22
Q9	220	11	7.1	0.26	20
Q11	220	2.9	]0;1.9[	0.048	15
Q13	220	2.4	3.9	0.16	11
Q15	220	11	3.3	0.15	16
Q17	220	3.4	7.9	0.26	15
Q19	220	12	2.7	0.17	15
Q21	220	11	1.9	0.12	21
Q23	220	2.7	8.1	0.25	14

J-3 PM quantification on cut quartz filters

The quartz fibre filters were cut in a specially made cutting mould into two pieces of different areas (see section 4.5.2). In order to determine the amount of PM on each filter piece, the exposed areas were calculated and a homogeneous particle load was assumed. Figure J-3 shows an illustration of the larger filter piece and necessary parameters for the calculation of the exposed area. The rim around the filter, where the plastic ring was sitting, has already been subtracted. Tables J-16 and J-17 contain the summarised results. In order to determine the actual area of exposure on the filter pieces, it is necessary to first calculate the centre point angle β of the two small triangles T1 and T2 (green). This is done with aid of the cosine definition [cos(β) = x/r]. Hence, the angle α is obtained by subtracting 2β from 360°.

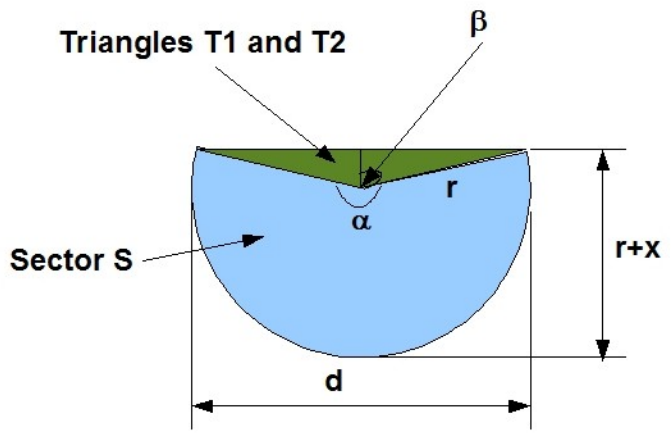

Figure J-3 – Illustration of the large quartz filter piece including calculation parameters

Now the area of the blue sector (**A_s**) can be calculated according to the formula:

$$A_S = \frac{\alpha}{360°} \cdot r^2 \cdot \pi$$ r: radius of filter

The area of the two triangles (**A_{T1}** and **A_{T2}**) is identical and given by the formula:

$$A_{T1} = \frac{r^2}{4} \sin 2\beta$$

The area A_{T1} is taken times two and added to A_s giving the total exposed filter area of the large filter piece (**A_L**). Moreover, the exposed filter area of the smaller piece (**A_{sm}**) is then easily determined by subtraction of A_L from the area of the total exposed filter: **$A_{Tot} = r^2 \cdot \pi$**.

The masses of PM on both the small (m_s) and the large (m_L) filter pieces are obtained by setting both ratios (area ratio and mass ratio) equal to each other and solving the equations for both [$m_s = m_{tot} - m_L$] and [$m_L = m_{tot} - m_s$] cases (m_{tot}: total mass of PM on whole filter).

These considerations are expressed in the following formulas:

$$\frac{A_L}{A_{sm}} = \frac{m_L}{m_s} \quad \text{with} \quad m_s = m_{tot} - m_L \quad \text{and} \quad m_L = m_{tot} - m_s$$

$$\rightarrow \quad m_s = \frac{m_{tot}}{\left(\frac{A_L}{A_{sm}} + 1\right)} \quad \text{and} \quad m_L = \frac{m_{tot}}{\left(\frac{A_{sm}}{A_L} + 1\right)}$$

Table J-16 – Parameter values of large filter piece

Sample	d [cm]	r + x [cm]	r [cm]	x [cm]	β [°]	α [°]
Q1	8.1	4.1	4.05	0.05	89.29	181.4
Q3	8.0	4.1	4.00	0.10	88.57	182.9
Q5	8.2	4.15	4.10	0.05	89.30	181.4
Q7	8.1	4.1	4.05	0.05	89.29	181.4
Q9	8.1	4.15	4.05	0.10	88.59	182.8
Q11	8.05	4.1	4.03	0.075	88.93	182.1
Q13	8.05	4.1	4.03	0.075	88.93	182.1
Q15	8.15	4.15	4.08	0.075	88.95	182.1
Q17	8.2	4.15	4.10	0.05	89.30	181.4
Q19	8.05	4.1	4.03	0.075	88.93	182.1
Q21	8.1	4.1	4.05	0.05	89.29	181.4
Q23	8.05	4.1	4.03	0.075	88.93	182.1

Table J-17 – Filter areas and PM loading

Sample	A_s [cm²]	$2*A_{T1}$ [cm²]	A_L [cm²]	A_{Tot} [cm²]	A_{sm} [cm²]	m_{tot} [mg]	m_L [mg]	m_s [mg]
Q1	25.97	0.20	26.17	51.53	25.36	30	15.2	14.8
Q3	25.53	0.40	25.93	50.27	24.33	12.9	6.7	6.2
Q5	26.61	0.20	26.82	52.81	26.00	14.9	7.6	7.3
Q7	25.97	0.20	26.17	51.53	25.36	19.7	10.0	9.7
Q9	26.17	0.40	26.57	51.53	24.96	10.9	5.6	5.3
Q11	25.75	0.30	26.05	50.90	24.84	6.8	3.5	3.3
Q13	25.75	0.30	26.05	50.90	24.84	5.0	2.6	2.4
Q15	26.39	0.31	26.70	52.17	25.47	7.8	4.0	3.8
Q17	26.61	0.20	26.82	52.81	26.00	7.9	4.0	3.9
Q19	25.75	0.30	26.05	50.90	24.84	9.2	4.7	4.5
Q21	25.97	0.20	26.17	51.53	25.36	10.4	5.3	5.1
Q23	25.75	0.30	26.05	50.90	24.84	6.9	3.5	3.4

The large quartz filter pieces and associated masses of PM (m_L) were used in the thermal/optical carbon analysis, while the small filter pieces (m_s) were analysed on the IC.

J-4 Error assessment of solution concentrations of all analysed ions

Since no certified NIST values were available, the standard deviations of the concentrations of the ions in solution were determined from the seven different amounts of SRM1648 analysed on the IC. The obtained solution concentrations of the SRM of tables J-4 and J-11 were multiplied with the solution volume (40ml) and divided by the total amount of SRM to normalise the determined mass of each ion to 1mg of SRM1648. The results are summarised in table J-18 and the 95% confidence intervals were obtained in the same manner as described in appendix H-1a.

Table J-18 – Error assessment of ion concentrations in solution

	Amount SRM in mg	SO_4^{2-} mg/mg	NO_3^- mg/mg	F^- mg/mg	Cl^- mg/mg	Na^+ mg/mg	NH_4^+ mg/mg	K^+ mg/mg	Ca^{2+} mg/mg
ICSRM1	1.8	0.24	0.032	0.00124	0.0033	0.036	0.0064	0.0025	0.049
ICSRM2	7	0.15	0.015	0.00055	0.0032	0.012	0.0076	0.0019	0.047
ICSRM3	3.5	0.20	0.019	0.00089	0.0034	0.023	0.0067	0.0022	0.048
ICSRM4	5.3	0.22	0.021	0.00079	0.0043	0.016	0.0092	0.0025	0.058
ICSRM5	7.8	0.18	0.016	0.00064	0.0035	0.011	0.0079	0.0020	0.048
ICSRM6	8.5	0.15	0.013	0.00051	0.0032	0.012	0.0079	0.0020	0.047
ICSRM7	11.5	0.18	0.014	0.00062	0.0037	0.011	0.0078	0.0020	0.049
	mean	0.19	0.019	0.00075	0.0035	0.017	0.0076	0.0022	0.049
	s	0.03	0.007	0.00026	0.0004	0.009	0.0009	0.0002	0.004
	r.s.d.	**±17%**	**±36%**	**±34%**	**±11%**	**±55%**	**±12%**	**±11%**	**±7.5%**
	95% c.i. in%	**±16%**	**±33%**	**±31%**	**±10%**	**±51%**	**±11%**	**±10%**	**±6.9%**

Appendix K

K-1 Thermal/optical carbon analysis of Taiyuan samples

The measured, blank corrected results of the thermal/optical carbon analysis of the Taiyuan samples are summarised in table K-1. The average blank value (average of blanks Q6, Q12, Q22) of **(0.79±0.38)μg/cm²** was subtracted from all samples. This, of course, only affects the organic and total carbon figures since there is no elemental carbon in the blanks. The results have been corrected after comparison with the sucrose standards, which were analysed after eight samples and at the end.

Table K-1 – TOA results on the quartz filters

Sample	OC in μg/cm²	EC in μg/cm²	TC in μg/cm²	EC/TC in %
Q1	104	44.4	149	29.8
Q3	18.8	7.27	26.1	27.9
Q5	37.8	20.4	58.2	35.0
Q7	43.6	18.8	62.3	30.1
Q9	20.6	11.9	32.6	36.6
Q11	8.77	3.75	12.5	30.0
Q13	11.4	4.66	16.1	29.0
Q15	19.1	7.17	26.3	27.3
Q17	26.4	11.2	37.5	29.7
Q19	12.9	6.69	19.6	34.1
Q21	14.5	10.8	25.3	42.7
Q23	18.6	12.1	30.8	39.5

In order to calculate the actual **amounts** of each carbonaceous fraction **on the whole quartz filter**, each area mass from table K-1 of each filter was multiplied with the whole filter area from table J-17. The results are summarised in table K-2.
The **atmospheric mass concentrations** were determined by dividing the carbonaceous masses on the whole filter (table K-2) with the corresponding air volumes sampled (0.1·t in m³), in the same way as in the previous methods.
The concentrations of the carbonaceous fractions of the PM on each filter in the atmosphere are gathered in table K-3.

Table K-2 – Masses of carbonaceous fractions on whole quartz filter

Sample	OC in mg	EC in mg	TC in mg
Q1	5.36	2.29	7.68
Q3	0.95	0.37	1.31
Q5	2.00	1.08	3.07
Q7	2.25	0.97	3.21
Q9	1.06	0.61	1.68
Q11	0.45	0.19	0.64
Q13	0.58	0.24	0.82
Q15	1.00	0.37	1.37
Q17	1.39	0.59	1.98
Q19	0.66	0.34	1.00
Q21	0.75	0.56	1.30
Q23	0.95	0.62	1.57

Table K-3 – Atmospheric mass concentrations of carbonaceous fractions

Sample	t [min]	OC in μg/m³	EC in μg/m³	TC in μg/m³
Q1	660	81.2	34.7	116
Q3	460	20.5	7.94	28.5
Q5	440	45.4	24.5	69.9
Q7	330	68.1	29.4	97.3
Q9	220	48.3	27.9	76.4
Q11	220	20.3	8.68	28.9
Q13	220	26.4	10.8	37.2
Q15	220	45.3	17.0	62.4
Q17	220	63.4	26.9	90.0
Q19	220	29.8	15.5	45.3
Q21	220	34.0	25.3	59.3
Q23	220	43.0	28.0	71.3

K-2 Thermograms of the TOA analysis of Taiyuan samples

The 12 thermograms of the thermal/optical carbon analysis of the Taiyuan samples are included in the following pages.

Appendix L

L-1 Bulk PM_{10} concentrations of Taiyuan samples on Teflon and quartz filters

The bulk atmospheric PM_{10} concentrations (c_{PM10}) have been calculated by applying the following formula:

$$c_{PM10} = \frac{m_{PM}}{\dot{V} \cdot t}$$

with m_{PM}: collected mass of PM_{10} on either Teflon or quartz filters

$\dot{V}$: volume flow of the pump (0.1m³/min), same for Teflon and quartz

t: sampling time for Teflon or quartz filters.

Table L-1 – Atmospheric bulk PM_{10} concentrations of Teflon and quartz filter samples from Taiyuan

Teflon	$\dot{V}$ in m³/min	m_{PM} in mg	t in min	c_{PM10} in μg/m³	**Quartz**	m_{PM} in mg	t in min	C_{PM10} in μg/m³
T51	0.1	32.3	660	**489**	**Q1**	30.0	660	**455**
T53	0.1	11.4	460	**248**	**Q3**	12.9	460	**280**
T55	0.1	14.1	440	**320**	**Q5**	14.9	440	**339**
T57	0.1	18.7	330	**567**	**Q7**	19.7	330	**597**
T59	0.1	8.7	220	**395**	**Q9**	10.9	220	**495**
T61	0.1	5.9	220	**268**	**Q11**	6.8	220	**309**
T63	0.1	2.7	220	**123**	**Q13**	5.0	220	**227**
T65	0.1	8.8	330	**267**	**Q15**	7.8	220	**355**
T67	0.1	12.3	440	**280**	**Q17**	7.9	220	**359**
T69	0.1	11.7	330	**355**	**Q19**	9.2	220	**418**
T71	0.1	13.4	330	**406**	**Q21**	10.4	220	**473**
T73	0.1	7.5	330	**227**	**Q23**	6.9	220	**314**
			mean	***329***			mean	***385***
			s	122			s	105
			r.s.d	**37**			r.s.d	**27**

L-2 Gauss' error progression (GEP) law

The GEP was used to calculate: using $c.i. = t \cdot {}^{s}/_{\sqrt{n}} = 2.201 \cdot {}^{s}/_{\sqrt{12}}$

a) 95% c.i. of the As/Se ratio ($\Delta\overline{R}_a$):

$$\Delta\overline{R}_a = \sqrt{\left(\frac{\partial R_a}{\partial m_{As}} \cdot \Delta\overline{m}_{As}\right)^2 + \left(\frac{\partial R_a}{\partial m_{Se}} \cdot \Delta\overline{m}_{Se}\right)^2}$$

$$\Delta\overline{R}_a = \sqrt{\left(\frac{\Delta\overline{m}_{As}}{m_{Se}}\right)^2 + \left(-\frac{m_{As}}{m_{Se}^2} \cdot \Delta\overline{m}_{Se}\right)^2}$$

with $\Delta\overline{m}_{As}, \Delta\overline{m}_{Se}$: 95% c.i. of As, Se masses: (0.53μg, 0.81μg); and m_{As}, m_{Se}: mean As, Se masses (table H-6): 1.07μg, 1.57μg;

→ $\Delta\overline{R}_a = 0.49$

b) 95% c.i. of the NH_4^+/SO_4^{2-} ratio ($\Delta\overline{R}_b$):

$$\Delta\overline{R}_b = \sqrt{\left(\frac{\partial R_b}{\partial m_{NH}} \cdot \Delta\overline{m}_{NH}\right)^2 + \left(\frac{\partial R_b}{\partial m_{SO}} \cdot \Delta\overline{m}_{SO}\right)^2}$$

$$\Delta\overline{R}_b = \sqrt{\left(\frac{\Delta\overline{m}_{NH}}{m_{SO}}\right)^2 + \left(-\frac{m_{NH}}{m_{SO}^2} \cdot \Delta\overline{m}_{SO}\right)^2}$$

with $\Delta\overline{m}_{NH}, \Delta\overline{m}_{SO}$: 95% c.i. of NH_4^+, SO_4^{2-} masses: (7.01μg, 5.63μg); and m_{NH}, m_{SO}: mean NH_4^+, SO_4^{2-} masses (table 26): 11.78μg, 11.78μg;

→ $\Delta\overline{R}_b = 0.76$